Atrial Fibrillation: Unravelling the Significance of Lysosomes In Atria Under Normal and Pathological Conditions



RASANJINI THAMALI PRANITHA AYAGAMA

Linacre College

University of Oxford

Submission for the degree of Doctor of Philosophy

Michaelmas 2021

This thesis was supervised by

Professor Rebecca Ann Beatrice Burton

Department of Pharmacology

And

Professor Frances Platt

Department of Pharmacology

Abstract

Lysosomes are responsible for the degradation of intracellular and extracellular macromolecules. They also play roles in signalling relevant to cardiac function and cardiac disease, however, the extent of altered lysosomal function in Atrial fibrillation (AF) is unknown. This thesis describes the development of a fractionation method and label-free quantitative proteomics using guinea-pig atrial tissue lysate (TL), endo-lysosome (EL) and mitochondria (Mito) fractions. Over two thousand proteins were detected, of which 564 were more abundant in EL than TL. The resulting lysates contained atrial, mitochondrial and EL-specific proteins. Significant EL proteins recovered included catalytic activity proteins. Protein enrichment and networks were studied.

The developed fractionation method was applied to goat left atrial AF and sham control samples, including network and pathway analysis. Regulated proteins discovered by proteomics were validated with Western blotting, including Ras-related protein 11 (RAB11). In addition, lysosomal assays (beta-galactosidase and beta-hexosaminidase) were performed. Out of 2104 proteins, levels of 340 proteins in TL, 113 in mito and 148 in EL were significantly altered. EL fractions showed enrichment for EL specific proteins including GAA, clathrin light chain B (CLTB), T-complex protein 1 subunit beta (CCT2), and vacuolar protein-sorting-associated protein 25 (VPS25).

KEGG pathways analysis highlighted mitochondrial oxidative-phosphorylation OXPHOS, and AMPK pathway protein upregulation, indicating a potential increased ATP energy demand in AF samples. Upregulation of protein processing suggests increased vesicular trafficking, potentially related to increased metabolic energy demand. The downregulation of autophago-lysosome fusion proteins such as dynein, dynactin and dynamin indicate a possible disruption in the cellular degradation of macromolecules during chronic AF.

The data presented in this thesis therefore provides evidence to support the role of the lysosome as an important organelle that may play a role in AF pathology.

Statement

The Negative Impact of COVID19

The study conducted here presents the significance of lysosomes in atria under (normal) physiological and (atrial fibrillation) pathological conditions and is a collaborative project with the laboratory of Prof Ulrich Schotten, Maastricht University, Netherlands. The initially planned experimental scale of this project was broad in that it involved the development of a method to identify endo-lysosomal proteins using label-free quantification (LFQ) proteomics. Furthermore, the project aims included the application of the endo-lysosome isolation method on the atrial fibrillation goat model to understand dysregulation of proteins, predict molecular pathways using pathway analysis, application of the regulated protein inhibitors on cell cultures to identify pathology and the application of electron microscopy to quantify structural or morphological changes.

The original experimental plan was to be executed between different departments and facilities. Unfortunately, when the COVID19 pandemic started, I lost a year of my research due to strict, distant working rules set at different departments. After much negotiations with the Target Discovery Institute, Oxford, I was able to apply the method that was developed for guinea pig atrial to atrial fibrillation goat model tissue. Additionally, my supervisor was able to establish a collaboration with a commercial

company to perform transcriptomics. More goat tissue samples had been planned for inclusion in this study but the atrial fibrillation goat model facility in the Netherlands has remained closed as a result of the pandemic and it was therefore unfortunately not possible to obtain more tissue samples to increase n numbers. As a result, the number of samples used in the study are unfortunately a limitation. Additionally, I was supposed to learn and perform electron microscopy imaging and quantitative analysis at the Oxford Brookes University or Sir William Dunn School of pathology, however this was not possible with the distant working rules that were put in place from March 2020.

Despite these challenges, I completed a major part of my research to address the original aims of the project, such as developing the density gradient-based organelle isolation method, applying that method on atrial fibrillation goat model, and molecular pathway interpretations to understand lysosomal protein dysregulations in atrial fibrillation pathology.

Abbreviations

AF	Atrial fibrillation
AMPK	Adenosine mono phosphate – activated protein kinase
BCA	Bicinchoninic acid assay
BLAST	Basic local alignment search tool
cDNA	Complementary DNA
CID	Collision-induced dissociation
COXIV	Cytochrome c oxidase
COPI	Coat protein complex I
COPII	Coat protein complex II
CTSD	Cathepsin D
CV	Conduction velocity
CICR	Calcium-induced calcium release
CAMKII	Calcium-calmodulin-dependent protein kinase 2
CPSF	Cleavage and polyadenylation specificity factor
CStF	Cleavage stimulation factor
CTD	Carboxyl tail domain
DADs	Delayed after-depolarizations
DAG	Directed Acyclic Graph

DCM	Dilated cardiomyopathy
DNA	Deoxyribonucleic acid
ECM	Extra cellular matrix
ER	Endoplasmic reticulum
ERK	Extracellular signal - regulated kinase
ESCRT	Endosomal sorting complexes required for transport
EL	Endo - lysosome
eIFs	Elongation initiation factors
FADH2	Flavin Adenine Dinucleotide
FDR	False - discovery rate
FP	Fibrous pericardium
GAA	Lysosomal-α- glucosidase
GAPDH	Glyceraldehyde 3-phosphate dehydrogenase
GO	Gene Ontology
GYG1	Glycogenin-1
HCN4	Potassium/sodium hyperpolarization-activated cyclic nucleotide - gated channel 4
IVC	Inferior vena cava
I_{K1}	Inward rectifier K+ current
KeGG	Kyoto Encyclopedia of Genes and Genomes
LA	Left atria

LAA Left atrial appendage

LC MS/MS Label-free liquid chromatography with tandem mass spectrometry

LKB1 Liver kinase B 1

LOPIT Localisation of organelle proteins by Isotope-tagging

LSD Lysosomal storage disorders

LV Left ventricle

Lamp2 Lysosome-associated membrane glycoprotein-2

LFQ Label free quantitative

LEB Lysosome enrichment buffer

LIB Lysosome isolation buffer

Mito Mitochondria

MO25 Mouse protein 25

MVBs Multivesicular bodies

mTORC1 mechanistic target of rapamycin complex 1

MA Plot M and A values plot

mRNA messenger RNA

MALDI-ToF Matrix - Assisted Laser Desorption Ionization - Time of Flight

mtDNA mitochondrial DNA

m/z mass to charge ratio

4-MU Fluorophore 4-methylumbelliferone

NAADP	Nicotinic acid adenine dinucleotide phosphate
NADH	Nicotinamide Adenine Dinucleotide - Hydrogen
NADPH	Nicotinamide adenine dinucleotide phosphate oxidase
NCBI/ Ensembl-EBI	National Center for Biotechnology Information/European Molecular - Biology Laboratories European Bioinformatics Institute
NOX2	NADPH oxidase2
NC	Nitrocellulose membrane
NPPA	Natriuretic peptides A
OXPHOS	Oxidative Phosphorylation
PBS	Phosphate buffered saline
PEL	Procedures Establishment License
PIC	Protease inhibitor cocktail
PHI	Phosphatase inhibitor
PRIDE	Proteomics identifications
PTP	Permeability transition pore
PV	Pulmonary Veins
PTM	Post-translational modifications
PKA	Protein kinase A
PVI	Pulmonary vein isolation

PCA Principal Component analysis

RA Right atria

rDNA Ribosomal deoxy ribonucleic acid

RNA Ribonucleic acid

rRNA Ribosomal ribonucleic acid

RPKM Reads Per Kilo base Million

RT-PCR Reverse transcriptase polymerase chain reaction

RV Right ventricle

RP Refractory period

ROS Reactive oxygen species

Rab7a Ras-related protein Rab-7a

RYR2 Ryanodine receptor 2

STRAD STE- related adaptor protein

SDS/PAGE Sodium dodecyl sulphate – polyacrylamide gel electrophoresis

SERCA Sarcoplasmic/endoplasmic reticulum calcium ATPase

SP Serous pericardium

SVC Superior vena cava

SNP Single Nucleotide Polymorphisms

SR Sarcoplasmic reticulum

TAK1 TGF-β-activated kinase 1

tRNA Transfer ribonucleic acid

TPC Two-Pore Channels

TF2E Transcription initiation factor IIE

TL Tissue Lysate

V-ATPase V-type proton ATPase

Table of Contents

Abstract…….....3

Statement…….....5

Abbreviations……..7

Chapter 1……21

Introduction……..21

1.1 Anatomy of the heart..... 21

1.1.1 Pericardium..... 23

1.1.2 Atria, ventricles and the anatomy of the chambers..... 25

1.1.3 Morphology of atria..... 26

1.1.4 Ventricular geometry 28

1.1.5 Role of atria in the process of cardiac filling 31

1.2 Atrial Fibrillation..... 35

1.2.1 History of Atrial fibrillation 38

1.2.2 Principal AF–maintaining mechanisms..... 39

1.2.3 Oxidative stress in cell 45

1.2.4 Animal models of Atrial Fibrillation 48

1.3 Current pharmacological therapies for treating Atrial Fibrillation 49

1.3.1 Cardiac rate control 50

1.3.2. Cardiac rhythm control..... 51

1.3.3 Catheter ablation 53

1.4 Physiological and functional identity of the lysosome 54

1.4.1 Lysosome in cellular autophagy; Intracellular degradation 58

1.4.2 Phagosome formation and phagocytosis 63

1.4.3 Cellular apoptosis related to AF: Potential lysosomal involvement in AF disease condition/progression 65

1.4.4 What are the Two-Pore Channels (TPC)? Why are they important? ... 66

1.5 Genomic and proteomic expression in the cell 69

1.5.1 Gene expression - Transcription in eukaryotes 70

1.5.2 Transcriptomics 73

1.5.3 Protein expression – Translation 75

1.5.4 Proteomics 78

1.5.5 Mass spectrometry 79

1.6 Proteomic application on disease pathology to identify lysosomal protein regulations 82

1.7 Hypothesis and aims 83

Chapter 2 85

A modified density gradient proteomic-based method to analyse endolysosomal proteins in cardiac tissue 85

2.1 Introduction 86

2.2 Experimental model and subject details 92

2.2.1 Method details 93

2.2.2 Quantification and statistical analysis 99

2.2.3 Network analysis 101

2.3 Results 102

2.3.1 Density gradient approach toward acidic organelle isolation from C. porcellus atria 102

2.3.2 Validation of lysosomal proteins using lysosomal enzymes and immunoblotting assays 103

2.3.3 Differential protein distribution using quantitative proteomic analysis 111

2.3.4 Functional networks within endo-lysosomes 112

2.3.5 PANTHER gene annotation pathway analysis 114

2.3.6 Organelle expression profile 116

2.3.7 Pathway analysis of EL, endosome, and lysosomal proteins..... 116

2.4 Discussion 120

2.5 Limitations of the study 127

Chapter 3…… 129

Protein expression in lysosomes and acidic organelles in a goat model of induced atrial fibrillation…….. 129

3.1 Introduction..... 129

3.2 Methods..... 136

3.2.1 Sample preparation..... 136

3.2.2 Liquid chromatography-tandem mass spectrometry analysis 138

3.2.3 Quantification and statistical analysis of mass spectrometry data.. 140

3.2.4 Network analysis 142

3.3 Results 147

3.3.1 Principal Component Analysis (PCA) 147

3.3.2 Violin plot analysis 150

3.3.3 Heat map analysis 154

3.3.4 Pearson co - efficient correlation analysis 159

3.3.5 Point plot analysis 163

3.3.6 Volcano plot analysis 166

3.3.7 Atrial fibrillation protein regulation enrichment comparison to the total human proteome 170

3.3.8 Molecular pathways interpreted in tissue lysate of AF goat model.. 175

3.3.9 Mitochondrial regulations in atrial fibrillation - results highlights ... 207

3.3.10 Lysosome and acidic organelle pathways regulated in atrial fibrillation 221

3.4 Discussion 237

Chapter 4…… 242

mRNA expression in goat atrial fibrillation tissue – A quantitative transcriptomics study…….. 242

4.1 Introduction 242

4.1.1 From Gene regulation to protein expression: How does transcriptomics evaluate proteomics? 244

4.1.2 Brief introduction to the importance of rRNA 246

4.1.3 rRNA and high ATP energy consumption 247

4.1.4 rRNA processing in the cell..... 248

4.1.5. AMPK Activation 250

4.2 Methods..... 250

4.2.1 Sample preparation..... 250

4.2.2 RNA qualification and quantification..... 251

4.2.3 Work flow..... 252

4.2.4 Library preparation for transcriptome sequencing 253

4.2.5 Clustering and sequencing 254

4.3 Data analysis..... 255

4.3.1 Quality control..... 255

4.3.2 Mapping to reference genome 255

4.3.3 Novel gene prediction..... 256

4.3.4 Quantification..... 256

4.3.5 Differential expression analysis..... 256

4.4 Results 257

4.4.1 Principal Component Analysis (PCA) Plot 257

4.4.2 Distance matrix heatmap..... 258

4.4.3 Heat map..... 259

4.4.4 MA plot..... 260

4.5 Transcriptomics observations in goat AF tissue samples 262

4.5.1 Down regulation of the rRNA processing pathway in the nucleolus and cytosol 262

4.5.2 AMPK activation of GLUT4 vesicle translocation to the plasma membrane..... 266

4.5.3 AMPK Activation of macroautophagy 268

4.5.4 AMPK activation of Lipophagy..... 271

4.5.5 The mechanistic Target of Rapamycin (mTOR) antagonism by 4F2 cell-surface antigen heavy chain (SLC3A2) 273

4.6 Discussion 276

Chapter 5……. 279

Quantitative Analysis of lysosomal proteins using biochemical assays 279

5.1 Introduction..... 279

5.2 Methods..... 285

5.2.1 Tissue homogenization 285

5.2.2 Human plasma sample selection 286

5.2.3 Protein quantitation assay for AF and sham goat tissue 287

5.2.4 Protein quantitation assay for human plasma samples 287

5.2.5 SDS/PAGE gel preparation and Western blotting..... 288

5.2.6 Lysosome hydrolase activity assays..... 289

5.2.7 Statistical analysis 290

5.3 Results 290

5.3.1 Cathepsin D expression in goat model - Atrial fibrillation 290

5.3.2 Cathepsin D expression in human plasma - AF patients and healthy donors..... 295

5.3.3 Western blotting evaluation for selected protein regulations observed in atrial fibrillation..... 298

5.3.4 Lysosome hydrolase activity assays..... 303

5.4 Discussion 308

5.5 Limitations to Study..... 312

Chapter 6…… 314

Conclusions…….. 314

6.1 Summary..... 326

6.2 Future directions 328

References…….. 330

Appendix……. 394

Appendix 1..... 394

1.1 Key proteins identified in EL fraction of guinea pig atria..... 394

1.2 Enzyme assay activities from Tissue Lysate, Mitochondrial fraction and Endo-lysosome and remainder fractions..... 401

1.3 GO analysis enrichment for cell component..... 402

1.4 Comparison of proteomic data between human and guinea pig atria 410

Appendix 2..... 411

2.1 Complete figures of proteomic pathway analysis 411

2.2 The Most significantly regulated proteins – Tissue Lysate (TL) fraction 417

2.3 The Most significantly regulated proteins Mitochondrial (Mito) fraction 426

2.4 The Most significantly regulated proteins – Endolysosomal (EL) fraction 429

Appendix 3 434

3.1 The complete pathways of transcriptomic pathway analysis 434

Appendix 4…… 440

Chapter 1

Introduction

1.1 Anatomy of the heart

The mammalian heart is a four-chambered, hollow fibromuscular organ (Bittihn, 2015), with the shape of an irregular cone (Mahadevan, 2014). It is a well-designed circulatory system to provide oxygen, nutrients and circulate cellular waste out of the tissue to maintain the life and biological balance of the system. The human heart is protectively located in the thoracic region between two lungs obliquely in the middle of the mediastinum and posterior to the sternum, costal cartilages and resting on the superior surface of the diaphragm. The whole heart is surrounded by the pericardium (Paul and Iaizzo, 2015) (Figure 1:1 The position of the heart in the thorax).

In addition, the heart is really the driving force for two central vascular circulatory systems, namely the pulmonary and systemic circulations (Figure 1:2). The right atrium (RA), right ventricle (RV), pulmonary arteries, pulmonary capillaries and pulmonary veins complete the pulmonary circulation. The pulmonary circulation circulates deoxygenated blood to the lungs' fine capillaries surrounding the alveoli

and returns the freshly-oxygenated blood to the heart for onward transit to the systemic circulation. The systemic circulation embodies the left atrium (LA), left ventricle (LV), aorta, systemic arteries, systemic capillaries and systemic veins, which conduct the oxygenated blood to the rest of the body (Katz and M, 2010 and Carlson, 2019) (Figure 1:2)).

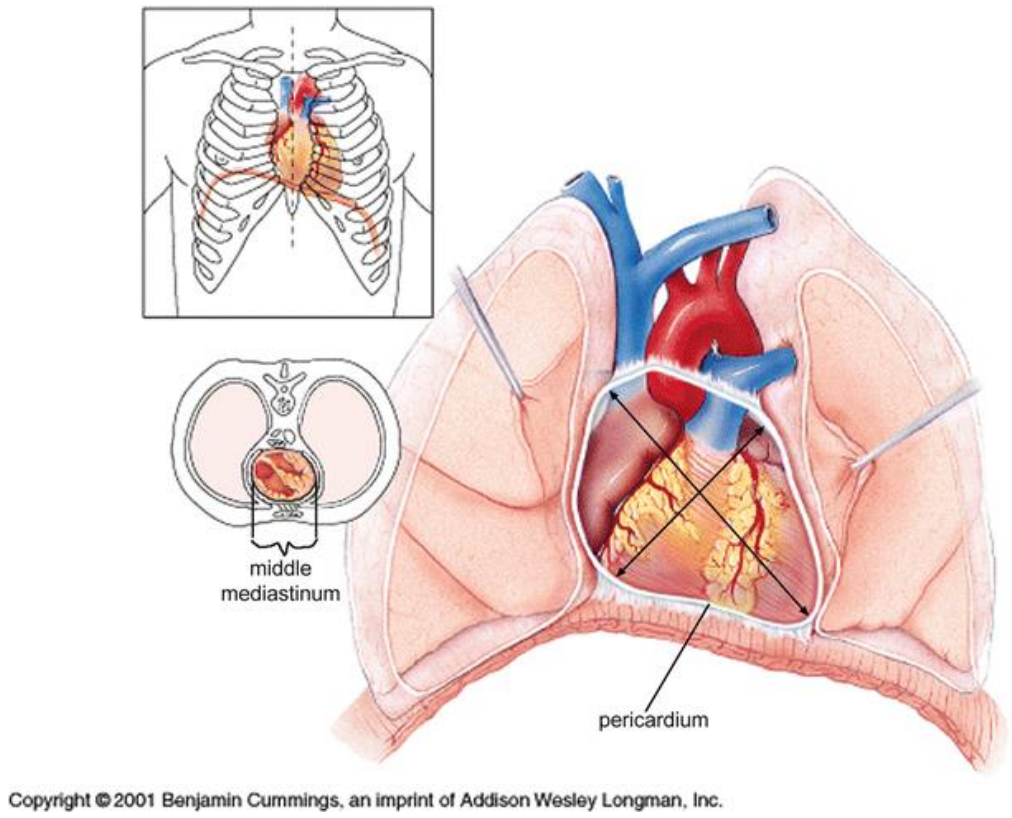

Figure 1:1: Heart's position in the thorax: *The heart is positioned posterior to the sternum and costal cartilages and rests on the superior surface of the diaphragm. Original figure from Benjamin Cummings., (2001), an imprint of Addison Wesley Longman Inc. Figure with permission from (Paul and Iaizzo, 2015).*

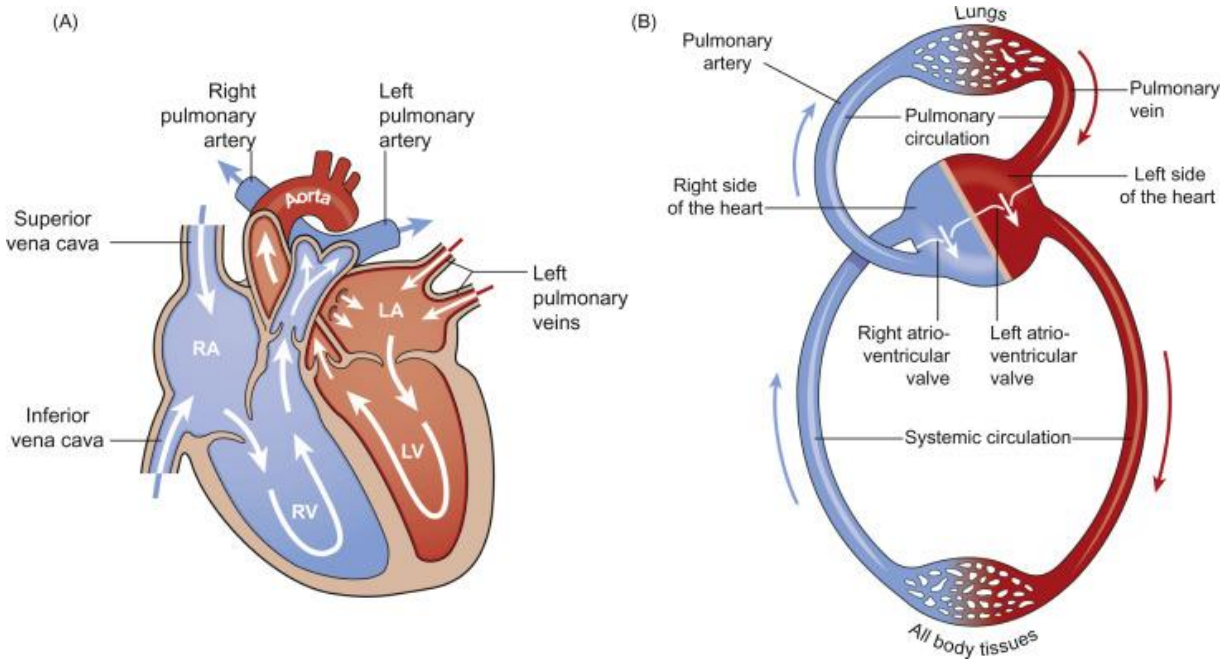

Figure 1:2: Pulmonary and systemic circulation of human heart: (A) Cross section of the cardiac circulation (B) Pulmonary and systemic circulation of blood. *Figure with permission from (Carlson, 2019). Original image from Waugh and Grant (2014).*

1.1.1 Pericardium

The pericardium is a fibrous sack where the heart is enclosed, and comprises three aligned layers (Figure 1:3). These are fibrous pericardium (FP) and serous pericardium (SP) (which consist of parietal and visceral layers separated by the pericardial cavity). FP is a tough, densely fibrous layer merged inferiorly with the central tendinous portion of the diaphragm, adventitia of the aorta, the pulmonary trunk and the superior vena

cava. At the same time, anteriorly, it is attached to the posterior surface of the sternum by sternopericardial ligaments (Whitaker, 2010 and Mahadevan, 2014).

The outer layer of the SP or the parietal layer is firmly applied to the inner surface of FP. The parietal layer is continuous with the epicardium, which covers the surface of the heart. Also, the pericardial cavity is situated between the two layers of the serous pericardium, which contains a thin fluid. This liquid helps the heart to glide through the pericardium without a friction while pulsating.

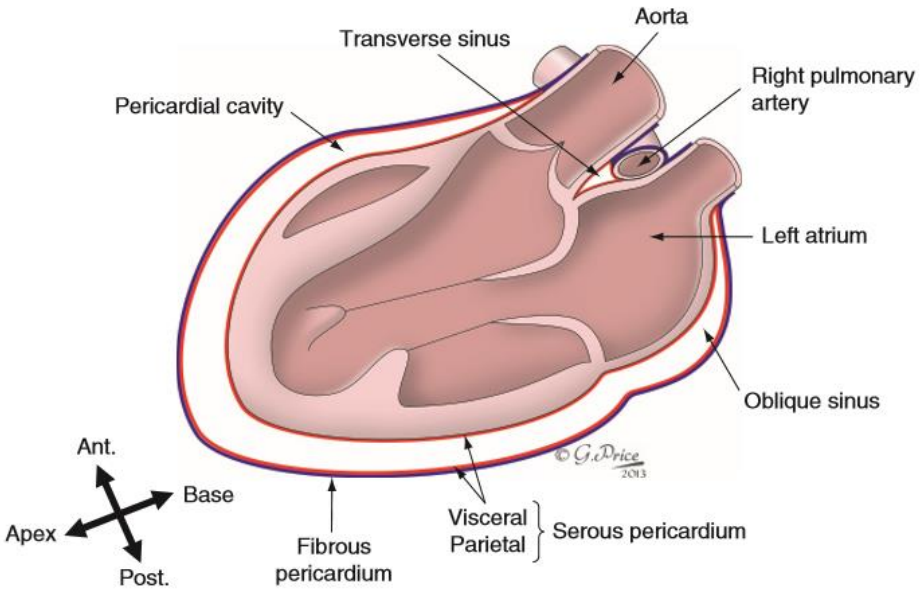

Figure 1:3: An arrangement of the pericardial cavity as seen in a parasternal long axis view
Figure with permission from (Anderson et al., 2013). Original figure created by G. Price.

1.1.2 Atria, ventricles and the anatomy of the chambers

The mammalian heart consists of four chambers (Figure 1:4 Major structural divisions of human heart chambers). The upper two chambers are the left and right atria (LA, RA), and the remaining two, left and right ventricles (LV, RV). In short, the atria collect the blood, contract and act to boost ventricular filling. LA receives blood from pulmonary system while RA receives from the systemic circulation. Whereas ventricles pump the blood out of the heart. The atria are positioned superior to the ventricles and separated by an atrioventricular groove or sulcus base. Ventricles are separated by a groove known as the anterior interventricular sulcus (the visible feature on the surface of the heart), which runs around the apex of the heart; the interventricular septum or the wall between the ventricles is situated internally to the sulci.

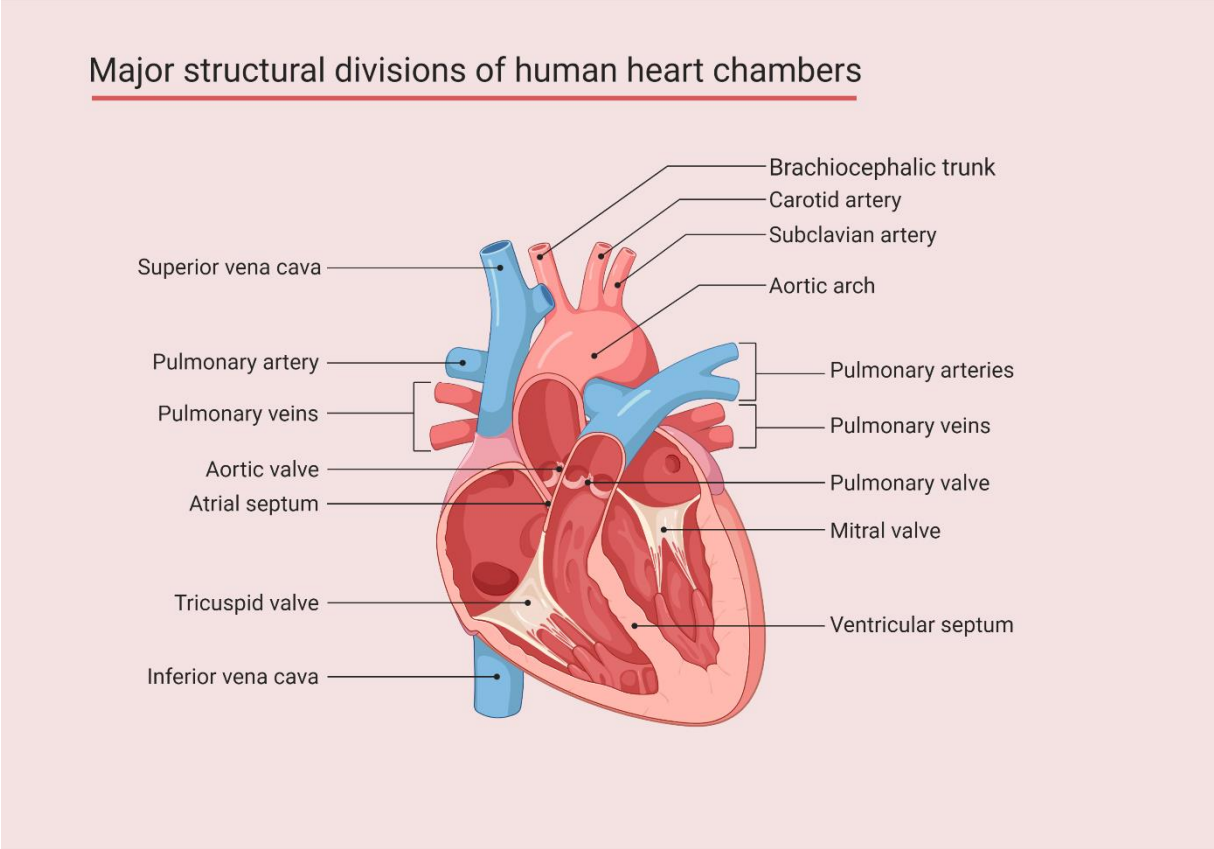

Figure 1:4: Major structural divisions of human heart chambers. *Image created with Biorender.com.*

1.1.3 Morphology of atria

The upper chambers of the mammalian heart consist of right and left atria, and their morphology and location differ according to the functional aspects. The right atrium (Figure 1:5) is an arrangement of the appendage, the vestibule of the tricuspid valve and the venous component, which receives the systemic venous return. The part of the internal right atrial wall and appendage is trabeculated. One prominent identification is

the exterior sulcus terminalis, the exterior groove and the prominent inner vertical ridge, called the crista terminalis. The septum separates both the atria. The left atrium (Figure 1:6) posterior walls consist of pulmonary veins, and the mitral opening. The mitral valve is situated at the inferior part of the left atrium (Wilcox's surgical anatomy of the heart, 4th edition, Whittaker R.H. 2010).

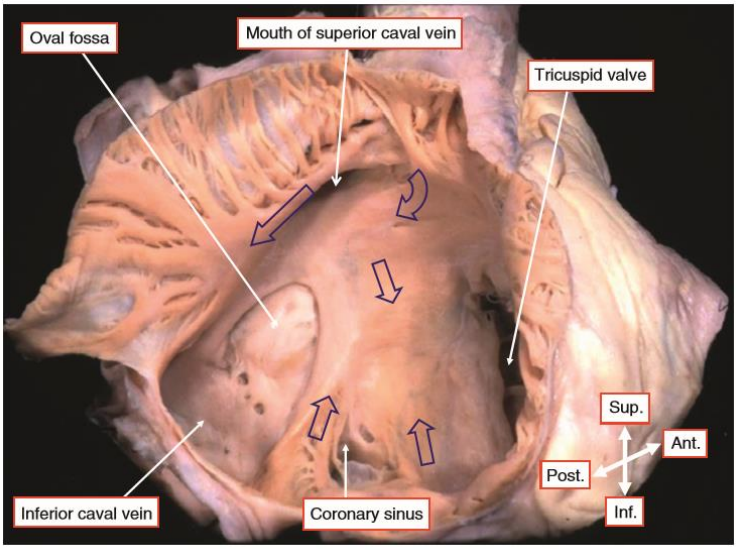

Figure 1:5: The anatomical orientation of right atrium. *Surgically opened right atrial appendage shows the interior muscle walls with conduction routes. (Arrows). Figure with permission from (Anderson et al., 2013).*

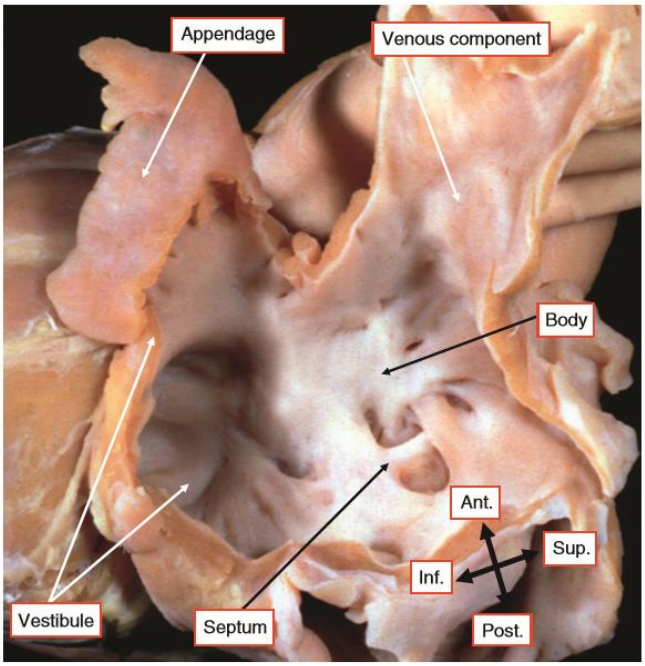

Figure 1:6: Left atrium in anatomical orientation showing surgically opened interior with the conduction sections. *Figure with permission from (Anderson et al., 2013)*

1.1.4 Ventricular geometry

The ventricles are described as three-dimensional thick-walled pressure vessels that have notable variations in the curvature and the thickness of the wall both regionally and temporally through the cardiac cycle (Vetter and Mcculloch, 1998).

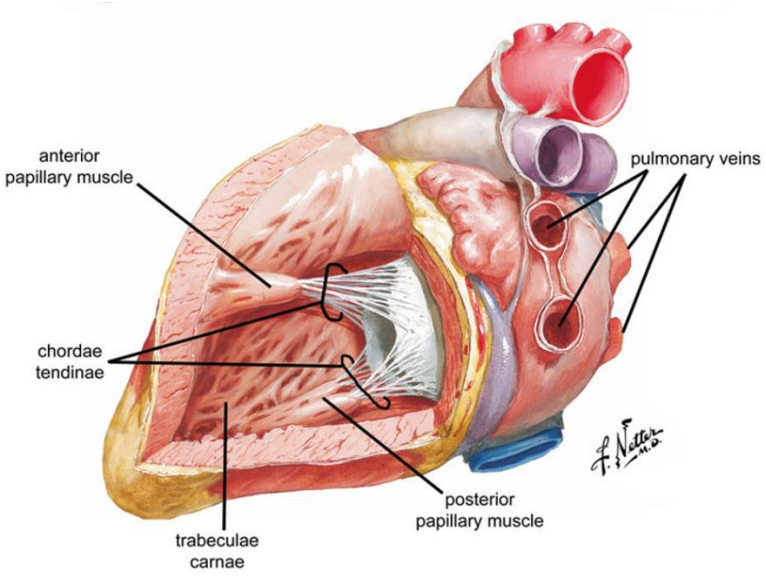

Figure 1:7: Internal anatomy of the left ventricle: *Left lateral area is mainly composed in to the left ventricle. Trabeculae carnae completes the inner surface of the ventricles. The interventricular septum separates right from left ventricle, Image Figure with permission from (Paul and Iaizzo, 2015); original image created by Frank H. Netter, www.netterimages.com.*

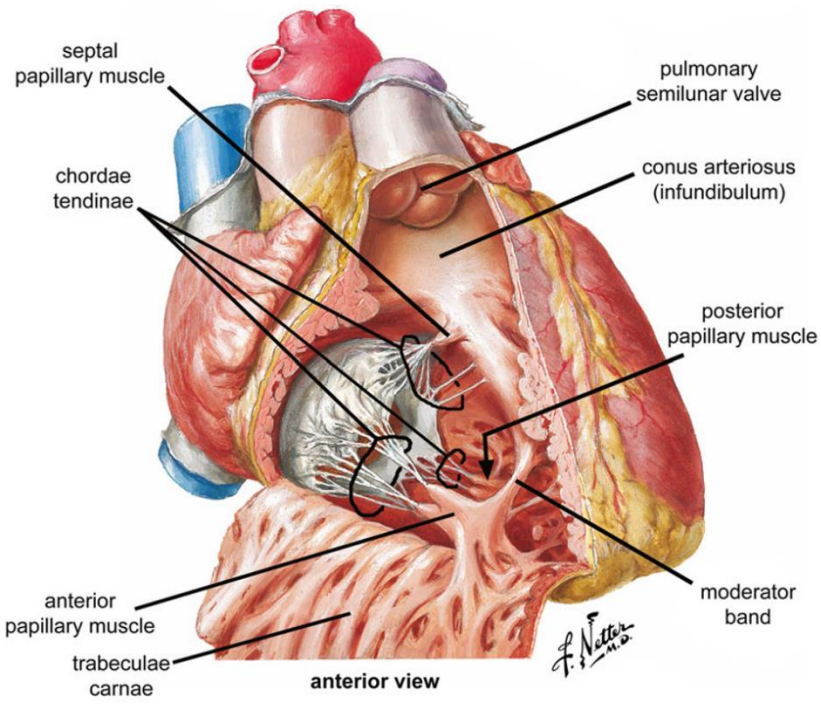

Figure 1:8: Internal anatomy of the right ventricle; *Trabeculae carnae is spread though out the inner right ventricle, and the septal papillary and posterior papillary muscles are attached to the chordae tendinae, and the pulmonary semilunar valve opens up to the conus arteriosus. Figure with permission from (Paul and Iaizzo, 2015); Original image created by Frank H. Netter, www.netterimages.com.*

In terms of the ventricular morphology, the containment has three components: inlet, apical trabecular and outlet parts. The inlet of the left ventricle (Figure 1:7) surrounds by the mitral valve and the tension apparatus. Furthermore, two distinguished papillary muscles and tendon chords support the two leaflets, an anterosuperior or aortic leaflet and a posteroinferior or mural leaflet. The aortic leaflet is in fibrous continuity with the aortic valve and is morphologically square shaped. The mural leaflet is supported by the parietal part of the left atrioventricular junction with a substantial junctional attachment and morphologically narrower than the aortic leaflet. The right ventricle contains (Figure 1:8) the tricuspid valve and its tension apparatus in the inlet section.

The valvar orifice contains the three leaflets structure lying in the anterosuperior, septal and inferior mural positions (Anderson *et al.*, 2013).

1.1.5 Role of atria in the process of cardiac filling

The cardiac conduction system consists of the following components: The pacemaker SA node located in the right atria at the base of the superior vena cava, which initiates electrical impulses throughout the right and left atria, causing them to contract. The AV node, located at the posterior of the annulus fibrosus, functions as an intermediate gateway providing an electrical connection between atria and ventricles, and delays the electrical impulses passing to the ventricles, providing time for ventricular filling. The AV node conducts the electrical impulse to the Bundle of His which then divides to the left and right bundle branches, extending further to the ventricles through Purkinje fibers (Katz and M.,2010). During the atrial contraction, the pressure ejects the blood to the ventricles through the tricuspid and mitral valves and the delayed action potential propagation through the AV node provides sufficient time for complete ventricular filling and atrial relaxation. The ventricular contraction increases the pressure in the ventricles that ejects the blood via pulmonary arteries and aorta (Farrell, 2011 and Athanasiou *et al*., 2017).

During AF, the electrical impulses can be initiated from sites in the atria other than the SA node, namely, ectopic sites such as at the pulmonary veins muscle sheath base, which will be discussed in detail under section 1.2.2. These unsynchronised electrical signals lead the whole atrium to fibrillate or quiver. The rapid impulses conducted by the ectopic foci eventually cancel the normal electrical impulses generated at the SA node. However, the refractory properties of the AV node cells function to minimise most of the unsynchronised electrical impulses. When the AV node receives irregular electrical impulses, this can lead to an irregularly- irregular ventricular rate.

Moreover, the reentry circuits (discussed in detail under section 1.2.2.2) of the atrial myocardium with various conductivity and electrical impulses, leaves some areas of the atrium to conduct slowly. For example, a slow conducting myocardium has a shorter refractory period causing rest and re-excitation faster than a normal myocardium in sinus rhythm. This electrical remodelling leads to faster and incomplete atrial filling during diastole and incomplete pumping of atrial blood to the ventricles during systole, leaving some volume of blood left in the atria, which can increase the risk of blood clot formation (Iwasaki *et al*., 2011). The cardiac conduction of a normal heart and an AF heart can be distinguished through an electrocardiogram (ECG) (Figure 1.9 and 1.10).

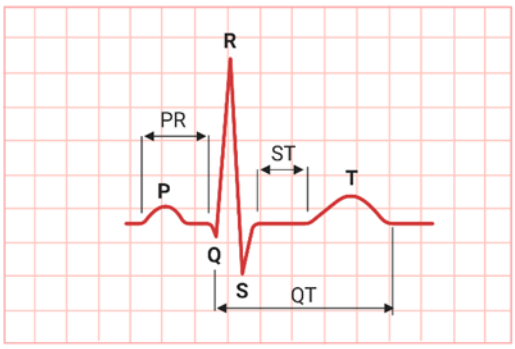

Figure 1.9: An illustration of a normal Electrocardiogram. *Image created with Biorender.com.*

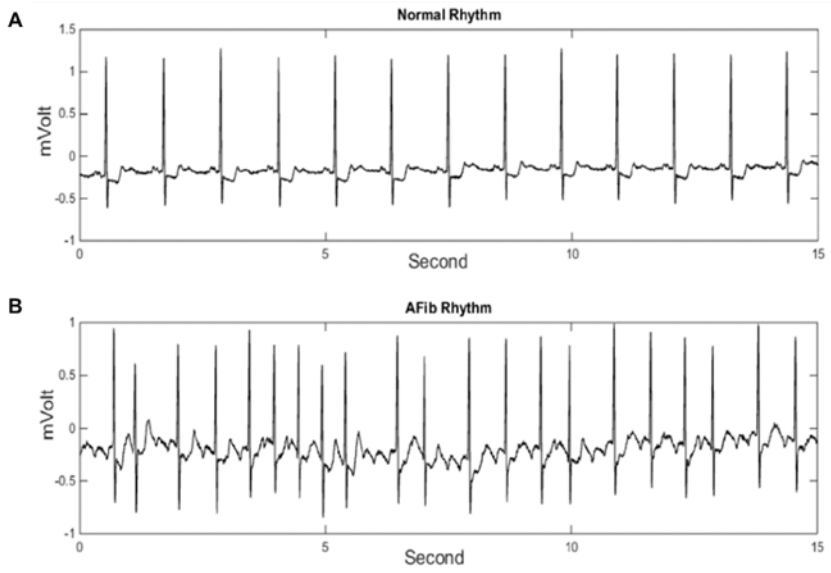

Figure 1.10: An ECG of a (A) normal sinus rhythm and (B) atrial fibrillation. *Figure with permission from (Taji et al., 2018).*

An ECG of a healthy individual consists of the following components, namely: P wave, QRS complex, and T wave (Figure 1.9). The P wave represents the depolarisation of

the atria. In contrast, the QRS complex represents the ventricular depolarisation, and importantly atrial repolarisation is within the QRS complex, but generally the atrial tissue repolarises in a less uniformed manner than ventricles, therefore the atrial repolarisation signal is much weaker to detect by the ECG. The T wave represents the ventricular repolarisation.

Furthermore, an ECG consists of intervals and segments (Figure 1.9), namely, PR interval with a normal duration range between 0.12 – 0.2 seconds (s) (Goldberger *et al*., 2018), which represents the electrical conduction from SA node to ventricles through AV node, and the QRS complex which typically lasts less than 0.12s (Katz and M.,2010).

The QRS complex represents the depolarisation of the ventricular septum, with an amplitude of less than 0.2mV, which lasts less than 0.03s (Surawicz & Knilans, 2008). At a constant heart rate, the distance between two R waves is equal from one electrical conduction to another, and the R and S wave amplitudes remain not less than 0.5mV in at one limb lead or 1mV in at least one precordial lead in general. The ST segment is the electrically neutral phase between the ventricular depolarisation and repolarisation. In a healthy individual, the baseline of the ST segment is around 0.10 mV, whereas, for females, the upper limit values are between 0.10 mV and 0.15 mV, and for males, it is between 0.30 mV and 0.35 mV (AH kashou *et al*., 2022). The QT interval is measured from the start of the QRS complex to the end of the T wave and

depends on the heart rate; therefore, an average healthy male has a QT corrected (QTc) value less than 450 ms and a healthy average female has a QTc value of 460 ms (Johnson & Ackerman, 2009).

An ECG of an AF patient has distinct features (Figure 1.10B), such as the absence of the P wave due to the interruption caused by the uncoordinated depolarisations of atrial myocytes. The iso-electric baseline of the ECG consists of irregular risings or the presence of the fibrillatory (f) waves caused by the multiple ectopic sites. The QRS complexes of AF are narrower and irregular, which lasts less than 120ms unless the presence of a bundle branch block; therefore, the distance between two R waves varies between the electrical conductions, typically ranging the clinical ventricular rate between 65 - 158 bpm (Husser *et al*., 2007).

1.2 Atrial Fibrillation

Atrial fibrillation (AF), in which the heart's upper chambers no longer contract in a coordinated fashion, is estimated to affect 2-4% of over 60s and more than 15% of the population over the age of 75 (www.nhlbi.nih.gov). AF is a significant cause of morbidity and mortality (Ruigómez *et al.*, 2002), for which pharmacologic approaches for rate or rhythm control remain suboptimal, primarily because of the lack of detailed mechanistic insights into the development and progress of this disease. The onset and the

progression of AF are highly complex. Atherothrombosis and thromboembolism (Spronk *et al.*, 2018), stress-related autophagy (Rinné *et al.*, 2017), cellular apoptosis (Papp *et al.*, 2012), atrial fibrosis (Nattel, 2017), atrial remodelling (De Souza *et al.*, 2010), microRNA (Shi *et al.*, 2013) and Single Nucleotide Polymorphisms (SNP) (Abunimer *et al.*, 2014), are among some of the identified causes for AF initiation or progression. Therefore, it is expected that the multifactorial nature of AF differentially regulates various structural and functional proteins (Ariyaratnam *et al.*, 2020) and (Thomas *et al.*, 2019) . Eventually, these protein irregularities prevail upon phenotypical expressions and underlying physiological failure in the heart.

Unravelling the onset and maintenance of AF could be aided by detangling the multifactorial nature of the disease progression where several factors expand from geometry, a person's age (www.cdc.gov), electrical state of the heart (Wasmer *et al.*, 2017) to anisotropic orientation for cell shape and size, excitability, myocardial fibrosis, gap junction distribution and function (Kotadia *et al.*, 2020). Cellular organelles of an arrhythmic heart are functionally, impaired (Xiao, 2011) bearing irregularities of metabolism networks (Adam *et al.*, 1993), protein-protein interactions and ion regulation leading to compromised electrical conduction. The functional and structural involvement of the Sarcoplasmic reticulum (SR) in calcium-induced calcium release (CICR) in cardiac arrhythmias has been extensively studied, yet the involvement of intracellular acidic organelles such as lysosomes and endosomes in diseased arrhythmic conditions such as AF is largely unknown.

Nearly two decades ago, a group of scientists from Oxford published key data showing that NAADP mobilises Ca^{2+} release from acidic stores of the cell (Churchill *et al.*, 2002). The initial studies of inducing exocytosis of cortical granules in the sea urchin eggs by microinjection of IP3 resulted in forming a fertilisation envelope to barricade polyspermy (David *et al.*, 1988 and Whitaker, 2006). Lysosomal involvement in Ca^{2+} release during egg fertilisation was discovered by a research team led by Antony Galione and Grant Churchill in the department of Pharmacology, Oxford (Churchill *et al.*, 2002). They provided the biochemical and pharmacological evidence that these reserve granules are Ca^{2+} stores, and these Ca^{2+} stores are lysosome-related acidic organelles that mobilised Ca^{2+} by NAADP in sea urchin eggs.

Lysosomal calcium signalling is a little-studied pathway in the heart which has been implicated in the adrenergic responses of both atrial (Collins *et al.*, 2011) and ventricular (Macgregor *et al.*, 2007) myocytes. Published work has suggested that inhibition of the lysosomal Ca^{2+} release pathway is protective against adrenergically-induced arrhythmias (Nebel *et al.*, 2013). Recent work in the department has shown that mice lacking the lysosomal Ca^{2+} release protein two pore channel 2 (TPC2) are protected from ventricular hypertrophy and arrhythmias (Capel *et al.*, 2015). Further, the pathway has been shown to require calcium-calmodulin-dependent protein kinase 2 (CAMKII) to function in its full amplification role (Mattiazzi and Kranias, 2011; Capel *et al.*, 2015). Deranged CaMKII signalling, over-expression and over-activity are a hallmark of atrial remodelling (Heijman *et al.*, 2014). An understanding of arrhythmogenesis depends on understanding a multitude of modulatory pathways

such, as the lysosomal Ca^{2+} release mechanism (Figure 1:11) and the measurement of complex activation patterns on a global scale.

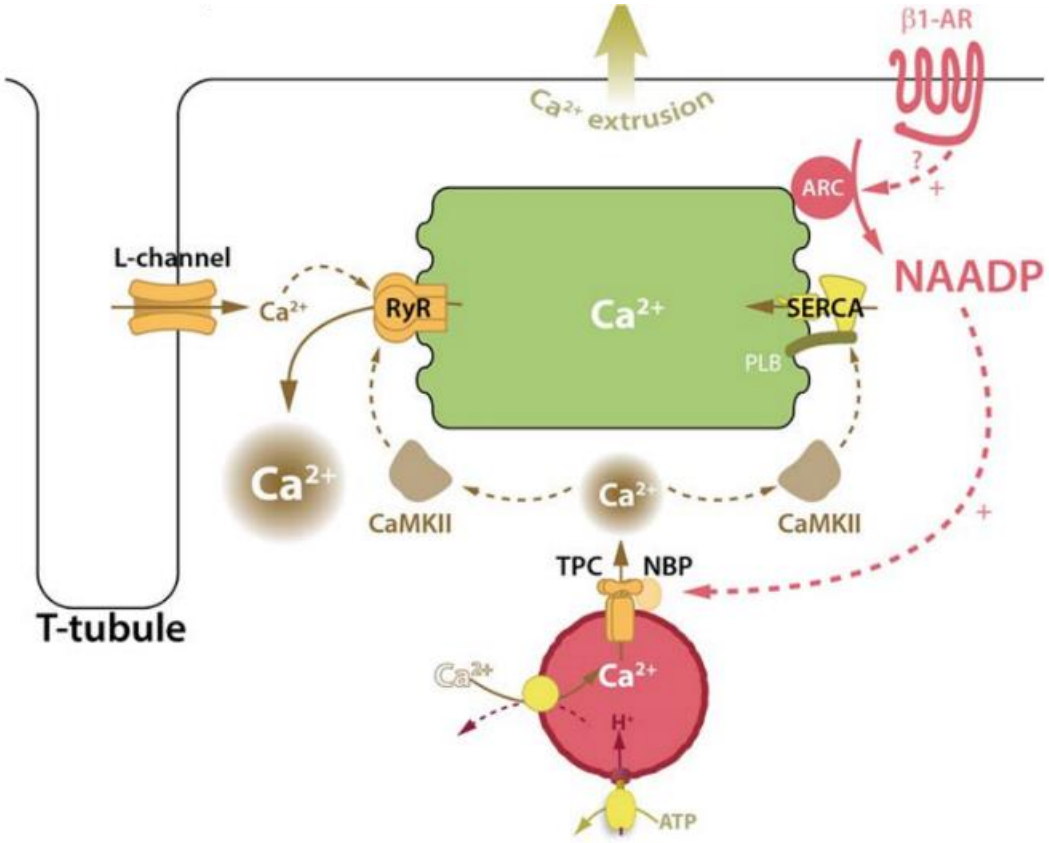

Figure 1:11: Proposed scheme for actions of NAADP in cardiac myocytes via activation of β-adrenoceptors. Figure with permission from (Capel et al., 2015).

1.2.1 History of Atrial fibrillation

Physicians first recognized AF in the late 1800s. It was named ‘Pulsus irregularis perpetuus’, ‘Rebellious palpitations’ or ‘Delirium cordis’ (Silverman et al 1994). In 1908 Hertz and Goodhart outlined atrial flutter and named by Jolly and Ritchie in 1911. In

1909 Lewis, Rothberger and Winterberg established using electrography that the origin of ‘Pulsus irregularis perpetuus’ is Auricular fibrillation (Silverman et al 1994). They are the first scientists who recognized the difference between the atrial flutter and fibrillation as the former represented a saw tooth configuration (equilateral triangle) in leads II and III (Friedrichs G *et al* 2000).

1.2.2 Principal AF–maintaining mechanisms

The mechanisms that trigger and re-entry to maintain the AF condition are of two types and they are the, rapid ectopic firing and reentries. The time and type of reentry exposure related to the clinical relationship to the type of AF, namely paroxysmal, persistent and permanent (Figure 1:12) (Iwasaki *et al.*, 2011).

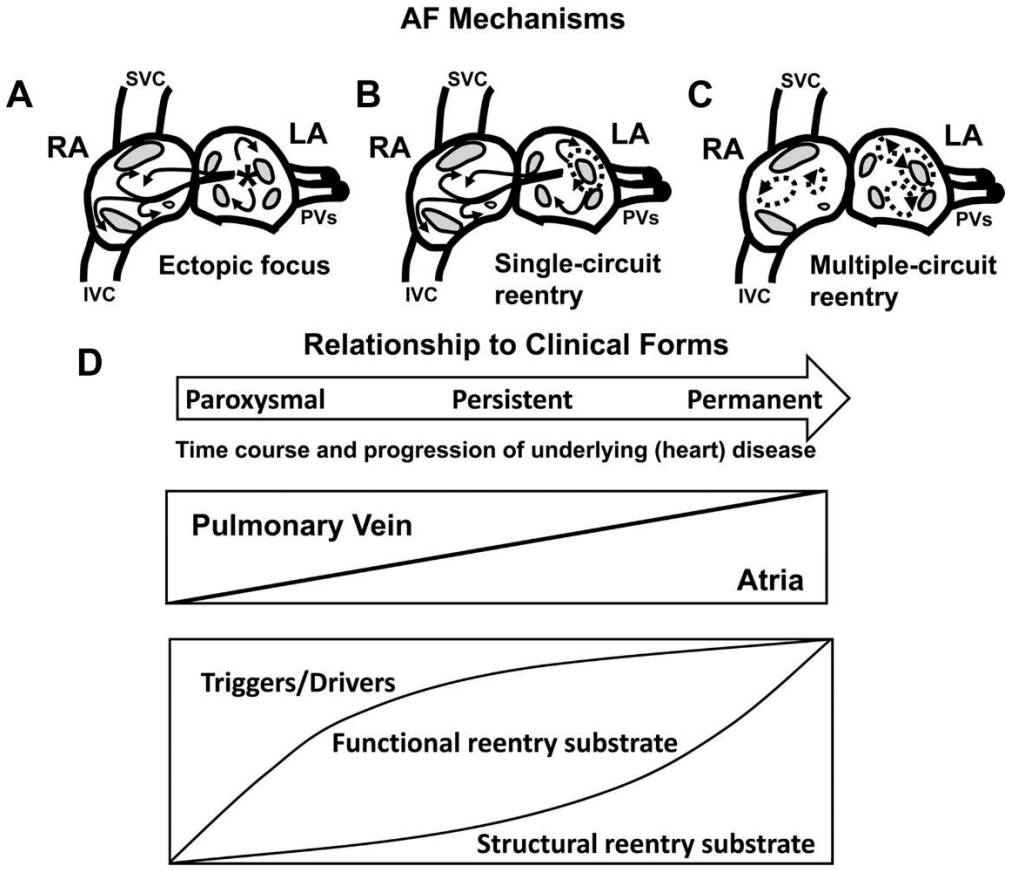

Figure 1:12: The main AF- maintaining mechanisms. *A. Ectopic focus firing, B. Single circuit re-entry. C. Multiple circuit re-entry. D. Clinically declared forms and their relation to mechanisms. The local triggers of AF are the predominance in paroxysmal AF, mainly from PV. Persistent to permanent AF progress with time and the initiation of functional and structural re-entry substrates predominate. (RA= right atria, LA=left atria, SVC= superior vena cava, IVC= inferior vena cava, PV= Pulmonary Veins; Figure with permission from (Iwasaki et al., 2011).*

1.2.2.1 Ectopic Firing

PV has a unique composition of transitional, pacemaker and purkinje cells that can provide a complex electrical conduction properties (Perez-Lugones *et al.*, 2003). During AF the abnormal electrical firing that generate locally from the PV area is

identified as ectopic firing, and this phenomenon was firstly identified by Haïssaguerre and team in 1998 (Haïssaguerre *et al.*, 1998).

After repolarization from a normal atrial cell action potential the cell remains at the resting potential (−65 to −80 mV). The high resting K^+ permeability through the inward rectifier K^+ current (I_{K1}), maintains the resting potential, and its regulated by (I_{K1}). Even though, HCN4 mRNA has been detected in human atrial samples from patients in sinus rhythm atrial cell (Stillitano *et al.*, 2008) the larger I_{K1} overwhelms the atrial cell and fails to manifest automaticity.

Therefore, the changes caused by balancing the decreased I_{K1} or enhanced I_f enhance the automaticity. During abnormal repolarization phases, abnormal secondary membrane depolarizations are involved by the early after-depolarizations. Action potential duration (APD) prolongation is the driver of early after-depolarization, which allows the recovery from L_{CaL} inactivation whilst the cell is still in a depolarised state. Therefore, the inward movement of the Ca^{2+} ions leads to a second excitation, In conditions such as congenital long QT syndrome the increased prevalence of AF is caused by these atrial APD prolongation led early afterdepolarizations (Johnson *et al.*, 2008).

The abnormal diastolic release of Ca^{2+} from SR causes the delayed after-depolarizations (DADs). In general, RYR receptors are closed during diastole but in the event of dysfunctional RYR receptors or if the SR is Ca^{2+} overloaded, the RYR may be opened in this phase remain open. During this time, the released Ca^{2+} ions are exchanged through the Na+ Ca^{2+} exchanger to 3 Na+ ions, and lead to a total depolarizing inward (+) ion movement, if large enough, this can trigger a full depolarization the DAD. One such example is congestive heart failure (Yeh *et al.*, 2008 and Pizzale *et al.*, 2008).

1.2.2.2 Re-entry

AF maintenance by re-entry can be of two types, either by a rapidly firing driver (Figure1:12A) or by irregular multiple re-entry circuits (Figure 1:12B), and there are two concepts of re-entry, either a spiral wave model or a leading circle model (Comtois *et al.*, 2005). The propensity for re-entrant activity to be maintained depends on the atrial substrate properties. Out of the two re-entry models, the leading circle model, re-entry circuits are spontaneously established in a length of a circuit or a wave length defined by the distance impulse can move in one refractory period (RP). Whereas the reduced RPs promote a circular re-entry model by stabilizing the spiral waves (Comtois *et al.*, 2005 and Allessie *et al.*, 2001) . AF re-entry circuits can increase by shorter wavelengths, therefore increased wavelengths reduce the amount of re-entry circuits.

Also, reduced conduction velocity (CV) and shortened RP can induce the AF re-entry cycles (Iwasaki *et al.*, 2011).

1.2.2.3 Atrial fibrillation trigger and substrate

The susceptibility to the development of AF depends on the multi environmental variables with the genetic predisposition. It is vital to understand the two key concepts that interact with the AF's initiation and interaction: Trigger and the substrate (Wijesurendra R and Casadei B, 2019). 'Trigger' is the rapid initiation focus for the arrhythmia such as ectopic beats which generate by atrial, great venous tissues (Chen *et al.*, 1999) or pulmonary veins initiating frequent paroxysms of AF (Haïssaguerre M. et. al.,1998), and the electrophysiological, mechanical and structural characteristics of the atria that maintain the arrhythmic condition (Figure 1.12) is the 'substrate'. The major site of triggers for AF is great venous tissues or pulmonary veins, initiating frequent paroxysms of AF (Chen *et al.*, 1999), although a range of sites have been recorded (Haïssaguerre M. et. al.,1998). As discussed above, AF promotes the initiation and sustaining of the AF by inducing specific tissue properties in the atria. The electrical induction of AF promotes sustaining of AF through decreased action potential duration. This phenomenon occurs via I_{CaL}, I_{to}, I_K, reduction, which shorten the action potential, and this electrophysiological alteration leads to the phenomenon called AF begets AF (Wijffels *et al.*, 1995).

The establishment of the substrate comprises a series of electrical and anatomical remodelling in the atria. Unlike familial AF, the substrate establishment observed in non-familial AF may be a result of multifactorial genetic disposition and the mean value of the fibrosis development in persistent AF is higher than paroxysmal AF (Figure 1:13 and 1:14). However, there is a vast variability observed among AF patients (Boldt A. et al).

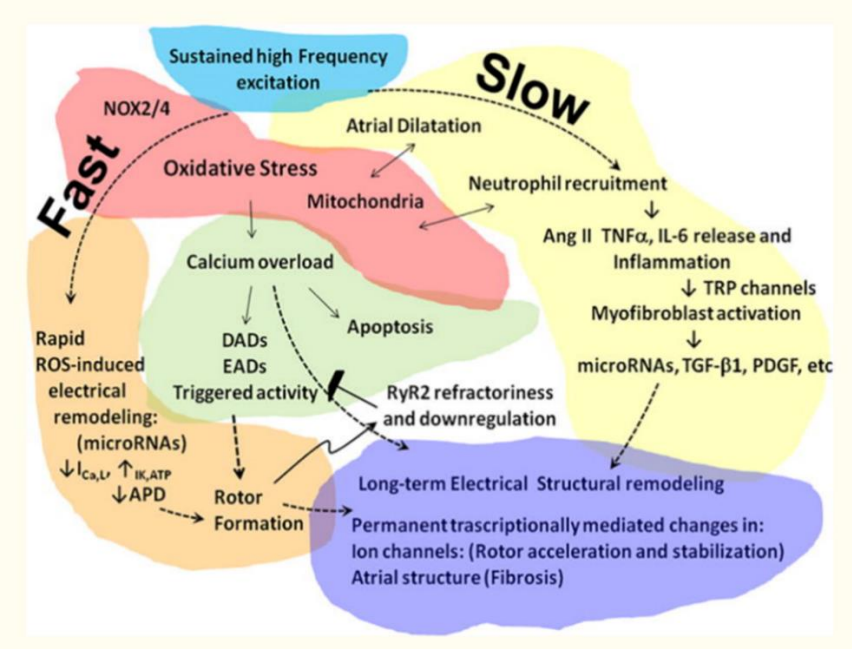

Figure 1:13: The long term pathophysiological events leading to atrial remodelling: *These events include calcium overload, mitochondrial oxidative stress, ROS induced electrical remodelling, apoptosis, atrial dilation, likely leading to long term structural and electrical remodelling. Figure with permission from (Jalife and Kaur, 2015).*

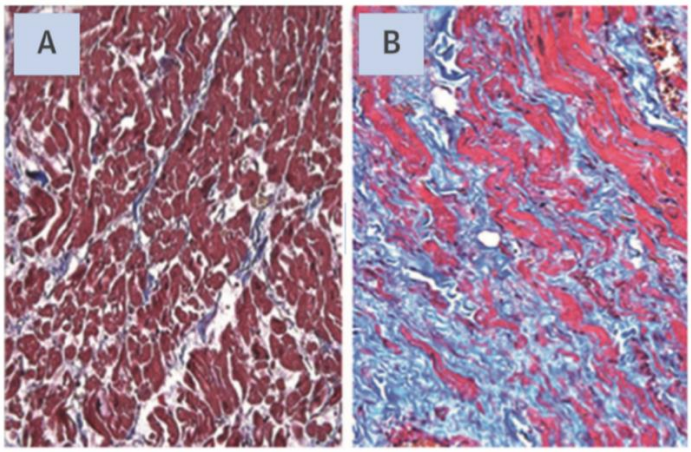

Figure 1:14: Light microscopy observation of Crista Terminalis showing AF-induced remodelling: *substrate for AF perpetuation: (A) Tissue from a patient with sinus rhythm and without a history of AF and (B) Patient with persistent AF showing high level of fibrosis. Figure with permission from (Kottkamp et al., 2015).*

1.2.3 Oxidative stress in cell

Oxidative stress in a cell is described as the imbalance between the cellular production of reactive oxygen species and the antioxidant defence system (Betteridge, 2000). In the atria, oxidative stress induces the endoplasmic reticulum (ER) stress levels, which can activate apoptosis (Long *et al.*, 2017). Oxidative stress, and irregular intracellular Ca^{2+} release via ryanodine receptor 2 (RyR2) promote AF, and RyR2 is oxidized in the chronic AF patients' compared with individuals in sinus rhythm (Xie *et al.*, 2015).

In AF and most cardiac disorders, the balance between protein synthesis, folding, and degradation or proteostasis is impaired (Sabath *et al.*, 2020 and Arrieta *et al.*, 2019).

Free radicals in the atria are formed by the products of many biochemical processes, especially the mitochondrial electron transport chain. Additionally, inflammation factors induced by activated neutrophils cause production of free radicals through the NADPH oxidase pathway. A free radical is an atom containing one or more unpaired electrons in the outer orbit of its atom, therefore capable of independent existence (Phaniendra *et al.*, 2015). The odd number of electrons in an atom of a free radical makes it unstable, hence highly reactive. The increased reactivity can obtain electrons from other molecules to retain stability (Table1:1 presents an array of free radicals formed under oxidative stress). Thus, the attacked molecule loses its electron and becomes a free radical itself or lose its functionality as a cell component, such as proteins, lipids or nucleic acids (Marnett, 2000) ; (Ylä-Herttuala, 1999) ; (Stadtman and Levine, 2000). Hence, free radicals can activate a cascade of chemical reactions, finally breaking down cellular senescence.

Free radical	Symbol	Half-life
Reactive oxygen species-ROS		
Radicals		
Superoxide	$O_2^{\bullet-}$	10^{-6} s
Hydroxyl	$OH^{\bullet}$	10^{-10} s
Alkoxyl radical	$RO^{\bullet}$	10^{-6}
Peroxyl Radical	$ROO^{\bullet}$	17 s
Non radicals		
Hydrogen peroxide	H_2O_2	Stable
Singlet oxygen	$^1O_2$	10^{-6} s
Ozone	O_3	s
Organic peroxide	ROOH	Stable

Table 1:1: Display some common free radicals present or produced in the cell, with their biological symbol and half-life in seconds*. Table with permission from (Phaniendra et al., 2015).*

However, reactive oxygen species (ROS) has been reported cardio protective (Cadenas, 2018), and the study conducted by Simon J. et al., 2021, reported that the disulphide modifications caused during the oxidation of protein kinase A (PKA). Regulatory Subunit PKARIα inhibits lysosome triggered Ca^{2+} release and protects against myocardial ischemia-reperfusion injury, therefore can be a novel target designing of cardio-protective therapeutics (Simon *et al.*, 2021). Furthermore, H_2O_2 selectively oxidize some targeted proteins, leading to conformational changes and activate signal transducers, for instance kinases, phosphatases and ion transporters (Cadenas, 2018).

1.2.4 Animal models of Atrial Fibrillation

In the early days, scientists realized that the deep understanding of the electrophysiological mechanisms in the heart could benefit the discovery of therapeutic strategies to improve patients' health. Therefore, they caused mechanical injuries and used artificial stimulation techniques on the atria to simulate clinical phenotypes that they observed in patients.

The artificial cardiac arrhythmia induction by programmed electrical stimulation concept was first discovered in 1967 (Durrer *et al.*, 1967). Over the years, AF has compelled scientists to thrive understanding the pathology; therefore, creating animal models that mimic the appropriate disease condition was vital to understand the underlying pathophysiological mechanisms. In 1997 Nattel et al. declared the necessary characteristics of an arrhythmic atrial model, namely (1) Relevance to the clinically observed arrhythmia to comprise the structural and functional abnormalities, (2) AF should be inducible and capable of being maintained chronically to ensure that it can be terminated by putative intervention and does not occur spontaneously, (3) Possibility to restore and maintain normal sinus rhythm. Several models of AF exist, including mouse (Ozcan *et al.*, 2015 and Wakimoto *et al.*, 2001), rabbit (Zhao *et al.*,

2013), pig (Clauss *et al.*, 2020), canine (Zhou *et al.*, 2002) and goat (Wijffels *et al.*, 1995 and van Hunnik *et al.*, 2018). The AF induction in goat is maintained by burst pacing for three weeks for short term AF, and for the long term, AF burst pacing carried for six months (Maesen *et al.*, 2013 and Verheule *et al.*, 2013).

1.3 Current pharmacological therapies for treating Atrial Fibrillation

Anti-arrhythmic drugs are used to either impair the transmission of impulses in tissues or suppress the abnormal pacemaker firing that rapidly conduct (www.heart.org). These are prescribed either as long-term oral consumption drugs or intravenous injections for emergency use. Long-term management of AF involves effectively managing symptoms with either rate or rhythm control strategies and prevent thromboembolism. To prevent embolic stroke caused by non-valvular AF, anticoagulant agents such as Dabigatran, Rivaroxaban, Apixaban, and Edoxaban are prevalent among the patients even though they exhibit some side effects of gastrointestinal bleeding (Cheung and Leung, 2017).

Oral anticoagulants are considered the more successful treatment for AF (Hart *et al.*, 2007 and Adam *et al.*, 2012). According to the NICE recommendation, the most

updated recommended anticoagulants are, rivaroxaban, apixaban, dabigatran, and edoxaban (www.nice.org.uk). Compared to AF patients not on anticoagulation, anticoagulation treated AF patients were reported to have a lower risk of death (Arbel *et al.*, 2019 and Hylek *et al.*, 2003). However, depending on the agent, anticoagulants have several disadvantages, for instance, dietary restriction, unpredictable nature of the pharmacokinetics and the risk of renal and hepatic diseases.

1.3.1 Cardiac rate control

Cardiac rate control is effective even for AF patients with rhythm control requirements. Some of the rate control treatments are calcium-channel blockers and β- blockers the latter of which may also be used with a combination with digoxin or calcium-channel blockers (Van Gelder *et al.*, 2016). The cardiac rate control is better than rhythm control because controlled heart rates are important during relapses of AF and suitable treatment for acute AF patients having acute recurrences. Moreover, it is ideal for AF patients over 80 years of age with minor symptoms (Wyse *et al.*, 2002 and January *et al.*, 2014), and rate control remains the only treatment once the rhythm control or ablation fails.

As evidenced by the literature, the current therapies are sub-optimal. Therefore, it is vital to explore molecular mechanisms to identify drug targets or biomarkers to promote

earlier diagnosis and more effective treatments. Lysosomes and endo-lysosomes in AF pathology are ideal organelles to study such targets as lysosomes play a central role in cellular homeostasis, and biomolecules are trafficked to the lysosome for degradation. Therefore, understanding the protein dysregulations in the AF pathology would provide researchers to develop novel drug targets and markers. The scope of this study is to use an AF goat model and identify the dysregulated proteins of lysosomes and proteins that target lysosomes in AF.

1.3.2. Cardiac rhythm control

Cardiac rhythm control is the cardioversion or acute restoration and maintenance of the sinus rhythm in AF patients. The irregular cardiac rhythm can lead to haemodynamic impairment, and protection against thromboembolism is vital as it leads to systemic embolism and stroke. The conductance of the rhythm control is based on the patient's symptoms such as comorbidity, general health issues, age, anticoagulation status and the types of AF such as paroxysmal, persistent, long-standing persistent, permanent and nonvalvular. The pharmacology recommendation in the antiarrhythmic drug therapy for AF patients depends on their renal function, the existence of the structural cardiac disorders, electro-cardiographical information and clinical comorbidities. Some of the rhythm control drugs are amiodarone and targeted sodium channel blockers, as an example flecainide and propafenone. Flecainide is an antiarrhythmic, membrane stabilizing agent recommended as a first-line drug for AF

patients without structural cardiac diseases for converting and suppressing of intermittent episodes of AF (January *et al.*, 2014 and Kirchhof *et al.*, 2016) . However, there are side effects for the use of flecainide, such as, ventricular proarrhythmic risk (Echt *et al.*, 1991). A clinical trial conducted for the morbidity and mortality in cardiac arrhythmic patients reported excess number of deaths due to after-shock acute recurrent myocardial infarction and arrhythmia in patients treated with flecainide (Echt *et al.*, 1991). Propafenone, which is an oral antiarrhythmic drug that is administered to prevent symptomatic AF recurrence after the cardioversion in patients without structural cardiac diseases. However, propafenone reported to cause common side effects, including, dyspnea, fatigue, palpitations, chest pain, anxiety, blurred vision, and gastrointestinal discomfort, whereas hepatotoxicity is reported as the long term side effect (NIH, 2012).

Furthermore, the direct cardioversion employment of bi-phasic defibrillators rather than the monophasic external defibrillators has been used and are more effective since they conduct low energy. To avert the risk of prevailing a stroke within 72 hours to 10 days, appropriate post cardioversion monitoring and adequate observation of electrocardiograms is vital. The pre-treatment with anti-arrhythmic drugs enhance the restoring probability of the sinus rhythm (Sulke *et al.*, 2007).

1.3.3 Catheter ablation

The catheter ablation was first introduced in the late 1960s as a recording design in cardiac science, and the transvenous catheter concept was first established during an electrophysiological recording of a patient who underwent a defibrillation procedure (Ghzally and Gerasimon *et al.*, 2020). Percutaneous catheter ablation (CA) is considered a current interventional cardiology procedure for AF rhythm control. However, this intervention procedure can require re-ablations, which is a considerable limitation and affects the overall success rate as a treatment. The lack of AF substrate pathophysiology and the longevity of pulmonary vein isolation (PVI) lines limits this method intervention (Kottkamp *et al.*, 2015).

1.4 Physiological and functional identity of the lysosome

The lysosome is the primary catabolic organelle of the cell that performs fundamental signalling, and metabolic functions, by responding dynamically to cellular stimuli. Lysosomal responses to the cellular stimuli can be an array of actions, such as lysosome number, lysosome position in the cell, size or enzymatic activity to influence the homeostasis.

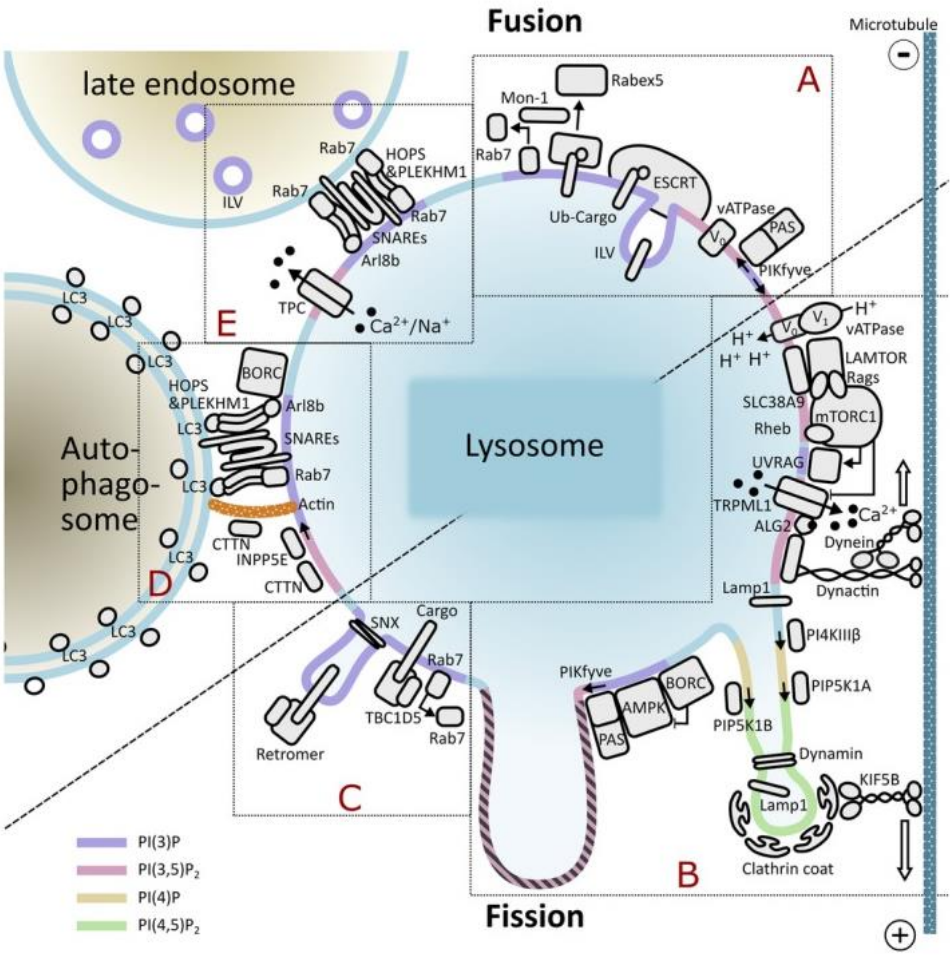

Figure1:15: A descriptive display of late endosomes/ lysosomes/ autophagosomes and their interactive proteins: *A. ESCRT related cargo proteins. B. Vesicle budding, fusion and fission related proteins. C. Sorting nexin and membrane fission proteins. D. Autophagosome and lysosome fusion proteins. E. Late endosome to lysosome and endo-lysosome fusion proteins. Phosphatidylinositol PIP proteins are colour coded according to the localization on lysosome. Figure with permission from (de Araujo et al., 2020).*

Morphologically, lysosomes are spherical organelles or vesicles, with ovoid or elliptical section profiles occasionally with temporary tubular extensions (Doeberitz and Wentzensen, 2008). Lysosomes are derived from Golgi apparatus and contain up to 50 hydrolases (Doeberitz and Wentzensen, 2008). The functional aspect of the lysosome is generally unique to all the cell types. The internal pH of the lysosome is

usually at pH 4.8, whereas cytosol is at neutral pH around 7.2, and acidity of the lysosome is maintained by proton pumps which pump H^+ ions to the lumen of lysosome across the lysosome membrane (Takenouchi *et al.*, 2015).

The primary function of the lysosome is degradation, and the degradation involves an array of macromolecules such as damaged organelles or processed unfolded proteins that are delivered through proteasomes or aggresomes.

Since the discovery by Christian de Duve in 1955 (De Duve *et al.*, 1955), the maintenance of cellular homeostasis was identified as the essential service provided by the lysosome. However, the lysosome's vivid physiological and functional identity is notably expanding every decade with research, including ion channel operation, nutrient and energy homeostasis, modulation of gene expression, regulation of immune responses, and cellular membrane repairment (Subothan and Roberto, 2019). Starting from single cells, plants to animals, the lysosome is the organelle with the highest distribution throughout the earth, from eukaryotes to prokaryotes, demonstrating the importance of lysosomes to life. After six and a half decades, the functional aspects of the lysosome and the related acidic organelles are still emerging (Capel *et al.*, 2015). Some of the major structural components and functional aspects of the lysosome are briefly described below.

Lysosome-associated membrane glycoprotein-2 (Lamp2)

Lamp2 is a lysosomal membrane protein and is considered a marker protein. Lamp2 is associated with starvation mediated lysosomal protein degradation (Sánchez-Lanzas and Castaño, 2018). Lamp2 is involved in major histocompatibility complex (MHC) mediated presentation of exogenous antigens, and during autophagy, Lamp2 plays a role in fusing auto-phagosomes with lysosomes (Hubert *et al.*, 2016).

V-type proton ATPase (V-ATPase)

V-ATPase is an ATP-driven proton pump required to acidify lysosomes, endocytic, and autophagic organelles, therefore vital for lysosome viability. V-ATPase-mediated lysosomal acidification is also linked to the control of Ca^{2+} efflux from lysosomes (Christensen *et al.*, 2002). Additionally, V-ATPase is essential for forming of intermediate compartments between early and late endosomes, generally defined as multivesicular bodies (MVBs) (Clague *et al.*, 1994). It's well understood that V ATPase is also associated with fusion and fission events of endo-lysosomes and lysosomes, therefore involved in the lysosome size (Baars *et al.*, 2007).

Ras-related protein Rab-7a (Rab7a)

Rab7a is a small GTPase that functions according to its GDP- bound and GTP- bound states. Additionally, it has roles in the regulation of endosomal trafficking (Tan and Tang, 2019) and vesicular trafficking (Daniloski *et al.*, 2021). Rab7a also associated in the fusion of phagosomes with lysosomes (Harrison *et al.*, 2003).

1.4.1 Lysosome in cellular autophagy; Intracellular degradation

Autophagy is the cellular survival mechanism predominated by the lysosome that leads a self-degradative process to precisely balance the sources of energy in critical situations such as nutrient or cellular oxidative stress.

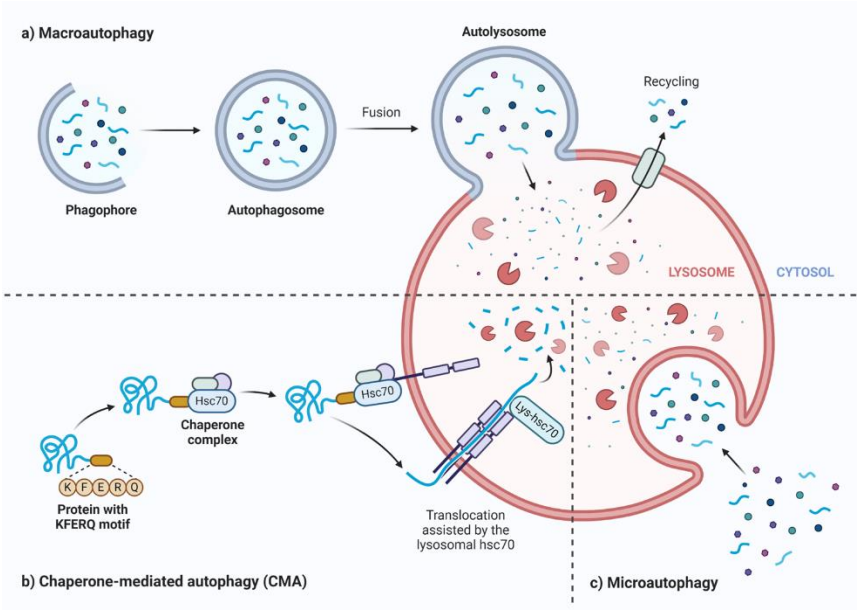

Figure 1:16: Three types of autophagy take place in the mammalian cell. *a. Macroautophagy; Generates energy under cellular stress conditions and remove the damaged organelles to adapt to the new nutrient deprived conditions and balance the cellular homeostasis: b. Chaperone- mediated autophagy; The lysosomal proteolysis pathway in the prolonged nutrient deprivation conditions: c. Microautophagy: Direct engulfment of the cytoplasmic molecules by the lysosomal membrane dynamics. Image reproduced with permission from (Bose et al., 2022).*

Autophagy is conducted in three mechanisms (Figure 1:16); Macroautophagy, which maintains the housekeeping of the cell by trafficking misfolded or aggregated proteins and disintegrating molecules to the lysosome for degradation; Chaperone mediated autophagy, which forms protein complexes/proteasomes to degrade proteins through ubiquitination; and Macro autophagy, a mechanism that leads protein aggregates, unable to unfold to the direct lysosomal degradation (Kaushik and Cuervo 2012). The cargo degradation through autophagy is conducted by forming a double membrane vesicle named the autophagosome, which contains cytoplasmic contents. The autophagosomes are later fused with lysosomes and turn in to auto lysosomes, where the targeted cargo degradation takes place (Hurley and Schulman 2014, Mizushima et

al 2008). Cellular energy levels are maintained by providing macromolecules that were degraded within the autolysosomes for the synthesis of new cellular components, hence these anabolic reactions thereby sustain cell homeostasis and metabolism (Lavandero *et al*., 2013). Despite maintaining cell survival, autophagy may lead to cell death when activated excessively or inefficiently, as occurs during certain pathological conditions or tissue development.

During the amino acid starvation, autophagy is induced above the baseline average through a series of molecular functional kinase activities in the adenosine mono phosphate – activated protein kinase (AMPK) and mechanistic target of rapamycin complex 1 (mTORC1) (Egan *et al* 2011).

1.4.1.1 Endocytosis; molecules trafficking cargo targeting lysosome

In 1963 Christian de Duve introduced the term “endocytosis” to include both the ingestion of large materials and the uptake of macromolecules or fluids through vesicles, which was also known as phagocytosis (cell eating) and pinocytosis (cell drinking) (Cooper, 2000).

Endocytosis is the remodelling system that maintains the membrane integrity of the cell. According to the specification and the extracellular and intracellular atmosphere of the cell, the plasma membrane, damaged organelles and the membrane receptor proteins are recycled and replaced (Inpanathan & Botelho, 2019) The lysosome is the final destination and the nexus of the recycling cargo that proceed with the degradation. The balanced circulation of the cellular cargo is conducted through mechanisms such as the Clathrin coated endocytic vesicles; a concomitant product of the endocytosis. The endocytic vesicles form through invagination and fission of the plasma membrane while carrying several different membrane proteins. The recycling and remodelling of the plasma membrane proteome renew the functional membrane integrity (Ross et al 2015).

Receptor mediated endocytosis or Clathrin mediated endocytosis is the selective uptake of macromolecules. These macromolecules bind to membrane surface receptors and later concentrate in Clathrin-coated pits. Cells also maintain Clathrin-independent endocytosis pathways, that uptake molecules in small invaginations of the plasma membrane. These invaginations are called caveolae and they are enriched in sphingolipids and cholesterol with a vesicle coat formed of Caveolin protein. Caveolae also mediate fluid uptake in the cell, a process known as micropinocytosis.

1.4.1.2 Endocytosis trafficking cargo to Lysosomes

Once macromolecules are internalized, Clathrin coated vesicles pinched off from the membrane fuse with early endosomes. The transmembrane fusing protein SNARE complexes and Rab GTPases (Rab proteins) associate to complete the fusion by interacting between vesicles and targeted membranes. After the fusion, early endosomes sort the cargo for further trafficking to the targeted membranes and compartments and the two major trafficking events that take place are, either, transport of the cargo to the lysosomes or recycling to the plasma membrane (Cooper, 2000) ;(Cooper and Hausman, 2007).

1.4.2 Phagosome formation and phagocytosis

Phagocytosis is a process of great biological value in the cellular system. It has been reported that apoptotic cell removal after a cardiac injury is an efficient step in recovery (Patil *et al.*, 2021). This receptor mediated process of the innate and adaptive immune systems was discovered over 100 years ago by Elie Metchnikoff and the past decades of studies revealed that phagocytosis plays a major role in tissue remodeling and homeostasis. Apart from the immune cells, the epithelial, endothelial and fibroblasts are capable of phagocytosis, led by complex receptor mediated signaling systems in the apoptotic atmosphere of a cell (Ronald and Valentin, 2011). Phagocytic receptors bind to ligand like molecules and decorate the particles to elicit engulfment and sequestration (Gray and Botelho, 2017; Levin et al 2016).

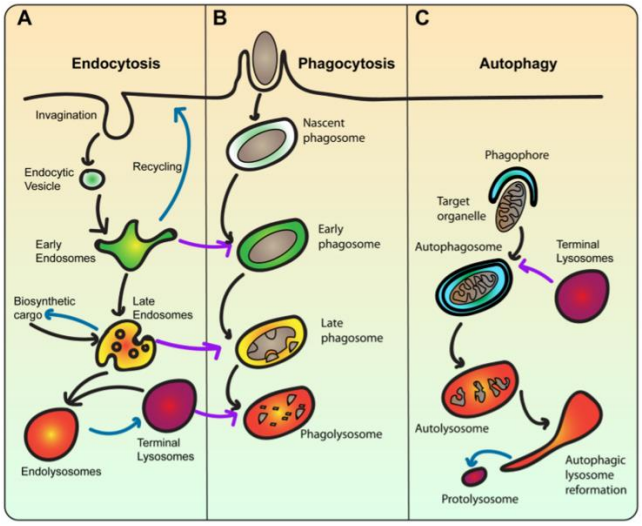

Figure 1:17: Lysosome as the terminal compartment for: *A. endocytosis, B. phagocytosis and C. autophagy. Figure with permission from (Inpanathan and Botelho, 2019).*

Molecules such as sphingosine -1-phosphate, fractalkine, lysophosphatidylcholine, Phosphotidylserine and ATP act as chemoattractant signals or apoptotic markers and with the support of exocytosis the phagosome pinches out to form a nascent phagosome (Figure 1.17), programmed to connect with early endosomes that later convert to late endosomes to fuse with lysosomes. The template organelle for the formation of phagosome and autophagosome is the endo-lysosome because it initiates the degradation process by a series of maturation steps (Bissig *et al* 2017 and Bright *et al* 2016). The maturation via Rab GTPases such as Rab 7 via its effectors PLEKHM1, FYCO1, SNARE complexes and tethering factors such as HOPS complex by binding LC3 (Zhao and Zhang, 2019; Yu and Melia, 2017) direct to the fusion of autophagosome to the lysosome. The phago-lysosome eventually degrade the enclosed particles, which are later recycled back to the endo-membrane system (Krishna et al 2016 and Krajcrovic et al 2013).

1.4.3 Cellular apoptosis related to AF: Potential lysosomal involvement in AF disease condition/progression

Oxidative stress has been shown linked to AF (Cadenas and Davies, 2000). The overproduction of oxidative by-products accumulates in the cytoplasm and leads to energy depletion. The lysosomal compartments undergo constant stress when ROS accumulate in the cell, mainly because of the insufficient functional capacity to meet the demands of autophagy. Moreover, enlarged and senescent mitochondria in the intracellular environment is a sign of deficiency in ATP production due to the reduced functionality in the inner membrane. Imperfect autophagic recycling of these critical organelles may underlie progressive mitochondrial damage (Terman *et al.*, 2003). Apart from oxidative stress, studies on cardiac specific inhibition of autophagy related 5 protein (Atg5), which caused severe cardiomyopathy in mice (Nakai *et al.*, 2007) also showed parallel decrement in the protein levels of lysosomal atrial Natriuretic peptides A (ANP), coded for the gene NPPA, Sarcoplasmic/endoplasmic reticulum calcium ATPase 2a (SERCA2a) and Phospholamban. Furthermore, Atg5-deficient hearts showed disorganized sarcomere structure and mitochondrial misalignment and aggregation. The measurements of intracellular Ca^{2+} transients indicated impaired Ca^{2+} cycling.

Cardiac myocytes gradually undergo pronounced age-related alterations because the myocardium is mainly composed of post mitotic cells. As a consequence, aberrant cytosolic proteins, often in aggregated form cause lipofuscin in lysosomes (intra-lysosomal un-degradable polymeric substance). This leads to insufficient capacity for autophagy of the lysosomal compartment, as a result enlarged and functionally defective mitochondria accumulate and aged lipofuscin-rich cardiac myocytes become overloaded with damaged mitochondria, leading to increased oxidative stress, apoptotic cell death, and the gradual development of heart failure (Terman *et al.*, 2008). Rising ROS production and obstruction of autophagy and increase of lipofuscin in cardiomyocyte causes faster apoptotic cell death and therefore, indicate that lysosomal destabilisation plays a significant role in the manifestation of myocardial ageing and a variety of cardiac pathologies.

1.4.4 What are the Two-Pore Channels (TPC)? Why are they important?

Lysosomal membrane contains multiple proteins with two of the most relevant ion channels being TRP and TPC. The NAADP- stimulated Ca^{2+} release mechanism occurs via TPCs (Calcraft *et al.*, 2009) in lysosome-related acidic organelles (Churchill *et al.*, 2002).

In 2015 Capel et al., published data showing the importance of TPC2 proteins for the physiology and pathophysiology of the heart. The results from this study define a role for NAADP and TPC2 at lysosomal/sarcoplasmic reticulum junctions and show that they are major contributors in the acute actions of β-adrenergic signalling in the heart and also in stress pathways linking chronic stimulation of β-adrenoceptors to hypertrophy and associated arrhythmias (Capel *et al.*, 2015).

More recently, in 2017, Aston et al. provided structural evidence of the intimate association between lysosome and SR in ventricular myocytes (Figure 1.18) (Aston *et al.*, 2017). They described the median separation between these two organelles is ~20nm in 2D electron microscopy and ~3.3 nm in 3D electron tomography, indicating these are realistic signalling micro-domains.

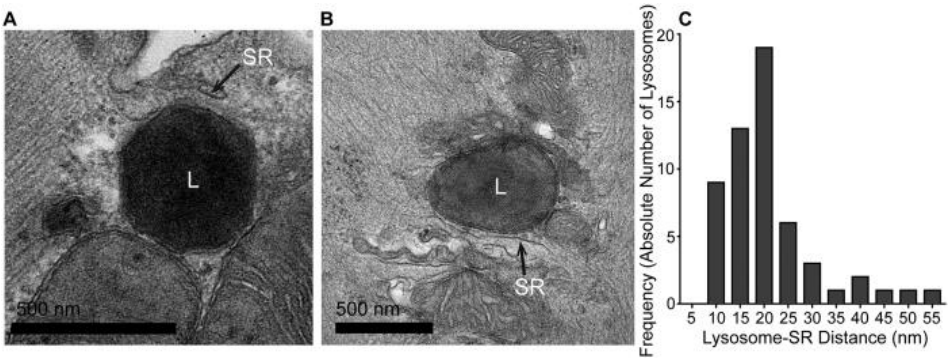

Figure 1:18 Lysosomes are in close proximity to the sarcoplasmic reticulum (SR) in rabbit ventricular myocytes, forming nanojunctions*. (A, B) Respectively, are lysosomes (L) in close proximity to the SR. (C) Population data chart displaying shortest distance from a lysosome membrane to the closest SR-membrane. Calculated Median distance 20 nm (13–24 nm), n = 56. Figure with permission from (Aston et al., 2017).*

Combining the fact that lysosomes are recognized as the major location for degradation of both intracellular and extracellular macromolecules and the ability of lysosomes to act as Ca^{2+} stores and participate in calcium signaling processes in the heart makes research investigating the role of lysosomes in fundamental cellular processes and their involvement in cardiac disease mechanisms a very interesting and timely study. Understanding the role played by lysosomes in the mechanisms underlying AF could prove important for the development of pharmacological therapies to treat AF.

1.5 Genomic and proteomic expression in the cell

The cell is the basic structural and functional unit of life. After its discovery in the 17th century by Robert Hooke, the fundamental concept of information and hereditary material for life emerged with Harold Clayton Urey (1893–1981) and Stanley Lloyd Miller's (1930–2007) experiments. They proved the biogenesis theory that biological molecules can be created from inorganic precursors through the famous Miller–Urey experiment (Miller, 1953).

The genetic basis of a eukaryote is coded in its genome, a sequence of deoxyribonucleic acid (DNA) that stores the hereditary information carried by the organism (Krebs *et al.*, 2017), and by a series of biological interactions, collectively called transcription and translation (Described in detail section 1.5.1 and 1.5.3 of this chapter). DNA sequences code for the production of ribonucleic acid (RNA) sequences that are converted to amino acid sequences to produce proteins (Described in detail, section 1.5.3 of this chapter) and are considered the functional units of the cell.

1.5.1 Gene expression - Transcription in eukaryotes

The transcription regulation between the prokaryotes and eukaryotes is fundamentally different. However, some of the regulatory mechanisms show similarity (Nelson and Cox, 2008). In this chapter I briefly focus on the eukaryotic transcription.

Transcription is considered the first step in the universal passage of biological information flow from genome to proteome (Nguyen and D'haeseleer, 2006). The hereditary information, such as RNA or proteins must be expressed for a cell to function. DNA is the original copy of the genetic information, which stores the cell's genetic code, yet is not used as the immediate source of instructions to run the cell. Instead, RNA generates functional copies of the genes. This process of transferring genetic information from genes to RNA is known as transcription. Therefore, the functional copies or the RNA molecules are referred to as transcripts (Clark, 2009).

Depending on the final product, genes are divided into two groups: Those whose final product is an RNA molecule (e.g., rRNA, tRNA or assorted regulatory RNA) and those whose final outcome is protein. In the second process, with several steps, the RNA transcript converts the information carried by its coding system to the protein as an intermediary product. As described above, this type of RNA molecule that carries

genetic data encoding a protein from a gene into the cell is known as mRNA. Here we give priority to the transcription of mRNA. Application of transcription analysis in AF is discussed in chapter 4 in detail (Clark, 2009).

The first step of the transcription is the opening of the chromatin template, and the process initiates by binding the enzyme RNA polymerase to the promoter region of the opened DNA template. Nucleosome octamers are removed from the promoter region before RNA polymerase binds to the promoter.

While RNA polymerase binds to the promoter, transcription factors bind to enhancers. Any protein needed for the initiation of the transcription but not part of RNA polymerase is described as a transcription factor. Transcription factors recognize the *cis*–acting sites on DNA and incorporate them into the initiation complex by associating with more factors.

The transcription mechanism consists of five steps: Pre-initiation, initiation, promoter clearance, elongation and termination. In the pre-initiation step, transcription factors bind to the DNA. Promoters are situated upstream of the transcription initiation site. The transcription initiation complex or the basal transcription apparatus is formed once the promoter region binds to the basal transcription factors and RNA polymerase-II are bound together. The binding region of the RNA polymerase is named ‘‘Core promoter’’,

and RNA polymerase begins to unwind the double helix DNA. Once the first bond with the nucleotide is made, the RNA polymerase must be released from the promoter, and this step is called ‘‘promoter clearance’’, which is the vital step to determine whether an active or a poised gene will be transcribed and is controlled by enhancers.

Transcription initiation factor IIE (TF2E) and Transcription initiation factor IIH (TF2H) are required for the DNA polymerase movement along with the linear template. RNA polymerase II depends on the phosphorylation of the carboxyl tail domain (CTD) to transit from the promoter and transcription factors to the elongating step. At the elongation step, RNA nucleotides are added to the DNA complementary strand and CTD process the mRNA strand while it is being synthesized and also after released by the RNA polymerase II.

Therefore, CTD act as an anchor point to dock for other proteins on the DNA polymerase II. As an example, once pre-mRNA is synthesized, guanylyl-transferase or the capping enzyme, which adds G residues to the 5’ end of the pre-mRNA, binds to the CTD and modify the mRNA strand. Moreover, splicing the mRNA strand is associated with CTD, where the recruitment of the SCAF proteins are docked to the CTD and bind to splicing factors.

At the near completion of the mRNA strand synthesis, RNA polymerase II identifies the termination identification or the polyadenylation identification sequence. Cleavage and polyadenylation specificity factor (CPSF) recruit's cleavage stimulation factor (CStF) to the transcribed polyadenylation identification sequence region binding site. Moreover, additional cleavage factors such as endonuclease are recruited and cleave the mRNA strand, and the poly-A polymerase enzyme adds multiple adenine residues to the 3' end of the mRNA strand and prevents further modifications through adenine. Poly-A binding proteins are then attached to the poly-A tail (Persson and Mueller, 2015).

Additionally, pre-mRNA that contain introns and exons undergo a spliceosome mediated splicing process to be converted into the mature mRNA form, which has only exons but not the introns. The matured mRNA strand will then be exported to the cytoplasm through the nuclear pores (Lewin *et al.*, 2011).

1.5.2 Transcriptomics

The activities of all RNA and their abundance in time and space is referred to as the total transcriptome. As RNA play the major role in protein synthesis, the analysis of RNA function through techniques such as microarray and next generation sequencing is called the transcriptomics or transcriptome studies. To understand the complex pathology of diseases such as AF, transcriptomics can be applied to study mRNA

expression (Liang, 2013) (a detailed presentation of the transcriptomics work flow is provided in chapter 4).

There are major scopes of studying transcriptomics. This method allows the study of underlying molecular mechanisms in a pathological condition to distinguish the cellular biological events such as cell differentiation and cell cycle, and possible identification of biomarkers in diseased states (Liang, 2013).

The transcriptomic platform is performed either by microarray or sequencing. The platform used in this study was RNA sequencing. The data generated from such next generation sequencing must be measured quantitatively to understand differential expression between two or more conditions. Moreover, different global visualization methods are applied to understand the data distribution. These methods include MA plots, PCA plots and similarity clustering.

The ratio intensity plot or the MA plot measures the fold change between more than two samples. However, it displays the average gene expression on the horizontal axis. The similarity clustering groups the similar genomic expressions across samples because genes with similar expression levels are presumed to co-expressed and have the same set of transcriptional factors; otherwise, they consist of similar cellular or biological functions. Additionally, genes with similar expressions assume that they can

be grouped and analysed together; for example, similar gene profiles have similar pathological phenotypes (Golub *et al.*, 1999 and Liang, 2013).

1.5.3 Protein expression – Translation

The complete process of protein synthesis, including transcription and translation, is considered the principle concept of molecular biology (Langston and Cookson, 2020). Once the genomic DNA is transcribed to RNA, the transcribed mRNA is translated to protein (Crick, 1970). In order to fulfil the correct biological functions of the proteins, the proteins must achieve their post-translational modifications, namely, methylation, phosphorylation, and glycosylation (Cooper and Hausman, 2007). Therefore, it is vital for cells the perform protein synthesis with careful regulation (Langston and Cookson, 2020). The hereditary information passed from DNA is encoded in the mRNA, and the functional unit of the encoded information is expressed in the form of proteins. The genetic code that encodes between base pairs of a gene and the corresponding amino acid sequence play a major role in translating the genomic information, and this process is carried out by the ribosome (Figure 1:19).

Translation consists of three stages: Initiation, elongation and termination. The elongation initiation factors (eIFs) coordinate the initiation. GTP bound eIF2 recruits tRNAs, while eIF3 and eIF4 form a complex with the ribosome to bind the mRNA

(Gingras *et al.*, 1999). Then the 5' cap of the mature mRNA binds to the eIF4E, and the 5' cap-bound eIF4E interacts with eIF4G to form the translation initiation complex associated with a small ribosomal unit (Richter and Sonenberg, 2005). Once the initiation process is completed, a set of elongation factors contribute to performing the elongation. These factors coordinate the tRNA positioning at the ribosome complex and insertion of tRNA bound new amino acids after the mRNA codon recognition. The peptide chains continue to grow with each peptide bond formed. Once the translation complex recognizes a stop codon, the termination of the peptide chain takes place, and the ribosome dissociates from the mRNA chain (Cooper and Hausman, 2007).

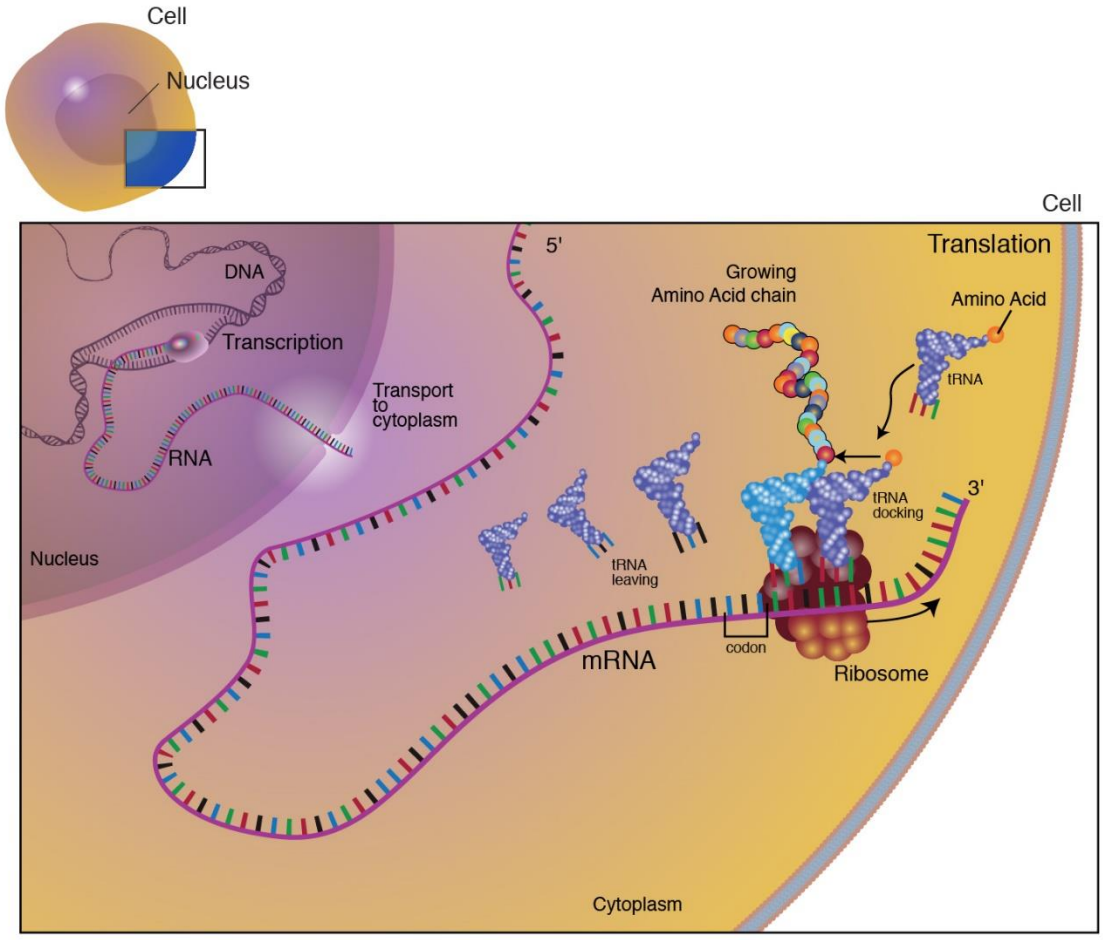

Figure 1:19: Protein translation. *mRNA strand is transcribed and exported to the cytoplasm in the cell, and the initiation complex is formed with small and large ribosome units together with eIFs. The GTP bound eIF2 recruits tRNA to the small ribosome subunit, and tRNA recruit the amino acids to the ribosome after reading the mRNA codons. The peptide chain keeps growing until the ribosome complex reads a stop codon to terminate the chain formation. (Courtesy: National Human Genome Research Institute: www.genome.gov/genetics glossary).*

1.5.4 Proteomics

The term ‘‘Proteomics’’ was first declared by Marc Wilkins in the mid-1990s, and the scope of proteomics is to understand the proteome expressed by a single species and this concept is functionally applied to study a set of proteins in a single system rather than a single protein in a single system. This technique was first driven by the researchers using 2D gel electrophoresis, and the initial proteomics workflow was built around Matrix-Assisted Laser Desorption Ionization - Time of Flight (MALDI-ToF) mass spectrometry. With time, proteomics technique has developed into gel-based samples to gel-free peptide separation technologies. The modern mass spectrometry peptide detection is followed by better and more sensitive data mining software to handle a high volume of generated data. The proteomic analysis is summarized depending on the task and scope of the targeted study: Protein level detection and quantification, protein modifications detection and quantification, subcellular localization protein detection and quantification and protein interactions detection and quantification (A detailed workflow of the proteomics is discussed in Chapter 2 and 3).

1.5.5 Mass spectrometry

Mass spectrometry is an analytical tool that can analyse biomolecules such as peptides or even DNA and RNA. However, in terms of proteomics, the scope is to analyse peptides to understand the interactions of proteins-proteins, proteins-RNA or proteins-DNA. Identifying the compounds in the instrumentation can be set even for the smallest size, such as peptides with three amino acids.

Mass spectrometry calculates the mass to charge ratio (m/z) of one or more molecules in a given sample. Therefore, the precise molecular weight of the biomolecules can be determined and supports identifying the isotopes (isotopes are atoms from a single element with a different number of neutrons). Isotope fractionation or mass fractionation discuss the subtle differences identified in the speed displayed by the different isotopes from the same element (Heide, 2014).

The mass spectrometry principle is based on the motion and momentum of ions and detects the ions of different masses on a mass spectrum. This principle is applied to ions to deflect in different angles in a magnetic or electric field according to their masses. (Figure 1:20).

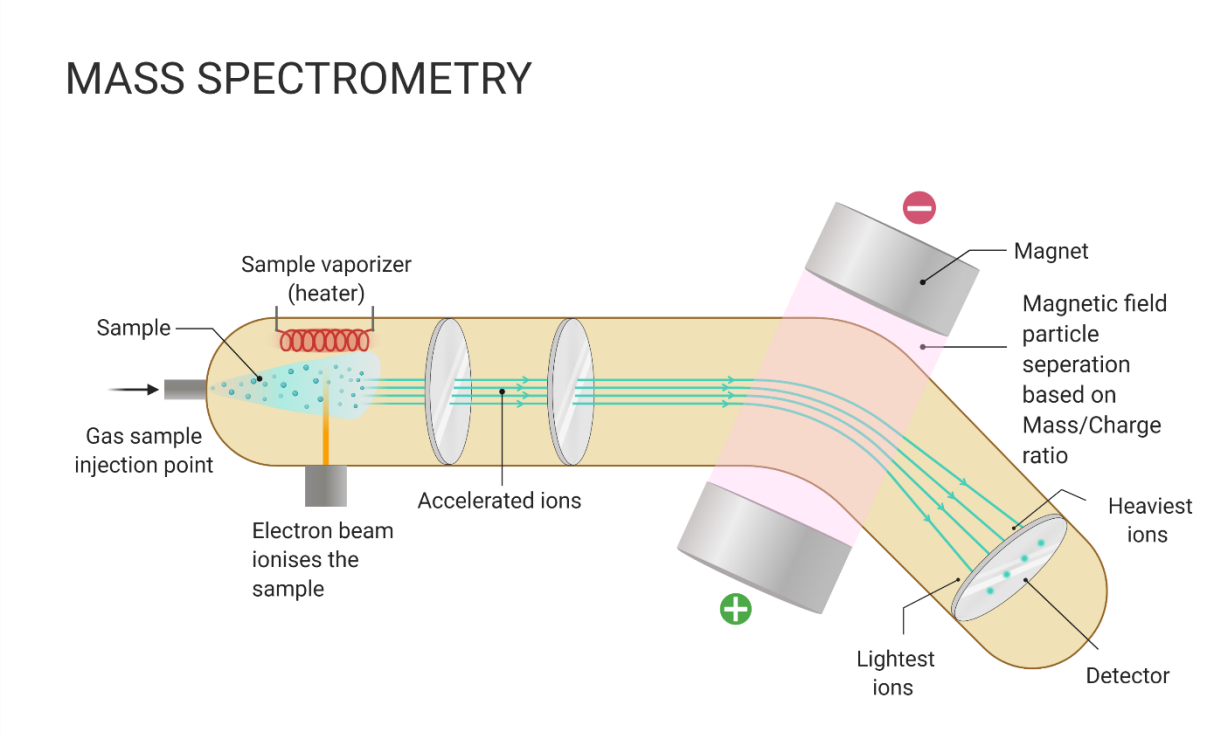

Figure 1:20: The principle of mass spectrometry technique. *Once the sample is injected to the mass spectrometer, the electron source ionizes the sample. The ionized particles are accelerated to the magnetic field and according to the mass of the charged isotopes the ions deflect at different angles. According to the points that charged isotopes landed, the particle detector at the end can detect the heaviest and lightest isotopes. Figure created using Biorender.com.*

The functional aspect of mass spectrometry is to generate a list of masses that can later be compared to the existing databases. However, this can lead to several limitations such as redundancies, unidentified peptide sequences that do not exist as a protein, fault discoveries and omissions. Mass spectrometry proteomics workflow is divided into two processes: top-down proteomics, and bottom-up proteomics.

Top-down proteomics comprises mass spectrometric analysis of the whole proteins and fragmentation during the analysis and comparing the masses against the published databases. Top-down proteomics is applied to the proteins with known sequences but unidentified post-translational modifications (PTMs). Therefore, if the mass spectrometric data quality is good, the top-down proteomics can identify PTMs by deducting the masses of the analysed fragments. In bottom-up proteomics, a mixture of proteins obtained from cells or tissues is digested into peptides before the mass spectrometric analysis. The proteomic analysis and workflow presented in this thesis followed the bottom-up mass spectrometric proteomics (Lovrić, 2011).

To identify and analyse proteins, proteomics as a method is advantageous over biochemical detection methods because proteomics simply require a measurable difference between sample groups to identify the protein regulations (Chandramouli and Qian, 2009). Moreover, the application of proteomics is broad. It can approach comparative differential expression between two or more samples, profiling proteomes, organelle localisation and identification of organelle-specific proteins, identification of post-translational modifications and interactions between the proteins (Alaoui-Jamali and Xu, 2006).

Furthermore, proteomics can be applied to different species in disease animal model studies such as AF, and proteomic analysis on different species leads to discover novel proteins. Even though unidentified proteome interpretation and conversion could

exclude unconfident proteins, leaving a higher number undetected. Moreover, the sensitivity of identifying low abundant proteins, which may require fractionation of samples according to their biological nature or organelle content (Ayagama *et al.*, 2021 and Mauri *et al.*, 2008) and ability to identify protein complexes with their correct isoforms, are limited to some mass spectrometry units (Siitari *et al.*, 2004).

1.6 Proteomic application on disease pathology to identify lysosomal protein regulations

Proteomics is an emerging technique that has overcome the challenge of understanding more proteins in a single technique. Therefore, efficient to recognise prominent pathways that are regulated in disease pathology. Therefore, it is equally important to increase the protein yield and detect low abundant proteins in a complex mixture of cells, such as tissue biopsies.

To overcome this challenge, fractionating cellular organelles and performing label free quantitative LFQ proteomics in each organelle fractions of disease models against the controls is currently an extremely promising approach. Unlike the high-throughput genomic screening, proteomics does not have an amplification step. Therefore, enrichment of the proteins in fractions is beneficial in molecular pathway analysis.

Chapter 2 that follows, describes a method to fractionate and yield an enriched endolysosomal fraction from a minimal amount of tissue biopsy sample to study endo lysosomal and lysosomal proteins using LFQ proteomics specifically in cardiac atria but more widely applicable to other tissue samples.

1.7 Hypothesis and aims

Since Christian De Duve's discovery of the lysosome in 1955 (De Duve et al., 1955), evidence for structural lysosomal abnormalities has emerged in several disease conditions. As examples, increased metabolic demand in the myocardium (Kottmeier and Wheat, 1967) increased the lysosome number in the atrial muscle tissue of mitral stenosis (Wheat, 1965), and in a dog model of atrial septal defects (Kottmeier et al. 1967). Recent studies provide sufficient evidence that AF cause metabolic demand in the atrium (Ausma et al., 2000); (Shingu et al., 2020); (Ghezelbash et al., 2015); (Kalifa et al., 2008). Furthermore, the early and recent data on lysosomal enzyme activity studies of the heart [(Youhotsky-Gore and Pathmanathan, 1968); (Comolli, 1971); (Wilson, 1972); (Lenders & Brand, 2021)] demonstrate that in certain disease conditions, such as Fabry disease, cardiac lysosomal activity can show dysregulation.

Understanding the dysregulations of lysosomal proteins such as, enzymes, and cargo proteins, that may significantly affect AF pathology.

I hypothesize that in AF, lysosomal proteins are dysregulated.

To investigate changes in lysosomal proteins, I will utilise proteomics to identify the significantly dysregulated proteins, transcriptomics to detect significantly dysregulated mRNA transcripts and further biochemical assays to confirm and validate the identified proteins of interest.

The experimental plan of the project is divided into two major sections.

1) Develop a novel method to identify endolysosomal proteins using a wild type Guinea pig.

2) Apply the developed method on a large-animal model of AF (goat) to identify the dysregulated lysosomal proteins and the metabolic pathways that may contribute to the lysosomal pathway or lysosomal cargo.

Chapter 2

A modified density gradient proteomic-based method to analyse endolysosomal proteins in cardiac tissue

Summary of contribution: This chapter presents a method developed to isolate and identify endolysosomal proteins from atria of guinea pig as published in Ayagama *et al.* 2021. I carried out the protocol development, conducted the quantification and statistical data analysis, pathway and functional network analysis, and all the experiments including, organelle isolation, SDS/PAGE, Western blots, enzyme activity and protein assays. Additionally, planning, designing, and writing the project. Figures reproduced from the paper were my own work. The liquid chromatography – tandem mass spectrometry analysis was performed by Roman Fischer and Georgina Berridge in the Target Discovery Institute, University of Oxford.

The methods and results detailed in this chapter have been published in Ayagama *et al.* (2021). The work presented here is my own except where stated otherwise, and has been reproduced here with permission of the authors.

2.1 Introduction

Early elegant ultrastructural and biochemistry based studies have looked into the levels of lysosomal enzyme activity in many organs, including the heart (Comolli, 1971); (Wilson, 1972); (Youhotsky-Gore and Pathmanathan, 1968), (Traurig, 1976). More than four decades ago, the importance of lysosomes in the heart was recognised (Wildenthal and Decker, 1980), and as early as 1964, an increased number of lysosomes was observed in the atrial muscle of chronically diseased or stressed hearts with acquired heart disease such as mitral stenosis (Wheat, 1965) Kottmeier *et al*. (1967) conducted studies in a dog model of atrial septal defects, and their data demonstrate an increase in the number of myocardial lysosomes in cells subjected to increased metabolic demands (Kottmeier and Wheat, 1967). However, these studies did not determine whether there was a correlation between the degree of stress and elevation in lysosome numbers.

In 1977, Wildenthal (Lundholm and Scherstén, 1975) and (Wildenthal *et al.*, 1977) looked at differences in cardiac lysosomal enzymes in detail and confirmed previous observations, relating to increase with age in the total activity of the lysosomal

proteinase, Cathepsin D (Comolli, 1971 and Hendley and Strehler, 1965). Since the identification of nicotinic acid adenine dinucleotide phosphate (NAADP) receptors in cardiac microsomes (Bak *et al.*, 2001), several papers have been published relating to the vital role of lysosomal Ca^{2+} signalling in the heart (Capel *et al.*, 2015 and Galione *et al.*, 2010).

Membrane-membrane junctions between lysosomes and the sarcoplasmic reticulum (L-SR junctions) are of particular interest; they have been hypothesised to couple Ca^{2+} signalling between these two organelles (Kinnear *et al.*, 2008). L-SR junctions may play an important role in cellular Ca^{2+} signalling as demonstrated in early studies on the Ca^{2+} mobilising messenger NAADP (Lee and Aarhus, 1995), which demonstrated that NAADP released Ca^{2+} from a store other than the Sarco/endoplasmic reticulum (S/ER) (Aarhus *et al.*, 1996), that could then trigger further Ca^{2+} release from the S/ER by Ca^{2+} induced Ca^{2+} release (CICR) (Lee and Aarhus, 2000) and (Cancela *et al.*, 1999), (Churchill and Galione, 2001 and Boittin *et al.*, 2002). NAADP synthesis and NAADP-mediated Ca^{2+} release from lysosomal pathways have not been explored in atrial arrhythmias such as AF. Proteomic characterisation of individual organelles (Au *et al.*, 2007), for example, can provide valuable information regarding their function in normal and disease states.

The concept of understanding proteins from a compartmentalisation (Larance and Lamond, 2015) perspective, their related properties and dynamic distribution in health and disease is critical for deciphering the phenotype of a cell. Significant advances in

mass spectrometry-based proteomics allow us to achieve multidimensional measurements of proteins with greater efficiency, enabling, for example, the generation of more detailed maps of the human proteome (Kim *et al.*, 2014). Relative quantification methods of samples include label-free quantification (LFQ) (Hoffert *et al.*, 2006), *in vivo* metabolic stable-isotope labelling (Wang *et al.*, 2002), stable-isotope labelling using chemical tags that are covalently attached *in vitro*, tandem mass tags and isobaric tags for relative and absolute quantification (recently reviewed by Larance and Lamond, 2015).

Methods available to analyse subcellular protein localisation in cells and tissues are diverse (Graham, 2001) and (Walker and Lloyd-Evans, 2015). Depending on the cell or tissue to be analysed, the choice of method carries its distinctive advantages and disadvantages. The subcellular fractionation methods most commonly combined with mass spectrometry-based analysis include differential centrifugation and either equilibrium gradient centrifugation or non-equilibrium gradient centrifugation (Larance and Lamond, 2015). One of the challenging issues encountered with subcellular fractionation is the slight density differences between individual organelle fractions. Advanced methods, such as localisation of organelle proteins by isotope tagging (LOPIT) (Dunkley *et al.*, 2004), offer advantages to differentiate large organelles, small intracellular vesicles and even large complexes such as ribosomes, purely based on their density and not requiring isolation and purification of organelles.

Over recent years, significant progress has been made in establishing a region and cell-type resolved quantitative proteomic map of the human heart (Doll *et al.*, 2017). The value of such approaches has been demonstrated by applying these data to define molecular changes in patients suffering from AF (Schröder *et al.*, 2010) . Mishandling of Ca^{2+} regulation in cardiac cells is closely linked to the pathophysiology of cardiac arrhythmias such as AF. To understand the contribution of the organelles involved in Ca^{2+} regulation (including lysosomes in addition to SR and mitochondria) to atrial function, a more detailed organelle-specific approach is required.

Relatively little is known about the protein composition of the lysosomes in cardiac atria. This study presents a flexible, low-cost, modified density gradient method for endo-lysosomal organelle isolation for processing small amounts of cardiac frozen atrial tissue biopsies to identify organelle protein better. We performed label-free mass spectrometry that allows us better to appreciate lysosomal function in physiological and pathophysiological states. Furthermore, Western blot analysis and lysosomal enzyme assays showed that the expression profile of the EL fraction was as expected, with minimum contamination from other organelles. Organelle-specific quantitative proteomics approaches such as this can help progress our understanding of the role of lysosomes in atrial physiology and pathophysiology, for example, by comparing protein composition from disease tissue samples or cell lines with those of healthy donors or patients.

An atrial endo-lysosomal organelle database would offer valuable data in studying cardiac physiology. The method described in this chapter, as published in Ayagama *et al*. (2021) shows the utility of a low cost, non-labor-intensive protocol involving density gradient ultra-centrifugation. Statistical analysis by volcano plot of quantified protein hits revealed 564 EL proteins significantly enriched in the EL fraction (false discovery rate of 0.05). In these proteomics data, we uncovered endo-lysosomal marker proteins (D'Souza *et al.*, 2019) Rab7A, VPS29, MAN2B1, LAMTOR1, LAMTOR2, LAMTOR3, LAMTOR5, RILP, ACP2, GBA, and GAA in the proteomics data, and LAMP2 from Western blot data. The guinea pig (*Cavia porcellus*) is a standard and well established small mammal model used in cardiovascular research, and the guinea pig cardiomyocyte electrophysiology, typical long plateau phase of the action potential, is more human-like than mouse or rat. This method offers flexibility in protocols involving minimal quantities of heart biopsies obtained during surgery. Using this approach, it will be possible to explore the contribution of lysosomes in health and disease, providing a technique to unravel novel mechanistic insights relating to changes in protein composition in diseased models that can then be related to functional data (Ayagama *et al* 2021).

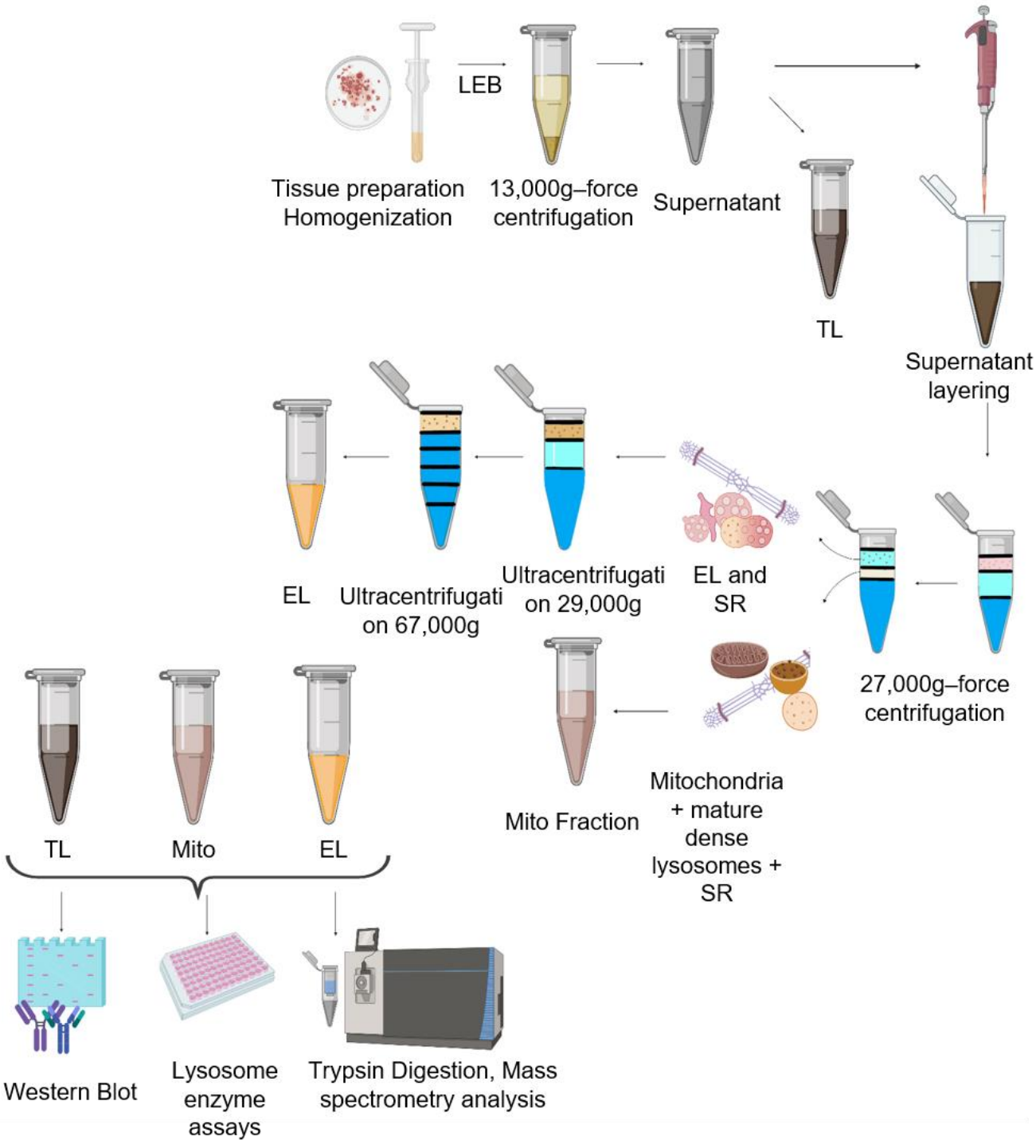
LEB
Tissue preparation
Homogenization
13,000g–force
centrifugation
Supernatant
TL
Supernatant
layering
EL
Ultracentrifugati
on 67,000g
Ultracentrifugati
on 29,000g
EL and
SR
27,000g–force
centrifugation
TL
Mito
EL
Mito Fraction
Mitochondria
+ mature
dense
lysosomes +
SR
Western Blot
Lysosome
enzyme
assays
Trypsin Digestion, Mass
spectrometry analysis

Figure 2:1: Flow chart of the acidic organelle isolation. *Top: Atrial tissue is homogenized using a Dounce homogenizer; after adding Lysosome enrichment buffer (LEB), tissue lysate is briefly centrifuged at 13,000 g-force, 4C for 2 min; supernatant is collected without disturbing the tissue pellet (tissue lysate, TL); centrifuge tube is layered with 750 µL of 2.5 M sucrose, 250 µL of Percoll, and 200 µL of TL; centrifuge at 27,000 g-force, 10 °C for 50 min: The mitochondria and SR accumulate at the biface of Percoll and 2.5 M sucrose and are carefully collected (mitochondria + SR enriched fraction). The area above the turbid white layer consists of endosomes and endo-lysosomes with minimum contamination of SR, and this fraction is collected for further removal of SR by centrifuging at 29,000 g-force 15 °C for 30 min; for the differential density gradient centrifugation step, centrifuge tube is carefully loaded with the different density gradients made of sucrose, Percoll and ddH2O (starting from 1.3 g/mL, 1.11 g/mL, 1.07 g/mL, 1.05 g/mL, 1.04 g/mL). The fraction collected from above the turbid white layer is pipetted (200 µL) on top of the 1.04 g/mL Percoll; the tube is centrifuged at 67,000 g-force at 4 °C for 30 min, and the top fraction consists of endo-lysosomes + endosomes. Bottom: Protein validation is performed using Western blot, lysosome enzyme assay, and proteomic analysis. (Flow chart created using Biorender.com) Figure published and reproduced with permission from (Ayagama et al., 2021)*

2.2 Experimental model and subject details

Animals

All experiments were performed in accordance with Home Office Guidance on the Animals (Scientific Procedures) Act 1986 (UK). Hearts were rapidly isolated from six healthy adult Duncan Hartley male guinea pigs (350-400g, Envigo, UK), following cervical dislocation and immediately perfused with ice-cold heparinized phosphate buffered saline (PBS). Both left and right atria were dissected, snap frozen in liquid nitrogen and stored at 80 °C until required. All animals were purchased from Envigo,

UK. All experimental protocols (Schedule 1) were approved by the University of Oxford, Procedures Establishment License (PEL) Number XEC303F12.

2.2.1 Method details

2.2.1.1 Tissue homogenization

Frozen atrial tissue biopsies (100 mg) were thoroughly cleaned in PBS and weighed. A minimum of 100 mg tissue is required to perform proteomics and biochemistry (enzyme assay and Western Blots). Each atrium was quartered and gently homogenized using a 7 mL Dounce homogenizer in Lysosome isolation buffer (LIB) [Containing 1:500 protease inhibitor cocktail (PIC) and phosphatase inhibitor (PHI) (Bio vision), (PhosSTOP Roche)]. Preparations were further homogenized in 1 mL Dounce homogenizer and transferred to chilled 1.5 mL ultracentrifugation tubes (Beckmann coulter). Sample preparations were mixed at a ratio of 1:1.5 Lysosome enrichment buffer [(LEB) (Biovision, containing 1:500 PIC)] to homogenate by inverting tubes, and were stored on ice for 5 min until the centrifugation.

2.2.1.2 Isolation of acidic organelles by fractionation

Samples were centrifuged at 13,000 g for 2 min at 4 °C (TLX Beckmann Coulter Ultra Centrifuge) and the resulting supernatant, corresponding to the TL was collected. Further fractionation was processed using 75% of the collected TL. 1.5 mL ultracentrifuge tubes were underlaid with 750 µL of 2.5 M sucrose (Fisher Scientific) followed by 250 µL of Percoll (Santa Cruz Biotechnology). 200 µL TL was layered on top of the Percoll layer and centrifuged at 27,000 g 50 min at 10 °C. The supernatant layer just above the turbid white, mitochondrial fraction (Mito fraction) was carefully removed, and the Mito fraction itself was collected separately. The collected supernatant was retained and repeated for a further centrifugation step at 29,000 g 30 min at 15 °C (500 µL of underlaid 2.5 M sucrose with overlaid 500 µL Percoll). The supernatant above the sucrose and Percoll intermediate was collected for further fractionation. Firstly, ultracentrifuge tubes were underlaid with 2.5 M sucrose and overlaid with a series of Percoll dilutions (1.11 g/mL – 1.04 g/mL in ddH2O). The ultracentrifuge tubes were centrifuged at 67,000 g 3 30min at 4°C. The fraction at 1.04 g/mL was collected and labeled as the endolysosomal fraction (EL) (Figure 2:1). N = 3 guinea pigs were used for Western Blots and proteomic analysis. A separate n = 3 biological triplicate was used for the lysozyme enzymatic analysis. The reproducibility of the fractions produced using biological triplicates can be found in Figure 2:4.

2.2.1.3 Lysosomal hydrolase activity assays

Lysosomal hydrolase activities were performed in EL, Mito fractions and TL. To fluorometrically measure the lysosome enzyme levels, artificial sugar substrates containing the fluorophore 4-methylumbelliferone (4-MU) were used. For measuring β-hexosaminidase activity, 3 mM 4-MU N-acetyl-β-D-glucosaminide (Sigma Aldrich) in 200 mM sodium citrate buffer, pH 4.5 and 0.1% Triton X-100 was used as substrate. For β-galactosidase activity, 1 mM 4-MU β-D-galactopyranoside (Sigma Aldrich) in 200 mM sodium acetate buffer, pH 4.3, 100 mM NaCl, and 0.1% Triton X-100 was used as substrate. The reaction was stopped by adding chilled 0.5 M Na_2CO_3, and the released fluorescent 4-MU was measured in a Clariostar OPTIMA plate reader (BMG Labtech, Ortenberg, Germany) with an excitation at 360 nm and emission at 460 nm. A standard curve for free 4-MU was used to calculate the enzyme activity. Results were calculated as total Units of enzyme activity (nmol/hr) and normalised with respect to protein content.

2.2.1.4 Protein quantitation assay

Sample fractions EL or TL were mixed at a ratio of 1:1 with radio-immunoprecipitation (RIPA) buffer (Thermo Scientific). Protein concentrations of all tissue fractions and TL were determined using the Bicinchoninic acid assay (BCA Protein Assay Kit, Thermo Scientific). Bovine serum albumin was used as a protein standard, and serial dilutions were prepared from the initial stock concentration of 2 mg/mL to prepare a standard curve. To ensure accuracy and reproducibility, protein assays were performed in triplicate. Absorbance values were measured at 562 nm. Protein concentrations were calculated by linear regression analysis.

2.2.1.5 SDS/PAGE gel preparation and Western blotting

Sample fractions EL and TL were solubilised, and proteins denatured using SDS/PAGE loading buffer (bio rad) and 2-mercaptoethanol (Sigma-Aldrich). Proteins were separated by gel electrophoresis (NW04120BOX, NuPAGE 4%–12% Bis-Tris protein gels, 20X MES buffer). The gel was transferred to nitrocellulose membrane (NC) (Bio-Rad) for protein transfer (X-cell-II blot module, Thermo Fisher Scientific). NC membrane was incubated in 5% skimmed milk. The primary antibodies anti LAMP2

(1:500, PA1-655, Thermo Fisher Scientific), anti-COX IV (1:1,000, Abcam, ab16056) and anti-Phospholamban (1:1,000, Abcam, ab85146) were incubated. Goat anti-rabbit antibody (1:2,500, Dako P0448) was used as the secondary antibody to detect the protein markers of lysosomes, mitochondria and SR, respectively. The secondary antibodies were detected via chemiluminescence using Westar Supernova (XLS3, 0020, Cyanogen) and the protein bands were visualized in a ChemiDoc XRS + imager (Bio-rad with image Lab software).

2.2.1.6 Liquid chromatography-tandem mass spectrometry analysis

Liquid chromatography-tandem mass spectrometry analysis was performed by Roman Fischer and Georgina Berridge at the Target Discovery Institute, University of Oxford. The samples were reduced by adding 5 µL of 200 mM dithiothreitol (30 min at room temperature), and 20 µL of 200 mM iodoacetamide was added to alkylate (30 min at room temperature). The protocol was followed by methanol-chloroform precipitation. Protein pellets were resuspended in 6 M urea in 400 mM Tris-HCl, pH 7.8. In the next step, diluted 1 M Urea was used (diluted using 400 mM Tris-HCl, pH 7.8), and the proteins were digested using trypsin overnight at 37 °C (trypsin was used in a ratio of 1:50). Peptides were acidified using formic acid, and the final concentration of formic acid was 1%. Then the samples were desalted on Sola HRP SPE cartridges (Thermo

Fisher Scientific), and peptides were dried entirely in a Speed-Vacuum for up to 3-6 hours.

Samples were further desalted online (PepMAP C18, 300 µm x 5 mm, 5 µm particle, Thermo Fisher Scientific) for 1 min at a flow rate of 20 µL/min and separated on an EASY-Spray column (PepMAP C18, 75 µm x 500 mm, 2 µm particle, ES803, Thermo Fisher Scientific) over 60 min using a gradient of 2–35% acetonitrile in 5% DMSO, 0.1% formic acid at 250nL/min. Separation and analysis was performed on a Dionex Ultimate 3000 RSLC system coupled to an Orbitrap Fusion Lumos platform (both Thermo Fisher Scientific) using standard parameters (Universal Method (Davis *et al.*, 2017)) . MS scans were acquired at a resolution of 120,000 between 400 and 1,500 m/z and an AGC target of 4.0E5. MS/MS spectra were acquired in the linear ion trap (rapid scan mode) after collision-induced dissociation (CID) fragmentation at a collision energy of 35% and an AGC target of 4.0E3 for up to 250 ms, employing a maximal duty cycle of 3 s, prioritising the most intense ions and injecting ions for all available parallelisable time. Selected precursor masses were excluded for 30 s (Davis *et al.*, 2017).

Raw data was analysed with assistance from Dr Holger Kramer from Biological Mass Spectrometry and Proteomics Facility, MRC London Institute of Medical Sciences, Imperial College London. Mass spectrometry data quantitative analysis were performed using the MaxQuant software platform (Cox and Mann, 2008) (version 1.6.2.3). Database searches were carried out against the UniProt *C. porcellus*

database (UP000005447_10141). A reverse decoy database was created, and results displayed at a 1% FDR for peptide spectrum matches and protein identifications. Search parameters included: trypsin, two missed cleavages, fixed modification of cysteine carbamidomethylation and variable modifications of methionine oxidation and protein N-terminal acetylation. Label-free quantification was performed with the MaxLFQ algorithm with an LFQ minimum ratio count of 2. 'Match between runs' function was used with match and alignment time limits of 0.7 and 20 min, respectively. The mass spectrometry proteomics data have been deposited to the ProteomeXchange Consortium via the PRIDE partner repository with the dataset identifier PXD021277 (reproduced with permission from Ayagama *et al.*, 2021).

2.2.2 Quantification and statistical analysis

2.2.2.1 Quantitative analysis of mass spectrometry data

Quantitative analysis of significant differences between the protein abundance of EL and TL samples and data visualisation was performed using the Perseus software platform (Tyanova et al., 2016) (version 1.5.2.4) using LFQ values of biological replicates. Data for peptides where more than two values were absent from six

biological replicates were excluded from the quantitative analysis and distributions of excluded values between the EL and TL fractions are represented in the Venn analysis shown in Figure 2:5B. Remaining data with no more than 2 missing values were uploaded as a data matrix in Perseus with the respective LFQ intensities as main columns. The data matrix was reduced by filtering based on categorical columns to remove protein groups only identified by site, reverse decoy hits and potential contaminants. A total of 2,436 proteins remained after filtering. Groups of biological replicates for EL and TL fractions were defined in categorical annotation rows. Data were log transformed (log2(x)) and normalised via median subtraction. Missing data points were imputed based on normal distribution and visualized as LFQ intensity histograms (per biological replicate) with imputed values shown separately (Figure 2:5A). Within the EL fraction, this corresponded to only 7% of proteins, and the inclusion of imputed values did not affect the normal distribution of data as confirmed using D'agostino and Pearson omnibus K2 test (Graphpad Prism v8). Principal component analysis (PCA) (Figure 2.4F) was performed on 100% valid values. A volcano plot was generated based on LFQ intensities applying two-way Student's t-test to probe for significant difference of protein abundance between EL and TL samples (Figure 2.6A). A permutation-based false-discovery rate (FDR) was determined with 250 randomizations and S0 = 0.1 (default). Out of the total 2,436 proteins, 1,254 proteins were accounted with 99% confidence level at 5% FDR. Of these 690 proteins were significantly depleted in EL compared to TL, and 564 proteins were significantly enriched in EL (Figure 2.6A).

For comparison with previously published proteomic data for human atria (Doll et al., 2017) LFQ intensity histograms were plotted for pooled TL data from the current study and compared with LFQ intensities published by Doll et al. (2017) for human left and right atria (Figure in appendix, A1:1)

2.2.3 Network analysis

Statistically enriched proteins acquired from the volcano plot were used for the functional networks, using Cytoscape (Shannon *et al.*, 2003) (Version 3.7.2) and Panther pathway analysis software (Mi *et al.*, 2021) (Figure 2.6B). The lists of *C. porcellus* proteins were converted to H. Sapiens with UniProt ID-retrieve and mapped to identify the reviewed proteins with 100%–50% similarity in the molecular function through molecular pathways. To investigate associations and relations between EL proteins, the Cytoscape 3.7.2. programme was used, and protein interactions were extracted from the STRING, KEGG and Reactome databases. Medium confidence of 0.4 was selected for the protein match to the molecular networks. STRING identified a total number of 125 proteins in a single functional network and 7 proteins in a detached cluster within the endo-lysosomal compartment.

564 of the highest abundant EL fraction proteins were selected and clustered into a main network, and applied perfused force directed layout on the network using

clusterMaker 2.8.2 (Morris *et al.*, 2011). Functional enrichment analysis was performed for the two clusters. Pearson correlation coefficient, heat maps, PCA and histograms (Figures 2.4 and 2.5A) were produced to assess the reliable correlation between the sample triplicates. The heat maps were produced using Euclidian distance and K-mean clustering. Plots were generated using Perseus software (v. 1.5.2.4) and presented for publication using Instant Clue (Nolte *et al.*, 2018). The protein profile plots were created using Pearson clustering. The unavailability of the characterized whole guinea pig proteome limitation was minimized by automatic selection of 100%–50% overlapped proteins with the closest species in the phylogenetic tree, and these automatic selections were performed by proteome databases such as Uniprot, and proteomic tools Perseus, String, Panther Pathway, and Cytoscape.(Ayagama *et al.*, 2021).

2.3 Results

2.3.1 Density gradient approach toward acidic organelle isolation from *C. porcellus* atria

An overview of the workflow is shown in Figure 2:1. In order to capture lysosomal-specific proteome data in guinea pig (*C. porcellus*) atrial frozen biopsies, I further developed a density gradient organelle isolation protocol based on previous work

(Graham, 2001 and Lamberti *et al.*, 2015). The first stage was to eliminate tissue debris and plasma membrane by brief ultra -centrifugation. The supernatant enriched in SR, Mito, lysosomes, endosomes, and endo-lysosomes (ELs) were then separated by differential density gradient based ultra-centrifugation. The much denser organelles such as crude Mito with mature lysosomes and most of the SR content were separated from the soluble fraction at this stage. A high degree of purity of the EL-enriched fraction was achieved by a repeated ultra-centrifugation step and confirmed by Western blot (Figure 2:4B). The final fraction was then subjected to differential density gradient levels to partition proteins into specific compartments with respective buoyant densities.

2.3.2 Validation of lysosomal proteins using lysosomal enzymes and immunoblotting assays

The comparison of proteomic data with previously published data for human atria (Doll et al., 2017) was performed by Samuel J Bose, Department of Pharmacology, University of Oxford. The main fractions, tissue lysate (TL), EL, and Mito, were validated for organelle enrichment by lysosome enzyme assays and Western blotting (Figures 2.4A and 2.4B). Lysosomal activities of β-galactosidase and β-hexosaminidase were assayed in TL, Mito, EL, and the remaining gradient fractions

from Dunkin Hartley guinea pig atria (Figure 2.4A, N = 3). Figure 2.4A shows total units of activity for each enzyme in each fraction.

Western blotting was conducted to analyse the presence of EL membrane proteins by blotting against LAMP2 (Figure 2.4B). The absence of the predominant organelles such as SR and mitochondrial membranes were examined by the SR marker protein phospholamban and inner mitochondrial membrane marker protein COX IV. I observed clear band visibility of LAMP2 in all the biological replicates of EL and TL. Phospholamban and COX IV were negligible in EL (Figures 2.4B and 2.3A. In addition, Western blotting was carried out using glyceraldehyde 3-phosphate dehydrogenase as a loading control (Figure 2.3B).

Sample intensity distributions showed high similarity, with Pearson correlation coefficients of >0.9 (TL) and >0.8 (EL) for intra-group comparisons (Figure 2.4C), with density histograms of the LFQ intensity data assuring the near-normal distribution of protein intensities between the TL and EL in three biological replicates showing technical reproducibility (Figure 2:5A).

In comparison, the distribution of protein intensities from our data was compared with that previously published for human atria by Doll et al. (2017), with both data sets showing similar patterns of distribution (Figure A1:1).

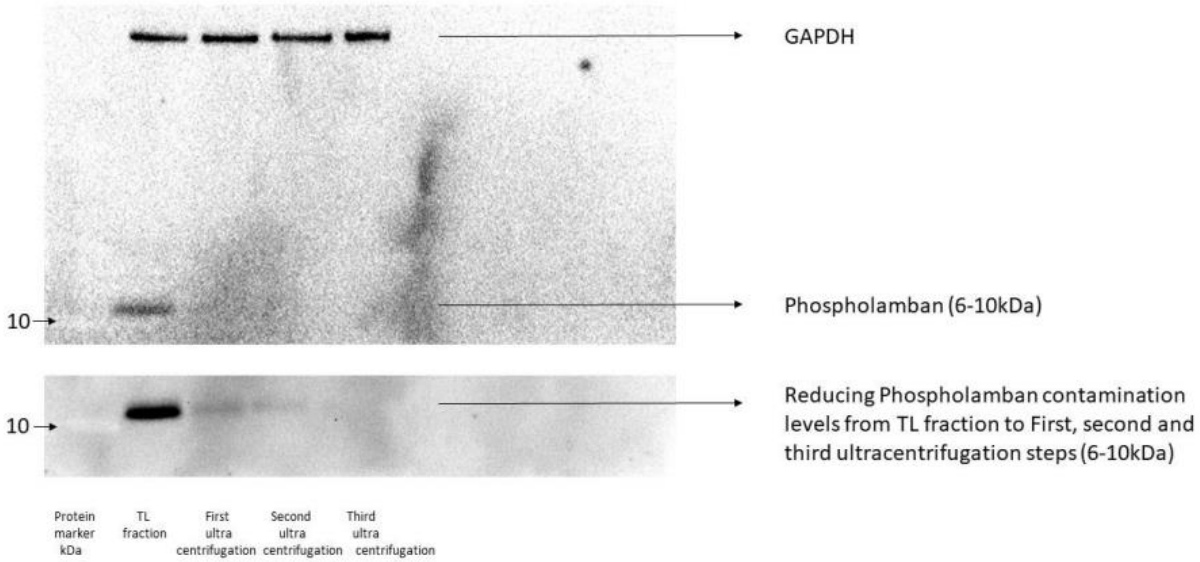

Figure 2:2 Confirmation of purity of EL enriched fractions, related to Figures 2:1 and 2:4. *Western blot demonstrates increasing purity of EL enriched fractions as shown by reduced levels of phospholamban from the TL fraction to the first, second and third ultracentrifugation steps. Bottom panel shows same blot without GAPDH antibody. Figure published and reproduced with permission from (Ayagama et al., 2021)*

A

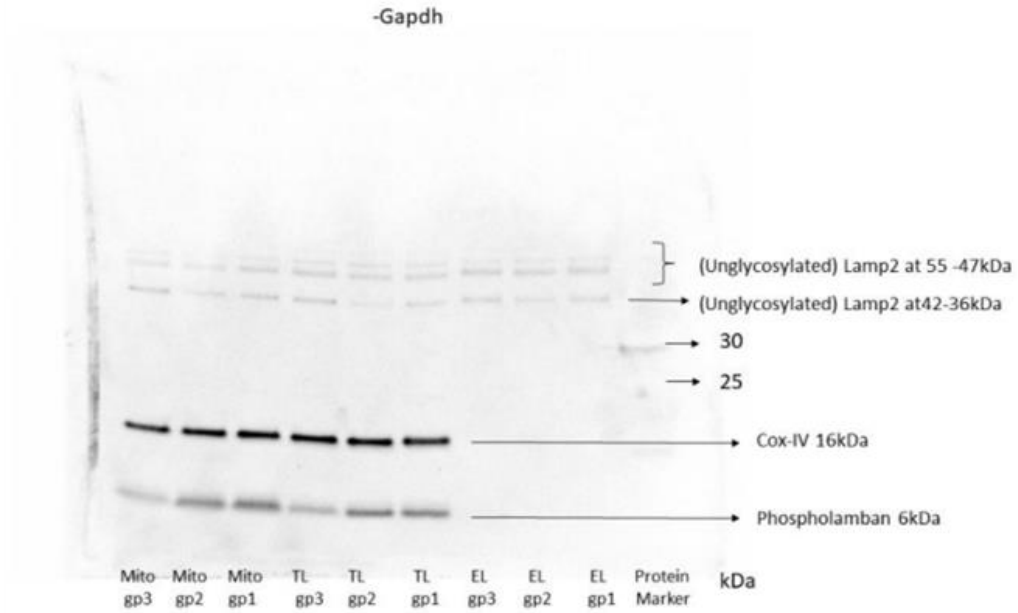
-Gapdh
(Unglycosylated) Lamp2 at 55 -47kDa
(Unglycosylated) Lamp2 at42-36kDa
30
25
Cox-IV 16kDa
Phospholamban 6kDa
Mito gp3
Mito gp2
Mito gp1
TL gp3
TL gp2
TL gp1
EL gp3
EL gp2
EL gp1
Protein Marker
kDa

B

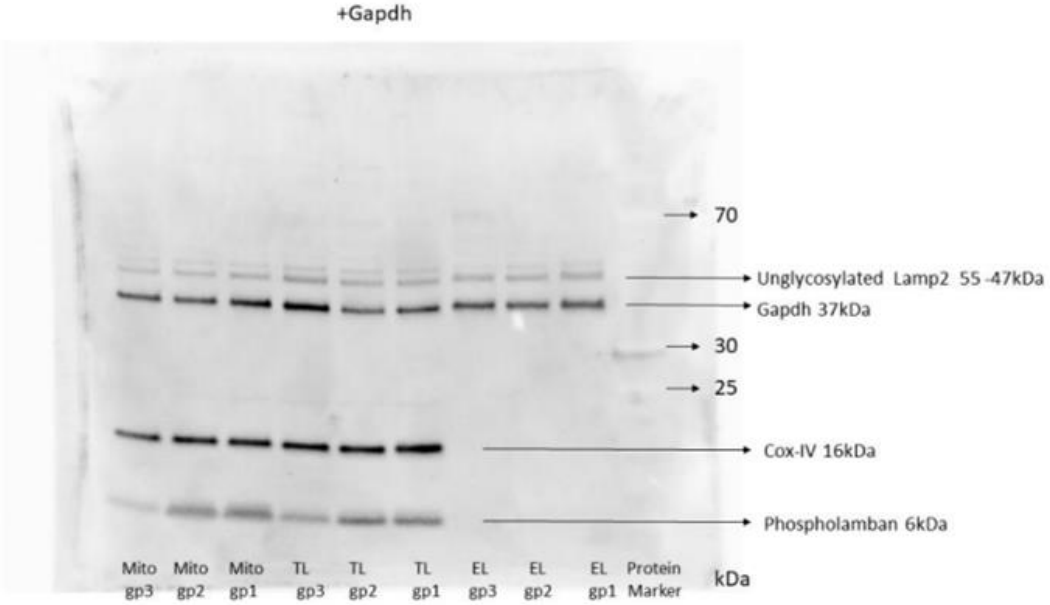
+Gapdh
70
Unglycosylated Lamp2 55 -47kDa
Gapdh 37kDa
30
25
Cox-IV 16kDa
Phospholamban 6kDa
Mito gp3
Mito gp2
Mito gp1
TL gp3
TL gp2
TL gp1
EL gp3
EL gp2
EL gp1
Protein Marker
kDa

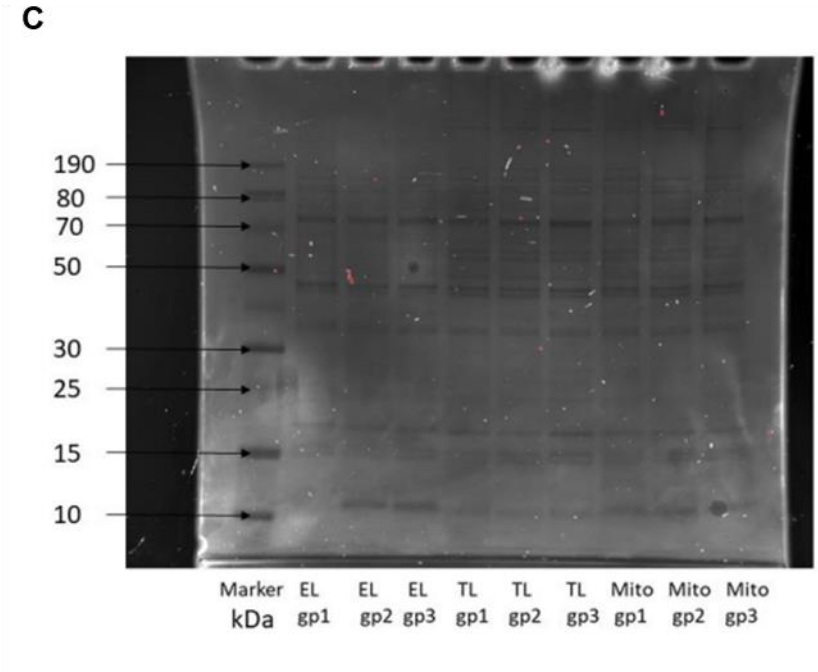

Figure 2:3 Western blots for markers for lysosome (LAMP2), Mitochondria (COXIV) and SR (phospholamban), related to Figure 2:4. A, *Complete Guinea pig (n = 3) Western blot corresponding to Figure 2:4B. The Western blots of the guinea pig atrial tissue used for lysosome assays displayed positive COXIV bands for the presence of mitochondria in Mito fraction and TL. EL fractions did not display bands for COXIV.* ***B,*** *Guinea pig (n = 3) Western blots including Gapdh loading control.* ***C****, Coomassie stained gel demonstrating protein loading. Figure published and reproduced with permission from (Ayagama et al., 2021)*

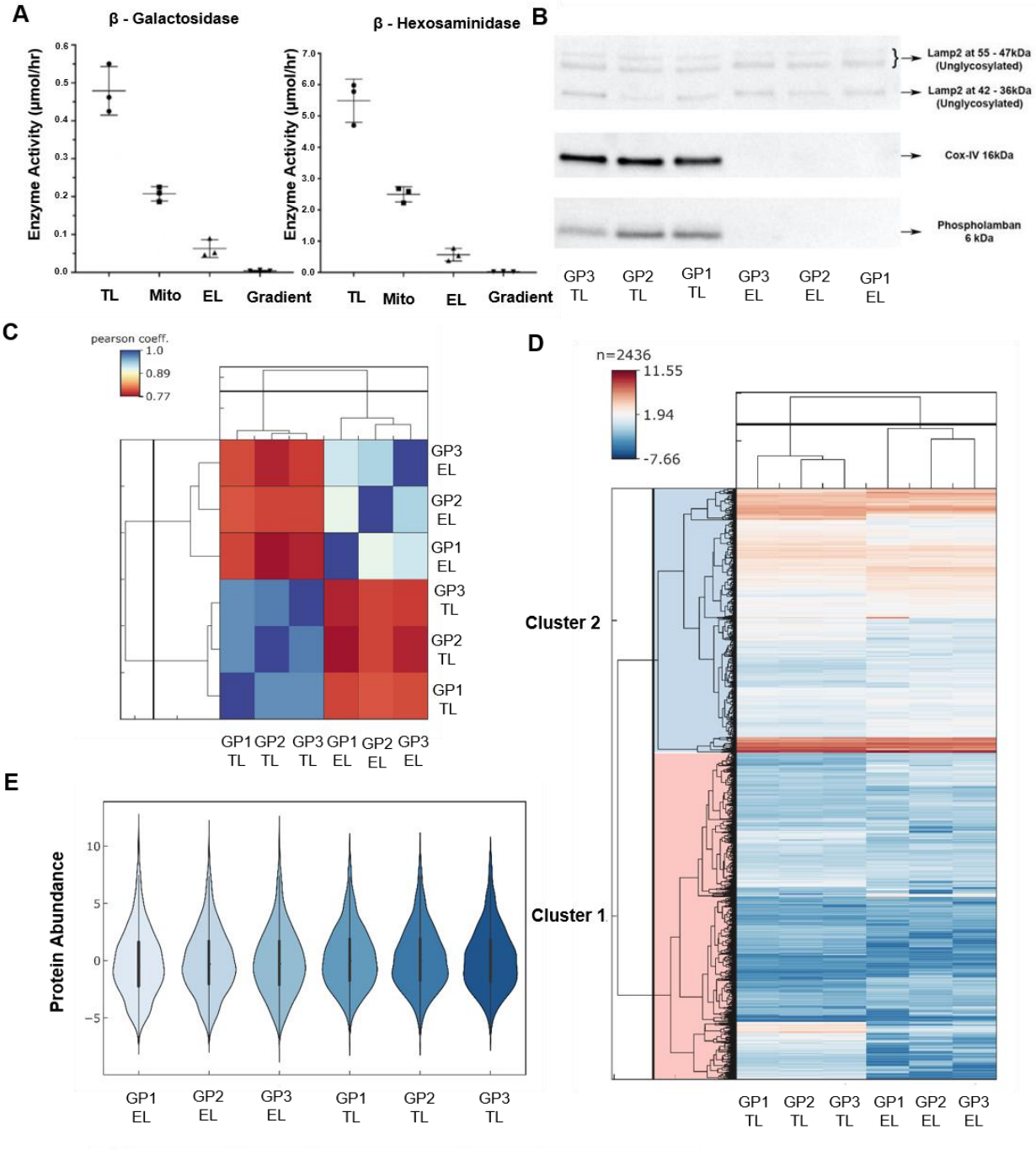
A
β - Galactosidase
β - Hexosaminidase
Enzyme Activity (µmol/hr)
TL
Mito
EL
Gradient
B
Lamp2 at 55 - 47kDa (Unglycosylated)
Lamp2 at 42 - 36kDa (Unglycosylated)
Cox-IV 16kDa
Phospholamban 6 kDa
GP3 TL
GP2 TL
GP1 TL
GP3 EL
GP2 EL
GP1 EL
C
pearson coeff.
1.0
0.89
0.77
D
n=2436
11.55
1.94
-7.66
Cluster 2
Cluster 1
E
Protein Abundance
F
Component 2 (14.1 %)
Component 1 (69.9 %)

Figure 2:4. Expression of protein abundancy and technical reproducibility

(A) Beta – galactosidase and Beta – hexosaminidase enzyme activities in adult guinea pig atria (n = 3). Lysosomal hydrolase activities (total Units G SD) were measured in EL, Mito (which contain dense lysosomes) and as well as TL using artificial 4-MU-substrates. (B) Western blots performed in guinea-pig atrial tissue: LAMP2, COXIV and Phospholamban (n = 3). Identification of lysosome, mitochondria, and SR organelle levels between (TL) and EL fraction. For clarity, only relevant rows and columns are shown. (C) Pearson co-efficient correlation plot values show the positive or direct correlation between the reliability of the triplicated samples. (D) Heatmap of z-scored protein abundances (LFQ intensities) of the differentially expressed proteins after unsupervised hierarchical clustering. (E) Violin plot shows distribution of peptide abundance from EL fraction to TL among the triplicates. (F) Principal component analysis (PCA) of the six atrial samples based on their proteomic expression profiles. Each data point represents the total protein groups in each sample as a single vector. The components 1 and 2 represent the spatial resolution among the vectors. The average of vectors corresponds to a point in the K-space. Component one explains 69.9% of the variation, component two 14.1%. Red: TL, Blue: EL. Panels (C and D) generated using Perseus 1.5.2.4 and redrawn using Instant Clue (Nolte et al., 2018). Figure published and reproduced with permission from (Ayagama et al., 2021)

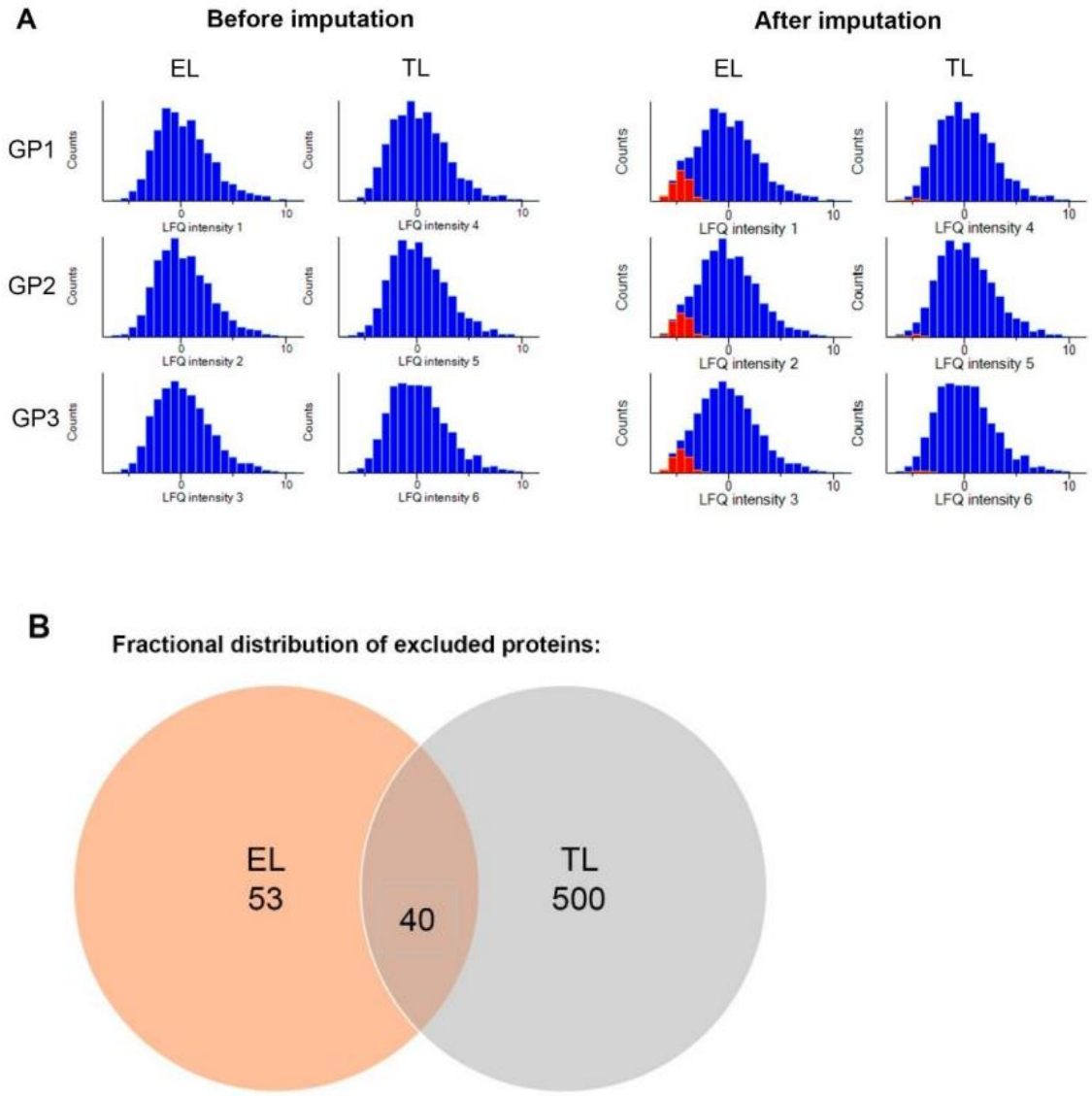

Figure 2:5. Technical reproducibility of proteomic measurements and representation of quality control. A, *Histograms generated before (i) and after (ii) inclusion of imputed values: Histograms are produced of the triplicated LFQ intensity datasets, demonstrating the normal distribution of protein intensities. In ii, contributions of imputed values are shown separately in red. Data was median subtracted for normalisation.* ***B,*** *Venn diagram representing relative distribution between fractions for proteins with more than two missing values that were excluded from subsequent analysis; EL = 53, TL= 500 and 40 proteins were detected in both EL+TL. Figure published and reproduced with permission from (Ayagama et al., 2021)*

2.3.3 Differential protein distribution using quantitative proteomic analysis

For overall assessment of functional protein resemblance between the fractions, unsupervised hierarchal clustering was employed on 2436 *C. porcellus* proteins. Gene ontology annotations identified a statistically different abundance of protein groups between the fractions (FDR<0.05). A heat map was generated (Figure 2.4D), where color representation from blue to red demonstrates lowest to highest relative abundance of the protein groups in EL compared with TL. The protein groups represented in white showed no significant difference between the protein intensity leading to different levels of expression in the protein groups. The differential distributions of protein abundance from EL to TL are demonstrated using violin plots in Figure 2.4E. Principal component analysis (PCA) reduced the data dimensions for simpler interpretation (Figure 2.4F). As indicated in Figure 2.4F, vector deviation of 69.9% was observed between TL (red symbols) and EL fractions (blue symbols). An exceptional 14.1% segregation was observed in the first biological replicate of EL. I observed a higher level of mitochondrial proteins in the TL vectors than in EL, such as proteins involved in electron transport chain (e.g.: A0A286XXR8/NDUFB4, H0V9U7/NDUFB9 (Wu *et al.*, 2016b)), whereas EL contained proteins from endosomal and endocytic trafficking pathways (e.g.: A0A286XGA7/TOM1 (Masters *et al.*, 2017), A0A286XNV7/ADIPOQ (Wang *et al.*, 2017), A0A286Y1Z7/ CDC42 (Sirokmány *et al.*, 2006)). The molecular functional differences were clearly distinguished in the PCA plot.

2.3.4 Functional networks within endo-lysosomes

Proteins demonstrating differential abundance between TL and EL fractions were identified using volcano plot (Figure 2:6A). Of a total of 2,436 quantified proteins, 690 accounted as depleted in EL, demonstrating higher abundance in TL fractions (Figure 2:6A, blue), whereas 564 proteins accounted for the most enriched hits corresponding to higher abundance in EL (Figure 2.6A, red). The functional networks of the quantified, statistically significant enriched proteins acquired from volcano plot analysis were mapped using several genomic and proteomic annotations (detailed description in methods section). The STRING network created by Cytoscape generated 125 proteins involved in a single functional network, and 7 proteins displayed a detached cluster that were not connected to any functional edge (Figure 2:6B).

The biological interactions of the leading network (Figure 2:6B) display a single network which is based on 4 functional annotations. These annotations are based on information from published databases, experiments, co - occurrence and co-expression data (www.cytoscape.org) (Shannon *et al.*, 2003). A color scale depicts the functional annotations.

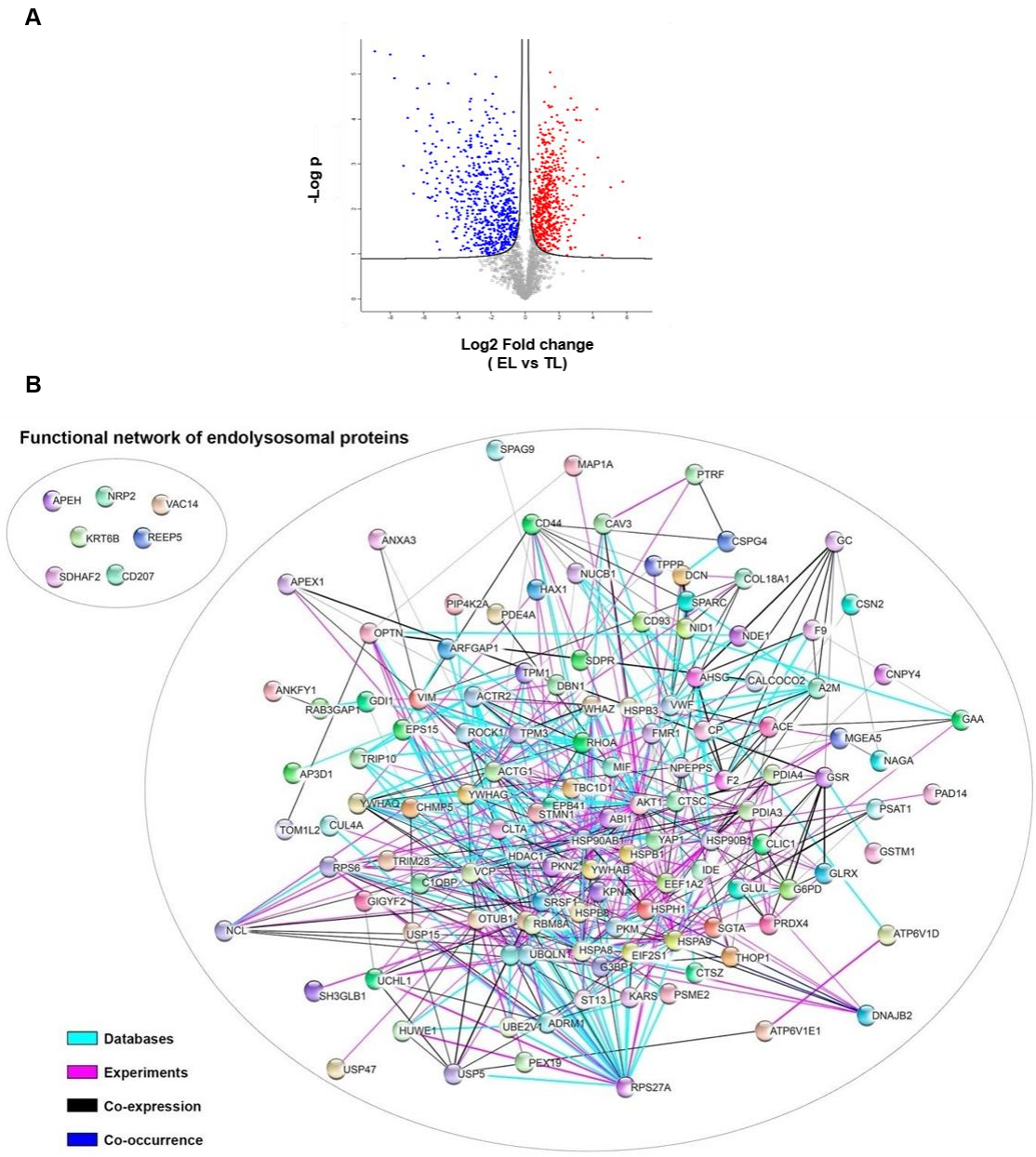

Figure 2:6 Profile of the endolysosomal proteins in EL fraction at a glance

(A) *Volcano plot is plotted against the –log2 transformation of the p values vs. the protein abundance differences in EL and TL. Significantly higher abundant proteins in EL compared with TL are highlighted in red and less abundant in blue, respectively (FDR 0.05).* ***(B)*** *EL fraction proteins were clustered using Cytoscape consortium 3.7.2 with String, KeGG, GO, and Reactome pathway annotations. Proteins were clustered using median confidence score (0.4) and the molecular pathway parameters (edges) were filtered to databases, experiments, co-expression, and co-occurrence. Figure published and reproduced with permission from (Ayagama et al., 2021).*

and the fading of the color displays the strength of the evidence. In addition to the EL network analysis, I performed a separate functional enrichment analysis using gene ontology (GO) pathway analysis; the most abundant protein IDs of the EL fraction were converted to human protein IDs and uploaded to the GO analysis software ShinyGO v0.61 (Ge *et al.*, 2020). Using cell component filtration, the 10 most significant cell components were identified. The highest number of protein IDs (188) belonged to the vesicle trafficking component, suggesting the identified EL proteins are localized to the endo-lysosome route of the cell (Schröder *et al.*, 2007) and (Martin-Serrano *et al.*, 2003) (Data table A1:3 ,presented in the appendix).

2.3.5 PANTHER gene annotation pathway analysis

The protein profile of EL (Figure 2:7A) and TL (Figure 2:7B) was analyzed using the PANTHER pathway database (www.pantherdb.org) using a total of 1,254 quantified proteins. The most enriched EL fraction proteins (564) and the proteins most abundant in TL (690) were plotted with mapped gene identifiers, using pie charts to demonstrate the overall representation of protein groups by molecular function categories.

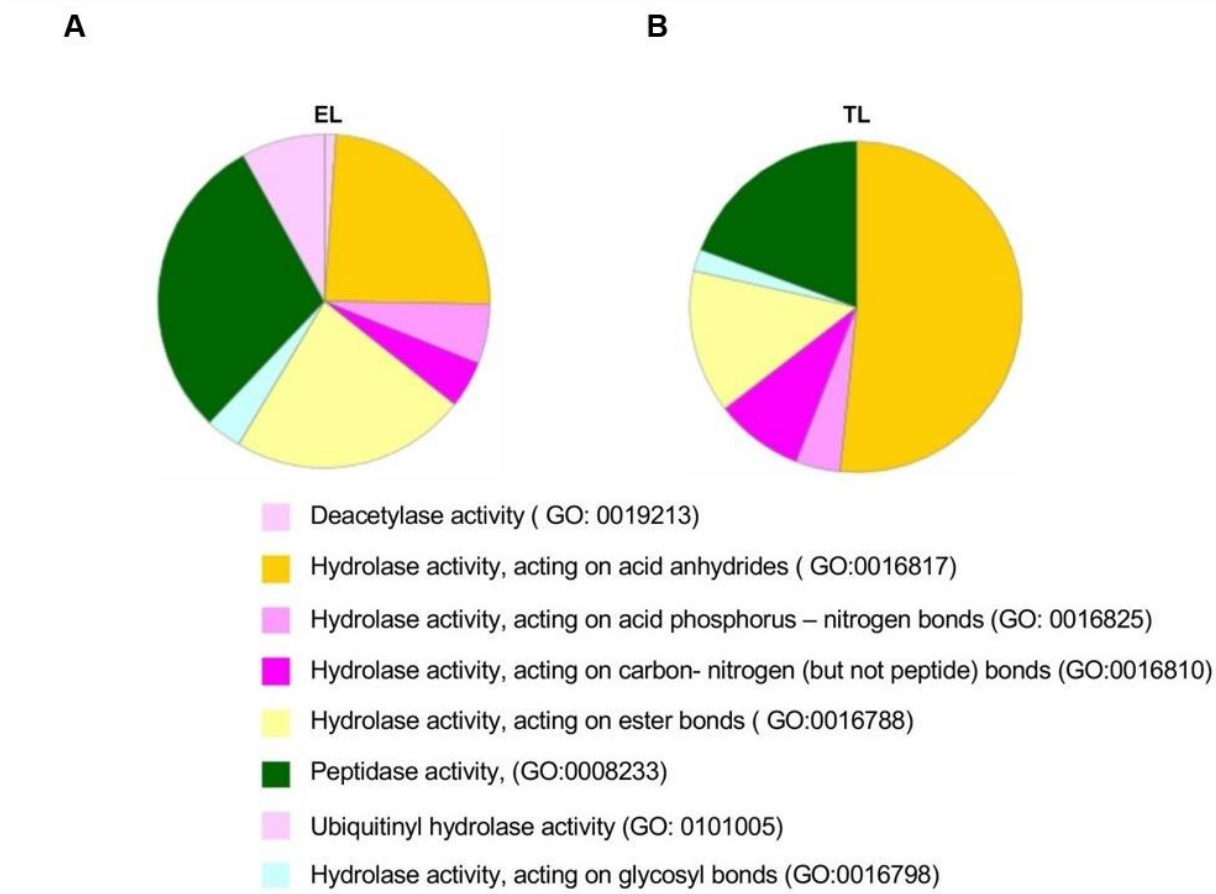

Figure 2:7. Gene ontology panther pathway analysis
*(**A** and **B**) The molecular function of the endo-lysosome fraction (EL) showed 39% of catalytic activity, whereas the molecular function of the tissue lysate (TL) showed 42.8% of catalytic activity. The catalytic hydrolase activity was further analysed for individual hydrolase activity, EL fraction (A) showed higher peptidase activity compared with TL (B). Figure published and reproduced with permission from (Ayagama et al., 2021).*

The EL fraction and TL displayed, respectively, 39% and 42.8% of the catalytic activity. The catalytic representation of the EL and TL was categorized according to the hydrolase enzyme groups. The percentages between EL and TL were, respectively, as follows: peptidase (29.9%, 19.4%), hydrolase acting on carbon-nitrogen (but not peptide) (4.8%, 8.6%), hydrolase acting on ester bonds (23.8%, 14%), hydrolase acting

on acid anhydrides (25%, 51.6%), hydrolase activity acting on glycosyl bonds (2.4%, 2.2%), and hydrolase activity acting on acid phosphorus-nitrogen bonds (4.8%, 4.3%). Lysosome-specific cathepsins were highly abundant in the peptidase category found in the EL fraction. In contrast, cytochrome oxidases of mitochondrial origin were highly abundant in TL.

2.3.6 Organelle expression profile

Our data demonstrate the presence of lysosomal markers β -galactosidase, β -hexosaminidase, Rab7A, and LAMP2 in our EL preparations and the absence of markers from mitochondria (COX IV) and ER (Calnexin protein) (Bagshaw *et al.*, 2005), with fewer cytochrome C reductase proteins (ER marker; H0VNA2/CYC1, A0A286Y030/NDUFA4 in EL and A0A286XMD6/UQCRFS1, CYC1, NDUFA4, A0A286XTF9/UQCRB, H0W408/UQCRQ, H0VIM6/UQCR10 in TL) (Bagshaw *et al.*, 2003). Key proteins identified are summarized in Table A1:1 provided in the appendix.

2.3.7 Pathway analysis of EL, endosome, and lysosomal proteins

Most of the proteins identified had a direct connection with the structural biology of endo-lysosomes, lysosomes, and functions related to their membranes, whereas some

proteins identified had a functional role in lysosome biogenesis and endocytic processes. The following sections provide details of some of the key proteins identified in our study, as well as their known associations according to previously published data.

a) Proteins involved in endosomal/ lysosomal functions

Multiple proteins linked to endocytosis, including AP2A1, LRP1, and APOE (Actis Dato *et al.*, 2020) were identified. AP2A1 is a key regulator of endosomal/lysosomal protein sorting pathways (Nakatsu and Ohno, 2003), whereas LRP1 and APOE are involved in cholesterol metabolism (Bilousova *et al.*, 2019). H0UWL7/ ACE and H0VDM6/ITGB1 have been recognized in hypertrophic cardiomyopathy disease pathways (Yuan *et al.*, 2017 and Wang *et al.*, 2020). HSPA8 is linked to Parkinson's disease, where it is involved in the impairment of lysosomal autophagy. HSPA8 may contribute to lysosomal storage disorders (LSDs) as a functional component of lysosome vesicle biogenesis (Rudenok *et al.*, 2019). Many Rab proteins were categorized under Rab-regulated trafficking, membrane trafficking, and endocytosis (Table (A 1:1)). I found numerous proteins, such as V-type ATPase proton pumps commonly expressed in lysosomes and lysosome-related organelles, including ATP6V1D (A0A024R683) (Schröder *et al.*, 2007) (Table (A 1:1)). In addition, I identified the endosomal proteins Flotillin-1 (A0A286XE27) (Schröder *et al.*, 2007) and CHMP5 (Q9NZZ3) (Martin-Serrano *et al.*, 2003) in our EL fractions.

Atrial tissue-specific protein markers such as myosin heavy chain 6 (MYH6/A0A286Y2B6), myosin heavy chain 7 (MYH7B/H0V2M2), peptidylglycine alpha amidating monooxygenase (PAM/H0VJZ4), and natriuretic peptide A (NPPA/H0VXX0) reported in previous cardiac proteomic studies (Doll *et al.*, 2017) were identified in our TL.

b) Acidic organelle proteins related to cellular Ca^{2+} and ion channels

EEA1, a phosphoinositide binding domain, and b1-integrin, which has a functional role related to two-pore channels (TPCs), were observed in our proteomic profiles (Nguyen *et al.*, 2017) and (Itoh and Takenawa, 2002). Inhibition of TPC function in metastatic cancer cells has been shown to prevent trafficking of β1-integrin, leading to accumulation within EEA1-positive early endosomes and preventing cancer cell migration (Nguyen *et al.*, 2017).

EH domain-containing proteins function as retrograde transport regulators and retrograde trafficking mediates the transport of endocytic membranes from endosomes to the trans-Golgi network (Zhang *et al.*, 2012). Our study identified several proteins involved in retrograde transport and trafficking including EHD 2 and 4, Ankyrin, Vps 35, and Annexin A. A 2010 study by Gudmundsson et al. (2010) showed that EHD1-4

directly associate with Ankyrin, providing information on the expression and localization of these molecules in primary cardiomyocytes and demonstrating that EHD1-4 are co-expressed with ankyrin-B in the myocyte perinuclear region. Significant modulation of EHD expression follows myocardial infarction, suggesting that EHDs may play a key role in regulating membrane excitability in normal and diseased hearts (Gudmundsson *et al.*, 2010). Retrograde transport is important for many cellular functions, including lysosome biogenesis where Vps35, a subunit of retromer, interacts with the cytosolic domain of the cation independent mannose 6-phosphate receptor to mediate sorting of lysosomal hydrolase precursors to endosomes (Arighi *et al.*, 2004). Annexin A2, another protein involved in acidic organelle Ca^{2+} binding and the endocytic pathway, is capable of active Ca^{2+} dependent plasma membrane resealing in vascular endothelial cells (Koerdt and Gerke, 2017), interacts with the lysosomal N-ethylmaleimide-sensitive factor attachment protein receptor (SNARE) VAMP8, and facilitates binding of VAMP8 to the autophagosomal SNARE syntaxin 17 to modulate the fusion of auto-phagosomes with lysosomes (Bustos *et al.*, 2017).

Dysferlin (DYSF) acts as a Ca^{2+} sensor in Ca^{2+} triggered synaptic vesicle-plasma membrane fusion in myocytes (Rubi *et al.*, 2015). Mutations in DYSF cause limb-girdle muscular dystrophy type 2B (LGMD2B) due to defective Ca^{2+} dependent, vesicle-mediated membrane repair (Liu *et al.*, 1998). Loss of DYSF causes death of cardiomyocytes, notably in aging hearts, leading to dilated cardiomyopathy and heart failure in patients with LGMD2B (Wei *et al.*, 2015). These observations in conjunction

with our data demonstrate the need for further studies related to the role of DYSF in cardiac atrial pathology.

Annexin 6, involved in Ca^{2+} binding to cellular membranes such as those of acidic organelles including late endosomes (de Diego *et al.*, 2002), were identified from our proteomic studies. As a regulator of the apical membrane events of the placenta, Annexin 6 binds in both a Ca^{2+} dependent and in a Ca^{2+} independent fashion (Riquelme *et al.*, 2004). Annexin 6 is also involved in the trafficking events between endocytic compartments and lysosomes leading to degradation of low-density lipoproteins (LDLs) (Pons *et al.*, 2001).

2.4 Discussion

This chapter presents a modified density gradient method of EL organelle isolation suitable for use with frozen cardiac tissue samples of at least 100 mg (Ayagama *et al.*, 2021). After confirming the identity and purity of these fractions using enzyme activity assays (Figure 2:4A) and Western blots (Figures 2:3 and 2:4B, I performed label-free liquid chromatography with tandem mass spectrometry (LC-MS/MS) peptide analysis and presented a comprehensive data set of *C. porcellus* EL focused organelle proteomics.

The importance of lysosomes for cardiac protein turnover and the role that changes in these organelles have to this function has been known for several decades (Wildenthal and Decker, 1980). Despite this, lysosomes have remained relatively understudied in terms of a possible role in cardiac pathogenesis. Several lysosomal storage diseases may present with cardiac abnormalities as part of disease progression, e.g. hypertrophy and conduction dysfunction in Anderson-Fabry's disease (Nair *et al.*, 2019) and (Linhart and Elliott, 2007). More recently, a role for lysosomes and endo-lysosomes as acute signaling organelles has been identified in a number of cell types (Zhu *et al.*, 2010) and (Burton and Terrar, 2021) including both atrial (Collins *et al.*, 2011) (Capel *et al.*, 2015)and ventricular (Capel *et al.*, 2015) , (Aston *et al.*, 2017 and Macgregor *et al.*, 2007) cardiomyocytes. These observations spark a renewed interest in the function and protein composition of lysosomes and endo-lysosomes in this tissue. However, proteomic databases of cardiac lysosomes have not been published to this point.

The involvement of lysosomes in cardiovascular disease has been of interest for decades. Early observations presented in patients undergoing open-heart surgery suggested that the number of lysosomes in the right atrium is increased in patients with atrial septal defects (Wheat, 1964), (Wheat, 1965) and (Kottmeier and Wheat, 1967) . Following these observations, in 1967, Kottmeier and Wheat (Kottmeier and Wheat, 1967) pursued experiments to see if similar findings could be produced in an experimental model. They found that the number of lysosomes increased significantly following the creation of atrial septal defects in dogs, with the most marked increase

occurring in the right ventricle providing early evidence to support the role of the lysosome as an important intracellular organelle which is related to cellular stress.

Cardiomyocytes are responsible for the beat of the heart and make up the bulk of cardiac tissue by volume (Tang *et al.*, 2009). These cells are structurally specialized for excitation-contraction coupling, containing large numbers of contractile filaments and mitochondria by volume. Although cardiomyocytes dominate heart tissue volume, non-myocytes (e.g. fibroblasts, endothelial cells, vascular smooth muscle) are greater by nuclear number (Kohl and Camelliti, 2007), (Pinto *et al.*, 2016). Consequently, whole tissue analysis of the cardiac proteome is dominated by contractile, mitochondrial, and cell/ECM structural proteins. For instance, Doll et al. (2017) found 25% of identified protein molecules were from just six proteins in human heart tissue samples, of which two were contractile and two structural (Doll *et al.*, 2017). Robust conclusions regarding the effects of physiology and disease on the proteome of other organelles therefore requires accurate enrichment of the organelle of interest. An elegant method to purify endo-lysosomes from cultured HeLa cells utilizing superparamagnetic iron oxide nanoparticles was published in 2017 (Tharkeshwar *et al.*, 2017). A similar approach utilising the uptake of latex beads was shown to allow endosome purification in cultured macrophages (Lamberti *et al.*, 2015). Both of these methods, however, rely upon the uptake of particles to live cells, limiting their utility for analysis of frozen samples, such as might be available from large-animal and/or patient biopsies for clinical cardiac projects. The LOPIT method (Dunkley *et al.*, 2004) on the other hand requires proteomic runs of a large number of cellular fractions, making it prohibitively expensive

for smaller research groups. Instead, I focused on improving the specificity and purity of samples produced by density-based fractionation.

Lysosomes and endo-lysosomes at different stages of their maturation pathway show a wide variety of densities which overlap markedly with other cellular organelles (Graham, 2001), (Hibbs *et al.*, 1965), (Wolff and Pertoft, 1972), (Peters and De Duve, 1974). By allowing the densest lysosomes to be collected with the Mito fraction, I was able to separate a highly purified EL fraction at a density of 1.04 g/mL containing over 1,200 identifiable proteins by LC-MS/MS analysis. The PRIDE database entry PRIDE: PXD021277). Isolation of this fraction from three separate frozen *C. porcellus* atrial tissue preparations clearly established the technical reproducibility of our method, as indicated by correlation and principal component analyses (Figures 2:4C and 2:4F). Figure 2:4A shows the average (GSD) total enzymatic activity of both for β -galactosidase and β -hexosaminidase when compared with either TL or mitochondrial fractions (Figure 2:4A in each fraction). Although there was only about 10% of each enzyme activity in the EL fraction, contamination from either mitochondria or SR (which can also be found in a range of densities after tissue homogenization) (Graham, 2001) was minimal and confirmed by Western blot analysis, showing that the EL fraction was devoid of COX IV and phospholamban staining, respectively (Figures 2:4B and 2:3). The mitochondrial fraction, which contains mature dense lysosomes and the denser endo-lysosomes, retained 56% of the total enzyme activity. Assay of the pooled remaining gradient fractions contained less than 0.5% of the total activity. I recovered

only 67% of the total activity of each enzyme which was likely to be because of the very low protein concentration in the EL fractions (~100mg/ml) (see appendix table A1.2).

Quantitative proteomic comparisons of TL and EL from three cardiac atrial *C. porcellus* fractionations demonstrated enrichment of endosomal and endocytic trafficking pathways at the expense of mitochondrial proteins such as components of the electron transport chain. In particular, these data identified enrichment of a range of known lysosomal markers within the EL fraction: β -galactosidase, β-hexosaminidase, β-glucosidase, Rab7, and LAMP2.

The EL proteomic data identified the presence of multiple protein hits relevant to diseases that have been linked to dysfunctional lysosomal enzymes. These include lysosomal α-glucosidase (GAA), a key lysosomal enzyme involved in the degradation of glycogen in lysosomes (Hermans *et al.*, 1991), the lysosomal protective protein/cathepsin A/H0VMB1, which serves a protective function by regulating stability and activity of β -galactosidase and neuraminidase enzymes (Galjart *et al.*, 1991) and also plays a role in galactosialidosis (Zhou *et al.*, 1996), Clusterin/H0VVP2, identified as a potential biomarker for the LSD mucopolysaccharidosis (Skrinjar *et al.*, 2018), and Decorin, a protein that when dysregulated contributes to cardiac fibrosis or fibrotic stiffness (Heras-Bautista *et al.*, 2019). Glycogen phosphorylase, brain form, is a lysosomal enzyme identified in our EL fraction that regulates glycogen mobilisation (Mathieu *et al.*, 2016) and plays a prominent role as the only marker protein elevated

in the early-stage of asymptomatic patients with Fabry disease (Doykov *et al.*, 2020). In addition a major complement of lysosomal cathepsins was identified in these proteomic data that have been previously linked with cardiovascular diseases, including cathepsins B, C, D, and Z (Guo *et al.*, 2002), (Moheimani *et al.*, 2012), (Wolinsky *et al.*, 1978), (Letronne *et al.*, 2016), (Wu *et al.*, 2017), (Thottath *et al.*, 2019) and (Campden and Zhang, 2019). The successful identification of such disease-related proteins highlights the potential for use of these techniques in understanding the role of lysosomal proteins in pathology.

Detection of proteins specific to the atria, such as natriuretic peptides A (NPPA/ANP), highlights the utility of such methods to study atrial cardiovascular diseases. The NPPA gene is expressed primarily in the heart, where the expression level is higher in atria than ventricles (Potter *et al.*, 2006).

An important protein detected in the EL fraction was Rab7, a small GTPase that belongs to the Rab family, known to control transport to late endocytic compartments such as late endosomes and lysosomes (Guerra and Bucci, 2016). Rab7 promotes lysosomal biosynthesis and maintains lysosomal function (Distefano *et al.*, 2015). Rab7 is directly or indirectly involved in each event that occurs between early endosomes and lysosomes. Endo-lysosomes are known to serve as intracellular iron storage organelles (Ward *et al.*, 2014). Ferna´ndez et al. (2016) show that increasing intracellular iron causes EL alterations associated with impaired autophagic clearance,

increased cytosolic oxidative stress, and increased cell death and these effects are subject to NAADP (Fernández *et al.*, 2016). Cell death triggered by altered intra-lysosomal iron handling is abrogated by inhibiting RAB7A activity. Alterations in the activity of Rab7 may be associated with cardiovascular diseases, lipid storage disorders, and neurodegenerative diseases (Cataldo *et al.*, 2008), (Zhang *et al.*, 2009 and He *et al.*, 2019).

As mentioned in the introduction, previously studied lysosomal protein profiles such as Schröder et al., (2010) used liver cells for the lysosome isolations. The use of liver cells for lysosome isolation was to alter the density of lysosomes. These studies utilized injection of Triton to the animal models, which is metabolised by the liver lysosomes. Dextran accumulated hepatic lysosomes become enlarged and denser, so that both sedimentation coefficient and equilibrium density are increased in a sucrose gradient (De Duve and Wattiaux, 1966). In this endo-lysosome isolation protocol, such modifications or alterations were not used to manipulate the nature of the endo-lysosomes.

The fractionation method presented here can isolate cardiac lyso/endo-lysosomes in a robust and reproducible manner. I chose *C. porcellus* for this work due to its known electrophysiological similarities to human cardiomyocytes and long-established use for physiology data collection within the field (Terrar *et al.*, 2007). Given the interest in lysosomes and endo-lysosomes as catabolic, storage and acute signaling

compartments in cardiomyocytes, the use of this method for analysis of further species and in order to compare how the pathophysiology of clinical samples and disease models affects these organelles is of great interest for future research (Lübke *et al.*, 2009 and Sleat *et al.*, 2008). Knowledge obtained from a combination of experiments performed at many levels such as genes, proteins, single cells, in vitro tissue engineering, isolated cardiac tissue, whole organ, and in vivo cardiac studies, rather than a single model or experimental technique, will lead to improved strategies for diagnosis and treatment.(Ayagama *et al.*, 2021).

2.5 Limitations of the study

The modified density gradient protocol described in this study has the potential to identify lysosomal proteins using relatively small sample volumes. However, it is important to recognize that the proteins identified using this technique are likely to be an underestimate of the total proteins present within samples.

For example, this analysis did not detect TPC1 or TPC2 proteins, EL ion channels that would be expected to be present (Wang *et al.*, 2012), (Cang *et al.*, 2013 and Grimm *et al.*, 2014),. Detecting these proteins in proteomic screens is problematic primarily due to their hydrophobicity, low levels of expression and lack of trypsin cleavage sites in their transmembrane segment sites (Vit and Petrak, 2017). I did however observe β1-

integrin, which has a functional role related to TPCs (Nguyen *et al.*, 2017), in our EL fractions. Disrupted TPC function also halts trafficking of β1-integrin, leading to accumulation in EEA1-positive early endosomes (Nguyen *et al.*, 2017). More recently, the contribution of TPC2 and NAADP to acute and chronic β-adrenoceptor signaling in the heart has been demonstrated (Capel *et al.*, 2015). In addition, it is not possible to rule out the possibility that some small contamination of the EL fraction with early endosomal proteins may occur during the fractionation phase. For example, besides EL proteins, potential minor contamination from early endosomal proteins was discovered in the EL fraction such as EEA1, Rab1A, and Rab6A (Ayagama *et al.*, 2021).

Chapter 3

Protein expression in lysosomes and acidic organelles in a goat model of induced atrial fibrillation

3.1 Introduction

AF is considered the most common tachyarrhythmia with a prevalence of 2% in the population (Zoni-Berisso *et al.*, 2014). Moreover, AF is a significant cause of ischaemic stroke in most patients with cardiac disorders above the age of 75 (Samuthpongtorn *et al.*, 2021). The substantial atrial remodeling nature of AF progresses the disease and is self-sustaining (Botto *et al.*, 2003). This remodeling can be structural (Frustaci *et al.*, 1997), or electrical (Lee, 2013) in nature. Furthermore, organelle dysfunction is observed in AF progression (Pool *et al.*, 2021) and multiple studies are published on

structural and electrical remodeling (Lee, 2013) ; (Embi and Scherlag, 2014). However, organelle remodeling, such as that related to mitochondria or acidic organelles, has not been extensively studied. Moreover, the contribution of proteomics in AF studies has emerged recently (Doll *et al.*, 2017), but understanding the acidic organelle contributions in cellular metabolism, protein regulations, and the underlying alterations in the molecular mechanisms of AF are not fully understood.

The proteomic studies presented in this chapter are a unique approach to understanding AF pathology. In Chapter 2, I presented the development of a method to isolate endolysosomal proteins (Ayagama *et al.*, 2021) to increase the identification of endo-membrane system proteins trafficked to the acidic organelles, mainly lysosomes. In this chapter, I present an application of this method to study organelle protein changes in AF.

Goat is a better-suited animal model to human AF because of better tolerance than other animal models (Schüttler *et al.*, 2020). Therefore, sustained AF can be developed in goats and goat models can be used to conduct long term pacing studies (usually for 6 months) (Wijffels *et al.*, 1995). The goat AF model is well suited to study structural and electrical remodeling (Verheule *et al.*, 2013 and Verheule *et al.*, 2010), for example, fibrosis (Verheule *et al.*, 2013). Since this model can be paced for an extended period, it develops some AF features identical to persistent human AF, e.g., increased numbers of rotors with complex activation patterns and endocardial-epicardial

dissociation (Verheule *et al.*, 2010 and Eckstein *et al.*, 2011). Moreover, the AF goat model is ideal for studies of antiarrhythmic drugs (Wijffels *et al.*, 1999 and Eijsbouts *et al.*, 2006).

Proteomics can use as a competent method to identify a set of proteins in a single technique, contributing and enlightening to the current understanding of AF pathology. Proteomics function through standard algorithms, workflows and quantitative statistical methods that allow the researcher to conduct a reliable and robust regulated protein identification (Sühling *et al.*, 2018). This type of method is ideal for identifying potential biomarkers (Ko *et al.*, 2019). However, the multifactorial and the heterogeneous nature of AF as a disease (Nattel and Dobrev, 2016) ; (Xi and Cheng, 2015) ; (Schüttler *et al.*, 2020) remain a significant limitation in omics and biochemical studies. Additionally, the protein regulations found in molecular pathways are interpretations of published literature and databases, which provide a fundamental understanding. An establishment of the protein regulations as a pathway alteration needs further and extensive investigation.

This chapter discusses the proteins of major molecular events that occurred in the left atrial tissue of the induced atrial fibrillation goat model. Here I will discuss the primary pathways to understand how these changes potentially affect the lysosome and acidic organelles. We performed label-free quantitative mass spectrometric analysis of peptides, then quantified and identified the statistically significant proteins. These

proteins were then analysed using several molecular pathway tools such as GO, Reactome, Panther and KeGG to predict the most plausible dysregulated molecular mechanisms applicable to AF. Application of this newly developed method (that is described in chapter 2) on a disease such as AF was a practical usage of the method and protein regulations were able to apply to the Reactome pathway unlike the wild type *C. porcellus* models.

In this chapter, I performed an over representation study in GO analysis, using the most significantly regulated proteins identified in the AF goat model compared against the human proteome. The purpose of this study was to understand the highest represented biological processes and cellular components that were altered in the AF goat model, based on comparison against human data. Interestingly, under biological processes, vesicle-mediated transport between endosomal compartments (GO: 0098927) was identified with a 13.33-fold overexpression, early endosome to late endosome transport (GO: 0045022) was identified with an 11.59-fold overexpression, and regulation of vesicle-mediated transport (GO: 0060627) with a 2.65-fold overexpression compared to the expression in the human proteome.

In addition, I also found under the cellular components, endocytic vesicle lumen, cytoplasmic vesicle lumen phagocytic vesicle, endocytic vesicle membrane, vacuolar lumen, endocytic vesicle, secretory vesicle, vesicle lytic vacuole, lysosome, vacuole,

(cell junction, and cytoplasmic vesicle proteins overrepresented in the AF goat model LA compared to that of the human proteome.

The primary molecular pathways that affected the overall pathology of the atria identified were (i) the AMPK pathway and (ii) AMPK activated mitochondrial ATP production and related pathway to glucose intake. Furthermore, I observed that the mitochondrial oxidative phosphorylation (OXPHOS) and inflammation activated NADPH oxidase (NOX2) pathways exhibited a possible increase in the reactive oxygen species (ROS) as a byproduct. From the studies conducted in the Reactome pathway (https://reactome.org/) it appears that the ROS increased the cellular stress and changed several acidic organelle-related pathways, such as protein processing, folding, trafficking, and degradation that are participated by acidic organelles.

The major lysosome and acidic organelle pathways dysregulated in AF were: Protein processing and folding pathway; endosomal sorting complex required for transport (ESCRT); vesicle-mediated transport pathway; aggrephagy; proteasome pathway; lysosome biogenesis; gap junctional trafficking to lysosomes, internalisation and degradation. Major regulated pathways had sub pathways and are provided with a detailed description in this chapter.

A summary table of the presumably regulated pathways presented in this chapter are given in the table 1 and the proteins exhibited in these molecular pathways are listed in appendix Table A3:1, A3:2 and A3:3 with significant regulation levels.

Tissue fraction (TL)	Mitochondrial Fraction (Mito)	Endo-lysosome/Late endosome/ Lysosome fraction (EL)
AMPK pathway	**Respiratory electron transport chain and chemiosmosis pathway (Oxidative Phosphorylation)**	**ESCRT pathway**
NADPH Oxidase pathway	**GLUT4 translocation to plasma membrane**	**Lysosome as the hub for mTORC1 activation**
GAP junctional assembly pathway	**Mitochondrial Stress and ROS formation**	**Lysosome biogenesis**
Protein processing and folding pathway		**Gap junctions trafficking to lysosomes, internalization and degradation**
Vesicle mediated transport		
Proteasome pathway		

Table 3:1: A summary of the pathways discussed from TL, Mito and EL fractions

3.2 Methods

3.2.1 Sample preparation

Frozen AF and sham goat left atrial tissue biopsies were thoroughly cleaned in PBS and weighed. A minimum of 100 mg tissue is weighted in order to perform proteomics, transcriptomics and biochemical assays (enzyme assay and Western Blots). Each atrium biopsy sample was cut using sterile scalpels and gently homogenized using a 7 mL Dounce homogenizer in Lysosome isolation buffer (LIB) [Containing 1:500 protease inhibitor cocktail (PIC) and phosphatase inhibitor (PHI) (Bio vision), (PhosSTOP Roche)]. Preparations were further homogenized in 1 mL Dounce homogeniser and transferred to chilled 1.5 mL ultracentrifugation tubes (Beckmann coulter). Sample preparations were mixed at a ratio of 1:1.5 Lysosome enrichment buffer [(LEB) (Biovision, containing 1:500 PIC)] to homogenate by inverting tubes, and were stored on ice for 5 min until the centrifugation (Ayagama *et al.*, 2021).

3.2.1.1 Isolation of acidic organelles by fractionation

Tissue Lysate (TL)

Samples were centrifuged at 13,000 g x 2 min at 4 °C (TLX Beckmann Coulter Ultra Centrifuge) and the resulting supernatant, corresponding to the TL was collected (Ayagama *et al.*, 2021).

Mitochondrial Fraction (Mito)

Further fractionation was processed using 75% of the collected TL. 1.5 mL ultracentrifuge tubes were underlaid with 750 µL of 2.5 M sucrose (Fisher Scientific) followed by 250 µL of Percoll (Santa Cruz Biotechnology). 200 µL TL was layered on top of the Percoll layer and centrifuged at 27,000 g x 50 min at 10 °C. The supernatant layer just above the turbid-white, mitochondrial fraction (Mito fraction) was carefully removed, and the Mito fraction itself was collected separately (Ayagama *et al.*, 2021).

Endo-lysosome Fraction (EL)

The collected supernatant was retained and repeated for a further centrifugation step at 29,000 g x 30 min at 15 °C (500 µL of under-laid 2.5 M sucrose with over-laid 500 µL Percoll). The supernatant above the sucrose and Percoll intermediate was collected for further fractionation. Firstly, ultracentrifuge tubes were underlaid with 2.5 M sucrose and overlaid with a series of Percoll dilutions (1.11 g/mL – 1.04 g/mL in ddH2O). The ultracentrifuge tubes were centrifuged at 67,000 g x 30min at 4 °C. The fraction at 1.04 g/mL was collected and labeled as the endolysosomal fraction (EL) (Ayagama *et al.*, 2021). N = 3 biological replicates for each AF and Sham conditions were used in proteomic analysis.

3.2.2 Liquid chromatography-tandem mass spectrometry analysis

3.2.2.1 Preparation of samples

5 µL of 200 mM dithiothreitol was added to reduce the samples (30 min at room temperature) and alkylated with 20 µL of 200 mM iodoacetamide (30 min at room

temperature) followed by methanol-chloroform precipitation (A detailed protocol is provided in chapter 2). Pellets were re-suspended in 6 M urea in 400 mM TrisHCl, pH 7.8. Urea was diluted to 1 M using 400 mM Tris-HCl, pH 7.8, and the proteins were digested with trypsin in a ratio of 1:50 (overnight at 37C°). After the trypsin digestion, the samples were processed at the Target Discovery Institute, Oxford.

3.2.2.2 Mass-spectrometry

Liquid chromatography-tandem mass spectrometry was performed by Roman Fischer and Georgina Berridge in the Target Discovery Institute, University of Oxford according to a published protocol (Davis *et al*., 2017).

After acidifying to a final concentration of 1% formic acid, the samples were desalted on Sola HRP SPE cartridges (Thermo Fisher Scientific) and dried down in a SpeedVac (3-6 hours). Samples were further desalted online (PepMAP C18, 300 µm x 5 mm, 5 µm particle, Thermo Fisher Scientific) for 1 min at a flow rate of 20 µL/min and separated on an EASY-Spray column (PepMAP C18, 75 µm x 500 mm, 2 µm particle, ES803, Thermo Fisher Scientific) over 60 min using a gradient of 2–35% acetonitrile in 5% DMSO/ 0.1% formic acid at 250 nL/min. Separation and analysis was performed on a Dionex Ultimate 3000 RSLC system coupled to an Orbitrap Fusion Lumos platform (both Thermo Fisher Scientific) using standard parameters (Universal Method (Davis

et al., 2017)). MS scans were acquired at a resolution of 120,000 between 400 and 1,500 m/z. An AGC target of 4.0E5, and MS/MS spectra were detected using rapid scan mode in the linear ion trap after collision-induced dissociation fragmentation (CIDF) at a collision energy of 35%. An AGC target of 4.0E3 for up to 250 ms, employing a maximal duty cycle of 3 s, prioritizing the most intense ions and injecting ions for all available parallelizable time. Selected precursor masses were excluded for 30 s (Davis *et al.*, 2017).

Mass spectrometry data were analyzed quantitatively with the Progenesis QI software platform (Waters™ Cooperation, www.nonlinear.com) (version 4.2), and database searches carried out against the UniProt *C. hircus* database (UP000291000). Automatic processing was selected. All runs in the experiment were adjusted to the function suitability, and runs were aligned automatically. The peak picking selected between 10 and 75 min. The group runs option was set to conditions and relative quantitation using Hi-N was selected. Finally, proteins were grouped.

3.2.3 Quantification and statistical analysis of mass spectrometry data

Quantitative analysis for significant differences of protein regulation between the AF and sham conditions of TL, Mito and EL samples and data visualization were performed

using the Perseus software platform (Tyanova *et al.*, 2016) (version 1.6.15.0). Using protein intensity values of biological replicates, the protein groups were created and uploaded as a data matrix in Perseus with the respective protein abundances as main columns. The data matrix was reduced by filtering based on categorical columns to remove proteins where more than two intensity values were absent from six biological replicates, and remaining data with no more than 2 missing values were quantitatively analysed. A total of 2,104 proteins in TL, Mito and EL remained after filtering. Groups of biological replicates for TL, Mito and EL fractions were defined in categorical annotation rows. Data were log transformed (log2(x)) and normalised via Z score.

Missing data points were imputed based on normal distribution and visualized as normalised intensity histograms (per biological replicate) with imputed values. Principal component analysis (PCA) was performed on 100% valid values. A volcano plot was generated based on normalised intensities applying two-way Student's t-test to probe for significant difference of protein regulation between AF and Sham conditions of each TL, Mito and EL samples. A permutation-based false-discovery rate (FDR) was determined with 250 randomizations and S0 = 0.1 (default). The quantified proteins were accounted with 99% confidence level at 5% FDR.

3.2.4 Network analysis

The functional networks of the statistically enriched proteins acquired from the volcano plot were analyzed using Reactome (https://reactome.org) (Fabregat *et al.*, 2017) and Panther pathway analysis software (Mi *et al.*, 2021). *C. hircus* proteins were converted to H. Sapiens with UniProt Retrieve/ID mapping to identify the reviewed proteins with 100%–50% similarity in the molecular function through biological and molecular pathways.

The KeGG, STRING, GO and Reactome programmes were used in order to investigate associations and relations of the regulated proteins and protein interaction between AF and sham goat models of TL, Mito and EL. The protein match to the molecular networks aligned with medium confidence of 0.4 in the panther GO analysis. From each type of sample highest and lowest regulated proteins were selected for all the pathway studies. I applied perfused force-directed layout on the network using clusterMaker 2.8.2 (Morris *et al.*, 2011). Functional enrichment analysis was performed for the AF diseased and Sham conditions.

Pearson correlation coefficient, heat maps, PCA and histograms were produced to assess the reliable correlation between the sample triplicates. The heat maps were produced using Euclidian distance and K-mean clustering. Plots were generated using Perseus software (v. 1.6.15.0) and presented for publication using Instant Clue (Nolte *et al.*, 2018). The protein profile plots were created using Pearson clustering. The unavailability of the characterized whole *C. hircus* proteome limitation was minimized by selecting 100%–50% overlap of the proteins with the closest species in the phylogenetic tree. These selections were automatically identified by proteome databases such as Uniprot and proteomic tools Perseus, Reactome, String and Panther Pathway.

3.2.4.1 PANTHER Overrepresentation Test

To understand the pathway enrichment fold of the significantly regulated proteins of the AF goat model to that of the universal human proteome, a PANTHER Overrepresentation Test (Released 20210224) was performed using panther-gene ontology (Panther –GO). The annotation version and the released date was GO Ontology database DOI:10.5281/zenodo.5080993 released date 2021-07-02. The Fishers exact test was applied to calculate the statistically significant enrichment and FDR was considered for the correction.

3.2.4.2 Reactome

Reactome is a curated knowledge base that provides a manual platform that is easy to access and analyse biological data on molecular mechanisms of reactions and pathways. It provides an extended level of details on metabolic reactions and downstream pathways in various useful formats, including interactive diagrams and structured hierarchies. Although pathway information can be studied via scientific literature, it is mainly unavailable for computational re-use, and Reactome addressed this need by providing an easy-to-use interface. The metabolic interaction information is completed primary published literature and contains a variety of analysis tools that allow users to investigate experimental data. The analysed results can be exported in standard formats for further analysis or discussions (www.reactome.org) and (www.ebi.ac.uk).

The most significantly up and down regulated proteins of TL, Mito and EL fractions were selected and any protein with a significant regulation between 0.1 – 0.9 were removed as Reactome identifies proteins with a regulation level higher than 0.9 and lower than 0.1. The analysis was performed against Reactome version 77, and quantitative expression data were overlaid to visualize the extent of change in affected pathways and its progression through regulation levels. A binomial test is used to calculate the probability shown for each result, and the p-values are corrected for the multiple testing (Benjamini–Hochberg procedure) that arises from evaluating the

submitted list of identifiers against every pathway. The expression analysis produced a colour scaled representation to visualise the relative expression levels, and all the non-human identifiers have been converted to their human equivalent.

3.2.4.3 Gene Ontology pathway (GO pathway)

The significantly regulated proteins were uploaded to the Gene Ontology pathway analysis (GO), which divide the proteins to the three non – overlapping ontologies; Biological process, Molecular function and Cellular component. The ontology groups are presented in terms of nodes and edges; nodes are the main protein interactors and edges are the relation among the nodes/ protein interactors. This presentation of data is termed Directed Acyclic Graph (DAG). Genes or proteins are interacted using a procedure known as annotation process and each annotation is attributed with a database entry and a source. Moreover, the literature of the published data, co–occurrence, experimental data sets are chosen as the source, therefore, each protein is associated with the most significant interactions and each term or node can have multiple interactions or edges that describe its functionality (du Plessis *et al.*, 2011) (geneontology.org). Unlike KeGG pathways (described in the next paragraph), GO analysis illuminated over-representation of the given set of regulated proteins in the AF model, enabling its biological interpretation compared to the reference human proteome.

3.2.4.4 Kyoto Encyclopedia of Genes and Genomes Pathway (KeGG)

Kyoto Encyclopedia of Genes and Genomes Pathway or KeGG pathway is a collection of manually constructed biological pathways that represent the knowledge of the molecular interactions between proteins. It can be compared to the Gene Ontology as a gene set enrichment analysis. KeGG analysis is mostly used as a reference knowledge base and is designed to network primarily for metabolisms, including carbohydrate, lipid, ATP production/ energy, amino acids and nucleotides. Secondly, secondary metabolites such as vitamins, xenobiotics and cofactors. Thirdly, genetic information, environmental information and cellular processing. Finally, drug development, organismal systems and human diseases.

The KeGG pathway analysis of the AF vs Sham goat model lead to the cellular metabolism pathways. The significantly regulated proteins of *C. hircus* were converted to the parallel human identifiers and then the KeGG id numbers were retrieved using the Uniprot ID mapping retriever. There are four mapping tools available in the KeGG pathway, they are; Basic or reconstruct pathway, traditional search pathway, Join Brite tool and search and colour pathway. The AF vs Sham model data were searched using the search and colour mapping tool due to the colour representation, which more clearly demonstrates the regulations.

3.3 Results

3.3.1 Principal Component Analysis (PCA)

Principal component analysis is a reduced data dimension-interpretation of the protein groups' distribution between the sample groups and it is one of the most popular multivariate statistical techniques. A PCA plot can provide a window to a large data set by identifying the common vectors, therefore summarizing the variation (Aït-Sahalia Yacine and Xiu Dacheng 2015). As indicated in Figure 3:1, 3:2 and 3:3 the respective component 1 vector deviations of TL 42.8%, mito 46.1% and EL 52.8% were observed between AF (purple symbols) and Sham (green symbols) groups. An exceptional segregation of 30.8% in TL, 23.8% in mito and 15.1% in EL was observed in the first biological replicates of Sham groups, demonstrating that the variability is driven by the differential experiment groups rather than the variability within the biological replicates.

Tissue Lysate (TL)

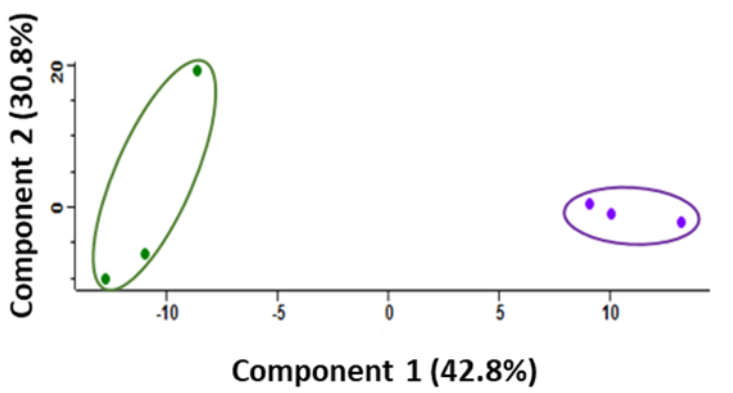

Figure 3:1: Principal component analysis of the Tissue Lysate (TL) fraction AF vs Sham goat models. *Graph shows a variability of 42.8% and 30.8% of component 1 and 2 between the AF (purple symbols) and Sham (green symbols) groups, based on the proteomic expression profiles. Each green or purple data point resembles the total number of protein groups in each sample as a vector. The spatial resolution between vectors are presented as component 1 and 2. Therefore, exhibiting that the variability is driven by the differential experiment groups rather than the variability within the biological replicates. Figure generated using Perseus 1.6.15.0.*

Mitochondrial fraction (Mito)

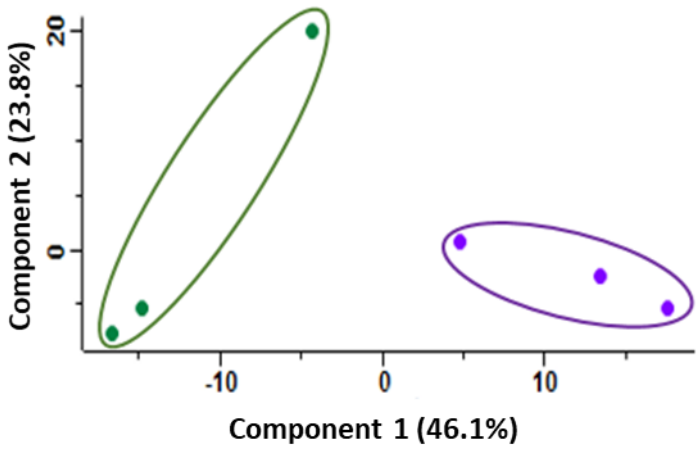

Figure 3:2: Principal Component analysis of the mitochondrial fraction (Mito) fraction AF vs Sham goat models. *The six samples of the AF and sham goats are showing the variability of 46.1% and 23.8% of component 1 and 2 between them. AF (purple symbols) and Sham (green symbols). The purple and green points, resemble the total protein groups belonging to each sample as a single vector, and the spatial resolution among the vectors are shown as a percentage in component 1 and 2. The sample groups assures that the variability is driven by the differential experiment groups rather than the variability within the biological replicates. Figure generated using Perseus 1.6.15.0.*

Endo-lysosome fraction (EL)

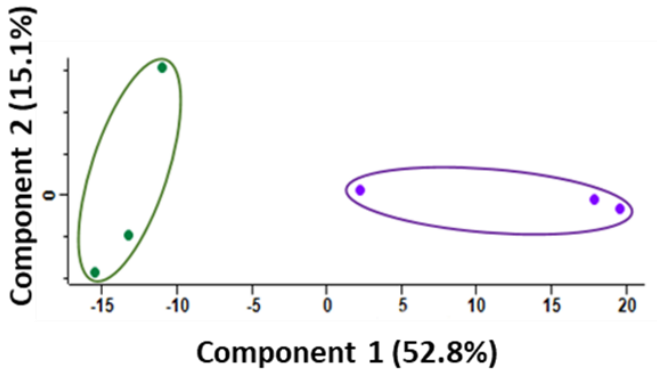

Figure 3:3: Principal Component Analysis of the Endo-lysosome (EL) fraction AF vs Sham goat models. *Graph shows the variability of 52.8% and 15.1% in component 1 and component 2 between the AF (purple symbols) and Sham (green symbols) groups. According to the protein expression profiles, each purple and green points represents the total protein groups in each sample as a single vector, therefore the component 1 and 2 resembles the spatial resolution among the vectors, assuring the variability driven by the differential experiment groups rather than the variability within the biological replicates. Figure generated using Perseus 1.6.15.0.*

3.3.2 Violin plot analysis

The violin plots were produced using the InstantClue omics tool (Nolte *et al.*, 2018). The protein intensities used were transformed to log2, normalised by z scoring, and AF vs Sham groups were colour-coded; a gradient of red for AF group and blue for sham group (Figure 3:4, 3:5, 3:6). This Violin plot represents a kernel density estimation of the underlying protein intensity distribution (The kernel estimated density distribution is the nonparametric representation of the probability density function of a random

variable (www.mathworks.com). The quantified protein intensity matrix used for the violin plot is created in Perseus 1.6.15.0 (Tyanova *et al.*, 2016).

A violin plot has a similar interpretation of data to that of a box plot and swarm plot. Based on the numerical values, it shows the distribution across the different categorical variations but, unlike the boxplot, the violin plot contains the kernel estimated density distribution.

Tissue Lysate (TL)

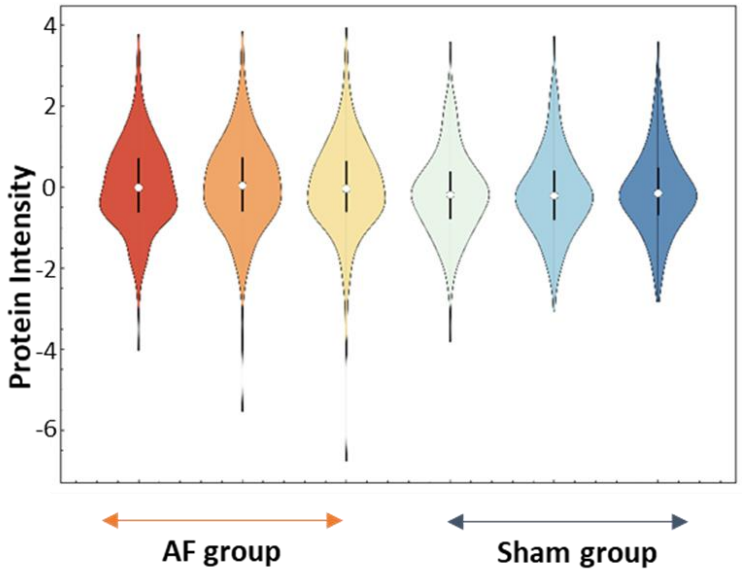

Figure 3:4: Violin plot of the Tissue Lysate (TL) fraction AF vs Sham goat models. *Represents a kernel density estimation of the underlying protein intensity distribution. The distribution of protein abundance from AF to Sham groups of TL between the biological replicates are represented with red and blue colour codes. Red= AF group, Blue= Sham group*

Mitochondrial fraction (Mito)

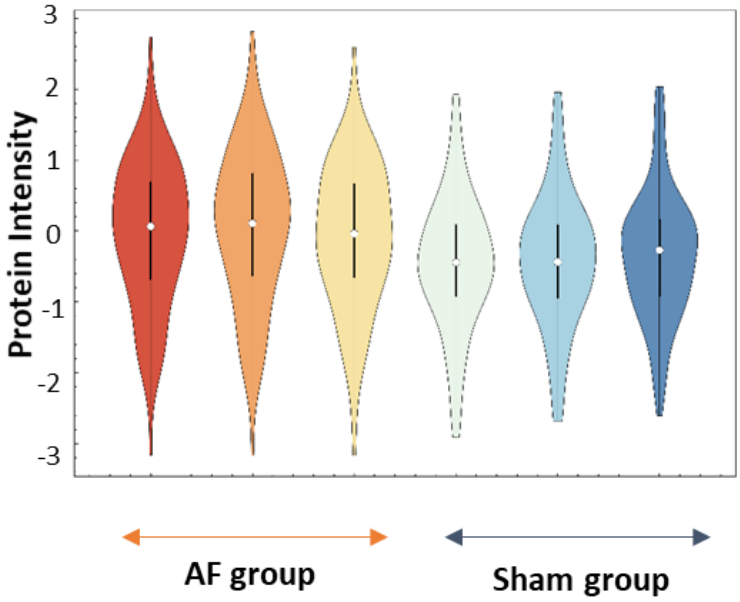

Figure 3:5: Violin plot of the Mitochondrial (Mito) fraction AF vs Sham goat models. *Graph shows distribution of protein abundance from sham to AF group between the biological replicates of mito fraction. Replicates are represented with red and blue colour codes. Red= AF group, Blue= Sham group*

Endo-lysosome fraction (EL)

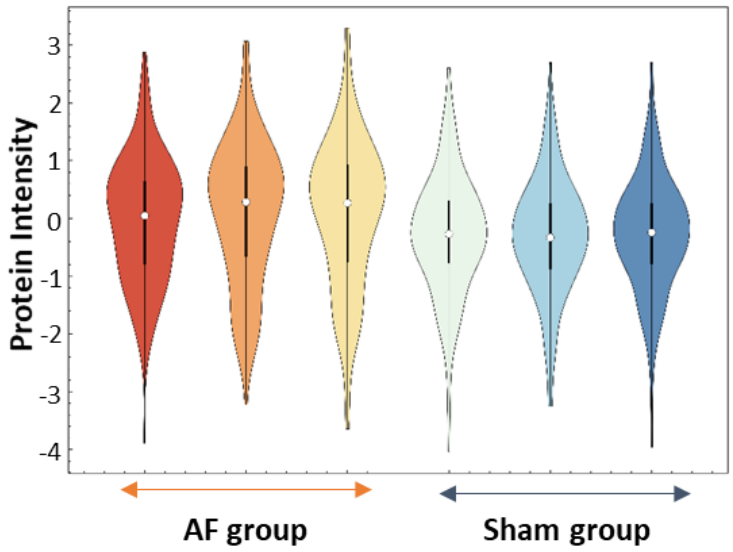

Figure 3:6: Violin plot of the Endo-lysosome (EL) fraction AF vs Sham goat models. *Graph shows the distribution of protein abundance from sham to AF group between the biological replicates of EL fraction. Replicates are represented with red and blue colour codes. Red= AF group, Blue= Sham group*

3.3.3 Heat map analysis

The heat or clustering maps were produced in InstantClue omics tool using Euclidian distance and K-mean clustering of the normalised protein intensities. The intensity values are obtained from the quantified matrix created in Perseus 1.6.15.0. Respectively in TL a total of 340 proteins, mito 113 proteins, and EL 148 proteins were categorized into protein clusters according to the protein intensities (TL= 2 clusters, mito = 3 clusters, and EL = 3 clusters). The regulation level variations are displayed

using colour codes (red and blue), where red represents the up regulation of the protein clusters and blue represents the down regulation of these clusters (Figure 3:7, 3:8, 3:9).

Tissue Lysate (TL)

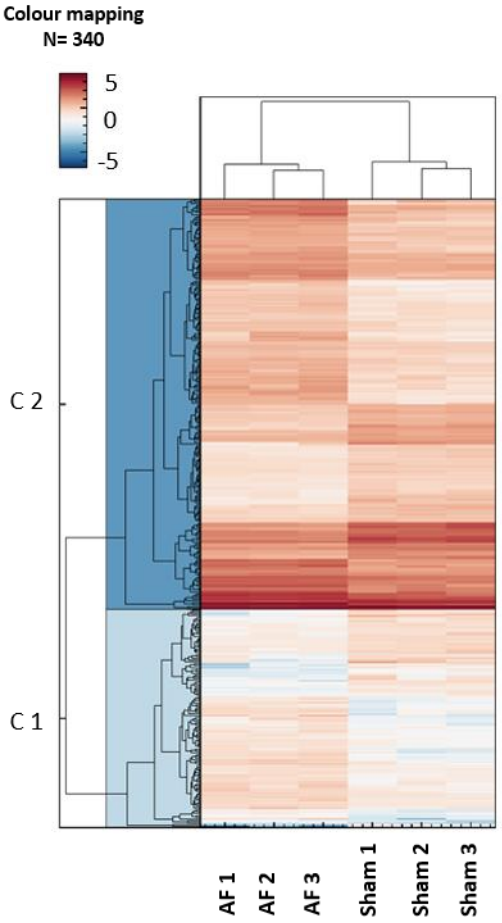

Figure 3:7: Heat map of the Tissue Lysate (TL) fraction AF vs Sham goat models. *Graph shows the protein clusters, identified after z scoring the intensities of the differentially expressed proteins under unsupervised hierarchical clustering and all the 340 proteins fall into two clusters (C1= cluster 1 and C2= cluster 2). The colour code blue to red represents the relative protein intensities from lowest to the highest, therefore according to the protein group clusters, the relative protein intensity differences display different levels of expression.*

Mitochondrial fraction (Mito)

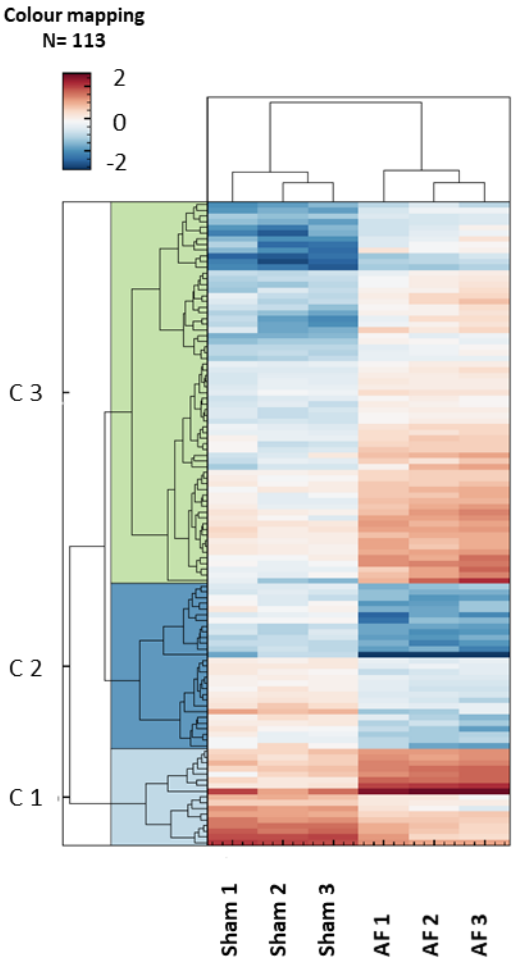

Figure 3:8: Heat map of the Mitochondrial (Mito) fraction AF vs Sham goat models. *Graph shows the protein clusters, identified after z scoring the intensities of the differentially expressed proteins under unsupervised hierarchical clustering and all the 113 proteins fall into three clusters (C1= cluster 1, C2= cluster 2 and C3= cluster3). The relative protein intensities from lowest to the highest are presented as a colour code blue to red. According to the protein group clusters, the relative protein intensity differences display different levels of expression.*

Endo-lysosome fraction (EL)

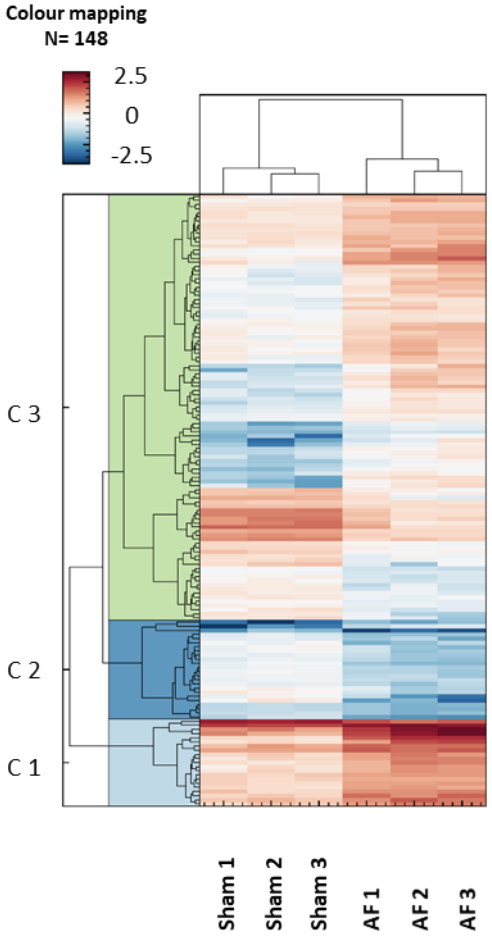

Figure 3:9: Heat map of the Endo-lysosome EL fraction AF vs Sham goat models. *Graph shows the protein clusters, identified after z scoring the intensities of the differentially expressed proteins under unsupervised hierarchical clustering and all the 148 proteins fall into three clusters (C1= cluster 1, C2= cluster 2 and C3= cluster 3). The colour code blue to red represents the relative protein intensities from lowest to the highest. The three protein group clusters are displaying the relative protein intensity differences, therefore the different levels of expression.*

3.3.4 Pearson co - efficient correlation analysis

The Pearson coefficient correlation estimates the true correlation between the given groups. Here the correlation ρ is calculated by an array of tests from -1, 0 to 1 and represent a range of interactions between two variables (AF and Sham) from perfect positive correlation through no correlation to negative correlation (Dytham., 2011). To measure both variables on a continuous scale, the quantified protein intensity data matrix created in Perseus version 1.6.15.0 was uploaded to InstantClue Omics tool to create the Pearson co-efficient correlation plot (Figure 3:10, 3:11, 3:12).

Tissue Lysate fraction (TL)

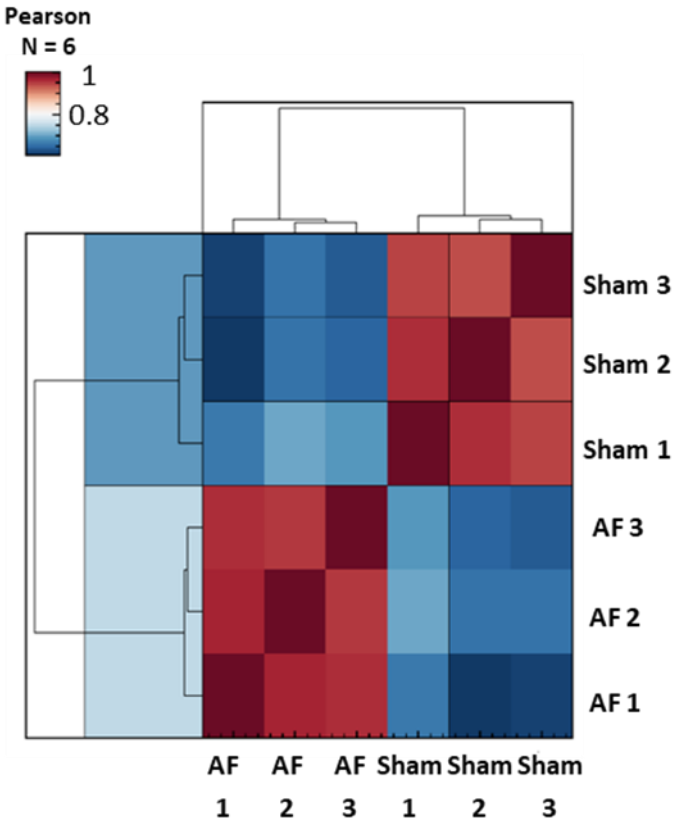

Figure 3:10: Pearson co – efficient correlation plot of the Tissue Lysate (TL) fraction AF vs Sham goat models. *Graph shows a positive correlation between the triplicated samples of TL. The correlation ρ is calculated by an array of tests from -1, 0 to 1 and represent a range of interactions between two variables (AF and Sham) from perfect positive correlation through no correlation to negative correlation. Red = highly likely, white= No correlation and Blue= highly unlikely.*

Mitochondrial (Mito) fraction

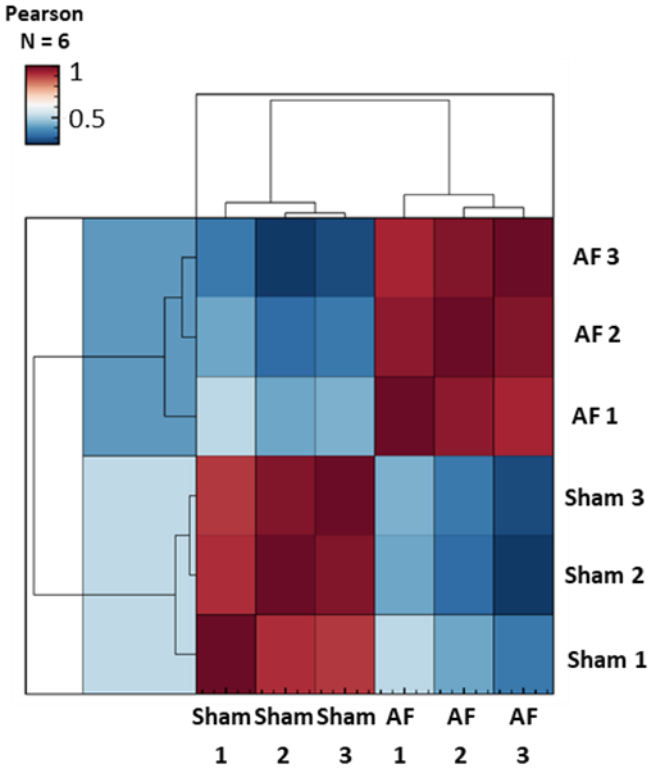

Figure 3:11: Pearson co efficient correlation plot of the Mitochondrial (Mito) fraction AF vs Sham goat models. *Graph shows a positive correlation between the triplicated samples of Mito fraction, between AF and Sham goat models. The correlation ρ is calculated by an array of tests from -1, 0 to 1 and represent a range of interactions between two variables (AF and Sham) from perfect positive correlation through no correlation to negative correlation. Red = highly likely, white= No correlation and Blue= highly unlikely.*

Endo-lysosome (EL) fraction

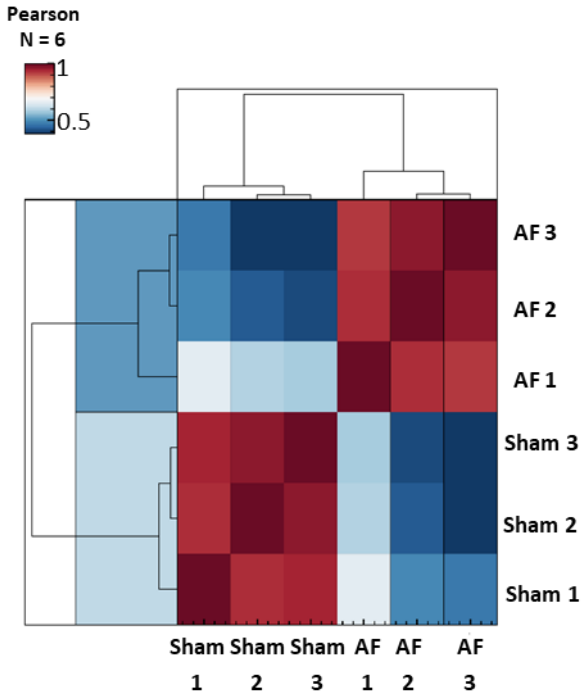

Figure 3:12: Pearson co efficient correlation plot of the Endo-lysosome (EL) fraction AF vs Sham goat models. *Graph shows a positive correlation between the triplicated samples of EL fraction. The correlation ρ is calculated by an array of tests from -1, 0 to 1 and represent a range of interactions between two variables (AF and Sham) from perfect positive correlation through no correlation to negative correlation. Red = highly likely, white= No correlation and Blue= highly unlikely.*

3.3.5 Point plot analysis

The point plot is created using the normalised protein intensities of the AF and Sham proteomic data and the protein intensities of the scatter plot points estimated the confidence intervals. A point plot portrays an estimate of central tendency or the probability distribution for a numeric variable using the position of scatter plot points with an indication of the unreliability around that estimate using error bars. Point plots are created using mean values therefore related to the distribution of values (Figure 3:13, 3:14, and 3:15).

Tissue Lysate (TL)

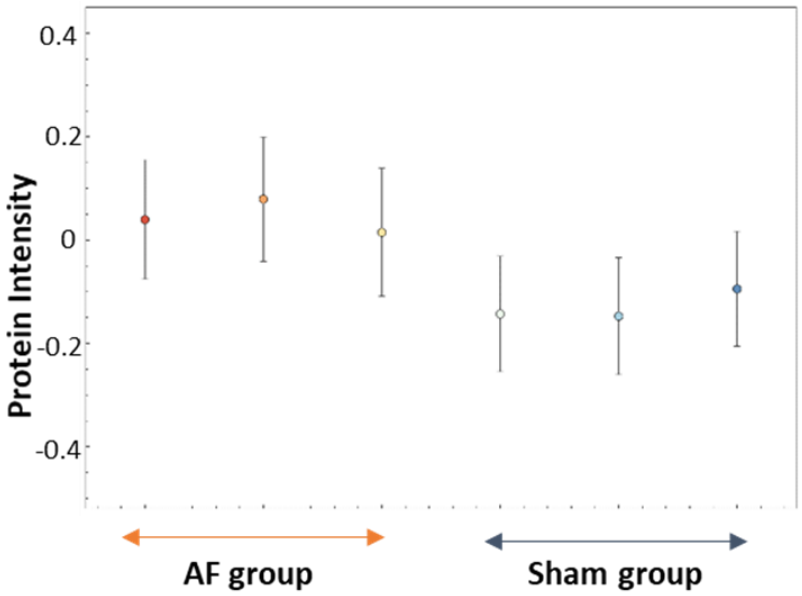

Figure 3:13: Point plot of the Tissue Lysate (TL) fraction AF vs Sham goat models. *Graph shows the confidence intervals between sham and AF groups of TL. The protein intensities of the scatter plot points estimated the confidence intervals. Here the point plot portrays an estimate of central tendency or the probability distribution for a numeric variable using the position of scatter plot points with an indication of the unreliability around that estimate using error bars.*

Mitochondrial (Mito) fraction

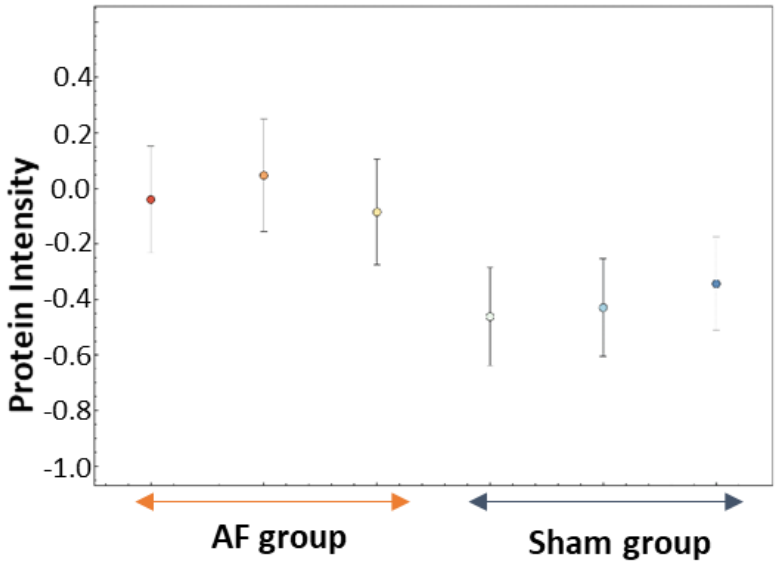

Figure 3:14: Point plot of the Mitochondrial (Mito) fraction AF vs Sham goat models. *Graph shows the confidence intervals between sham and AF groups in mito fraction. The protein intensities of the scatter plot points estimated the confidence intervals. Here the point plot portrays an estimate of central tendency or the probability distribution for a numeric variable using the position of scatter plot points with an indication of the unreliability around that estimate using error bars.*

Endo-lysosome (EL) fraction

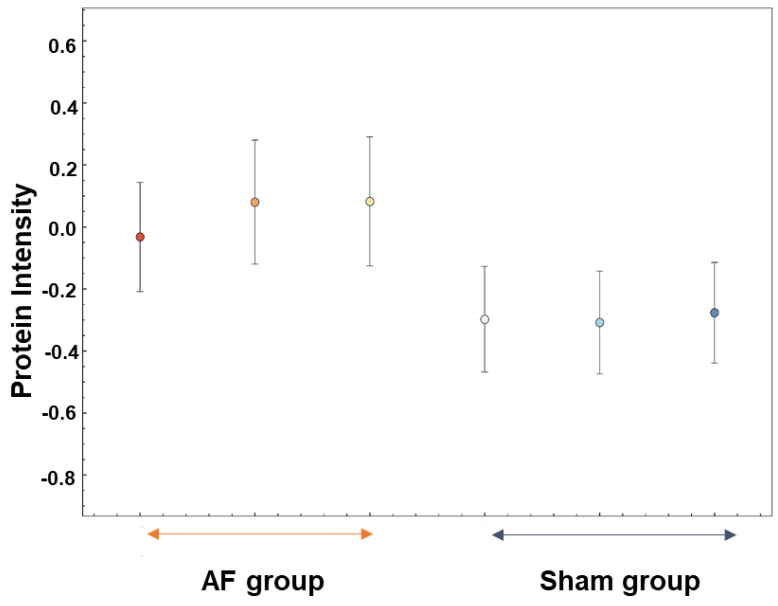

Figure 3:15: Point plot of the Endo-lysosome (EL) fraction AF vs Sham goat models. *Graph shows the confidence intervals between sham and AF groups of EL fraction. The protein intensities of the scatter plot points estimated the confidence intervals. Here the point plot portrays an estimate of central tendency or the probability distribution for a numeric variable using the position of scatter plot points with an indication of the unreliability around that estimate using error bars.*

3.3.6 Volcano plot analysis

Proteins demonstrating differential expression levels between AF vs Sham models were identified using volcano plots (Figure 3:16, 3:17, 3:18). Of a total 2,104 quantified proteins, respectively 205 proteins in TL, 75 in mito, and 93 in EL were upregulated protein hits corresponding to upregulated in AF (Figure 3:16, 3:17, 3:18 blue in colour data), whilst 135 in TL, 38 in mito, and 55 in EL accounted as depleted in AF (Figure 3:16, 3:17, 3:18 orange in colour data). The quantified, statistically significant enriched

proteins (*p*=0.05) acquired from volcano plot analysis were mapped using several genomic and proteomic annotations to generate functional networks. The volcano plot is created after z score normalisation of the protein intensities.

Tissue Lysate (TL)

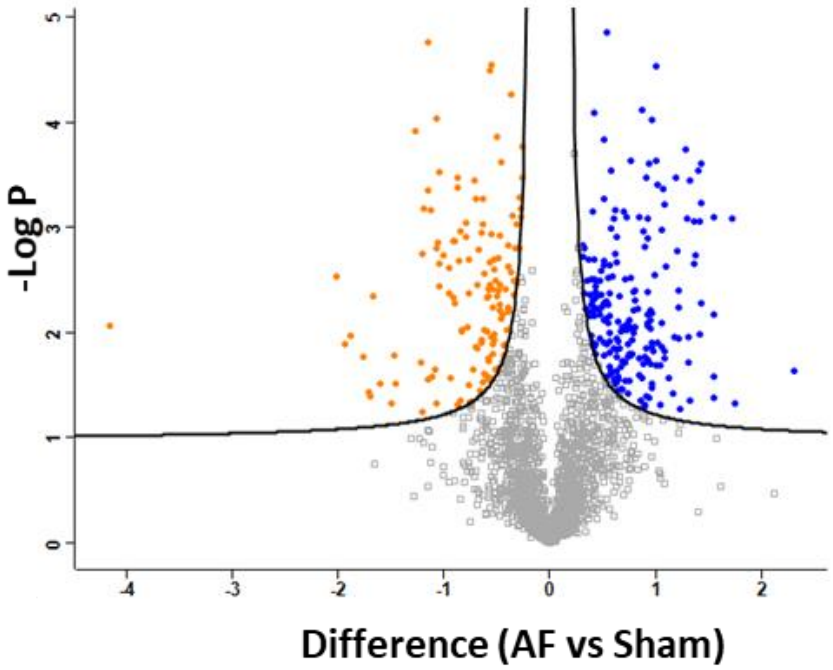

Figure 3:16: Volcano plot of the Tissue Lysate (TL) fraction AF vs Sham goat models. *Proteins demonstrating differential expression levels between AF vs Sham models were identified using volcano plot showing the significantly up and the down regulated proteins between the sham and AF conditions, and a total of 340 proteins were regulated, out of 205 were up regulated and 135 proteins were down regulated (Orange in colour represents significant down regulation and blue in colour represents significant up regulation of proteins (p=0.05) in AF goat model LA, TL).*

Mitochondrial (Mito) fraction

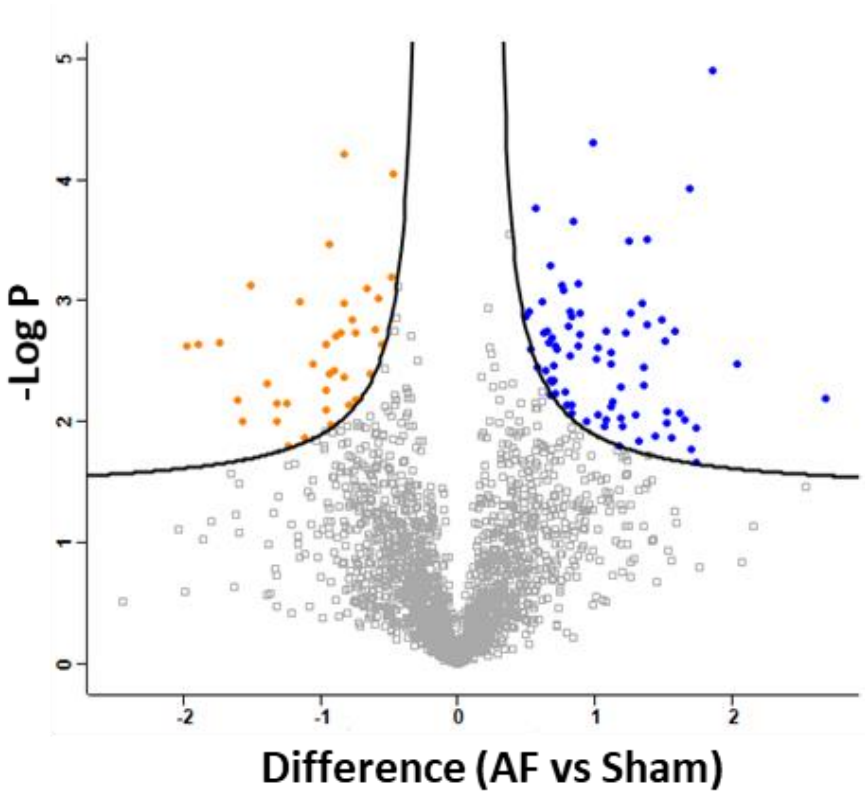

Figure 3:17: Volcano plot of the Mitochondrial (Mito) fraction AF vs Sham goat models. *Graph shows the significantly up and the down regulated proteins between the sham and AF conditions and 113 proteins showed a significant regulation, out of 75 were up regulated and 38 proteins were down regulated (Orange in colour represents significant down regulation and blue in colour represents significant up regulation of proteins (p=0.05) in AF goat model LA, mito fraction).*

Endo-lysosome (EL) fraction

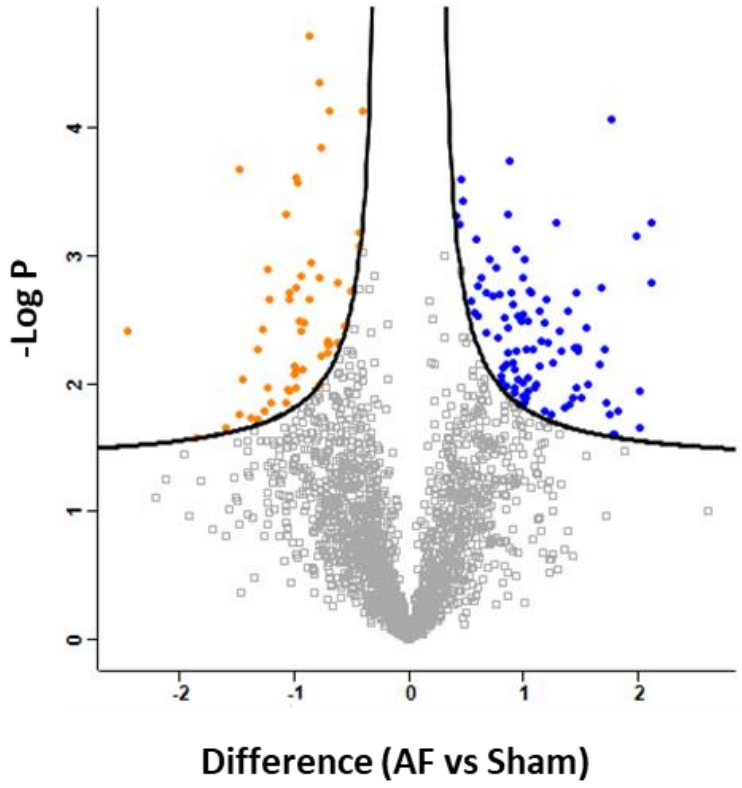

Figure 3:18: Volcano plot of the Endo-lysosome (EL) fraction AF vs Sham goat models. *Graph shows the significantly up and the down regulated proteins between the sham and AF conditions and 148 proteins showed a significant regulation, out of 93 were up regulated and 55 were down regulated. (Orange in colour represents significant down regulation and blue in colour represents significant up regulation of proteins (p=0.05) in AF goat model LA, EL fraction).*

3.3.7 Atrial fibrillation protein regulation enrichment comparison to the total human proteome

The most significantly regulated proteins in the AF goat model compared to the sham model were identified from the volcano plot. The *C. hircus* UniProt KB identifiers were converted to the human identifiers as described in the Methods (Ayagama *et al.*, 2021). The protein names followed with the log2 fold-change values were uploaded to the Panther – Gene Ontology (GO), and an overrepresentation test was conducted against the reference *Homo sapiens* proteome (Taxonomy ID: 9606).

The test was conducted on GO terms, biological process (GOBP) and cellular content (GOCC), and under the biological process, 280 terms were overrepresented. The highest enriched GO terms representing the top GOBP identified included GO terms related to energy metabolism and vesicle mediated trafficking pathways These enriched biological process terms followed by the fold enrichments are provided in Figure 3:19 and Table 3:2.

GO biological process	Fold enrichment
ribonucleoprotein complex disassembly (GO:0032988)	28.56
tubulin complex assembly (GO:0007021)	24.99
malate metabolic process (GO:0006108)	22.22
vesicle-mediated transport between endosomal compartments (GO:0098927)	13.33
glycolytic process (GO:0006096)	11.66
early endosome to late endosome transport (GO:0045022)	11.59
ATP generation from ADP (GO:0006757)	11.38
pyruvate metabolic process (GO:0006090)	8.74
glycogen metabolic process (GO:0005977)	8.00
fatty acid beta-oxidation (GO:0006635)	7.02
positive regulation of protein localization to plasma membrane (GO:1903078)	6.35
protein folding (GO:0006457)	5.80
fatty acid oxidation (GO:0019395)	5.76
fatty acid catabolic process (GO:0009062)	5.62
lipid oxidation (GO:0034440)	5.49
energy derivation by oxidation of organic compounds (GO:0015980)	5.44
oxidative phosphorylation (GO:0006119)	5.31
cellular oxidant detoxification (GO:0098869)	5.02
muscle contraction (GO:0006936)	4.20
electron transport chain (GO:0022900)	4.02
receptor-mediated endocytosis (GO:0006898)	3.80
response to reactive oxygen species (GO:0000302)	3.58
positive regulation of protein transport (GO:0051222)	3.45
regulation of actin filament-based process (GO:0032970)	3.36
response to oxidative stress (GO:0006979)	3.13
regulation of vesicle-mediated transport (GO:0060627)	2.65

Table 3:2: The top most biological processes of AF goat model LA were identified from the overrepresentation test.

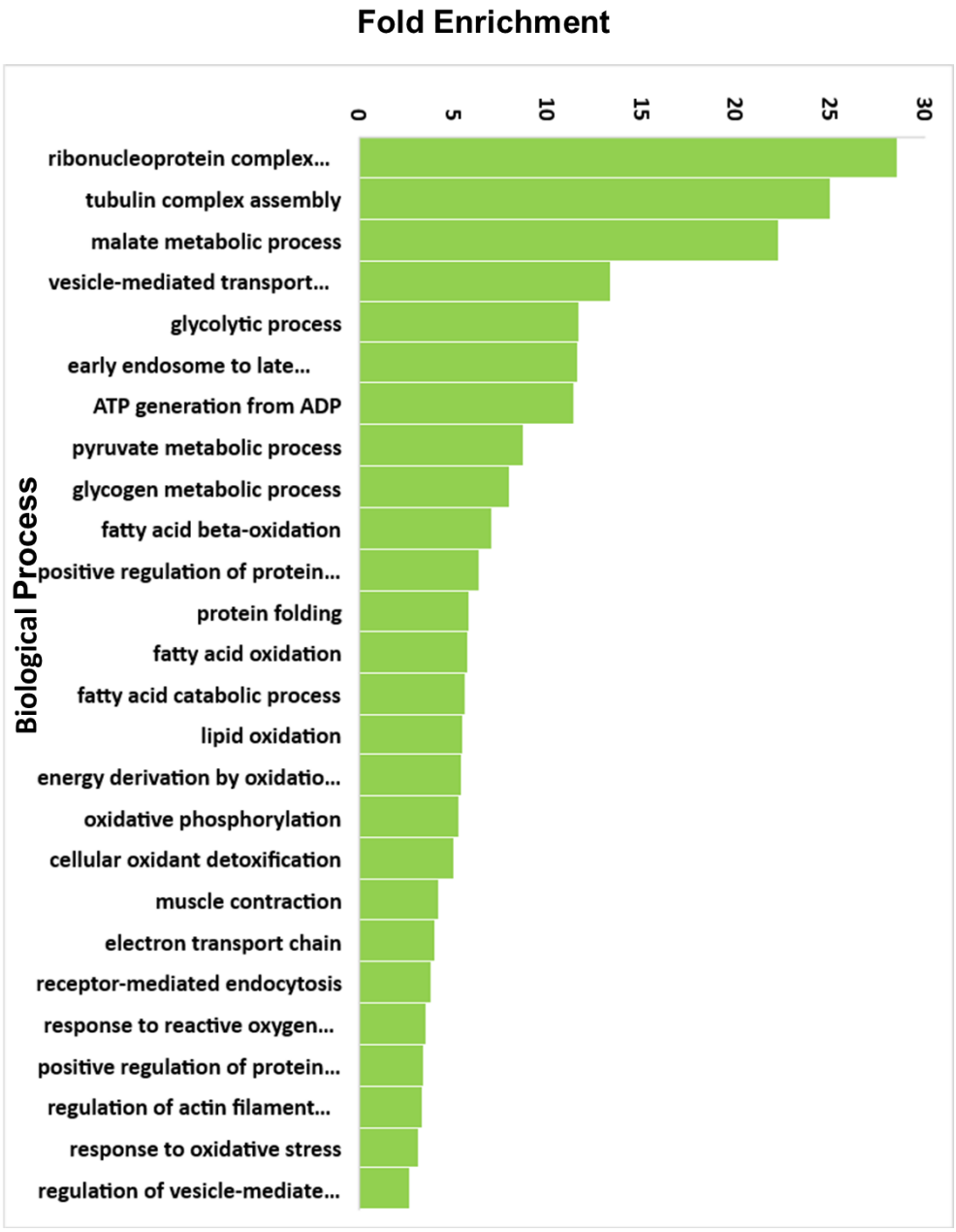

Figure 3:19: Atrial fibrillation protein regulation enrichment comparison to the total Human proteome. *Panther – GO overrepresentation test, Biological Process; most significantly regulated proteins of the AF goat model were compared against the Biological process GO terms of human proteome. An array of overrepresentations starting from 3 – 28.5 folds were observed. Most of the biological processes were functions leading to the cellular energy demand, oxidative stress, protein folding, endosomal transport and vesicle mediated transport. (Figure created using Gene Ontology pathway).*

Similarly, the most enriched Cellular Component GO terms enrichment was analysed. The most overrepresented cell components were muscle filaments, myofibrils, and sarcoplasmic reticulum (SR), which lead-calcium transient pathways, and proteasomes, lysosomes, phagocytic vesicles, cytoplasmic vesicles, which lead to the degradation pathway (Figure 3.20). The top most cell components identified from the over-representation test are included in the Table 3:3.

GO cellular component	**Fold enrichment**
muscle thin filament tropomyosin (GO:0005862)	49.99
cardiac myofibril (GO:0097512)	28.56
proteasome core complex alpha-subunit complex (GO:0019773)	24.99
sarcoplasmic reticulum lumen (GO:0033018)	20.00
proteasome core complex (GO:0005839)	13.33
endocytic vesicle lumen (GO:0071682)	12.12
proteasome complex (GO:0000502)	10.93
cytoplasmic vesicle lumen (GO:0060205)	5.35
vesicle lumen (GO:0031983)	5.32
phagocytic vesicle membrane (GO:0030670)	5.26
inner mitochondrial membrane protein complex (GO:0098800)	4.53
phagocytic vesicle (GO:0045335)	4.35
mitochondrial matrix (GO:0005759)	4.28
endocytic vesicle membrane (GO:0030666)	4.14
vacuolar lumen (GO:0005775)	3.85
endocytic vesicle (GO:0030139)	3.36
secretory vesicle (GO:0099503)	2.76
vesicle (GO:0031982)	2.61
lytic vacuole (GO:0000323)	2.57
lysosome (GO:0005764)	2.57
vacuole (GO:0005773)	2.35
cell junction (GO:0030054)	2.12
cytoplasmic vesicle (GO:0031410)	1.95
intracellular vesicle (GO:0097708)	1.95

Table 3:3: The top most cellular components of AF goat model LA were identified from the overrepresentation test.

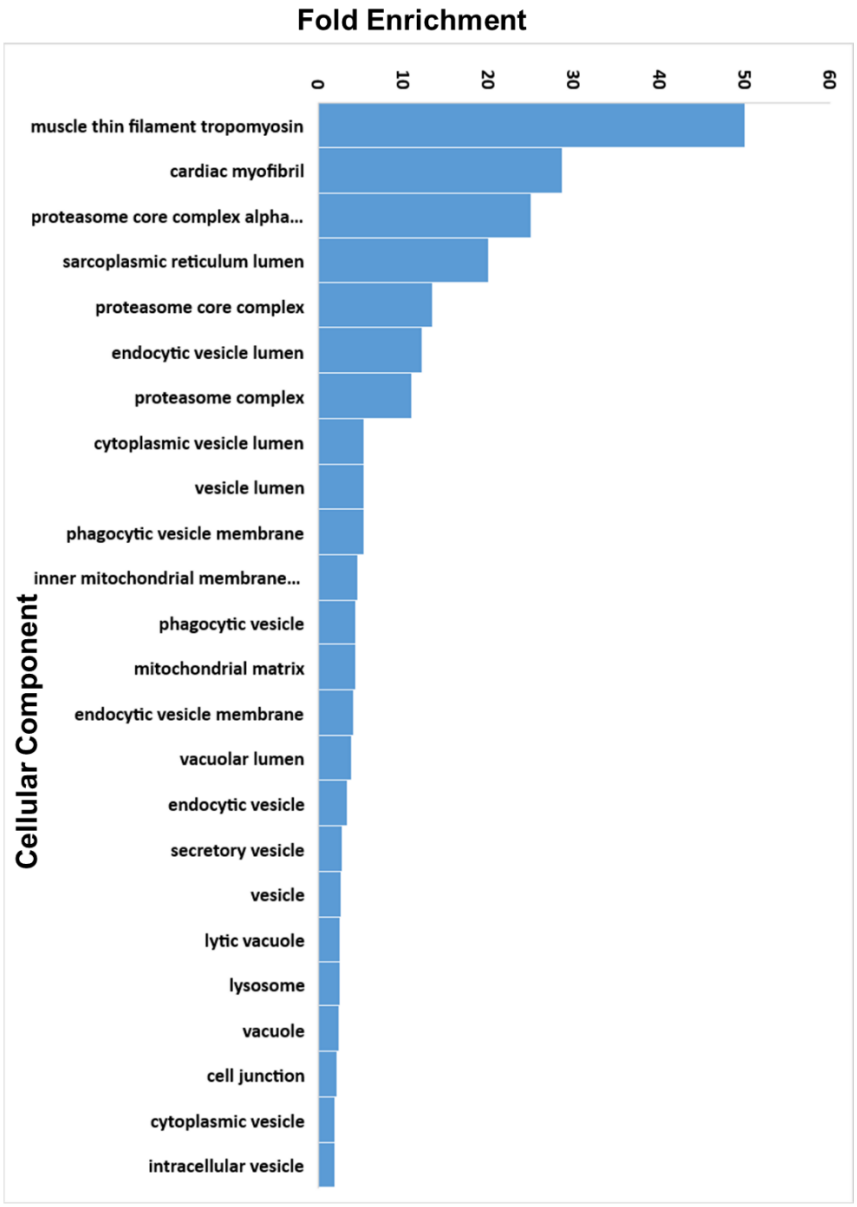

Figure 3:20: Atrial fibrillation protein regulation enrichment comparison to the total Human proteome*. Panther – GO overrepresentation test, Cellular Component; the most significantly regulated proteins of the AF goat model were compared against the cellular component GO terms of human proteome. An array of overrepresentations starting from 2 – 50 folds were observed, starting from muscle filaments, myofibrils proteasome complex, endocytic vesicles, vesicle lumen, lysosomes and phagocytic vesicles, that had the highest cellular component overrepresentation. (Figure created using Gene Ontology pathway).*

3.3.8 Molecular pathways interpreted in tissue lysate of AF goat model

This section discusses the main dysregulated proteins in TL fraction and the impact of the cellular energy-sensing mechanism AMPK pathway. Furthermore, the downstream effects of AMPK.

3.3.8.1 AMPK pathway

The AMP-activated protein kinase (AMPK) pathway was observed to be upregulated in the AF goat model of LA. Respectively, 5'- AMP-activated protein kinase subunit gamma-1 (PRKAG1/AMPK) log2 0.8- fold, calcium-binding protein 39 (CAB39/MO25) log2 0.5 fold, Serine/threonine-protein phosphatase 2A regulatory subunit A beta isoform (PPP2R1B/PP2A) log2 0.7-fold and Protein-serine/threonine kinase (PDK1) log2 0.5-fold were upregulated in the quantitatively analysed proteomic data. Similarly, transcriptomics results showed a significant upregulation in AMPK and are discussed in detail in chapter 4. Therefore, it is possible to assume that AMPK regulatory pathway protein upregulation played a role in the LA of the AF goat model.

Additionally, the NADPH oxidase pathway and gap junctional assembly related proteins such as Protein S100-A9 (S100A9) log2 1.17, Mitogen-activated protein kinase 3 (MAPK3) log2 1.4, Mitogen-activated protein kinase 12 (MAPK12) log2 0.5 and Mitogen-activated protein kinase 14 (MAPK14) log2 0.4, Clathrin light chain B (CLTB) log2 1.5-fold, tubulin α chain (TUBA4A) log2 1.088 up-regulation, and tubulin β chain (TUBB2A) log2 -1.07 were observed down-regulated.

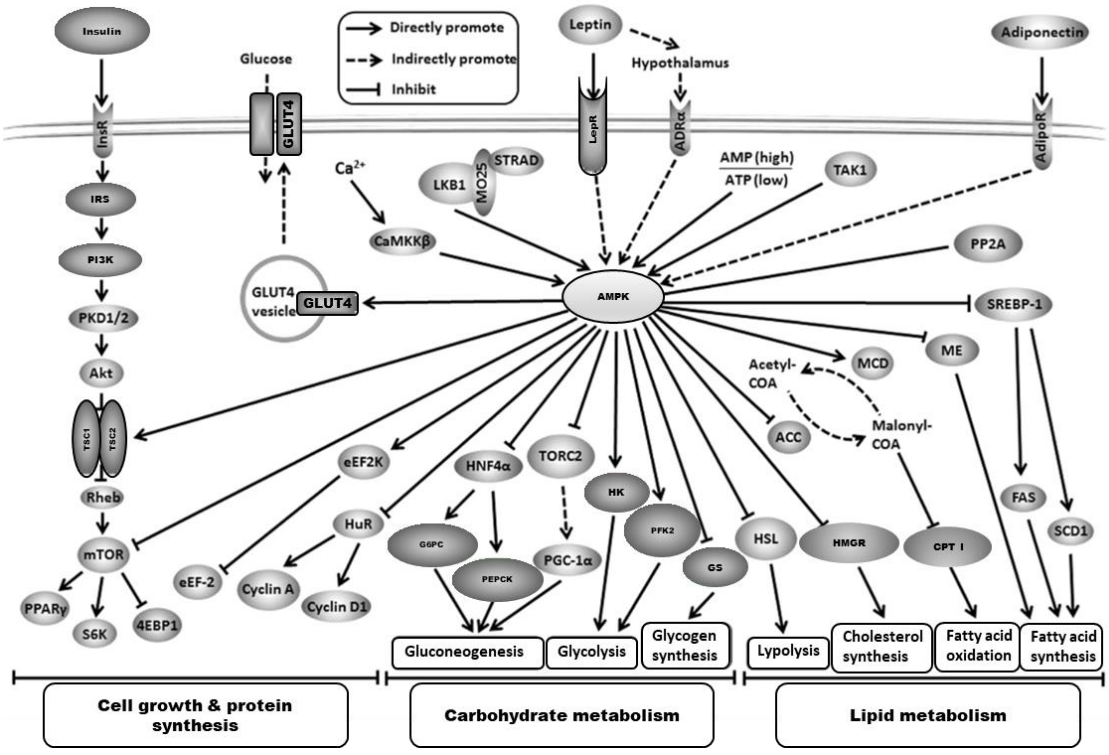

Figure 3:21: AMPK pathway activation through different effectors and the down stream biological paths. *AMPK is directly promoted by high AMP and low ADP levels/ATP depletion (LKB1,MO25, STRAD complex), Calcium induced CaMKK, and indirectly promoted by Laaeptin and adiponectin. In turn, AMPK upregulation increases the cellular glucose uptake through GLUT4 vesicles, glycolysis, and inhibits the cellular mechanisms that decrease ATP levels, such as gluconeogenesis, glycogen synthesis, cholesterol synthesis, and fatty acid synthesis. Moreover, AMPK pathway induce mTOR / S6K pathway to increase the cell growth and protein synthesis. Figure with permission from Wu Kun et.al.,2016.*

AMPK pathway is the central regulator of cellular metabolisms and processes (Figure 3:21) (Mihaylova and Shaw, 2011). AMPK is activated mainly by reduced adenosine triphosphate (ATP) levels in the cell, and the activation of AMPK cascades a series of downstream bio reactions that reprogram metabolism, autophagy, cell polarity and growth. AMPK is a robust sensor for intracellular adenosine nucleotide levels, and is therefore activated even at a modest decrease in ATP production, resulting in a relative increase in Adenosine monophosphate (AMP) or adenosine diphosphate (ADP). As a result, catabolic pathways increase the cellular ATP level while inhibiting the anabolic pathways.

According to the published data the AMPK pathway is activated by several mechanisms: **(1) Lowered cellular ATP path:** When cellular ATP levels are lowered, ADP or AMP binds to the γ regulatory subunits of the AMPK and causes a conformational change that protects the activating phosphorylation of AMPK. Allosterically bound AMP activates AMPK and induces threonine residue Thr-172 phosphorylation through α subunit by an upstream kinase LKB1 (Long and Zierath, 2006). Moreover, AMPK bound AMP inhibits protein phosphatases from dephosphorylating this Thr-172 site. **(2) Calcium triggered CAMKK activation:** A rise in intracellular calcium ions triggers calmodulin-dependent protein kinase kinase (CaMKK) activation of AMPK (Woods *et al.*, 2005). Moreover, AMPK response to calcium flux and phosphorylate on Thr172. This phenomenon takes place without

associating LKB1, via CAMKK2 kinase (Mihaylova and Shaw, 2011). **(3) Indirect AMPK activation by adipocyte hormone leptin:** α-adrenergic receptors are involved in activation of the sympathetic nerve-mediated effect of leptin on AMPK (Minokoshi *et al.*, 2012). AMPK is reported to be activated by the stimulation of Gq coupled α adrenergic receptors. **(4) TGF-β-activated kinase 1 (TAK1) induced AMPK activation:** AMPK heterotrimeric complexes can be directly activated by TAK1- TAK1-binding protein 1 (TAB1) complex through phosphorylation. TAK1 belong to Mitogen-Activated Protein kinase kinase kinase (MAP3K) family member, and AMPK activation through TAK1 signaling enhances the autophagy pathway. Additional studies have suggested that TAK1/MAP3K7 may also phosphorylate Thr172 and activate the downstream pathway (Long and Zierath, 2006).

Here, I discuss a particular set of proteins from the AMPK pathway regulated in the induced AF-goat model and their possible downstream reactions.

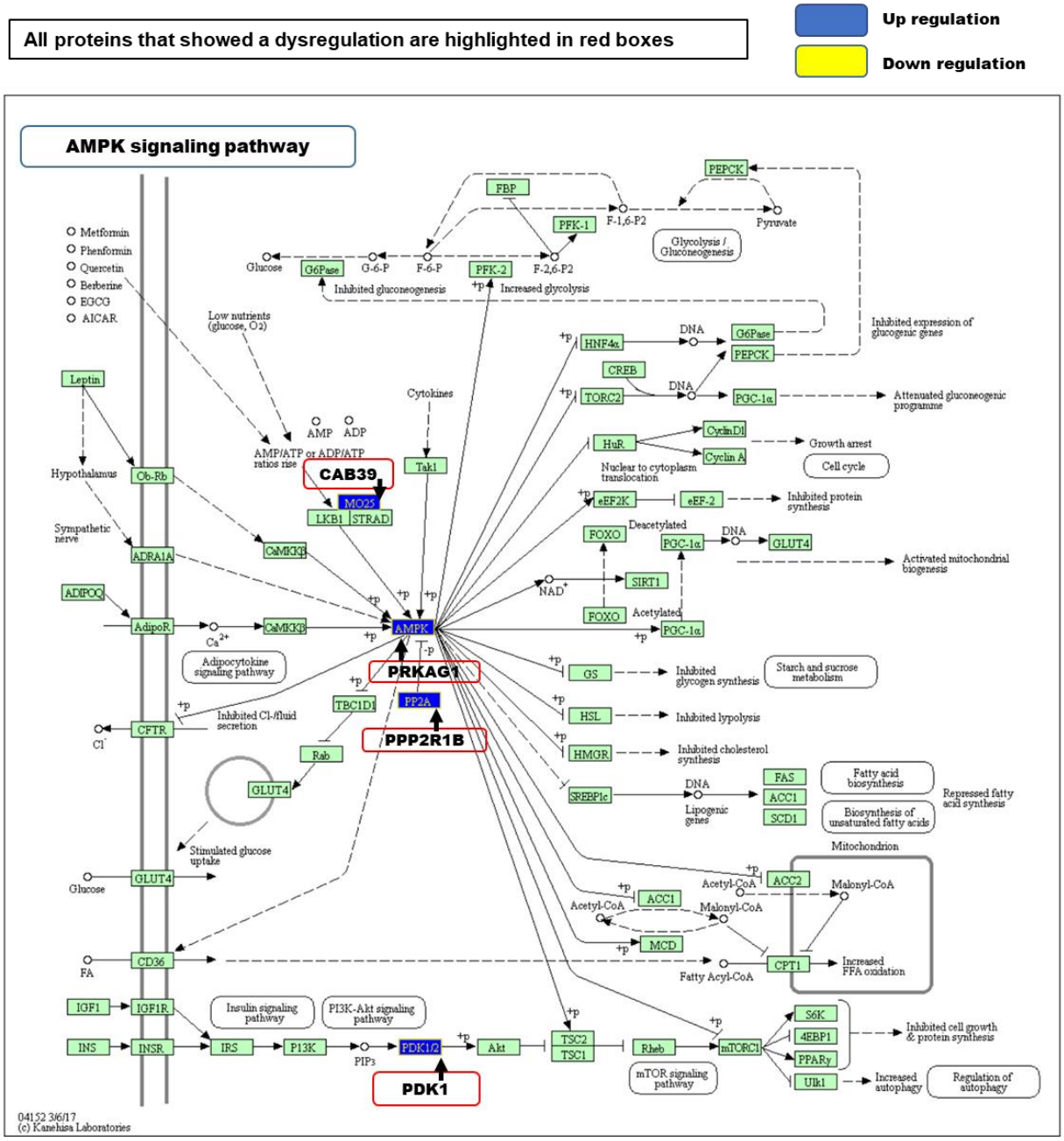

Figure 3:22: Observed protein regulations in AMPK pathway. *The allosteric activation of AMPK by AMP binding to AMPK promotes AMPK phosphorylation by the upstream kinase complex, (Liver kinase B 1, Mouse protein 25 and STE- related adaptor protein) LKB1 + MO25+STRAD, which presumed to have induced the AMPK protein upregulation in the AF goat model. The PDK1/2 protein was upregulated by log2 0.5 fold, which have a tendency to active the Akt pathway. The level of upregulation of the proteins observed are respectively: CAB39/MO25 log2 0.5 fold, PRKAG1/AMPK log2 0.7 fold, PPP2R1B/PP2A log2 0.7 fold and PDK1 log2 0.5 fold. (Arrow = Protein name, protein complex name or protein function. Red bordered boxes= regulated proteins from the query data set. +P = phosphorylating events. Blue = up regulation (log2 fold-change) and Yellow= down regulation (log2 fold-change)). Pathway analysed using KeGG database.*

Out of all the proteins in the AMPK signaling pathway activation mechanisms (Figure 3:21), I identified some significantly regulated proteins, especially from AMPK activation through ATP pathway, that were upregulated in the AF goat model (Figure 3:22). The upregulated proteins and their respective log2 fold-change levels were: Calcium-binding protein 39 (CAB39/MO25) log2 0.5 fold, 5'- AMP-activated protein kinase subunit gamma-1 (PRKAG1/AMPK) log2 0.8- fold, Serine/threonine-protein phosphatase 2A regulatory subunit A beta isoform (PPP2R1B/PP2A) log2 0.7-fold and Protein-serine/threonine kinase (PDK1) log2 0.5-fold.

CAB39/MO25 is part of the Serine/threonine-protein kinase STK11 or liver kinase B1 (LKB1) and STE- related adaptor protein STRAD protein complex (Zeqiraj *et al.*, 2009). CAB39 binds and activates STK11/LKB1, stabilising the interaction between CAB29, MO25 and LKB1. STRAD is a Pseudo kinase that acquires a closed conformation to that of an active protein kinase and binds LKB1 as a pseudo substrate, promoting a conformational change of LKB1 into an active form (Boudeau *et al.*, 2003). LKB1 controls the AMPK family proteins activity by acting as a key upstream regulator of AMPK by mediating phosphorylation. PPP2R1B is a scaffolding molecule that coordinates the assembly of the catalytic subunit of AMPK, and PDK1 plays a main role in the transduction of signals from insulin to PKB/AKT1 by activating the phosphorylation, therefore the signals propagated to downstream targets controlling cell division, survival, amino acid uptake, glucose uptake and storage (Pullen *et al.*, 1998). The activation of AMPK regulates processes including glucose intake, upregulation of ATP production, inhibition of the cell proliferation and growth that

consume ATP, activation of autophagy during nutrient deprivation, regulation of cellular polarity by cytoskeletal remodelling, cell apoptosis, and DNA damage response (Mihaylova and Shaw, 2011). The increased expression of the CAB39, AMPK, PP2A and PDK1 proteins in the induced AF could potentially lead to upregulation in the AMPK signaling pathway.

3.3.8.2 Nicotinamide adenine dinucleotide phosphate oxidase (NADPH oxidase) pathway

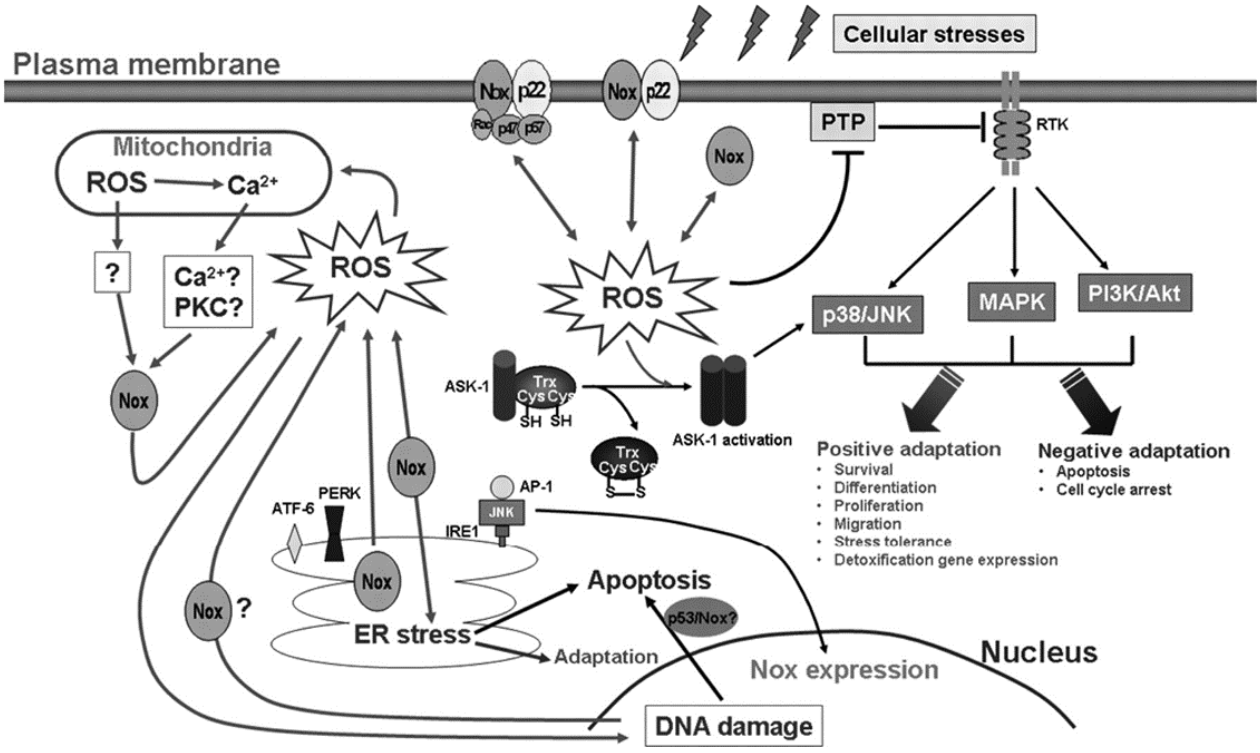

Figure 3:23: Network of cellular stress responses through NADPH oxidase-dependent reactions. *The ROS production vary on the cell types and different cellular stress conditions, such as mitochondrial ROS production, and NOX induced ROS production. These signaling pathways may result in cellular adaptation and tolerance to the stress, or cell apoptosis. Thioredoxin (trx). Schematic with permission from Jiang F et. al., 2011.*

The NADPH Oxidase (NOX) signaling system is a cellular stress-responsive mechanism (Jiang *et al.*, 2011). These stresses can be biological, physical or chemical initiatives and produce reactive oxygen species (ROS) (Figure 3:23). NADPH Oxidase 2, also known as Cytochrome b-245 heavy chain (CYBB), is a membrane-bound enzyme that generates superoxide. Besides membrane bound NOX2, cytosolic NOX

is also present in the cardiovascular system (Schröder *et al.*, 2017). In the cardiovascular system, the main isoforms present are NOX1, NOX2, NOX4, and NOX5.

NOX2 was the first NOX isoform discovered, in work from neutrophils (Hilenski *et al.*, 2004 and You *et al.*, 2013), and is comprised of two activating subunits necessary for its activity and a cytosolic component, which are, respectively: p47phox, p67phox and Ras-related C3 botulinum toxin substrate (RAC), a Rho family small GTPase protein that plays a crucial role in the activation of NOX. (Figure 3:23). NOX-mediated ROS activates the leading cell stress-response signalling network(s): mitogen-activated protein kinase (MAPK), p38 and c-Jun NH2-terminal kinase (JNK). Hence, NOX indirectly modulates both negative and positive cellular adaptations (Figure 3:23), such as cellular apoptosis activation after cellular damage and cell cycle arrest in the event of DNA damage, activation of cell proliferation at tissue damage, fibrosis and angiogenesis.

Moreover, the clinical study of Kim et al., 2005 showed a significantly higher NADPH-induced superoxide release from the RAA of AF patients (Kim *et al.*, 2005) and supporting these findings, a further clinical study performed on patients with in-hospital complications after cardiac surgery showed that the atrial derived superoxide independently associated with increased risk of AF in these patients (Youn *et al.*, 2013) ; (Kim *et al.*, 2005) ; (Antoniades *et al.*, 2012 and Mighiu *et al.*, 2021).

The proteins upregulated with their log2 fold changes were: Protein S100-A9 (S100A9) log2 1.17, Mitogen-activated protein kinase 3 (MAPK3) log2 1.4, Mitogen-activated protein kinase 12 (MAPK12) log2 0.5 and Mitogen-activated protein kinase 14 (MAPK14) log2 0.4. Therefore, the AF goat model obtained a possible overexpression of RHO GTPase activated NADPH oxidase through MAPK regulation. Moreover, the regulation levels interpret that the production of reactive oxygen and nitrogen species in AF goat model LA was considerably increased (Figure 3:24).

The predicted observations are supported by the functional roles of the upregulated proteins observed in the AF disease condition, such as; S100A9, a calcium- and zinc-binding protein. S100A9 plays a significant role in the inflammatory and immune response (Simard *et al.*, 2010). MAPK3 is a crucial member of signal transduction which plays a vital role in diverse biological functions such as cell survival through the regulation of translation (Sha *et al.*, 2017), transcription, cell adhesion (Shi *et al.*, 2012) and cytoskeletal rearrangements (Pullikuth and Catling, 2007). Moreover, the MAPK/ERK mechanism is also involved in endosomal recycling (He and Kogut, 2003) and lysosomal dynamics (Takemasu *et al.*, 2019).

MAPK12 is an essential component of the MAP-kinase signal-transduction pathway and plays a vital role in the cascades of cellular responses initiated by extracellular stimuli such as stress or pro-inflammatory cytokines (Enslen *et al.*, 1998).

MAPK14, which is an essential protein that is regulated by inflammatory stimuli (Xu and Derynck, 2010), and plays a role as a proteasome-mediated degradation regulator that controls the protein turnover of the cell (Qi *et al.*, 2007); Moreover, MAPK signaling has been observed in intracellular compartments such as endosomes, Golgi apparatus, endoplasmic reticulum (ER) and mitochondria (Mor and Philips, 2006).

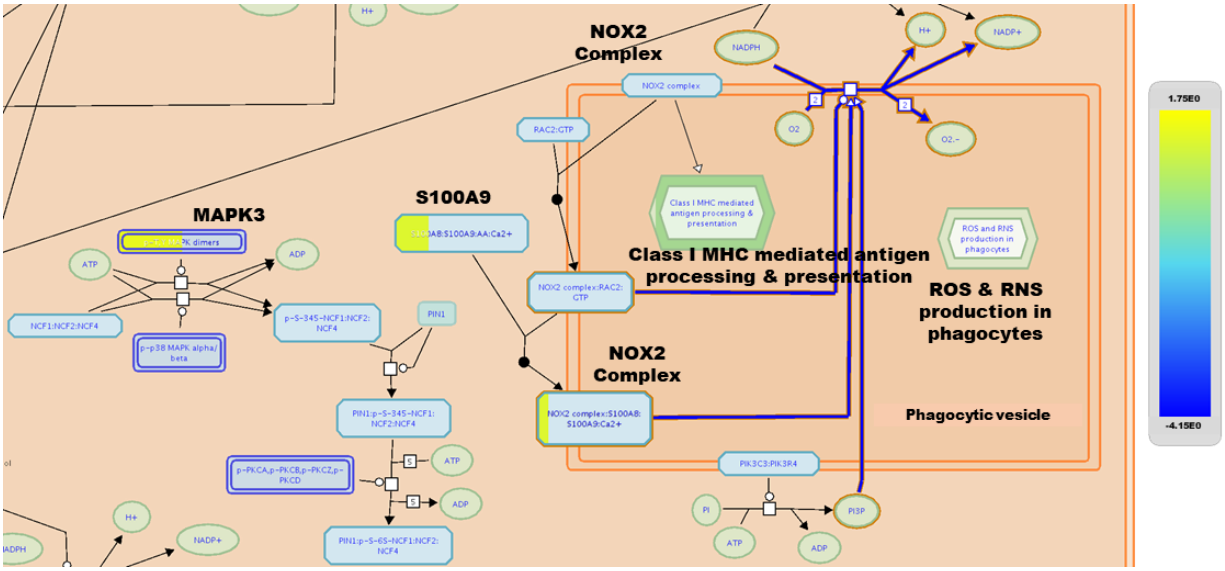

Figure 3:24: RHO GTPase activation of NADPH Oxidase. *The downstream reactions of the RHO GTPase activation of NOX2 signaling in AF included; the induced production of phagocyte oxygen radicals by NOX2 complex bound to Ras-related C3 botulinum toxin substrate 2 (RAC2) and Guanosine-5'-triphosphate (GTP), MAPK1 or MAPK3 phosphorylation of Neutrophil cytosol factor 1 (NCF1) at Serine/threonine-protein kinase Chk1 (Ser345) and S100A8:S100A9:AA: Ca(2+) binding to NOX2 complex. Protein S100-A9 (S100A9 with) log2 1.17, Mitogen-activated protein kinase 3 (MAPK3) with log2 1.4, Mitogen-activated protein kinase 12 (MAPK12) with log2 0.5 and Mitogen-activated protein kinase 14 (MAPK14) with log2 0.4 fold were upregulated (colour code=yellow to blue gradient yellow represent highest up regulation while blue represent highest down regulation, highest upregulation log2 fold 1.75E0 and lowest log2 fold -4.15E0. The protein complexes with complete or part-coloured representation showed the total molecules present from the query data set to complete the complex. Arrow = Protein, protein complex name or protein function) Figure created using www.reactome.com pathway analysis. The given figure is a cropped version from the original elaborated figure for the discussion and the original version of this figure is provided in the Appendix figure A2:1.*

3.3.8.3 Connexins and gap junction assembly

Gap junctions maintain a high degree of coordination between cells. Some of the main functions of gap junctions are exchanging electrical signals, ions and low molecular weight metabolites. Gap junctions in vertebrates are formed with connexin, which are multifaceted proteins connecting cytoskeletal junctional complexes in the cell and facilitating cytoskeletal elements' transport and assembly (Figure 3:25) (Laird, 2010).

Gap junctions of atrial cardiomyocytes are composed of Connexin43 (Cx43), while ventricles have a combination of Connexin40 (Cx40) and Cx43. Gap junctions are formed by clusters of adjacent intercellular channels permitting direct exchange of ions and biomolecules between cells. Furthermore these channels are composed of connexons or two hemi-channels or (Figure 3:26), each hemi-channel localized opposite to each other on each neighbouring cell. A hemi-channel comprises six transmembrane protein subunits of connexins: two connexons dock head-to-head in the cell's outer membrane, forming a tightly sealed, double-membrane intercellular channel (Gemel *et al.*, 2008). The activity of these intercellular channels is regulated, notably by intramolecular modifications such as phosphorylation, which appears to regulate connexin protein turnover, gap junction assembly and the gating of gap junction channels (Segretain and Falk, 2004) and (Laird, 2006).

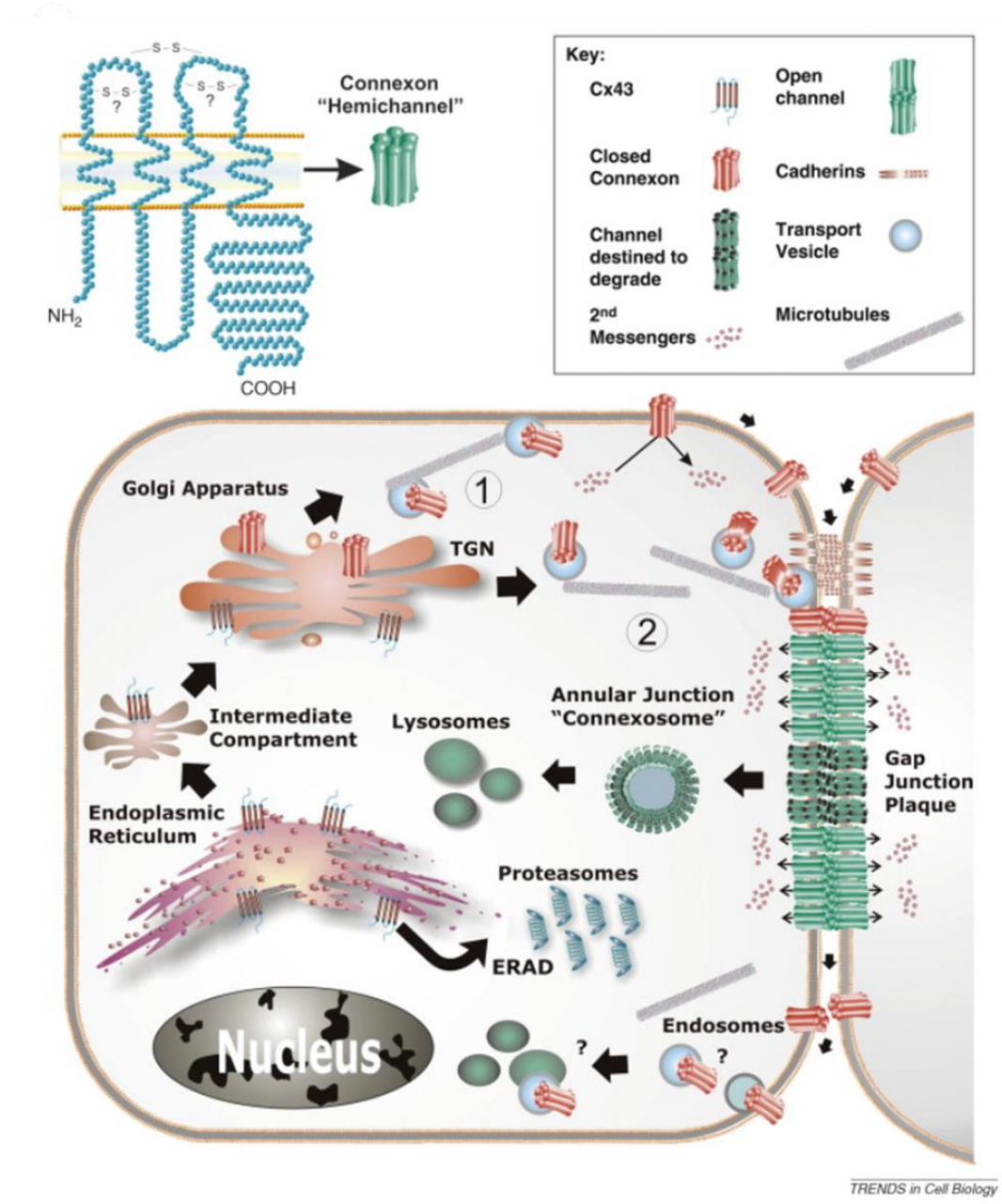

Figure 3:25: Gap junction lifecycle. *(i) Connexin43 hemichannels are formred as hexamers.. The connexin43 protein is synthesized and processed in the ER and intermediate golgi apparatus, and trafficked to the plasma membrane. (ii) The hemichannels are paired at the cell interface and form gap junctions. The unpaired connexons or hemichannels are constatntly reclycled through lysosome as annular connexosome vesicles. This phenomenon is called gap junction turn over. Both connexin delivery mechanisms are heavily dependent on microtubules. (Figure with permission from Laird D.W. et. al., 2010).*

Gap junctions are recycled through vesicle-mediated trafficking, from endosomes to lysosomes (Berthoud *et al.*, 2004), and internalized as connexosomes (Laird, 2010); moreover, the trafficking regulators play a role in directing the assembly or internalization of gap junctions as connexosomes between two cells, such as dynamin2 (DNM2), Adaptor protein complex 2 (AP2A2), CLTB (Piehl *et al.*, 2007), disabled 2 (DAB2), and Myosin VI. (Laird, 2010 and Berthoud *et al.*, 2004).

The proteomic data of the LA AF exhibited changes in some of the regulatory proteins that control the gap junction assembly (Figure 3.26). These include: Dynamin -2, AP2A2 and CLTB. The functional aspects of these proteins have a close resemblance in gap junction assembly, but with slight differences, such as Dynamin-2 (which is a microtubule-associated protein that provides motility with microtubule bundles, hence, a major component in vesicular trafficking processes such as endocytosis) and DNM2 (Yeung *et al.*, 2021) had a log2 -0.6-fold down-regulation in AF diseased condition.

AP2A2 is one of the component of the adaptor protein complex that transports vesicles in the cell. AP2A2 is involved in cargo selection and vesicle formation (Nakatsu and Ohno, 2003). Similar to DNM2, AP2A2 plays a significant part in vesicle trafficking, such as Clathrin-mediated cargo transport targeted to early endosome fusion (Hinrichsen *et al.*, 2003). AP2A2 binds to Clathrin and lipid molecules such as

polyphosphoinositides (Daboussi *et al.*, 2012). With log2 -0.3-fold down-regulation in AF diseased condition, AP2A2 protein down-regulation would be predicted to lead to a possible dysregulation in connexin transport dynamics (Piehl *et al.*, 2007).

CLTB is a self-assembling protein that coats vesicles and acidic organelles, hence is involved in trafficking, recycling and degradation pathways (Brodsky, 2016). CLTB showed a log2 1.5-fold up-regulation, which exhibits a possibility for a malfunction in the gap junction assembly and routing in the AF diseased condition.

Tubulin is a critical cytoskeletal protein that forms microtubules and is required for cellular motility and differentiation (Redeker, 2010 and Vemu *et al.*, 2017). The building block of the human microtubule is the α/β-tubulin heterodimer (Redeker, 2010). The proteomic data showed tubulin α chain (TUBA4A) to be up-regulated by log2 1.088, and the tubulin β chain (TUBB2A) showed a log2 -1.07 down-regulation. Formation and insertion of hemi-channels into the plasma membrane is a process that recruits microtubules and the discordant regulation of the tubulins may suggest that these essential biological functions are potentially altered in AF.

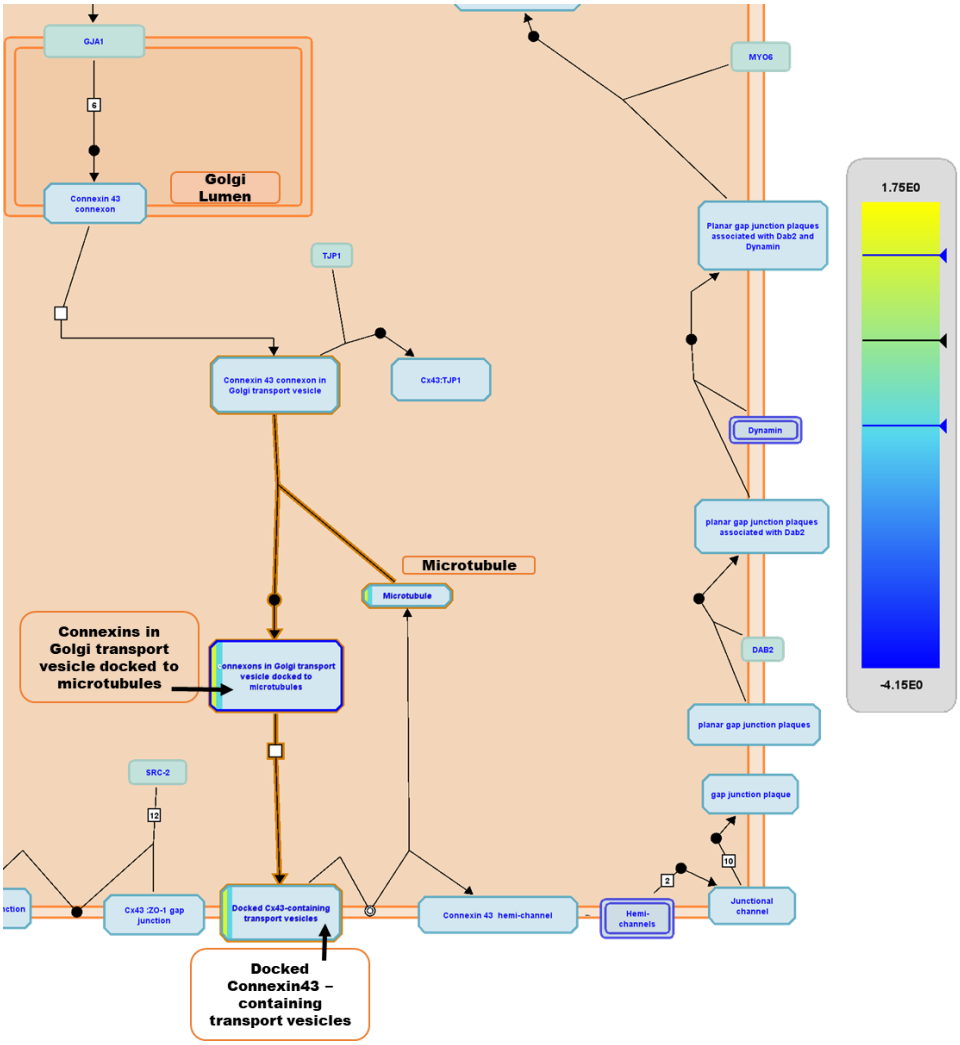

Figure 3:26: Gap junction assembly. *The pathway diagram showing the transport of connexons to the plasma membrane while using the discordantly regulated microtubule dependent trafficking from Golgi to plasma membrane. The assembly of gap junctions involves (1) synthesis of connexin polypeptides at the membrane sites of ER, (2) Homomeric and heteromeric oligomerization into connexon or hemi-channels, (3) Hemi-channel transport through the Golgi stacks, (4) Trans Golgi membrane storage of the hemi channels, (5) trafficking of connexons along the microtubules, (6) insertion of connexons into the plasma membrane, (7) lateral diffusion of hemi channels in the plasma membrane, (8) aggregation of gap junction channels into plaques, and (9) stabilization of peripheral microtubule plus-ends by binding to Connexin43- gap junctions (Segretain and Falk, 2004). Upregulated proteins were CLTB with log2 1.5 fold, TUBA4A with log2 1.088 fold, and down regulated proteins were AP2A2 with log2 -0.3 fold, and DNM2 with a log2 -0.6 fold. Arrow marks pointing to the events with protein regulations. (colour code=yellow to blue gradient yellow represent highest up regulation while blue represent most down regulated, highest upregulation log2 fold 1.75E0 and lowest log2 fold -4.15E0. The protein complexes with complete or part-coloured representation showed the total molecules present from the query data set to complete the complex. Arrow = Protein, protein complex name or protein function). Figure created using www.Reactome.com pathway analysis. The given figure is a cropped version from the original elaborated figure for the discussion and the original version of this figure is provided in the Appendix figure A2:2.*

3.3.8.4 Protein Processing and folding pathways

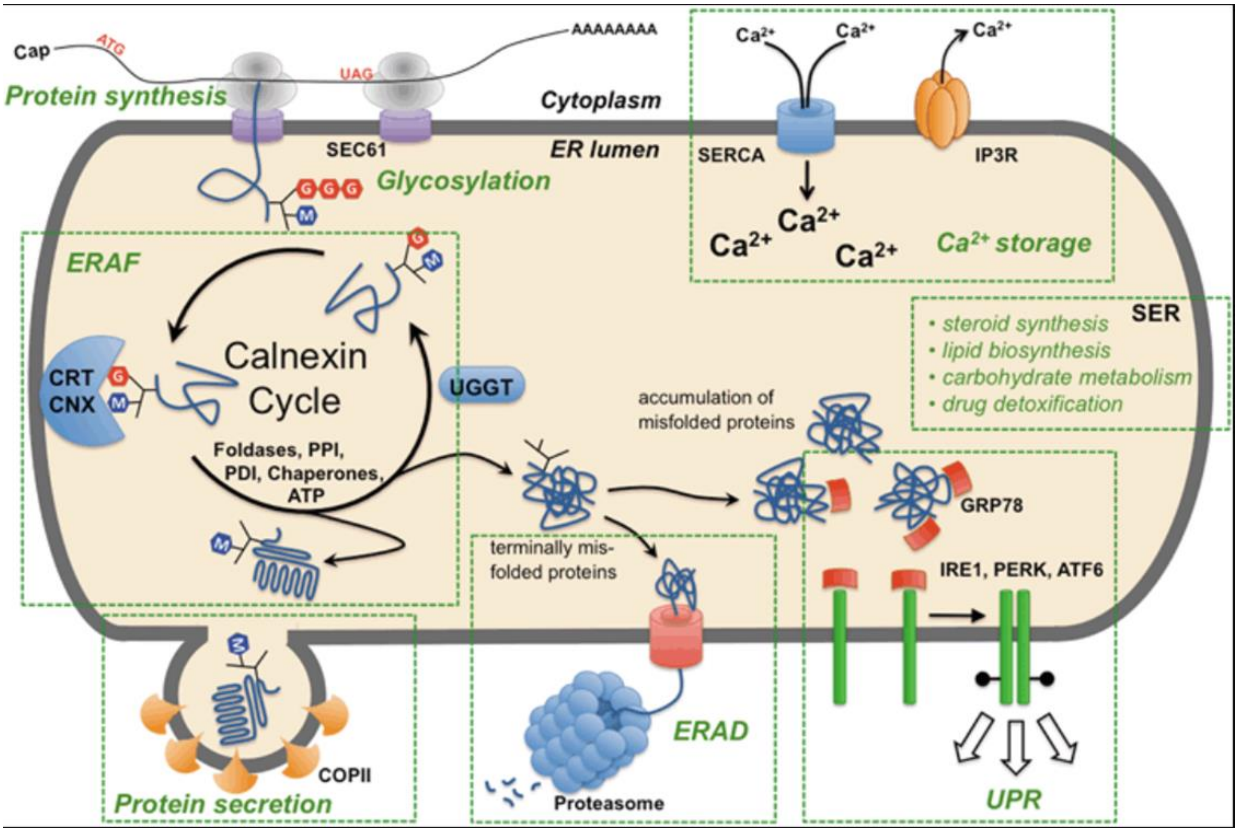

Figure 3:27 Protein processing and main functions of the endoplasmic reticulum in a healthy cell. *The diagram depicts, calcium signaling, protein synthesis by ribosomal RNA in the cytoplasm, internalization of the unfolded proteins. After the internalization of the protein, it undergoes a series of post translational modifications in the ER lumen, such as glycosylation. The N-glycosylated proteins are processed in the calnexin cycle to reveal misfolding. The ER quality controlling system select all the misfolded proteins and they will be degraded through proteasome formation or unfolded protein response path (UPR). Correctly folded proteins will enter the COPII coated vesicles. Figure with permission from (Healy et al., 2012).*

Ribosomes synthesize the proteins during the translation process, and once synthesized, proteins then enter the endoplasmic reticulum (ER) where they undergo further processing. The protein processing inside the ER consists of protein folding, post-translational modifications and one-third of eukaryotic proteins are targeted to the endomembrane system, hence processed and trafficked through ER. Once synthesized, proteins must be translocated from ribosomes to ER through sec61 translocon and processed in the ER.

The ER lumen has the most favourable environment for protein folding and maturation because the ER lumen supports oxidisation and promotes disulphide bond formation between protein complexes (Sevier and Kaiser, 2002). Furthermore, ER lumen is completed with protein regulators, adapters, chaperones and folding enzymes, such as foldases, heat shock proteins (HSP), peptidyl-prolyl cis-trans isomerases, oxidoreductases, glycan-modifying enzymes, lectins and co-factors to incorporate protein processing and folding to its natural state (Figure 3:27) (Healy *et al.*, 2012).

ER contain chaperone proteins that assemble and regulate the correct folding. As an example, calnexin and calreticulin ensure the correct folding of glycoproteins (Healy *et al.*, 2012). Additionally, the heat shock proteins such as HSP90, HSPB1, HSP70, and Heat shock protein beta-7 (HSPB7) are reported to be cardio protective (Maslov *et al.*,

2011) by inducing the protein refolding mechanisms (Żwirowski *et al.*, 2017). ER maintain three main protein processing mechanisms, namely, ER-associated folding (ERAF), ER-associated degradation (ERAD), and unfolded protein response (UPR) activation in recognition of misfolded proteins (Figure 3:27).

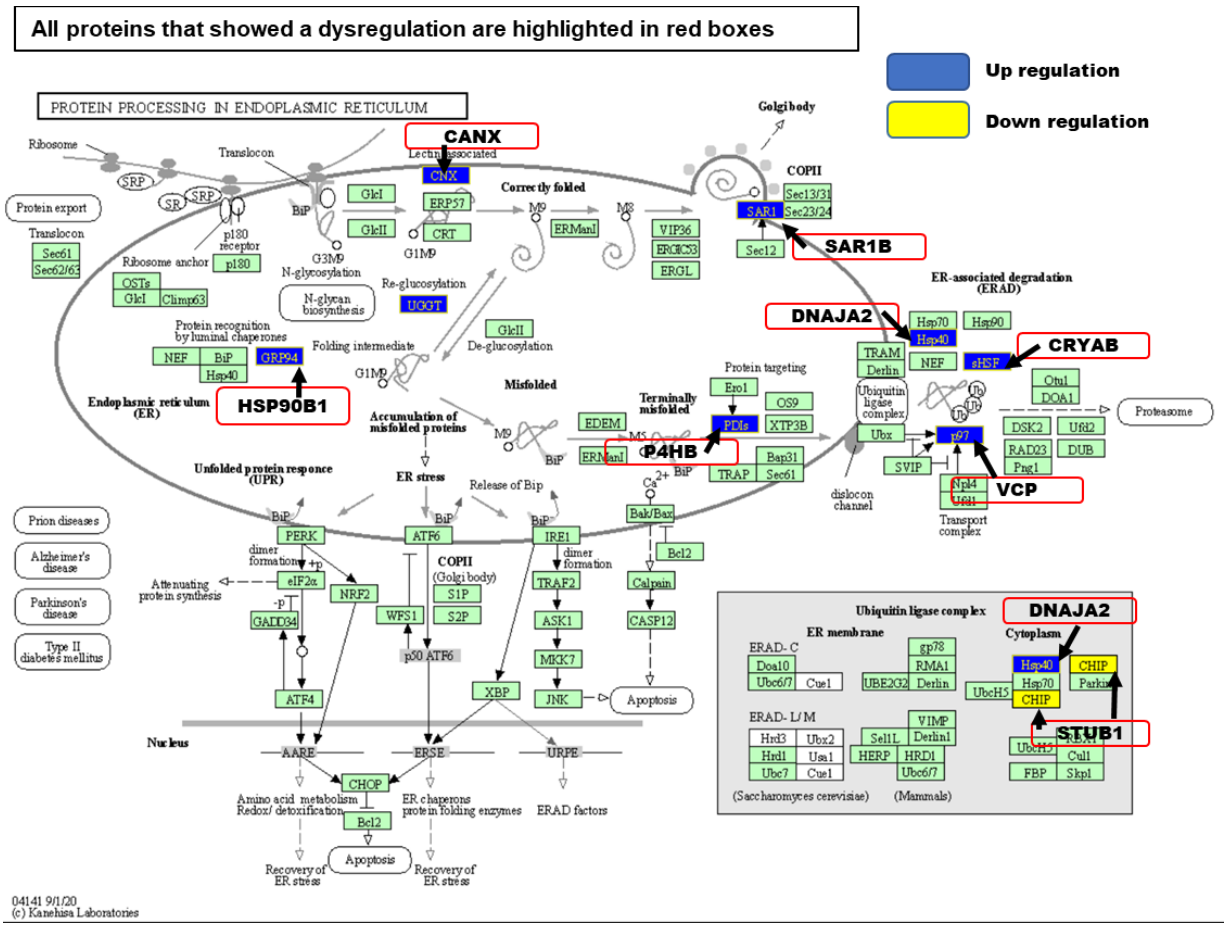

Figure 3:28: Proteins processing in the endoplasmic reticulum. *An array of protein processors were dysregulated in the LA AF goat model as indicated by the red boxes. Except for the down regulation of STUB1 protein by log2 -0.4 fold, all the other proteins were up regulated, namely; UDP-glucose: glycoprotein glucosyltransferase 1 (UGGT1) with 0.7 log2 fold, Calnexin (CNX) by log2 0.9 fold, Protein disulfide-isomerase (P4HB)by log2 0.6 fold, DnaJ homolog subfamily A member 2 (DNAJA2) by log2 0.7 fold, Alpha-crystallin B chain (CRYAB) by log2 0.5 fold, 15S Mg (2+)-ATPase p97 subunit (VCP) by log2 0.3 fold, GTP-binding protein SAR1b (SAR1B)by log2 0.9 fold. (Arrow = Protein name, protein complex name or protein function. Red bordered boxes= regulated proteins from the query data set Blue = up regulation (log2 fold-change) and Yellow= down regulation (log2 fold-change)). Pathway analysed using KeGG database.*

The protein processing and folding pathways of the AF diseased goat model exhibited a considerable amount of protein dysregulations (Figure 3:28). The list of proteins that exhibited significant regulations in AF are presented in Table 3:4.

Protein Name	**Gene name**	**Log2 Fold-change**
UDP-glucose: glycoprotein glucosyltransferase 1	UGGT1	0.70
Calnexin	CNX	0.90
Protein disulfide-isomerase	P4HB	0.60
DnaJ homolog subfamily A member 2	DNAJA2	0.70
Alpha-crystallin B chain	CRYAB	0.50
15S Mg (2+)-ATPase p97 subunit	VCP	0.30
GTP-binding protein SAR1b	SAR1B	0.90
E3 ubiquitin-protein ligase CHIP	STUB1	-0.40

Table 3:4: Proteins regulated in the protein processing pathway.

Proteins that I observed to be regulated in the protein processing pathway are major regulators and chaperones in the ER. A summary of the functions of these regulated proteins that were identified in the AF goat model is as follows:

UGG1 is a quality control protein of the protein folding mechanism which identifies minor misfolding defects in the glycoproteins. The re-glycosylated proteins are directed to the calreticulin for refolding, degradation and recycling (Arnold *et al.*, 2000). P4HB is a protein with multiple functions in the ER. P4HB forms, breaks or rearranges disulfide bonds, creating structural modifications to the proteins, and acts as a chaperone protein to inhibit the accumulation of misfolded proteins (Mezghrani *et al.*,

2000) and (Lumb and Bulleid, 2002). CRYB is a cardiac-specific chaperone protein that inhibits the accumulation of misfolded proteins in the cell under different stress conditions (Chung and Leinwand, 2008). SAR1B is a cargo protein attached to the ER membrane, which assembles the COPII coat complex for COPII mediated vesicle trafficking (Chen *et al.*, 2021).

Hsp90 chaperone protein kinase-targeting subunit (CDC37) is a co-chaperone, and 0.6 log2 fold upregulation was observed in the AF goat model. HATPase_c domain-containing protein (HSP90B1) is a chaperone protein that processes and transports secreted proteins in ER and translocate leaderless cargo into the ERGIC (endoplasmic reticulum-Golgi intermediate compartment) (Zhang *et al.*, 2020). A log2 fold-change of 0.4 up-regulation was observed in the HSP90B1. Heat shock protein beta-1 /Heat shock 27 kDa protein (HSPB1) that plays a role as a molecular chaperone (Rogalla *et al.*, 1999) to maintain denatured proteins into a folding-competent state and phosphorylate proteins to protect against oxidative stress was upregulated log2 0.7 fold-change. Furthermore, cardiac-specific and cardio-protective Heat shock protein beta-7 (HSPB7) (Surya *et al.*, 2018) showed a log2 1.4 fold upregulation.

As part of the protein processing pathways, I also observed discordant protein regulations in the post-chaperone in tubulin folding pathway and tubulin folding intermediates formation by CCT/TriC. The tubulins displayed the below regulations in

the AF goat model: Tubulin alpha chain (TUBA4A) upregulation with 1.08 log2 fold-change and Tubulin beta chain (TUBB2A) down-regulation with -1.07 log2 fold-change.

I also observed an array of chaperone proteins and regulators dysregulated in the AF goat model. Most of these proteins were upregulated, which could signify that an increased amount of misfolded proteins were generated and that the left atrial tissue may have adapted a compensatory mechanism to reduce the accumulation of the protein aggregates by upregulating the proteins as mentioned above.

3.3.8.5 Vesicle mediated transport

Vesicle-mediated transport is a prominent cellular activity responsible for trafficking proteins, lipids, or carbohydrate moieties between an array of specific membrane-bound compartments. Hence the selectivity of the trafficking pathway is precise from one compartment to another. In the eukaryotic cell, vesicle-mediated transport plays a significant role to balance almost all the molecular mechanisms (Cooper, 2000).

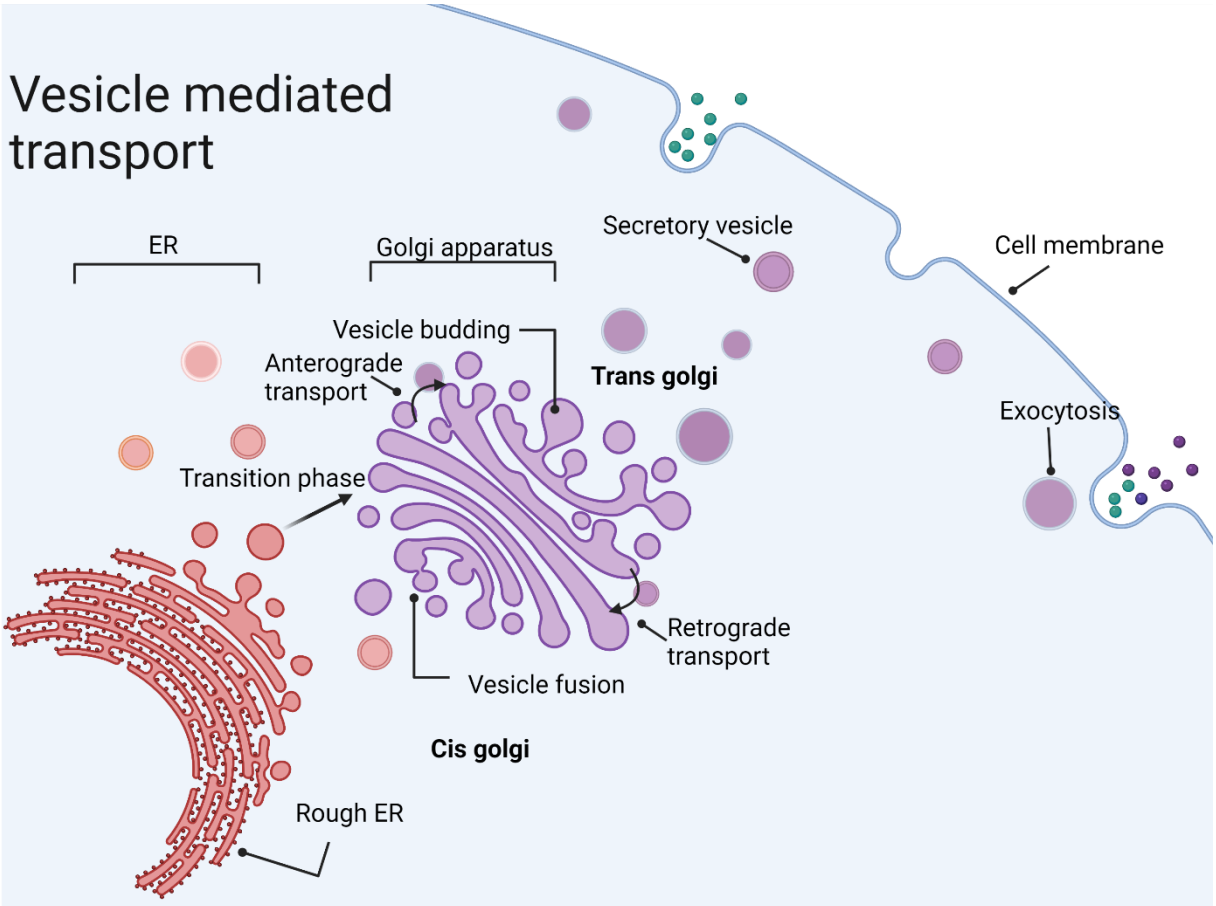

Figure 3:29: A schematic representation of vesicle mediated transport. *The initiation of the cargo transport is at the endomembrane. After cellular cargo, such as lipids, carbohydrate moieties and proteins are selected and transported across ER to the Golgi apparatus through transition vesicles. The cargo targeted towards the end such as plasma membrane or lysosome through the endocytosis or any other vesicle mediated path are considered anterograde transport vesicles, whereas, vesicles that retrieve the native proteins back to ER- Golgi network are labelled as retrograde transport vesicles. Figure created with Biorender.com.*

Vesicle-mediated trafficking of the cellular cargo is initiated at specific membranes, such as ER and Golgi apparatus. A distorting membrane conformation initiates the vesicle budding, usually with the operational support of regulatory proteins. Two types of coated vesicles generate during the vesicle-mediated transport. The first type is clathrin coated vesicles. These clathrin coated vesicles transport cellular cargo from the Golgi network to the lysosome or traffic extracellular contents into the cell at the plasma membrane through endocytosis. The second type is non-clathrin coated, or COP (coat protein) coated vesicles, and they originate at either ER or Golgi. The non clathrin coated vesicles are again subdivided into COPI mediated, and COPII mediated vesicles. COPII mediated vesicles originate or bud from ER and target their cargo forward to the Golgi network, whereas COPI mediated vesicles originate at Golgi apparatus or inter ER- Golgi network and retrieve the native ER or Golgi proteins back to the respective locations to maintain a constant cargo transport (Figure 3:29) (Cooper, 2000).

Furthermore, Rab11A and B were significantly upregulated in the proteomic data. Rab11A was found to be significantly up regulated in the TL fraction exhibiting a log2 0.5-fold increase, whereas, Ras-related Rab11B or Rab11B was upregulated by log2 0.4-fold. These small GTPase proteins are essential regulatory proteins in the vesicle-mediated transport system (Goswami *et al.*, 2021). Activated Rab11 proteins binds with specific effectors such as Rab11 family-interacting protein 3 (RAB11FIP3) to promote vesicle trafficking (Hales *et al.*, 2001) ; (Grosshans *et al.*, 2006 and Welz *et al.*, 2014), and recruit effectors to form vesicles. Moreover, Rab11 proteins are associated with

fusion and tethering (Welz *et al.*, 2014). Rab11 is localized to the trans-Golgi network, and involved in the cellular recycling pathway, supporting the traffic of membrane components to the plasma membrane (Table 3:1) (Urbé *et al.*, 1993).

Vesicle-mediated transport is one of the primary mechanisms driving autophagy, the cellular housekeeping process that balances energy retrieval. Autophagy is divided into three biological cascades, namely- Macroautophagy, Chaperone – mediated-autophagy and Microautophagy (Figure 3:30) (Bose *et al.*, 2022).

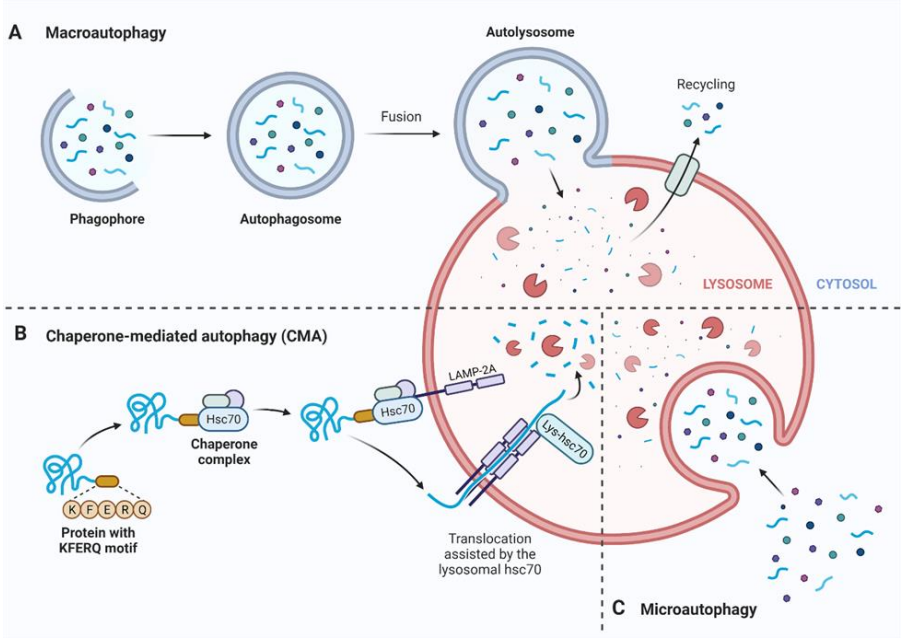

Figure 3:30: Pathways of autophagy. *A. In macroautophagy, cytoplasmic organelles and its content is engulfed by a phagophore, and convert in to an autophagosome which later fuses with a lysosome. B. Chaperone mediated autophagy (CMA) functions through a complex of proteins called chaperons that unfolds and transport dismantled biomolecules to the lysosome. Hsc70 protein play a major role in translocation of the chaperon complex to the LAMP-2A lysosomal membrane protein, which leads to the uptake of the degradable molecules to the lysosome lumen. Figure reproduced with the permission from (Bose et al., 2022).*

Autophagy is generally a survival mechanism for the cell, and dysregulation of this pathway has been reported in several diseases and disorders (Bravo-San Pedro *et al.*, 2017). This self-degradative process removes the aggregated or misfolded proteins, intruded pathogens and damaged cell organelles. Autophagy is focused on lowering cellular stress levels and balancing the sources of energy. Autophagy consists of key functional steps; (1) Nucleation or phagophore formation; (2) Conjugation of proteins Autophagy protein 5 (Atg5) and Autophagy protein 12 (Atg12); (3) Multimerisation of phagophore by interacting with Autophagy protein 16L (Atg16L); (4) Association of Microtubule-associated protein 1A/1B-light chain 3 (LC3) with the protruding phagophore; (5) selection of targeted or non-targeted molecules for degradation; (6) Fusion of lysosome and autophagosome and enzymatic degradation (Glick *et al.*, 2010).

Autophagy has two categories, they are: selective and non-selective autophagy. Removal of protein aggregates and misfolded proteins are removed by selective autophagy, precisely aggrephagy. In the AF goat model, I observed an upregulation of the aggrephagy process (Figure 3:31).

3.3.8.6 Aggrephagy and Proteasome pathway

I further discuss another possible dysregulated pathway under the selective autophagy process, namely, proteasome pathway (Kraft *et al.*, 2010), and both processed misfolded and aggregated proteins. Once the ER chaperone proteins identify the misfolded proteins, they interact with ubiquitin proteins. This process is ubiquitination and is a crucial step for degrading proteins through aggresome (Figure 3:31 and 3:32) and proteasome pathways (Figure 3:31 and 3:33).

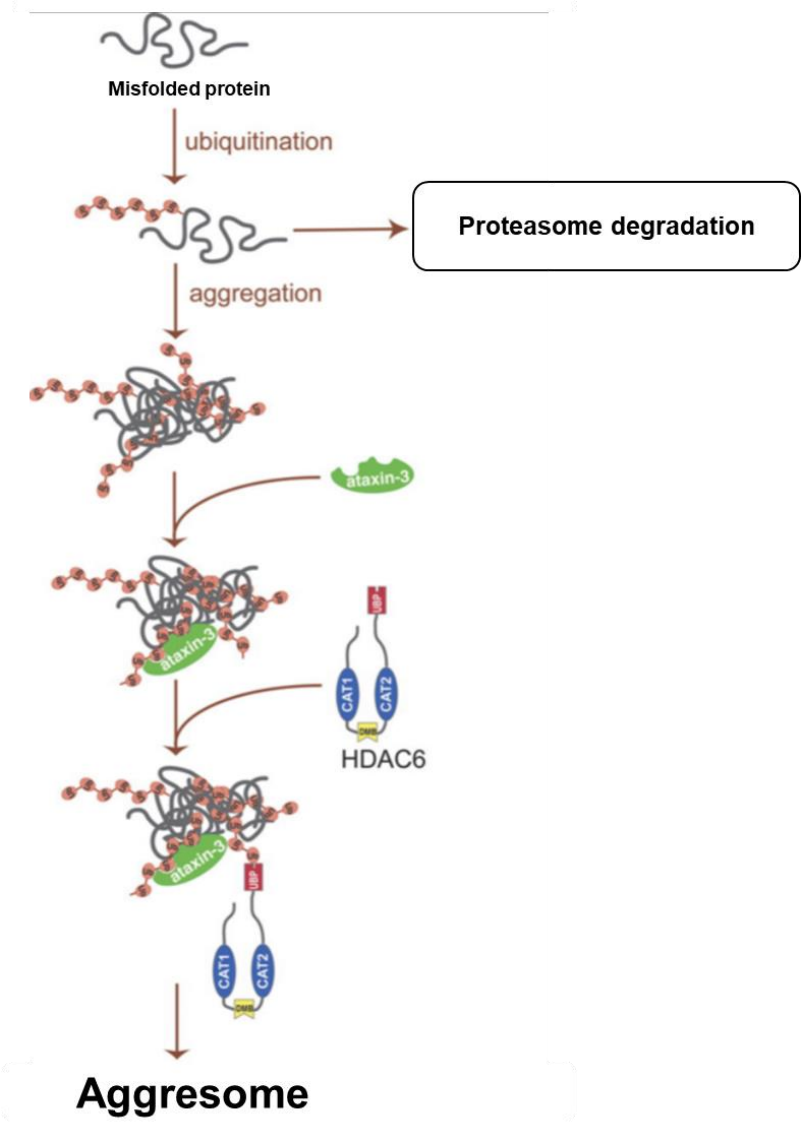

Figure 3:31: A schematic representation of an aggresome formation in a cell. *The formation of ubiquitin proteasome and aggresome are both formed in the event of the misfolded protein accumulation. Ataxin-3 enzyme form a complex with the ubiquitinated proteins. These ubiquitin and HDAC6 complex leads the protein aggregates to the dynein proteins to transport the cargo to the aggresome. Figure with permission from (Ouyang et al., 2012)*

In the AF diseased condition, the aggrephagy process was overexpressed. The proteins related to both aggresome and proteasome formation are mainly ubiquitin. In the AF goat model I observed; ubiquitin carboxyl-terminal hydrolase 5 (USP5) with a

log2 0.3 fold upregulation, E3 ubiquitin-protein ligase PPP1R11 (PPP1R11) with log2 1.7 upregulation, probable ubiquitin carboxyl-terminal hydrolase FAF-X (USP9X) that prevents degradation of proteins through the removal of conjugated ubiquitin with log2 1.0 fold upregulation, tubulin α chain (TUBA4A) with a log2 1.088 upregulation and tubulin β chain (TUBB2A) with a log2 -1.07 down-regulation (Figure 3:32).

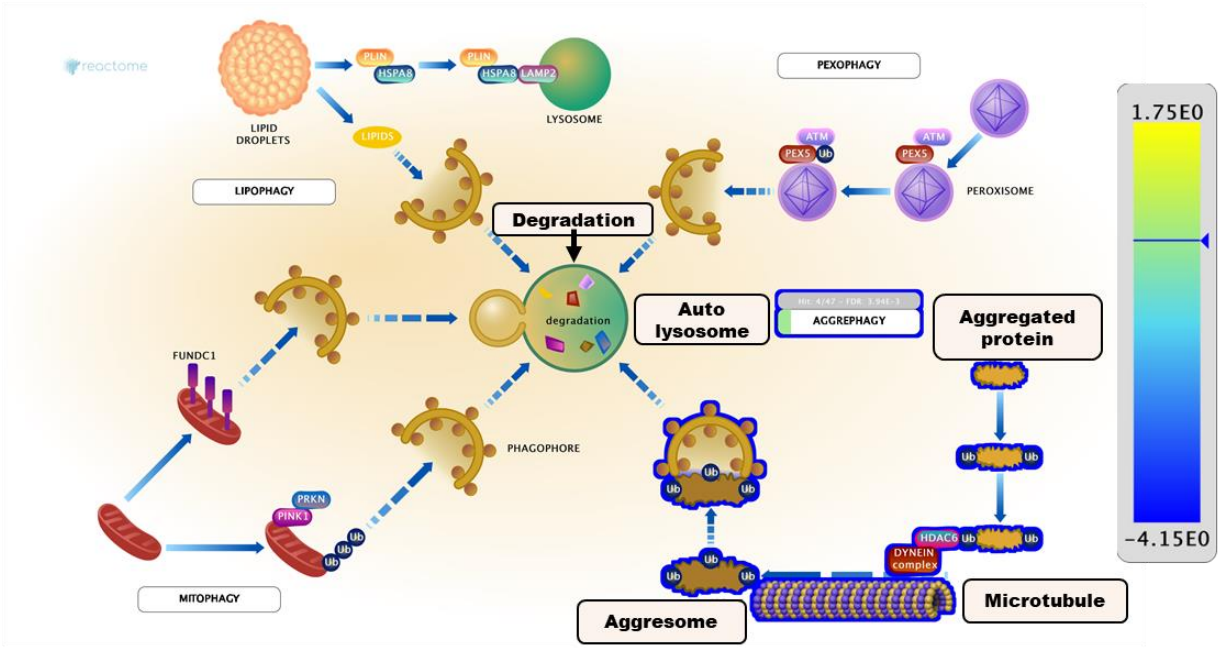

Figure 3:32: Aggresome formation in AF goat model. *The majority of the misfolded protein degradation was detected by then over expressed ubiquitin levels in the left atrial cells of the AF goat model. Proteins that were over expressed, namely: Ubiquitin carboxyl-terminal hydrolase 5 (USP5) by log2 0.3 fold, E3 ubiquitin-protein ligase PPP1R11 (PPP1R11) by log2 1.7 fold, Probable ubiquitin carboxyl-terminal hydrolase FAF-X (USP9X) by log2 1.0 fold, Tubulin α chain (TUBA4A) by a log2 1.088 fold. (Colour code=yellow to blue gradient; yellow represent highest up regulation while blue represent highest down regulation. Highest upregulation log2 1.75E0 fold and lowest log2 -4.15E0 fold. Grey box above the aggrephagy label indicates the pathway entities detected in the query dataset, the total number of entities in the pathway, and the FDR corrected probability score. The protein complexes with complete or part-coloured representation showed the total molecules present from the query data set to complete the complex. Arrow = Protein, protein complex name or protein function). Figure created using www.reactome.com pathway analysis.*

3.3.8.7 Proteasome pathway

The proteasome pathway displayed an upregulation of 26S proteasome non-ATPase regulatory subunit 9 and 11 (PSMD9 and PSMD11). PSMD9 showed a log2 0.8 and PSMD11 showed a log2 0.3 fold upregulation and these two proteins play roles as chaperones during the assembly of the 26S proteasome. 26S proteasome regulatory subunit 4 (PSMC1) which is a component of the 19S proteasome (Gómez-Garre *et al.*, 2012) and was upregulated with a log2 fold of 0.8 (Figure 3:33). PSMC1 is an ATPase of 19S proteasome multiprotein complex involved in the ATP-dependent degradation of ubiquitinated proteins (Gómez-Garre *et al.*, 2012).

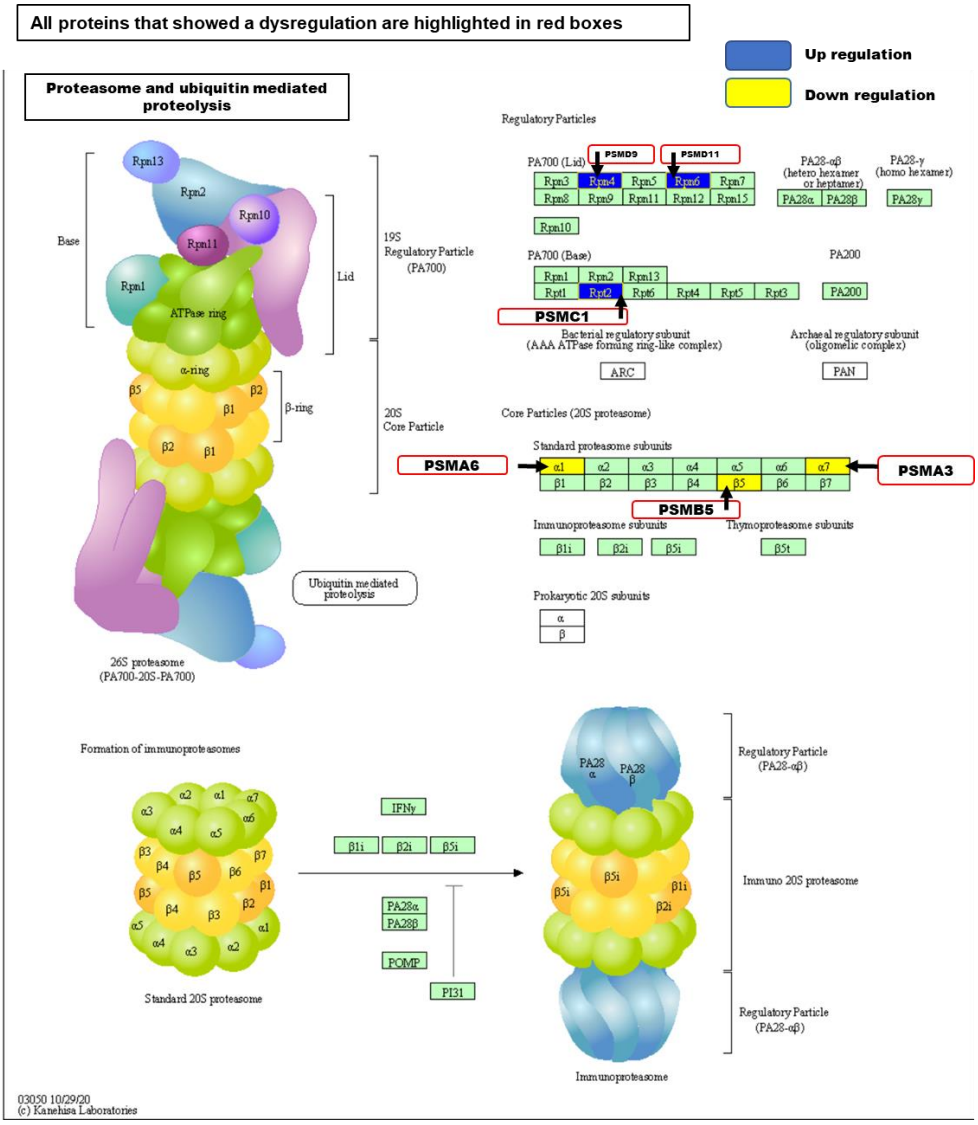

Figure 3:33: A KeGG pathway representation of proteasome assembly. *Proteasome is made of two units, 19S regulatory particle (PA700) and 20S core particle. PA700 regulatory particle (26S proteasome regulatory subunit) is divided into two categories, namely, PA700 (Lid) and PA700 (Base). Similarly core particle is divided into three categories, namely, standard proteasome subunits, Immunoproteasome subunits and Thymo-proteasome subunits. In the LA AF goat model, 26S proteasome regulatory subunit assembly some proteins showed a protein upregulation, namely; PSMD9 by a log2 0.8 and PSMD11 by a log2 0.3 fold and PSMC1 log2 fold of 0.8. (Arrow = Protein name, protein complex name or protein function. Red bordered boxes= regulated proteins from the query data set. Blue = up regulation (log2 fold-change) and Yellow= down regulation (log2-fold change)). Pathway analysed using KeGG database.*

3.3.9 Mitochondrial regulations in atrial fibrillation - results highlights

Mitochondria are considered the energy production unit in the cell. The primary pathway for ATP production is oxidative phosphorylation (OXPHOS). Increases in ATP production eventually lead to the possible reactive oxygen species (ROS) production (Liu, 1998 and Korshunov *et al.*, 1997). ROS is one known mediator of cellular stress in left atria (Liang *et al.*, 2018), and I observed a considerable elevation in proteasome and aggresome formation in the LA AF tissue.

Here, I discuss the downstream effects of the AMPK pathway, which lead to increased mitochondrial energy production and by-product ROS mediation in cellular stress. From the proteomic data of AF goat model; Apart from the mitochondrial OXPHOS, and ROS mediated oxidative stress, I discuss identified regulations in pathways such as GLUT4 translocation to plasma membrane, involved in the sub pathways with a connection to the vesicle mediated transport and cargo.

3.3.9.1 Respiratory electron transport chain and chemiosmosis pathway (Oxidative Phosphorylation)

The cardiac myocytes of AF require a high level of ATP energy due to its abnormal excitation-contraction coupling mechanism. Therefore, the OXPHOS pathway has been studied and reported in the AF pathology (Jeganathan *et al.*, 2017), and LA reportedly has lower ATP levels than RA in human and mice AF in Ozcan *et al*.,2019 studies (Ozcan *et al.*, 2019). Here, in this AF goat model LA, I observed protein regulations that support the findings of Ozcan *et al*., 2019.

The energy-rich molecules such as NADH and FADH2 are formed in glycolysis, fatty acid oxidation and citric acid cycle. Each NADH and FADH2 molecule contains an electron pair, and these electrons have a high transfer force. Hence, reducing the molecular oxygen and water releases a considerable amount of free energy used to generate ATP. This process is oxidative phosphorylation (OXPHOS) (Figure 3:29), and it is the primary source of ATP production. Generally, OXPHOS generates 30 molecules of ATP energy per molecule of glucose. During the process of ATP production superoxide and other types of ROS are produced in complex-I and complex-III (Dromparis and Michelakis, 2013).

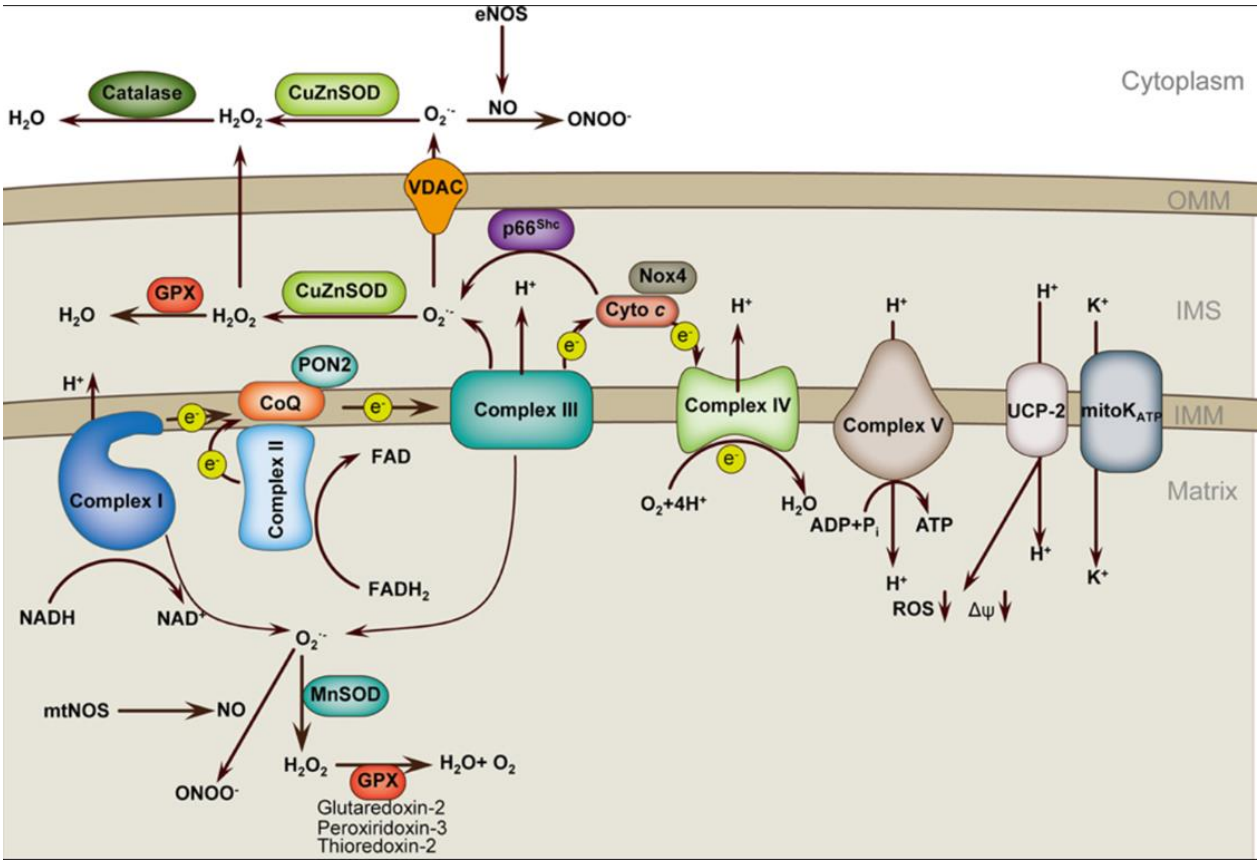

Figure 3:34: Mitochondrial oxidative phosphorylation and ROS production. *Respiratory chain complexes I–IV are located over the mitochondrial inner membrane, and proton gradient from I- IV drives the electron transfer. ATP generated by ATP synthase/ complex V. Electrons (e−) are passed from complex I to II, while NADH convert to NAD^+ and $FADH_2$ to FAD^+. From complex III to complex IV e− are transferred by cytochrome c complex. At the complex IV O_2 reduces to H_2O and the e− are accompanied with H^+ gradient across the inner mitochondrial membrane. The electrochemical gradient move across complex V or ATP synthase generate ATP from ADP. The leaked e− produce ROS and CuZnSOD convert superoxide to H_2O_2. ROS formation is further reduced by the UCP and mitochondrial K_{ATP}. Figure with permission from (Tang et al., 2014).*

Oxidative Phosphorylation is the primary cellular process of high scale ATP production in the inner mitochondrial membrane and matrix. ROS production takes place in the inner mitochondrial space. The highest number of proteins that were up regulated in the AF diseased condition belonged to Complex – I of the electron transport chain,

where, the highest level of ROS are produced and these proteins with their respective regulation levels related to the Figure 3:35 are presented in the Table 3:5.

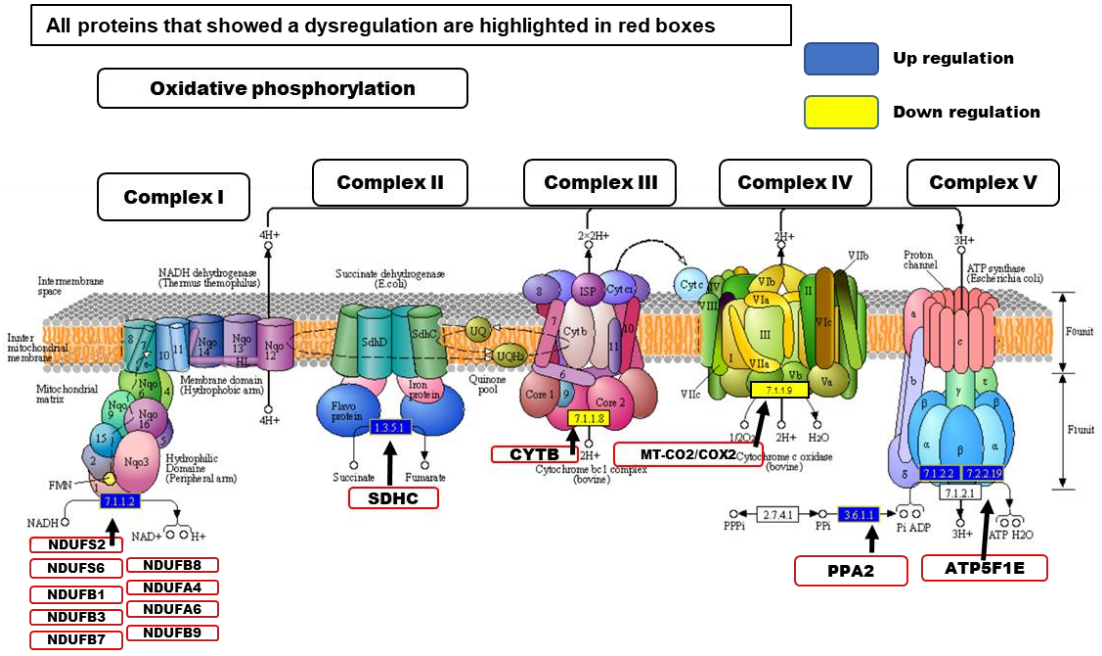

Figure 3:35: Respiratory electron transport chain and chemiosmosis pathway. *The electron transport chain of the oxidative phosphorylation pathway proteins showed a discordant protein regulation in the oxidative phosphorylation (OXPHOS). All proteins that showed dysregulation have been highlighted in red boxes. Thirteen proteins were over expressed in the AF condition except protein, CYTB. These upregulations were mainly from proteins in complex-I biogenesis. The up regulated proteins observed in the OXPHOS were; NADH dehydrogenase (Ubiquinone) 1 alpha sub-complex 4 (NDUFA4) with log2 1.2 fold, Protein arginine methyl transferase NDUFAF7 (NDUFAF7) with log2 1.06 fold, Complex I-49kD (NDUFS2) with log2 1.0 fold, NADH dehydrogenase [ubiquinone] iron-sulfur protein 4, mitochondrial (NDUFS4) with log2 0.9 fold, Complex I-B12 (NDUFB3) with log2 0.9 fold, Complex I-MNLL (NDUFB1) with log2 1.08 fold, Complex I-B12 (NDUFB3) with log2 0.9 fold, NADH dehydrogenase [ubiquinone] iron-sulfur protein 6, mitochondrial (NDUFS6)with log2 1.07 fold, NADH dehydrogenase [ubiquinone] 1 beta sub-complex subunit 8, mitochondrial (NDUFB8) with log2 1.02 fold, Complex I-B18 (NDUFB7) with log2 0.95 fold, Complex I-B22 (NDUFB9) with log2 0.85 fold, NADH dehydrogenase [ubiquinone] 1 alpha sub-complex subunit 6 (NDUFA6) log2 0.6 fold, Succinate dehydrogenase cytochrome b560 subunit, mitochondrial (SDHC), Cytochrome c oxidase subunit 7A1, , Cytochrome c oxidase subunit 2 (MT-CO2) with log2 -0.7 fold, Inorganic diphosphatase (PPA2) with log2 0.5 fold , and the chemiosmotic coupling ATP production protein ATP synthase subunit epsilon, mitochondrial (ATP5F1E) by log2 0.7 fold. Cytochrome b (CYTB) of cytochrome bc complex was down regulated by log2 -1.5-fold. (Arrow = Protein name, protein complex name or protein function. Red bordered boxes= regulated proteins from the query data set. Blue = up regulation (log2 fold-change) and Yellow= down regulation (log2 fold-change)). Pathway analysed using KeGG database.*

Protein Name	Gene name	Log2 Fold-change
NADH dehydrogenase (Ubiquinone) 1 alpha sub-complex 4	NDUFA4	1.20
Protein arginine methyl transferase NDUFAF7	NDUFAF7	1.06
Complex I-49kD	NDUFS2	1.00
NADH dehydrogenase [ubiquinone] iron-sulfur protein 4, mitochondrial	NDUFS4	0.90
Complex I-B12	NDUFB3	0.90
Complex I-MNLL	NDUFB1	1.08
NADH dehydrogenase [ubiquinone] iron-sulfur protein 6, mitochondrial	NDUFS6	1.07
NADH dehydrogenase [ubiquinone] 1 beta sub-complex subunit 8, mitochondrial	NDUFB8	1.02
Complex I-B18	NDUFB7	0.95
Complex I-B22	NDUFB9	0.85
NADH dehydrogenase [ubiquinone] 1 alpha sub-complex subunit 6	NDUFA6	0.60
Cytochrome c oxidase subunit 7A1	COX7A1	1.30
Cytochrome c oxidase subunit 2	MT-CO2	-0.70
Cytochrome c oxidase subunit 6A1	COX6A1	1.60
Inorganic diphosphatase	PPA2	0.50
chemiosmotic coupling ATP production-protein ATP synthase subunit epsilon	ATP5F1E	0.70
Cytochrome b	CYTB	-1.50

Table 3:5: The table presents the array of proteins regulated from the OXPHOS pathway.

NADH ubiquinone oxidoreductase (Complex – I) is the largest electron transport chain unit and catalyses the electron transfer from NADH to Quinone (Cecchini, 2003). The electron transfer through a series of redox reactions, and the inactive to active transition modulated by the cations in the Complex-I create a conformational change to the enzyme that drives the transition (Grivennikova *et al.*, 2001). The overall upregulations of Complex-I proteins observed in the AF condition provide us with a general understanding that the ATP production appears to have increased, with an elevated ROS production.

Succinate dehydrogenase (Complex-II) is the only component of ATP production that is associated with both the citric acid cycle and electron transport chain. Complex-II extends from the flavin, and iron-sulfur redox cofactors in the membrane-extrinsic domain to the quinone and the b heme cofactors in the membrane domain, and similar to Complex-I, Complex-II form reactive oxygen species, which is vital to understand the presumed functional changes I observe in the AF goat model.

Cytochrome C oxidase (Complex-IV) is a proton gradient contributor that transfers electrons to molecular oxygen to produce H_2O. I observed that most COX proteins were upregulated in AF while COX2 protein showed a slight down-regulation (log2 -0.7 fold).

ATP synthase or Complex-V is the main ATP generator through the proton gradient and the last enzyme to synthesize ATP molecules from ADP and an inorganic phosphate group (Yoshida *et al.*, 2001). The overexpressed ATP synthase proteins in the AF diseased condition might reflect an increased ATP energy demand in the AF pathology.

3.3.9.2 Mitochondrial Stress and ROS formation

Oxidative stress plays a significant role in several clinical conditions such as cancer (Roberts *et al.*, 2009 and Hardbower *et al.*, 2013) diabetes (Wright *et al.*, 2006), viral infections (Beck *et al.*, 2000), and is especially reported in cardiac disorders such as atherosclerosis (Singh and Jialal, 2006), ischemia-reperfusion injury (Xia *et al.*, 2014), cardiac hypertrophy (Maulik and Kumar, 2012), heart failure (Seddon *et al.*, 2007) and AF (Xie *et al.*, 2015).

Superoxide ($O_2^{\bullet-}$) is the prominent mitochondrial ROS. The production of $O_2^{\bullet-}$ in mitochondria is significant because it underlies oxidative damage in many pathologies and contributes to retrograde redox signaling in the cell. There are two types of reactive oxygen species: free radicals that are highly reactive (e.g. $O_2^{\bullet-}$) and non-radicals (e.g. HOCl, H_2O_2). Free radicals consist of one or more free or unpaired electrons, hence highly reactive to release the energy. When produced in higher concentrations, these free radicals react with any molecule in the cell and mostly with essential proteins or lipids that are abundantly available in the cell. Therefore, cells have adapted ROS sensitive antioxidant defense systems to reduce toxicity and cellular damage (Murphy, 2009) and (Dhalla *et al.*, 2000).

Mitochondrial $O_2^{\bullet -}$ are produced between mitochondrial matrixes in the outer mitochondrial space, and Complex-I is the predominant site of superoxide production (Figure 3:34 and 3:35).

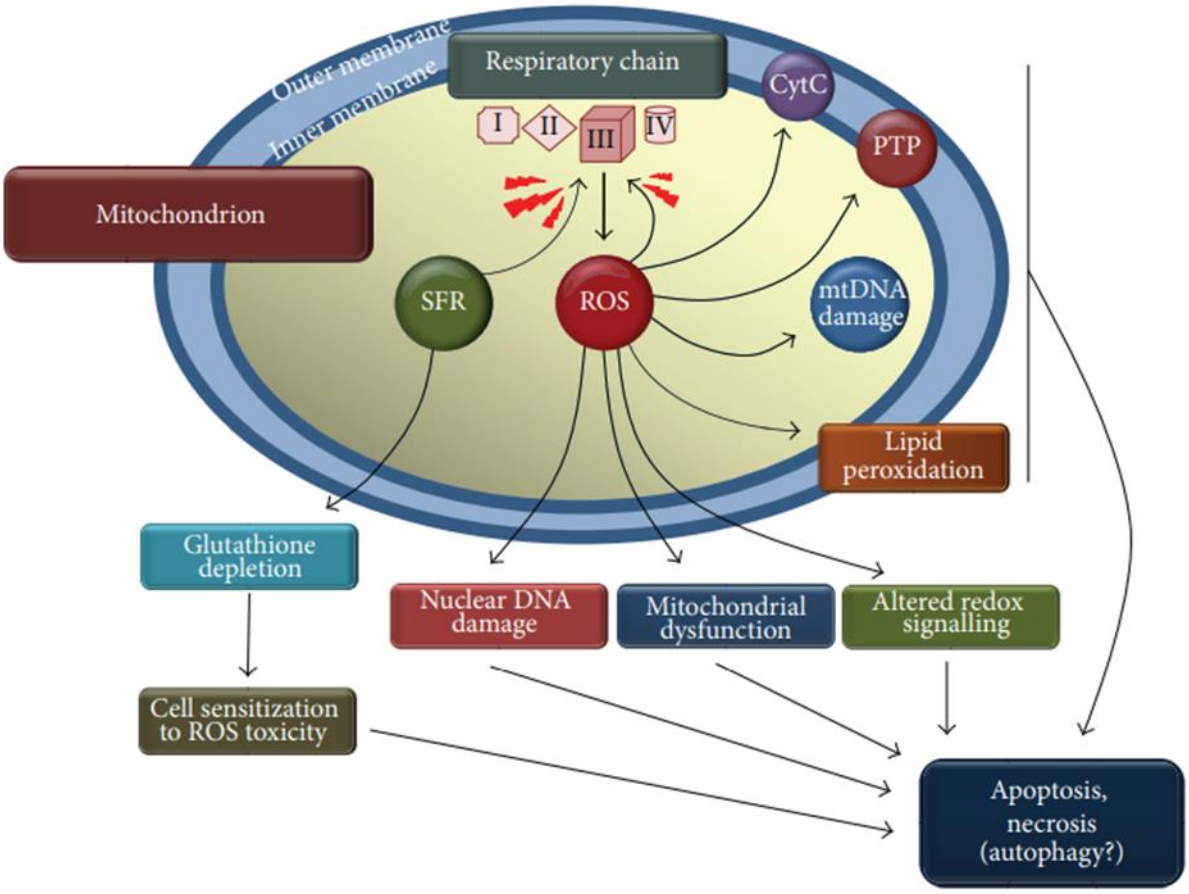

Figure 3:36: Schematic representation of mitochondrial ROS formation. *ROS initiate a cascade of toxic events culminating in apoptosis, necrosis, and cell survival mechanism, autophagy. Arrows are pointed to the commonly observed cellular toxic events generated by ROS. CytC: cytochrome C complex mediated electron leakage at the inner membrane of mitochondria; PTP: permeability transition pore ; I,II,III,IV; complexes of OXPHOS; mtDNA: mitochondrial DNA;. .Figure with permission from (Sestili and Fimognari, 2015).*

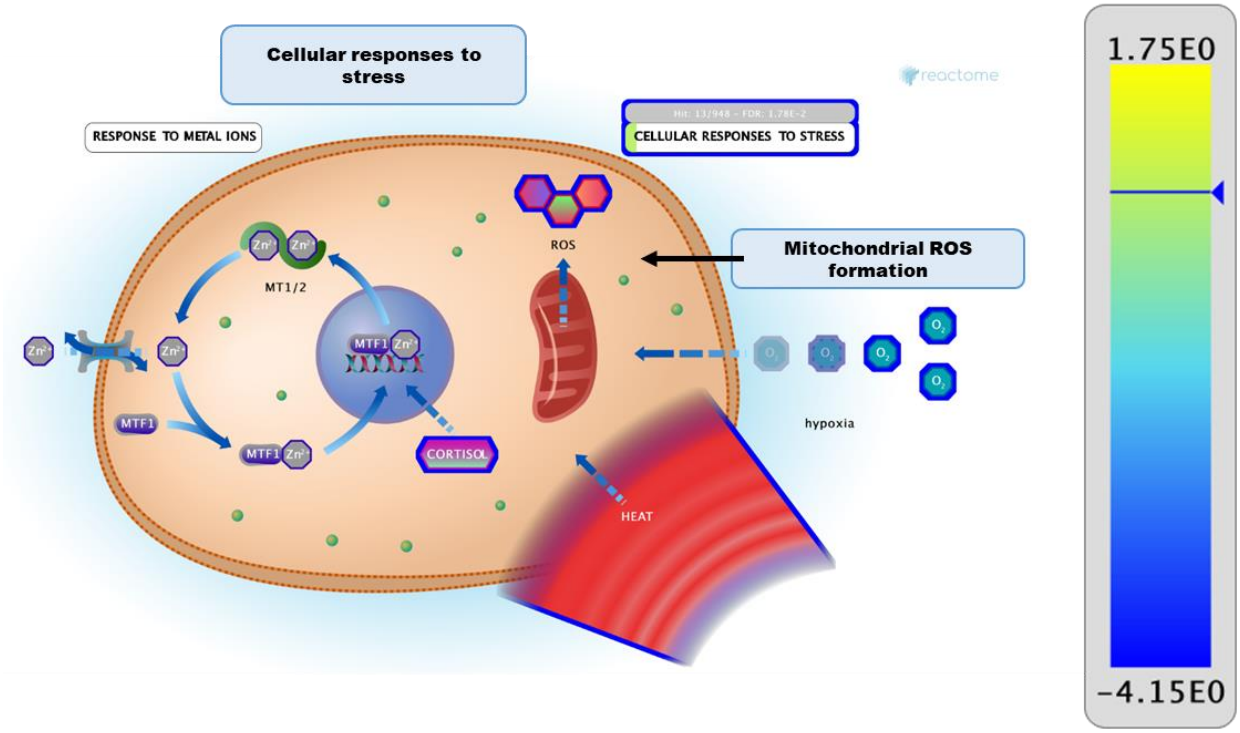

Figure 3:37: Mitochondrial ROS formation and cellular stress response. *Mitochondrial ROS formation exhibited a possible increase as Complex I proteins of electron transport chain were up regulated, namely; NADH dehydrogenase (Ubiquinone) 1 alpha sub-complex 4 (NDUFA4) with log2 1.2 fold, Protein arginine methyl transferase NDUFAF7 (NDUFAF7) with log2 1.06 fold, Complex I-49kD (NDUFS2) with log2 1.0 fold, NADH dehydrogenase [ubiquinone] iron-sulfur protein 4, mitochondrial (NDUFS4) with log2 0.9 fold, Complex I-B12 (NDUFB3) with log2 0.9 fold, Complex I-MNLL (NDUFB1) with log2 1.08 fold, Complex I-B12 (NDUFB3) with log2 0.9 fold, NADH dehydrogenase [ubiquinone] iron-sulfur protein 6, mitochondrial (NDUFS6)with log2 1.07 fold, NADH dehydrogenase [ubiquinone] 1 beta sub-complex subunit 8, mitochondrial (NDUFB8) with log2 1.02 fold, Complex I-B18 (NDUFB7) with log2 0.95 fold, Complex I-B22 (NDUFB9) with log2 0.85 fold, NADH dehydrogenase [ubiquinone] 1 alpha sub-complex subunit 6 (NDUFA6) log2 0.6 fold. (colour code=yellow to blue gradient yellow represent highest up regulation while blue represent highest down regulation, highest upregulation log2 fold 1.75E0 and lowest log2 fold -4.15E0. Grey bar above the label indicates the number of pathway entities that are represented in the query dataset (13 entities were found in the query data set out of 948 of total reference entities), the total number of entities in the pathway, and the FDR corrected probability score. The protein complexes with complete or part-coloured representation showed the total molecules present from the query data set to complete the complex. Figure created using www.reactome.com pathway analysis.*

Protein Name	Gene name	Log2 Fold-change
NADH dehydrogenase (Ubiquinone) 1 alpha sub-complex 4	NDUFA4	1.20
Protein arginine methyl transferase NDUFAF7	NDUFAF7	1.06
Complex I-49kD	NDUFS2	1.00
NADH dehydrogenase [ubiquinone] iron-sulfur protein 4, mitochondrial	NDUFS4	0.90
Complex I-B12	NDUFB3	0.90
Complex I-MNLL	NDUFB1	1.08
NADH dehydrogenase [ubiquinone] iron-sulfur protein 6, mitochondrial	NDUFS6	1.07
NADH dehydrogenase [ubiquinone] 1 beta sub-complex subunit 8, mitochondrial	NDUFB8	1.02
Complex I-B18	NDUFB7	0.95
Complex I-B22	NDUFB9	0.85
NADH dehydrogenase [ubiquinone] 1 alpha sub-complex subunit 6	NDUFA6	0.60

Table 3:6: The observed protein regulations in the mitochondrial cellular stress response.

As discussed above, mitochondrial superoxide is predominantly produced at Complex-I (Figure 3:35 and Figure 3:37), and I observed in the AF goat model, that the highest number of OXPHOS proteins over expressed were from the Complex-I (Figure 3:35). These upregulated proteins are presented in Table 3:6.

3.3.9.3 Translocation of GLUT4 to the plasma membrane

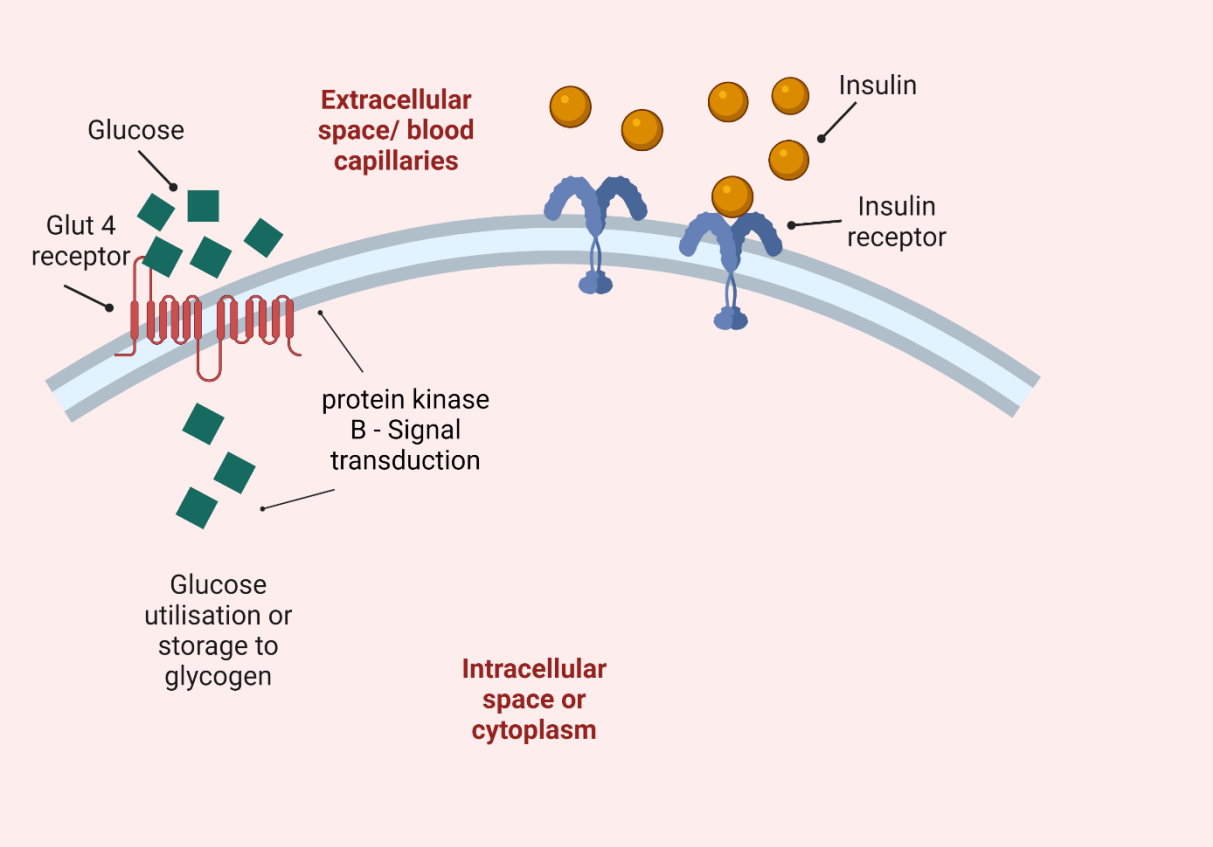

Figure 3:38: GLUT4 translocation to the plasma membrane. *In the event of an increased ATP demand in the cell the circulatory glucose will be taken up by the cells through insulin receptor mediated path. When insulin binds to the insulin receptor, protein kinase B induces translocation of GLUT4 to the cell surface; Figure created with Biorender.com.*

Glucose transporter type 4 or GLUT4 is a prominent glucose mediator between the cell and extracellular environment. When insulin binds to the receptors at the plasma membrane, vesicles with GLUT4 transporters translocate from cytosol to the plasma membrane (Figure 3:38) (Koshy *et al.*, 2010). In healthy cells, insulin promotes the removal of excess glucose from the circulatory system and GLUT4 transports the glucose to store in cells. Moreover, insulin requires the phosphatidylinositol 3-kinase (PI3K) signalling mechanism to activate GLUT4 storage vesicles. Furthermore, high concentrations of phosphatidylinositol 4,5 bisphosphate (PIP2) were reported to regulate cytoskeleton with proteins such as Caveolin (CAV1) and, interestingly, where PIP2 concentrations were low, insulin-stimulated GLUT4 translocation was reportedly impaired (Hoffman and Elmendorf, 2011).

Moreover, some studies discover that insulin remodels the actin filaments (Brozinick *et al.*, 2007) into a cortical mesh in skeletal muscles to translocate GLUT4 vesicles (Hoffman and Elmendorf, 2011) back to the cytoplasm (Klip, 2009 and Koshy *et al.*, 2010). The tethering function of the cortical actin mesh associate with syntaxin 4, soluble N-ethylmaleimide sensitive factor-attachment-protein receptors proteins (SNAREs) and SNARE vesicle-associated membrane protein 2 (VAMP2) to regulate the fusion and docking of the GLUT4 storage vesicles with the plasma membrane (Watson and Pessin, 2007).

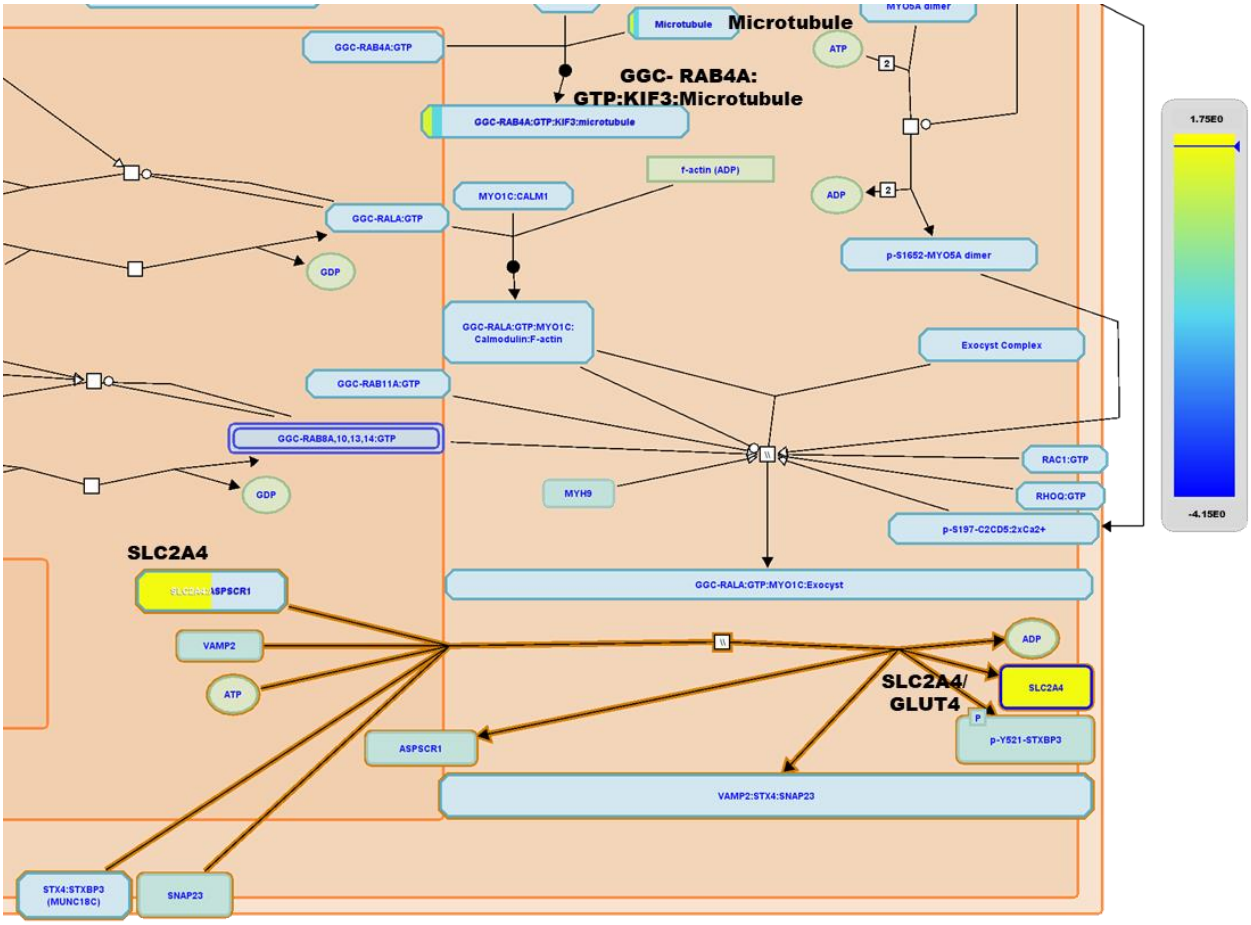

Figure 3:39: GLUT4 translocation to plasma membrane: *The pathway analysis of Reactome exhibited a possible interaction between the plasma membrane and GLUT4 vesicle trafficking. Under this pathway all the detected proteins were upregulated, such as, SLC2A4 or GLUT4 by log2 1.55, CAV1 by log2 0.6-fold, and NSF by log2 1.55. (colour code=yellow to blue gradient yellow represent highest up regulation while blue represent highest down regulation, highest upregulation log2 fold 1.75E0 and lowest log2 fold -4.15E0. The protein complexes with complete or part-coloured representation showed the total molecules present from the query data set to complete the complex. Arrow = Protein, protein complex name or protein function) Figure created using www.reactome.com pathway analysis. The given figure is a cropped version from the original elaborated figure for the discussion and the original version of this figure is provided in the Appendix figure A2:3.*

As discussed above, insulin stimulates glucose uptake. However, it has been reported that AMPK activation induces glucose uptake through GLUT4 vesicles (Wu *et al.*, 2016a) without phosphatidylinositol 3-kinase (PIK3CA) activation (Figure 3:21) (Bergeron *et al.*, 1999). In the LA of AF goat model I observed an AMPK upregulation by log2 0.8-fold (Figure 3:22), moreover GLUT4 protein (labelled by its gene name SLC2A4) was upregulated by log2 1.55-fold, exhibiting a possible upregulation in GLUT4 vesicle translocation to the plasma membrane. Therefore, one conclusion consistent with these sets of upregulations is that in the AF goat model the AMPK may have induced the glucose uptake through GLUT4 vesicles to compensate the increased energy demand. However, the levels of insulin in the AF goat LA tissue were not measured, and PIK3CA was not significantly regulated in the proteomics analysis.

Interestingly, the lysosomal α-glucosidase (GAA) enzyme was significantly upregulated in the EL fraction of AF goat model LA (Table A3:1), and Glycogenin-1 (GYG1) was significantly upregulated in the Western blotting experiments (discussed in chapter 5 in detail). Therefore, I observed a pattern or a possible link between SLC2A4/GLUT4, GYG1 and GAA proteins as they are functional proteins of glycogen metabolism. As I described above, GLUT4 transport glucose to the cell, whereas GYG1 is a self-priming protein in glycogen synthesis (Lomako *et al.*, 2004), and GAA is a lysosomal residing enzyme that degrades glycogen (Hoefsloot *et al.*, 1988). Glycogen granules (Yosefy *et*

al., 2021) and accumulation (Embi and Scherlag, 2014) in the atria of murine and goat models of AF are previously reported as structural remodelling in AF pathology. Furthermore, myofibrils are reported to be replaced by glycogen in AF goat models (Embi and Scherlag, 2014).

Furthermore, GLUT4 vesicle translocation to the plasma membrane is supported by caveolin and Vesicle-fusing ATPase N-ethylmaleimide-sensitive fusion protein (NSF), the tethering and docking proteins of GLUT4 vesicles (Kanzaki and Pessin, 2003). In the AF goat model CAV1 and NSF proteins showed a significant upregulation, respectively CAV1, log2 fold-change of 0.6, and NSF log2-fold change of 1.55 (Figure 3:39).

3.3.10 Lysosome and acidic organelle pathways regulated in atrial fibrillation

I hypothesize that the AMPK pathway plays a critical role in AF goat model protein expression. With the increased ROS mediated cellular stress, an array of dysregulations have taken place in the acidic organelles. It is possible to postulate that misfolded proteins have increased by observing the increase in aggrephagy and proteasome processes. Furthermore, the vesicle-mediated transport, gap junctional

assembly, and its degradation in the lysosome have increased as the downstream effects of the AMPK pathway.

Here I discuss the acidic organelle related pathways that were dysregulated in the LA of the AF goat model.

3.3.10.1 Endosomal sorting complex required for transport (ESCRT)

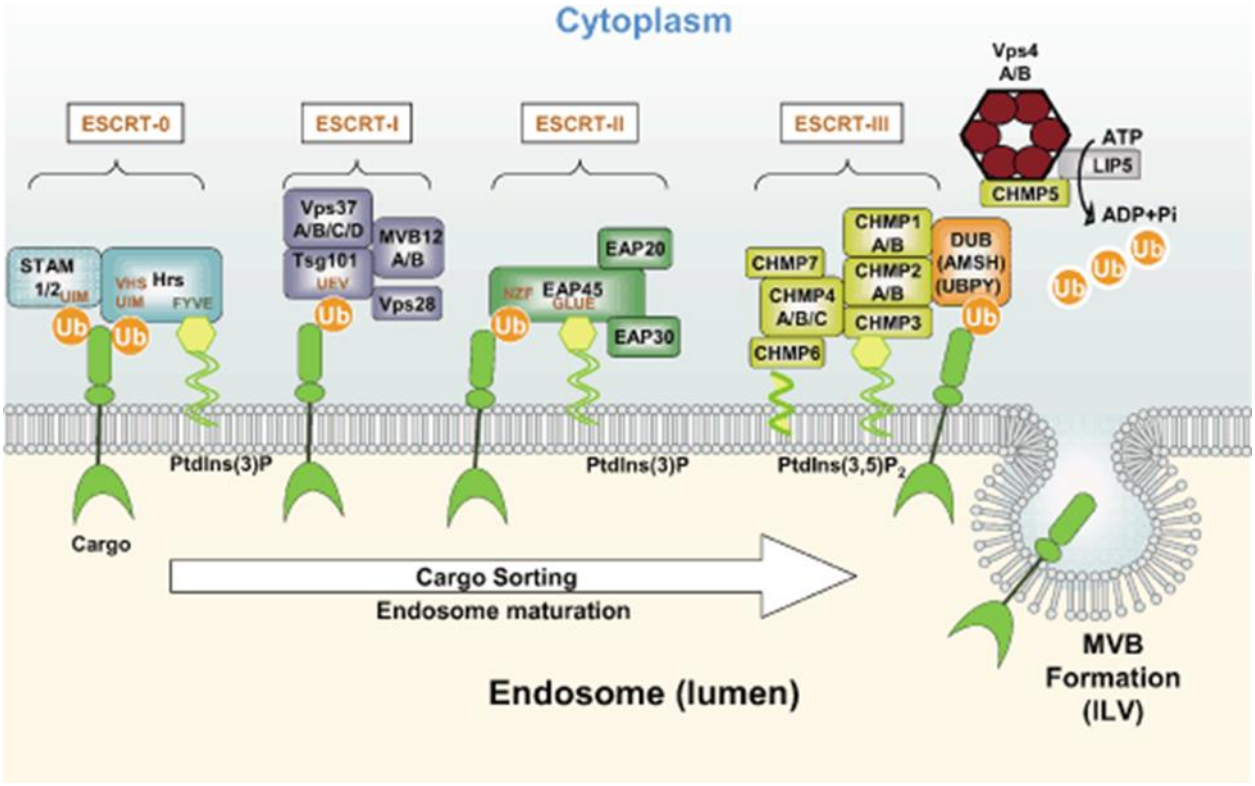

Figure 3:40: Diagram shows the cargo sorting events of Endosomal Sorting Complex (ESCRT). *The ubiquitinated proteins firstly interact with ubiquitin-interacting motif (UIM) and are recognized by ESCRT-0 complex. Secondly, Via Tsg101 ubiquitin E2 variant (UEV) recruit ESCRT-I complex for the protein cargo, Thirdly, ESCRT-III complex associate with membrane bound CHAP proteins and finally ubiquitin is removed from the cargo by deubiquitinating enzyme (DUB). The membranes invaginate to form multi vesicular bodies and cargo is internalized. Figure with permission from (Tanaka et al., 2008).*

ESCRT is a cascade of biological events that assemble and sort a multi-complex protein cargo unit to control the formation of multivesicular bodies (MVB) (Figure 3:40). MVB directed cargo is then targeted to lysosomal degradation, and ESCRT regulates and sorts the ubiquitinated membrane proteins to the endosomes. Defects in ESCRT can lead to dysregulation of membrane receptor traffic and recycling (Tanaka *et al.*, 2008).

MVB is an intermediate organelle of early and late endosomes; the bioactive marker lipid such as Lyso-bisphosphatidic acid and Ras-related protein Rab-7 (RAB7) are present in the MVB. RNA interference studies conducted by Vanlandingham P.A. *et al*., 2009 reported that the lack of Rab7 protein blocks the exit of late endosomes to MVB (Vanlandingham and Ceresa, 2009). Here in the AF goat model studies, I observed a compatible outcome to the 2009 study and a downregulation of RAB7 with concurrent downregulation of the ESCRT pathway, which would be expected to reduce MVB formation.

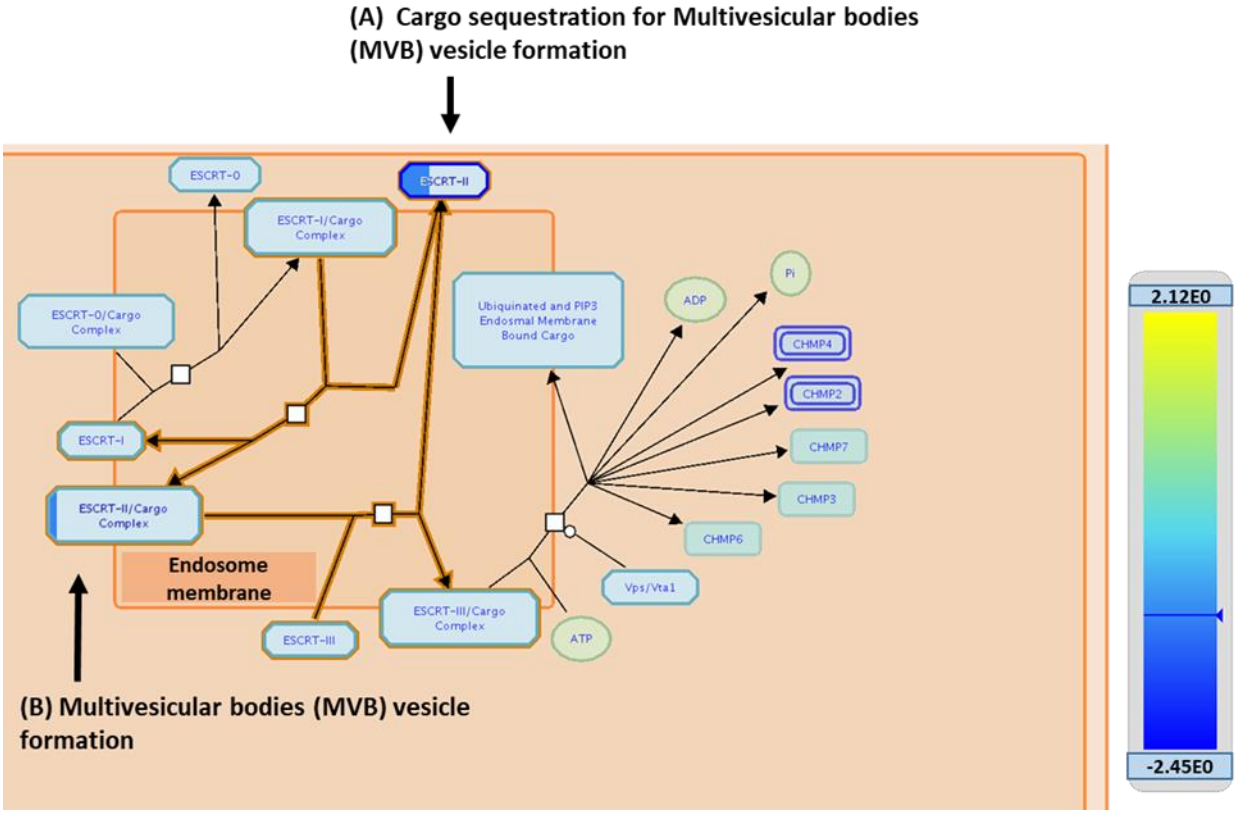

Figure 3:41: ESCRT pathway. *The left atrial cells of the AF goat model showed a possible down regulation of the multivesicular body formation in the ESCRT pathway. I observed a down regulation in the proteins such as ESCRT-II complex subunit VPS25 (VPS25) and Ras-related protein Rab-7a (Rab7a) respectively by log2 -1.03 fold and log2 -0.5 fold. (Colour code = yellow to blue gradient yellow represent highest up regulation while blue represent highest down regulation. Highest upregulation log2 1.75E0 fold and lowest log2 -4.15E0 fold. The protein complexes with complete or part-coloured representation showed the total molecules present from the query data set to complete the complex. Arrow = Protein, protein complex name or protein function) Figure created using www.reactome.com pathway analysis. The given figure is a cropped version from the original elaborated figure for the discussion and the original version of this figure is provided in the Appendix figure A2:4.*

The ESCRT pathway in the AF diseased condition showed a down-regulation in the ESCRT-II complex and its cargo (Figure 3:41). Proteins such as ESCRT-II complex subunit VPS25 (VPS25) was downregulated with -1.03 log2 fold, and Rab7A was downregulated with -0.5 log2 fold. As mentioned earlier, Rab7A a tethering factors

recruiting protein (Gutierrez et al., 2004) and (Vanlandingham and Ceresa, 2009) plays a critical role in the transition of late endosomes to MVB in the ESCRT pathway, and lysosome biogenesis through autophago-lysosome formation (Press et al., 1998) Similarly, Rab2A, a protein associated with autophago-lysosome formation (Ding et al., 2019) was down regulated in AF goats by log2 -0.7-fold and VPS25 is one of the main regulatory components of the ESCRT complex-II that sort the endosomal cargo proteins to the MVB and recruit the ESCRT-III complex (Table 3:1) (Im et al., 2009). Hence, I hypothesize that downregulation of the VPS25, Rab7A and Rab2A in the LA AF diseased condition can possibly affect the downstream lysosomal cargo.

3.3.10.2 Lysosome as the hub for mammalian target of rapamycin complex 1 (mTORC1) activation

In the AF goat model LA, the following upregulations of proteins were observed; Ras-related GTP-binding protein A (RRAGA) or RagA was upregulated by log2 0.7 fold, AMPK activating (CAB39/ MO25) by log2 0.5 fold, Mitogen-activated protein kinase 3 (MAPK3) or ERK1/2 by log2 1.8 fold and Protein-serine/threonine kinase (PDK1) by log2 0.6 fold (Figure 3:42).

The Rag family proteins RRAGA or RagA and Ras-related GTP-binding protein B (RRAGB) or RagB are Ras like small GTPases that play a major role in amino acid stimulated mTORC1 activation by recruiting mTORC1 to lysosome (Kim *et al.*, 2014). The 2008 studies of Kim E. *et al*., showed in Drosophila genetic studies that the Rag GTPases regulate cell growth, autophagy, and animal viability under starvation (Kim *et al.*, 2008). Moreover, Rag GTPases activate mTORC1 in response to amino acid signals (Kim *et al.*, 2008 and Sancak *et al.*, 2008).

The mTORC1 signaling hub is the lysosome (Menon *et al.*, 2014) and it is composed of mTOR raptor, rapamycin-sensitive protein, regulated by nutrients and growth factors. mTOR integrates signals from hormones, nutrients, cellular oxygen, and energy levels to control a variety of vital cellular processes including, transcription, mRNA translation, proliferation, differentiation, cytoskeletal organization, and

autophagy (Hay and Sonenberg, 2004) ; (Sarbassov *et al.*, 2005) ; (Wullschleger *et al.*, 2006) and (Yang and Guan, 2007). Under nutrient-rich conditions, activated mTORC1 pathway inhibits autophagy and promotes cell growth (Rabanal-Ruiz *et al.*, 2017) because mTORC1 is an anabolic cellular metabolism promoter, stimulating synthesis of protein, lipid, and nucleotides and blocking catabolic processes such as autophagy at the post-translational and transcriptional levels (Kim and Guan, 2015). Yet, whether the cell actively supports catabolic or anabolic processes is decided by close signalling interplay of mTORC1 with the energy sensor AMPK (Rabanal-Ruiz *et al.*, 2017).

Tuberous sclerosis 1/2 proteins (TSC1/2) are negative regulators of mTORC1 signaling by inducing as a GTPase-activating protein (GAP) for the small GTPase Rheb, an activator of mTORC1. TSC1/2 are activated by cellular stress promoters, such as energy or oxygen depletion (Göktuna, 2018) and inhibits mTORC1 activation (Kim and Guan, 2015). As discussed earlier, AMPK is a cellular ATP sensor and a kinase that can phosphorylate many substrates (Mihaylova and Shaw, 2011). One such protein is the RAPTOR protein which, when phosphorylated, acts to inhibit mTORC1 (Gwinn *et al.*, 2008) or TSC2 to induce the TSC1/2 complex activity (Inoki *et al.*, 2003).

Extracellular signal-regulated kinase (ERK) phosphorylation leads to TSC1-TSC2 dissociation and impairs TSC2 ability to inhibit mTOR signaling (Ma *et al.*, 2005). PDK1 phosphorylate and activate protein kinase B (also known as Akt) (Dangelmaier *et al.*, 2014). TSC2 is inactivated by Akt-dependent phosphorylation. Inactivation of TSC2

relieves the inhibitory effects of the TSC1-TSC2 complex on Rheb and mTOR complex 1 (mTORC1), therefore activating mTORC1 (Huang and Manning, 2009). Recently, a model has emerged showing mTORC1 activation occurs at the lysosome and is mediated through an amino acid sensing cascade involving RAG GTPases, Ragulator and vacuolar H+-ATPase (v-ATPase) (Jewell *et al.*, 2013). mTORC1 is inhibited under starvation conditions by the energy sensor AMP-activated protein kinase (AMPK) and by amino acid signalling. Furthermore, Rag ATPases recruit mTORC1 to the lysosome surface in the presence of amino acids. GTP-binding protein Rheb (RHEB) activates mTORC1 to induce apoptosis (Kim and Guan, 2015).

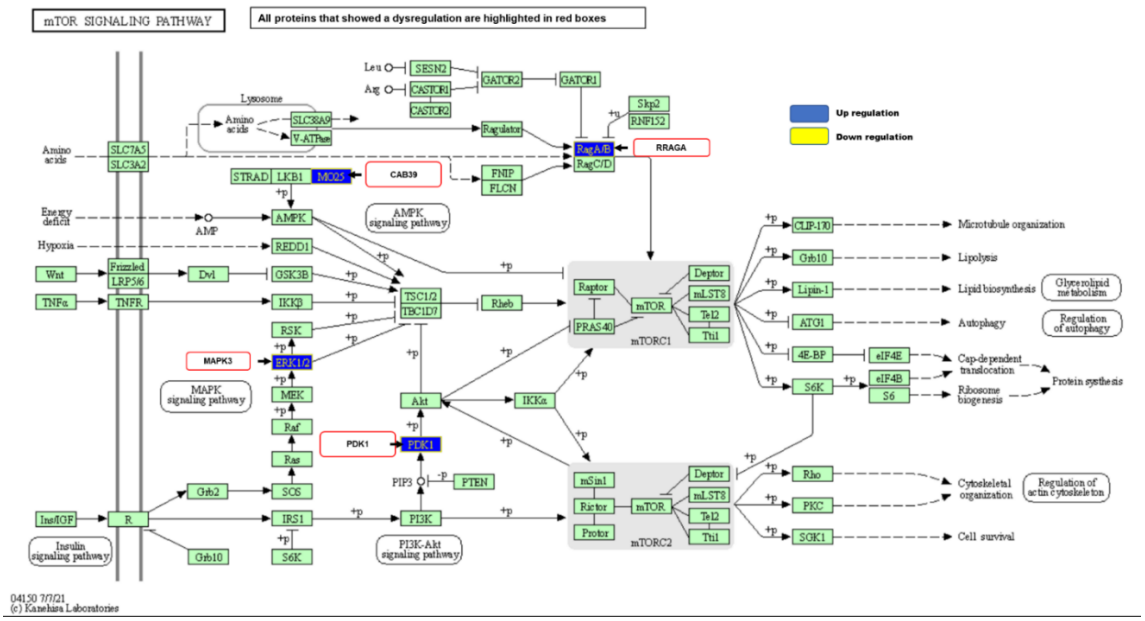

Figure 3:42: mTOR signaling pathway. *The AF goat model of LA showed up regulation of the proteins: Ras-related GTP-binding protein A (RRAGA) or RagA by log2 0.7 fold, AMPK activating (CAB39/ MO25) by log2 0.5 fold, Mitogen-activated protein kinase 3 (MAPK3) or ERK1/2 by log2 1.8 fold and Protein-serine/threonine kinase (PDK1) by log2 0.6 fold. (Arrow = Protein, protein complex name or protein function. +P = phosphorylating events. Blue = up regulation (log2 fold-change) Pathway analysed using KeGG database.*

3.3.10.3 Lysosome biogenesis

As discussed previously in detail, the vesicle trafficking pathway is a fundamental membrane trafficking process with a targeted cargo delivery between the cellular compartments. Adaptor protein AP-1 is a member of the AP complex family proteins, which play a significant role in Clathrin–coated vesicle biogenesis (Nakatsu *et al.*, 2014). Once the AP protein complex sorts the targeted cargo, Clathrin is recruited by the AP proteins to propel the vesicle formation via self-assembly (Nakatsu *et al.*, 2014).

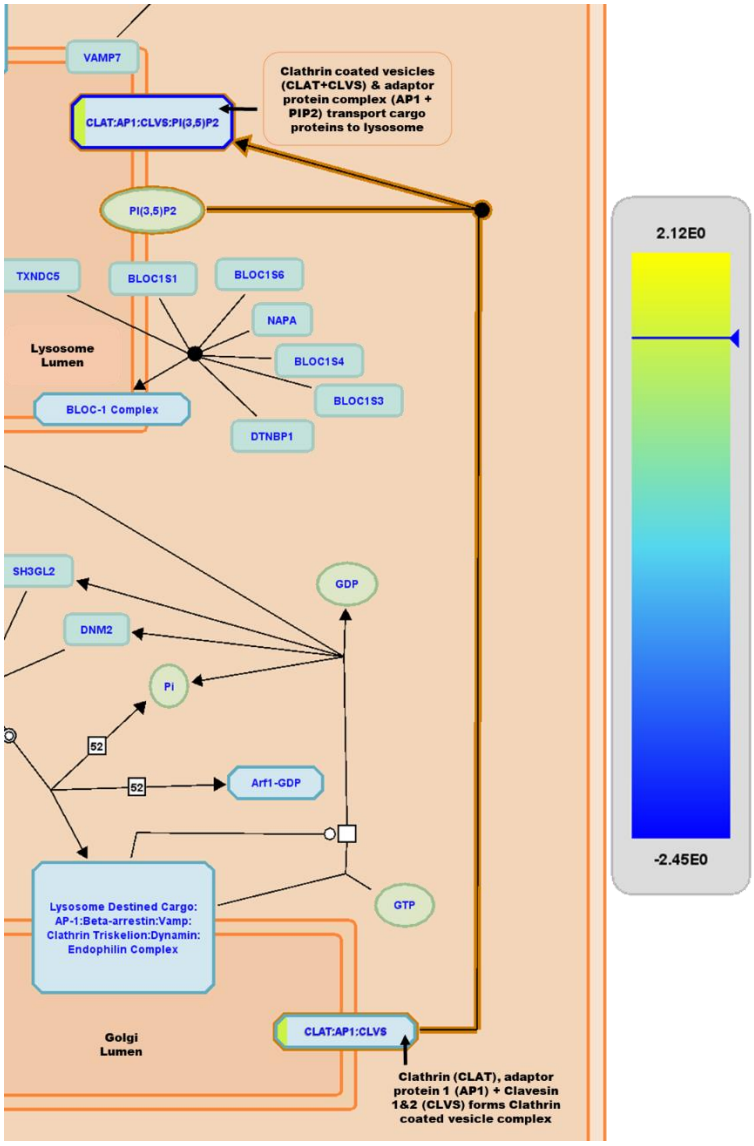

Figure 3:43: Lysosome biogenesis path. *Lysosome destined cargo is carried to the lysosome through clathrin mediated transport. Clathrin triskelions complex associate with lysosome destined cargo, AP1, beta-Arrestin and Vamp proteins, and dynamin form a collar around the vesicle budding for fission. This process is driven by GTPase. In the LA of the got AF model I observed an over expression of Clathrin coated vesicle traffic to the lysosome membrane. Formation of vesicles with Clathrin, AP1 protein complex and Clavesin proteins and its pathway to the lysosome was highlighted in the Reactome studies. (Colour code=yellow to blue gradient; yellow represent highest up regulation while blue represent highest down regulation. Highest upregulation log2 2.12E0 fold and lowest log2 -2.45E0 fold. The protein complexes with complete or part-coloured representation showed the total molecules present from the query data set to complete the complex. Arrow = Protein, protein complex name or protein function). Figure created using www.reactome.com pathway analysis. The given figure is a cropped version from the original elaborated figure for the discussion and the original version of this figure is provided in the Appendix figure A2:5.*

One 2003 study by Lefkir Y. *et al.* showed that the precursor lysosomal enzymes are transported to the lysosome by AP1 and Clathrin-mediated vesicles through the trans-Golgi network (Lefkir *et al.*, 2003). The AP1: clathrin protein complex binds to phosphatidylinositol 3,5-bisphosphate (PIP2), a phospholipid located in the lysosomes. This interaction supports the transport of the vesicle cargo to the endosomal - lysosomal network (Katoh *et al.*, 2009), and in the AF goat model (Figure 3:43), Clathrin (CLTB) protein was upregulated from 1.5 log2 fold. It is possible that in AF, some areas of Clathrin-mediated lysosome biogenesis could be upregulated.

3.3.10.4 Gap junctions trafficking to lysosomes, internalization and degradation

As discussed previously under Connexins and gap junction assembly there was an increase in expression of gap junction assembly proteins in the LA of the AF goat model. Similarly, in the EL fraction, I observed a likely increase in gap junctional degradation through lysosomes. Gap junctional proteins or connexins have a short-term structural conformation. Hence they are constantly recycled by the cell (Figure 3.25) (Berthoud *et al.*, 2004).

The gap junctional protein complexes have three known degradation pathways: (1) Direct trafficking of connexin dimers to the lysosome for degradation (Strous and van Kerkhof, 2002), (2) Misfolded connexins are translocated to the proteasome through ER and degrade in the proteasome pathway (Laing and Beyer, 1995), (3) Gap junctional plaque formation and degradation through lysosome (Laing *et al.*, 1997).

In the LA AF goat model, I observed a possible upregulation in the formation of double membraned vesicles or gap junctional plaques (Figure 3:44) (Berthoud *et al.*, 2004).

Connexins are translated and inserted into the Golgi compartment, and at the protein transition from ER to Golgi, Connexins are oligomerized into hexamers or connexons. These connexons or hexamers are trafficked from the trans-Golgi network to the plasma membrane. Later, these connexons arrange in appositional plaques. Participation of endocytosis and lysosomes in the degradation of gap junctional plaques was proposed more than 20 years ago after observing intracellular vesicle-like double-membrane structures resembling gap junctions in transmission electron micrographs. These studies suggested that gap junctional plaques (or fractions of them) were internalized by endocytosis. Internalized gap junctional plaques fuse with lysosomes, and degradation of connexins takes place in the lysosome (Berthoud *et al.*, 2004).

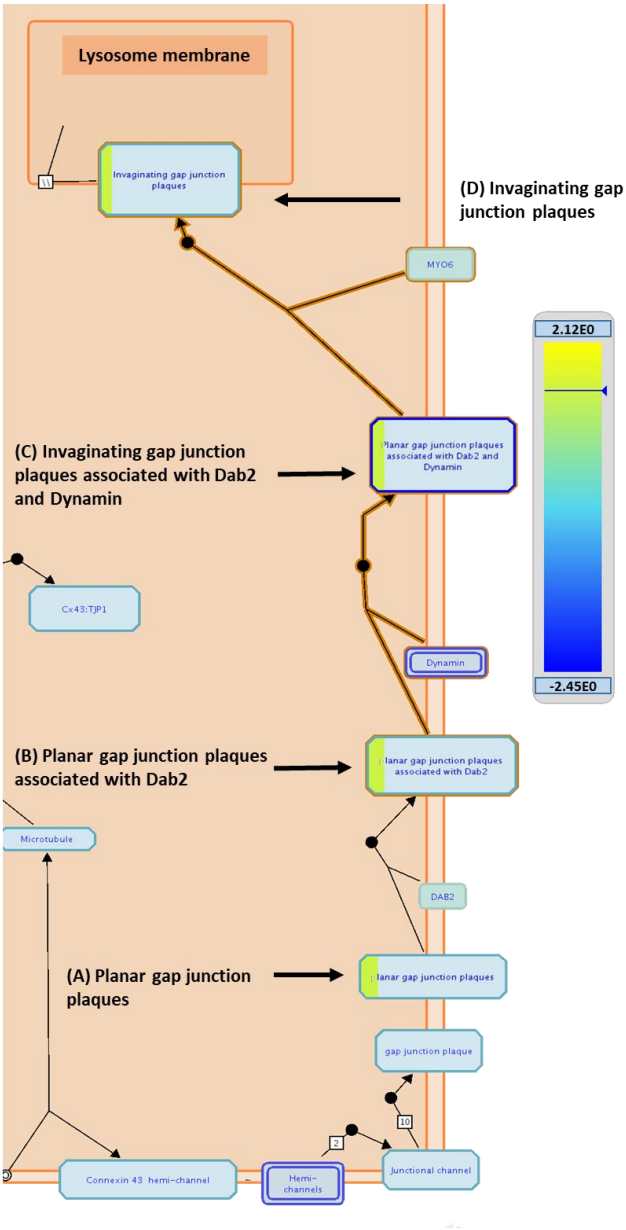

Figure 3:44: Pathway representation of gap junction trafficking to lysosomes, internalization and degradation. *In the AF goat model I observed; (A) increased planar gap junction plaques formation (B) Disabled homolog 2 (Dab2) protein of the plasma membrane associates with the hemi channels or planar gap junctions (C) Invagination of gap junctions form double membraned annular gap junctional plaque vesicles and transported to lysosome membrane by dynamin (D) internalization of gap junctional annular plaque vesicles at the lysosomal membrane for the degradation. (Colour code=yellow to blue gradient; yellow represent highest up regulation while blue represent highest down regulation. Highest upregulation log2 2.12E0 fold and lowest log2 -2.45E0 fold. The protein complexes with complete or part-coloured representation showed the total molecules present from the query data set to complete the complex. Arrow = Protein, protein complex name or protein function). Figure created using www.reactome.com pathway analysis. The given figure is a cropped version from the original elaborated figure for the discussion and the original version of this figure is provided in the Appendix figure A2:6.*

3.4 Discussion

This chapter presents the results of quantitative proteomic analysis to understand protein level changes in the goat AF model LA. Analysis of significantly regulated proteins in the TL, Mito and EL fractions identified and interpreted the possibility of some of the molecular pathways that have been affected by the disease. Understanding the potential dysregulations of proteins in a multifactorial disease such as AF (Schüttler *et al.*, 2020) using label-free proteomics allows the possibility to discover pilot information on pathway dysregulations leading to acidic organelles that can be studied further.

One of the important pathways identified in the AF goat model was the AMPK pathway and is predicted to be regulated in the AF goat model because AMPK is the main pathway that senses and controls the ATP energy levels in a cell (Chakraborty *et al.*, 2020). AMPK balances ATP demand in the cell by regulating several pathways, such as upregulation of glycolysis, glucose uptake through GLUT4 vesicles, downregulation of fatty acid synthesis (Hardie, 2011), and cholesterol synthesis (Jeon, 2016). Moreover, in the event of cellular ROS mediated stress, AMPK can stimulate autophagic processes to remove the accumulated cytotoxic materials and aggregated misfolded proteins (Jang *et al.*, 2018 and Xia *et al.*, 2018).

The Reactome pathway interpretations showed that, GLUT4 protein that transport glucose inside the cell was upregulated (Figure 3:39). Moreover, in the EL fraction of AF goats, a log2 0.4-fold upregulation of GAA was observed, degrading glycogen in the lysosome. (Zirin *et al.*, 2013 and Adeva-Andany *et al.*, 2016). Furthermore, in Chapter 5, a significant (*p=0.007*) upregulation of GYG1 was observed in the Western blotting providing evidence for the increased glycogen synthesis or an accumulation of glycogen may proceed in the AF goat model (Embi *et al.*, 2014). The glycogen deposits are identified as structural or a cellular remodelling of AF goat LA (Ausma *et al.*, 2003 and Embi *et al.*, 2014). According to the Hout *et al*., 2001 studies (Van den Hout *et al.*, 2001), it was indicated that a considerably higher level of recombinant human α-glucosidase was required to reduce the abnormal levels of stored glycogen in the cardiac and skeletal muscles. The proteomic data up-regulation of GAA levels with the upregulated GLUT4 and GYG1 proteins can lead to the hypothesis that as part of the structural remodelling (Embi and Scherlag, 2014) LA of AF goat model, a potential link to the GAA. Therefore, it is presumable that to compensate for the upregulation of either glycogen levels or glycogen synthesis GAA enzyme was upregulated in AF pathology. Additionally, GAA significant upregulation was detected only in the EL fraction, suggesting that the modified density gradient proteomics-based method that I developed to analyse endolysosomal proteins in cardiac tissue is a suitable method for analysing endolysosomal protein composition (Ayagama *et al.*, 2021).

Furthermore, Rab11A and B that plays a role as regulatory proteins in the vesicle - mediated pathway (Grosshans *et al.*, 2006 and Goswami *et al.*, 2021) were

upregulated. They recruit effector proteins such as RAB11FIP3 and associate in the fusion and tethering (Hales *et al.*, 2001 and Welz *et al.*, 2014). Rab11 is localized to the trans-Golgi network and involved in the cellular recycling pathways, supporting the traffic of membrane components to the plasma membrane (Urbé *et al.*, 1993). The study published in Kessler *et al*., 2000 suggested that Rab11 participates in GLUT4 vesicle trafficking of glucose transport (Kessler *et al.*, 2000).

Moreover, lysosomal acid ceramidase (ASAH1), which hydrolyses sphingolipid ceramides and converts them to sphingosine and free fatty acids (Yu *et al.*, 2018a) was observed to be downregulated by log2 -0.6-fold. Deficiency of ASAH1 enzyme leads to the lysosomal storage disorder, Farber disease (Li *et al.*, 1999). Furthermore, OCIA domain-containing protein 1 (OCIAD1) was downregulated by log2 -1.04-fold and OCIAD1 is a lysosomal protein that attaches to either α-actin IV or β-actin. Thus, OCIAD1 was identified to be associated with the cytoskeletal proteins. However, it has been reported that OCIAD1 downregulation inhibits lysophosphatidic acid (LPA)-induced cell adhesion to laminin, collagen I, and cell attachment to integrin (Wang *et al.*, 2010).

I observed an array of lysosomal proteins such as Rab7A and Rab2A, which are autophago-lysosomal fusion associated proteins (Press *et al.*, 1998). Additionally, DNM2, which scission the lysosomes from auto-lysosomal tubules to promote autophagic flux , DYNC1I2 and AP2A2 proteins that act as motor proteins in vesicle

trafficking (Ansar *et al.*, 2019) early endosome fusion (Hinrichsen *et al.*, 2003) to gap junction assembly (Laird, 2010) were downregulated in AF goat model. Therefore, acidic organelle fusion and related dynamics might be affected in AF goat model LA.

The molecular events discussed in this chapter that I observed in the AF goat model have been previously reported in other cardiac disorders (Dhalla *et al.*, 2000), including cardiac hypertrophy and congestive heart failure (Hill and Singal, 1996), atherosclerosis (Thong *et al.*, 1996), acute ischemic syndrome and ischemic-reperfusion injury. Cardiomyopathy (Dhalla *et al.*, 2000) and the molecular cascades regulated in the acidic organelle pathways could be possible downstream effects of the primary pathways such as AMPK.

The overexpression of ER protein processing and recycling is a prominent pathological issue in the AF goat model, and the comparison studies of the left atrial AF goat models to that of human proteome supported that pathways related to vesicle transport were overexpressed in the AF goat model (Figures 3:19 and 3:20).

From my studies on the LA AF goat model, I have learned that the lysosome, as an acidic organelle, is the hub of the mTORC1 pathway (Menon *et al.*, 2014) and can be affected by a series of molecular events in AF (Rabanal-Ruiz *et al.*, 2017 and Sciarretta *et al.*, 2018)

One of the major complexities of AF is that the disease changes occur over time (Schüttler *et al.*, 2020). The information obtained from the experimental subjects or patients can vary, and it may be years before the complete pathological phenotype appears. In this instance, goats were paced into persistent AF for six months, and a complete human AF compatibility, is limited.

It is important to evaluate the molecular pathways predicted in the proteomic studies in some other technique. In the next chapter, I present the transcriptomic analysis and the overlapping molecular pathways. In Chapter 5, I validated some of the proteins identified as regulated and related to these regulated proteins and conducted some lysosomal enzyme assays to identify enzymatic changes in the lysosome under AF conditions.

Chapter 4

mRNA expression in goat atrial fibrillation tissue – A quantitative transcriptomics study

4.1 Introduction

Transcriptomics is a high-throughput technique (Barh and Azevedo, 2017) to identify and characterise RNA, mainly mRNA or coding RNA. RNA profiling provides researchers with a comprehensive understanding of the hereditary to functional genomic conversion on a large scale. The application of transcriptomics to study the pathology of a disease compared to its wild type or control is widely used (Gladka *et al.*, 2018). Moreover, transcriptomics is applied to precise disease development; For instance, induced disease model organisms are subjected to transcriptomic analysis at controlled time points to understand the vital disease developing stages (Spies and Ciaudo, 2015) and (Alvarez-Fernandez *et al.*, 2021).

Furthermore, transcriptomics has been applied to complex disorders such as AF (Wijesurendra and Casadei, 2019) and (Roselli *et al.*, 2018). The current application of transcriptomics methods are used in understanding molecular pathway alterations. Especially understanding the epigenetics of AF, for instance, histone modifications (Song *et al.*, 2019) and hyper methylation (Shen *et al.*, 2017) are emerging areas to apply this technique. Notably, AF has been reported for structural remodelling such as fibrosis, and LA is reported for fibrosis over RA (King *et al.*, 2017) . However, the limitations of AF disease models and achieving the correct level of sustained AF with controlled time points are some of the obstacles following this technique (Victorino *et al.*, 2021).

Additionally, complex disorders such as AF must be Prevented or controlled and kept at bay by understanding the risk factors (Berg *et al.*, 2021). Therefore the large scale of differentially expressed genes identification is ideal for further examination to increase the potential biomarker identification through co-expressional proteins (Mantini *et al.*, 2020). Here in Chapter 4, the mRNA expression of the induced AF goat model is discussed by applying transcriptomic studies. The whole tissue lysates (same samples from that which was used in proteomics and Western blotting) were used to isolate mRNA, and genomic expression was quantified and the differential expression obtained. These differentially expressed genes were fed into Reactome and KeGG pathway analysis to study the pathway regulations.

4.1.1 From Gene regulation to protein expression: How does transcriptomics evaluate proteomics?

Proteins drive the functional tasks of the cell (Hahn, 2004). Therefore genetic instructions in DNA must be transcribed to a complementary messenger RNA (mRNA), and the mRNA instructions must be converted to its complementary amino acid sequence to translate into proteins.

This chapter discusses five major pathway events where transcriptional changes relatable with that of the proteomic differential expression analysis with a downstream connection to the lysosome and lysosomal cargo. The molecular pathways are rRNA biosynthesis, processing and modification down regulation, AMPK mediated macroautophagy upregulation, AMPK mediated GLUT4 translocation to the plasma membrane, AMPK mediated lipophagy and Solute carrier family 3 member 2 (SLC3A2) down regulation mediated mTOR inhibition. Based on changes in AMPK, which serves as the energy sensing regulator of the cell (Hardie *et al.*, 2012). Here we identified that the AF goat model of LA displayed energy depletion and consequent pathological pathway regulations.

Pathway upregulations such as macroautophagy, lipophagy and inhibition of mTOR by SLC3A2 showed that AF model transitioned to a cellular survival state by upregulating autophagy (Byun *et al.*, 2020), while, rRNA biosynthesis, processing; modification pathway downregulation, GLUT4 translocation to plasma membrane pathway and lipophagy upregulation implicated the role of AMPK in reversing cellular energy depletion (Hoppe *et al.*, 2009) ; (Klip *et al.*, 2009) and (Kaushik and Cuervo, 2016) in AF goat model LA.

Studying the complex biological pathways holistically requires an extensive and integrative approach to combine several omics data together, whilst a comprehensive understanding of a diseased condition requires multiple levels of techniques incorporated to understand and validate the overlapping areas of pathology, such as proteome, genome, transcriptome or metabolome (Jiang *et al.*, 2020) This chapter aims to present such a comparative approach of transcriptomics that builds upon that of the proteomics differential expression analysis that was discussed in the Chapter 3. Muti-omics tools were used to produce, analyse and conclude molecular pathways for the transcriptome interpretation. Nevertheless, these pathways do not represent overlap between proteomic and transcriptomics interpretation because of the biological gap between transcriptions to translation. The data was quantified to understand and learn the most significantly regulated genes related to lysosomal pathways in AF goat model LA.

4.1.2 Brief introduction to the importance of rRNA

Eukaryotic transcription is supported by RNA polymerases that recruit transcription factors to regulate initiation, elongation and termination. The RNA polymerases are, namely, RNA polymerase I, RNA polymerase II and RNA polymerase III. RNA polymerase I transcribes rRNA in the nucleolus. rRNA plays a significant role in transcription as they are structural RNAs that are transcribed, processed and assembled into ribosomes. RNA polymerase II synthesizes protein-coding pre-mRNAs. RNA polymerase III synthesises 5S rRNAs and tRNAs, which serve as the adaptors for the polypeptide chain synthesis in the translation process (Lewin *et al.*, 2011).

Ribosome assembly is processed in the nucleolus, maturated in the nucleus and trafficked to the cytosol to conduct transcription. Inhibiting any of the steps from the rRNA process can significantly reduce the energy consumption in the cell (Grummt and Voit, 2010). Additionally, it has been proven that cellular stress levels such as energy depletion, UV, gamma radiation or ROS can activate and respond to nucleolar stress signalling pathways (Boulon *et al.*, 2010).

4.1.3 rRNA and high ATP energy consumption

Intracellular energy balance is the primary adaption for cell survival, and in eukaryotic cells, the most energy-consuming process is ribosome biosynthesis (Murayama *et al.*, 2008). Therefore, rRNA synthesis downregulation is vital for maintaining intracellular energy homeostasis and cell survival under an energy demand in the cell (Murayama *et al.*, 2008). However, the mechanism that links energy-status fluctuation and ribosome biosynthesis is the least studied area (Murayama *et al.*, 2008). In 2008 studies by Murayama A. et al. provided evidence for this mechanism. Murayama's studies showed that a protein complex named eNoSC binds to (rDNA) locus (rDNA is the rRNA transcribing DNA) of the Sirtuin-1 (SIRT1) and Histone-lysine N-methyl transferase (SUV39H1) complex implying that a change in the NAD+/NADH ratio induced by reduction of energy could activate SIRT1, leading to deacetylation of histone H3 and dimethylation at Lys9 by SUV39H1, thus establishing silent chromatin in the rDNA locus and inhibiting transcription (Murayama *et al.*, 2008).

As discussed earlier, ribosome biogenesis by rRNA is a high energy-consuming pathway. The major cellular homeostasis AMPK pathway controls ATP energy consumption as part of the cell survival, and alteration of ribosome subunit biosynthesis is one strategy for energy conservation. In contrast, regulation of RNA Pol I transcription or rRNA processing (Chédin *et al.*, 2007) is another strategy (Grummt and

Voit, 2010). Furthermore, ribosome biogenesis by rRNA is required for cell growth and rapid cell proliferation. It has been reported that under ROS mediated or energy depletion cellular stress conditions, the AMPK pathway ceases cell proliferation and arrests the cell cycle to reduce high energy level consumption.

4.1.4 rRNA processing in the cell

rRNA comprises non-coding RNA, and forms the structural components of the ribosome. The ribosome is the central machinery of the protein synthesis or translation process. rRNAs contain secondary structures and actively recognise conserved areas of mRNA and tRNA strands, acting as a mechanical trigger that forces tRNA and mRNA to translate the sequence into proteins (Grummt, 2013). Furthermore, rRNA ribozyme activity regulates protein synthesis within the ribosome. rRNA are transcribed from rDNA. In eukaryotic cells and there are up to 5000 sets of rRNA genes and 10 million ribosomes. In the eukaryotic cell, the rRNA separates from the chromosomal fibers and assemble into the nucleolus, therefore the nucleolus is recognised as being the ribosome assembly location (Figure 4:1).

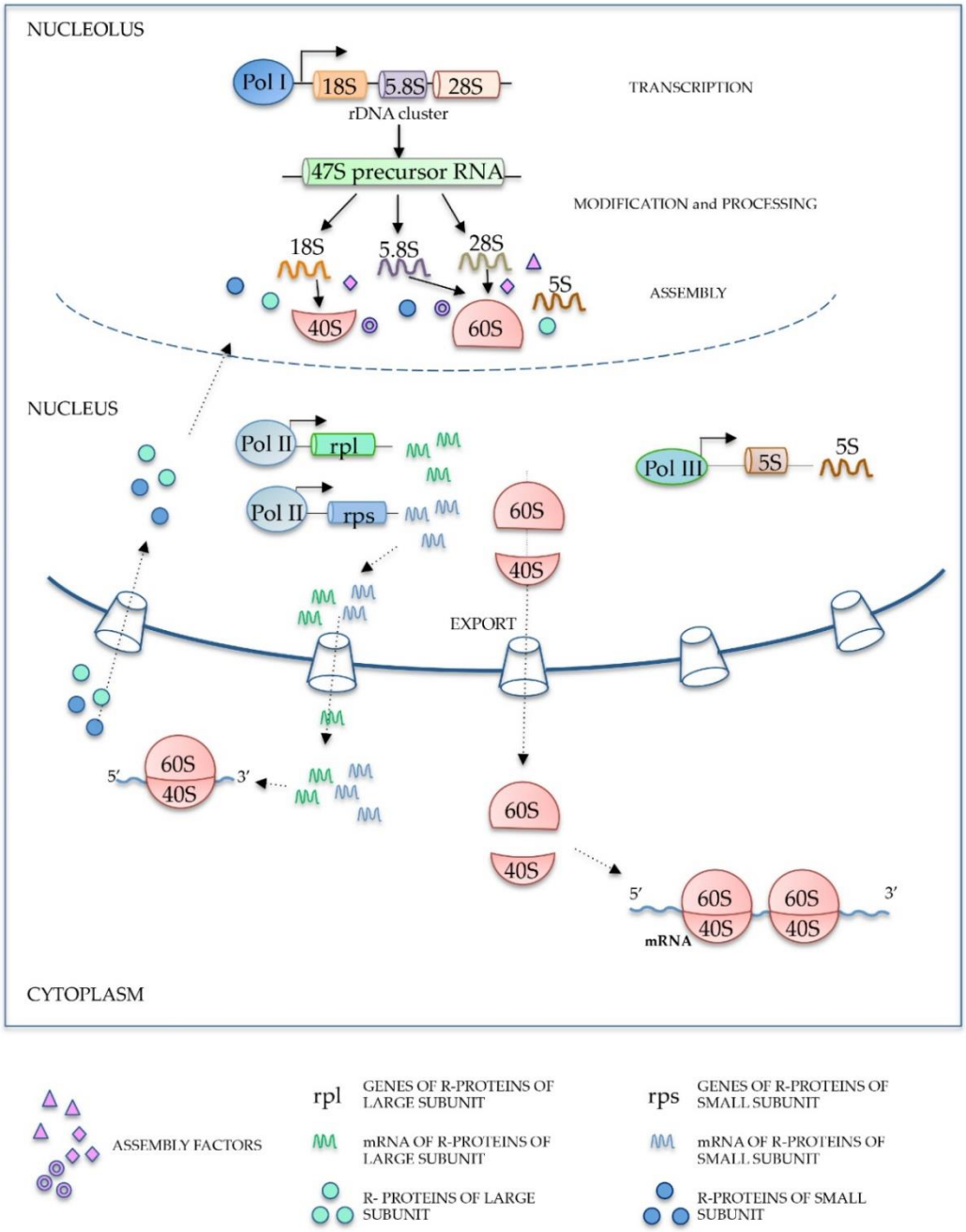

Figure 4:1: Ribosome biogenesis. *rRNA bio synthesis initiates in the nucleolus, and then transcribed from rDNA. The first 47S precursor RNA undergoes several modifications to assemble the 40S and 60S matured subunits. The external assembly factors are imported from cytosol. Once assembled, the matured rRNA polymerase I and polymerase II is trafficked from nucleus to cytosol. Figure with permission from (Russo and Russo, 2017).*

4.1.5. AMPK Activation

In the AF goat model LA, AMPK was found to be significantly up regulated in both proteomic (see Chapter 3) and transcriptomic studies. KeGG and Reactome analyses identified several pathways involving AMPK signaling where multiple targets were regulated in a consistent manner. These are discussed below.

4.2 Methods

4.2.1 Sample preparation

Due to the pandemic and lab shut down, RNA sequencing and transcriptomics data were analysed at Novogene Cambridge, an advanced genomics service.

Frozen goat AF and sham model LA tissue were rapidly collected at an RNase free workbench without contaminating, thawed in RNAlater stabilisation solution (AM7020, Invitrogen), and homogenised using bead disruption. 50 – 100 mg snap-frozen tissue samples were then solubilised in 1 ml Trizol (15596026, Thermo Fischer). Lysates were incubated at room temperature for 5 minutes and centrifuged at 12,000 x g for 5 min at

4°C. The collected supernatant was mixed with 200 µL of chloroform. Then, the lysate was vigorously shaken and centrifuged at 12,000 g at 4°C for 15 min. After 15 minutes, the upper clear aqueous phase was observed and transferred to a new centrifuge tube. Ice-cold isopropanol was added at a 1:1 volume ratio to the collected layer and mixed by inverting the tubes followed by centrifugation at 12,000 g for 30 min at 4°C. The pellet, which contained RNA, was collected, washed with 75% ethyl alcohol (10048291, Thermo Fisher), and dried.

4.2.2 RNA qualification and quantification

The RNA contaminants and degradation level was detected using 1% agarose gels, and the purity was checked using the NanoPhotometer® spectrophotometer (IMPLEN, CA, USA). RNA Nano 6000 Assay Kit of the Bio-analyser 2100 system (Agilent Technologies, CA, USA) was used to detect the RNA integrity and assess quantitation.

4.2.3 Work flow

After RNA was isolated from the samples, each step of the procedure needed to be monitored to achieve reliable data. Stepwise of the procedure, quality control was conducted, including sample tests (Figure 4:2).

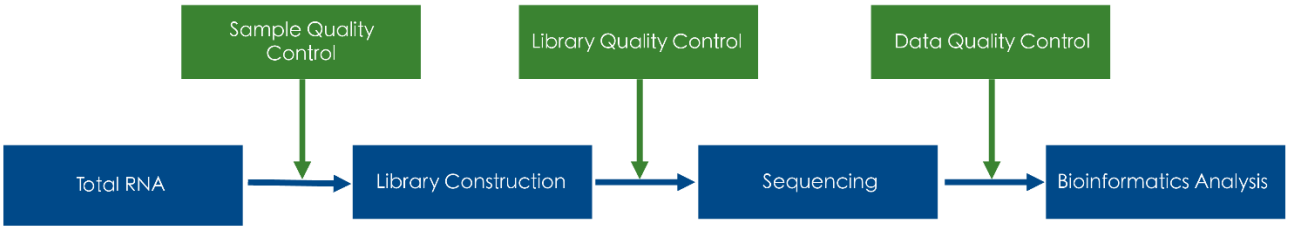

Figure 4:2: The general work flow of RNA sequencing to bioinformatics analysis. *(Figure provided by Novogene Cambridge genomics).*

4.2.4 Library preparation for transcriptome sequencing

RNA 1 µg per sample was obtained for the sample preparations, and NEBNext® Ultra TM RNA Illumina® (NEB, USA) Library Prep Kit was used for sequencing libraries preparation. The intact poly-A tailed mRNA was purified from total RNA using NEBNext poly- A mRNA magnetic beads coupled to thymine. Furthermore, cDNA synthesis was performed using NEBNext first-strand synthesis reaction buffer 5X, random hexamer primer, RNase, DNA polymerase I, and exonuclease. Then, the cDNA library was purified to hybridise, and 200 bp cDNA library fragments were chosen for PCR cycles. cDNA quality control was performed using Agilent Bioanalyser 2100 system (Figure 4:3).

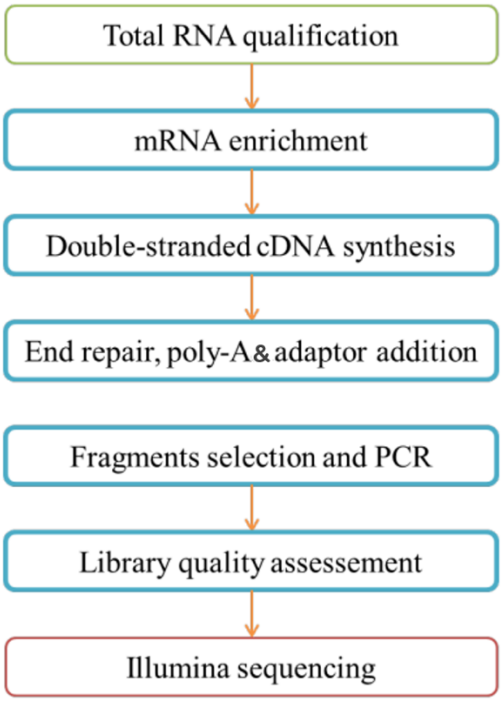

Figure 4:3: Process of mRNA enrichment and library preparation in a nutshell. *1 µg RNA per sample was used and mRNA was purified from total RNA. Double stranded cDNA was synthesised and the sequence end repaired, poly-A tail and adaptor was added. Fragments were then selected for polymerase chain reaction and the cDNA library quality assessments were performed. Sequencing was performed using next generation illumina. (Figure provided by Novogene Cambridge genomics).*

4.2.5 Clustering and sequencing

PE Cluster Kit cBot-HS was used for clustering the samples, and then sequenced using an Illumina and paired-end reads were generated.

4.3 Data analysis

4.3.1 Quality control

The poly-N and adapter reads were removed from the raw data and processed through fastp. Low quality reads Qscore over 50% was considered low quality and Qscore at 20 and 30 was considered as clean.

4.3.2 Mapping to reference genome

Reference genome and annotation files were directly downloaded from genome web browser National Center for Biotechnology Information/European Molecular Biology Laboratories-European Bioinformatics Institute (NCBI/Ensembl-EBI). Clean paired-end reads were mapped to the reference genome using HISAT2 (daehwankimlab.github.io/hisat2/manual/) software.

4.3.3 Novel gene prediction

Because transcriptome annotations are still incomplete to *C. hircus*, most RNA-seq studies will reveal novel genes and transcripts. For instance, the StringtTie (ccb.jhu.edu/software/stringtie/) tool assembles the transcript isoforms of each .bam file obtained from the mapping stage, and Gffcompare can compare StringTie assemblies to reference annotation files to identify novel genes.

4.3.4 Quantification

The mapped read numbers were counted using the feature for each gene, including known and novel genes. Reads Per Kilo base Million (RPKM) values of genes were assessed using the length and the read count mapped for an individual gene.

4.3.5 Differential expression analysis

Differential expression analysis was performed between a minimum of three biological samples per AF and control conditions, using DESeq2 v1.12.3 package. DESeq2

determine differential expression of a given data set using the negative binomial distribution, and adjusted *p* values were calculated considering the FDR values and performed Benjamini and Hochberg's statistical test. The adjusted *p* value (adj) < 0.05 was set as the threshold value, and those genes were listed as differentially expressed.

4.4 Results

4.4.1 Principal Component Analysis (PCA) Plot

Principal component analysis (PCA) was performed to analyse the sample distribution and to assess the reliable correlation between the sample triplicates between AF and Sham model groups by reduced data dimension for a simpler interpretation. As indicated in Figure 4:4, vector deviation of 69% was observed at PC1 between AF (red symbols) and Sham/control groups (light-blue symbols). An exceptional 15% segregation was observed in PC2, or the biological replicates within the groups. Since, PC1 value was higher than PC2, it can be concluded that the variance between the two conditions is higher than the variance within a group (Figure 4:4).

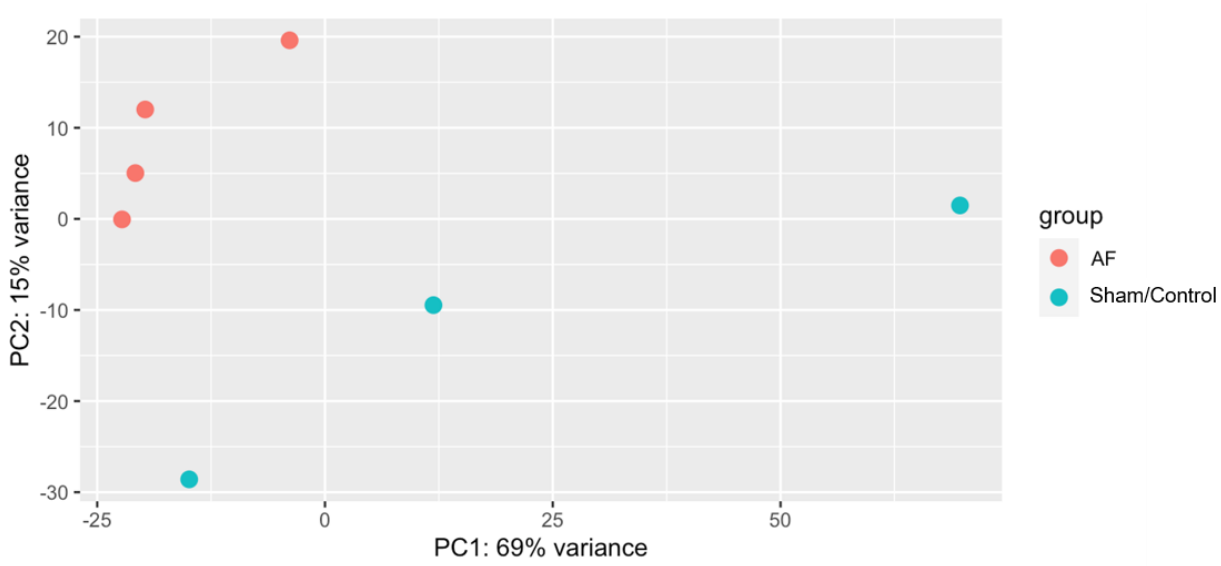

Figure 4:4: Principal component analysis (PCA) of the seven atrial samples based on their genomic expression profiles. *Each data point represents the total gene groups in each sample as a single vector. The components 1 and 2 represent the spatial resolution among the vectors. The average of vectors corresponds to a point in the K-space. Component one explains 69% of the variation, component two 15%. Salmon pink in colour: AF samples, Teal in colour: Sham/Control samples.*

4.4.2 Distance matrix heatmap

The distances between samples were analysed using hierarchical clustering and provided an overview of the similarities and dissimilarities between the samples. Sample distances were displayed using a range of shaded colour bar from dark blue to white, 0 being highly similar and displayed as dark blue and 200 being highly dissimilar represented in white colour (Figure 4:5).

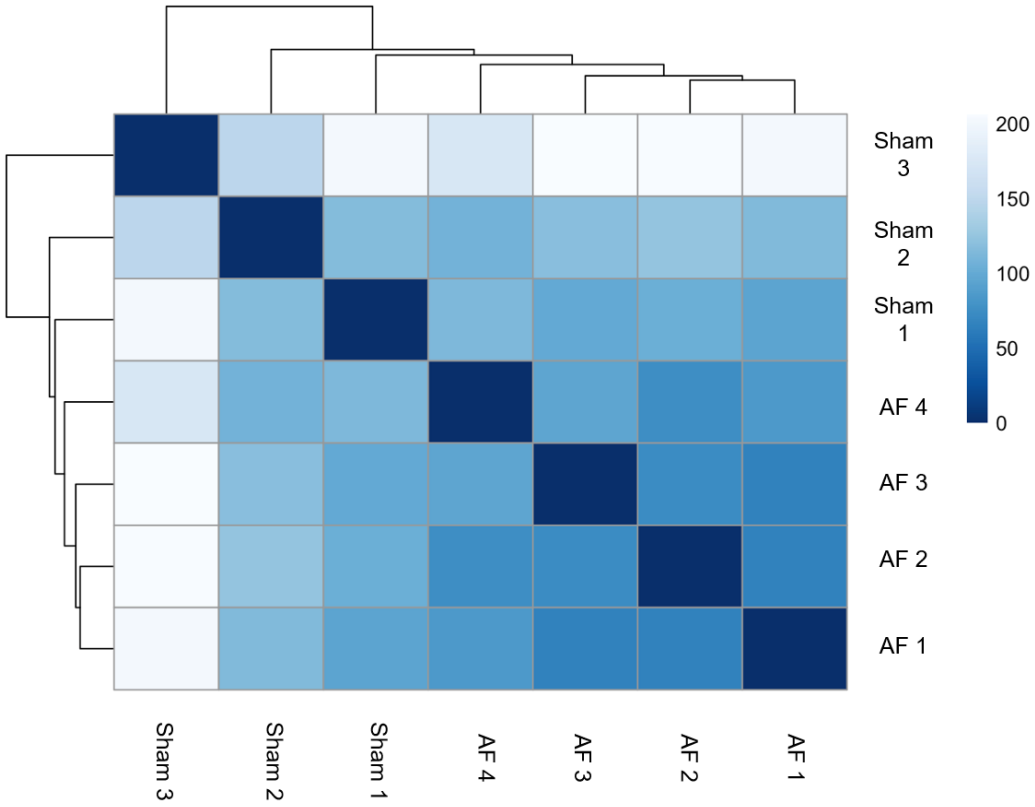

Figure 4:5: Distance Matrix Heatmap showing the distance between the samples according to their gene groups. *The similarity and dissimilarity was displayed by the colour code ranging from dark blue to white. 0 represents highly similar samples and 200 represents the highly dissimilar samples.*

4.4.3 Heat map

The top 200 most regulated genes were plotted to determine whether the samples cluster together by the diseased or non-diseased condition. All the AF goat samples of LA tissue were clustered together, similarly for the sham or control goat samples. Samples were clustered using hierarchical clustering (Figure 4:6).

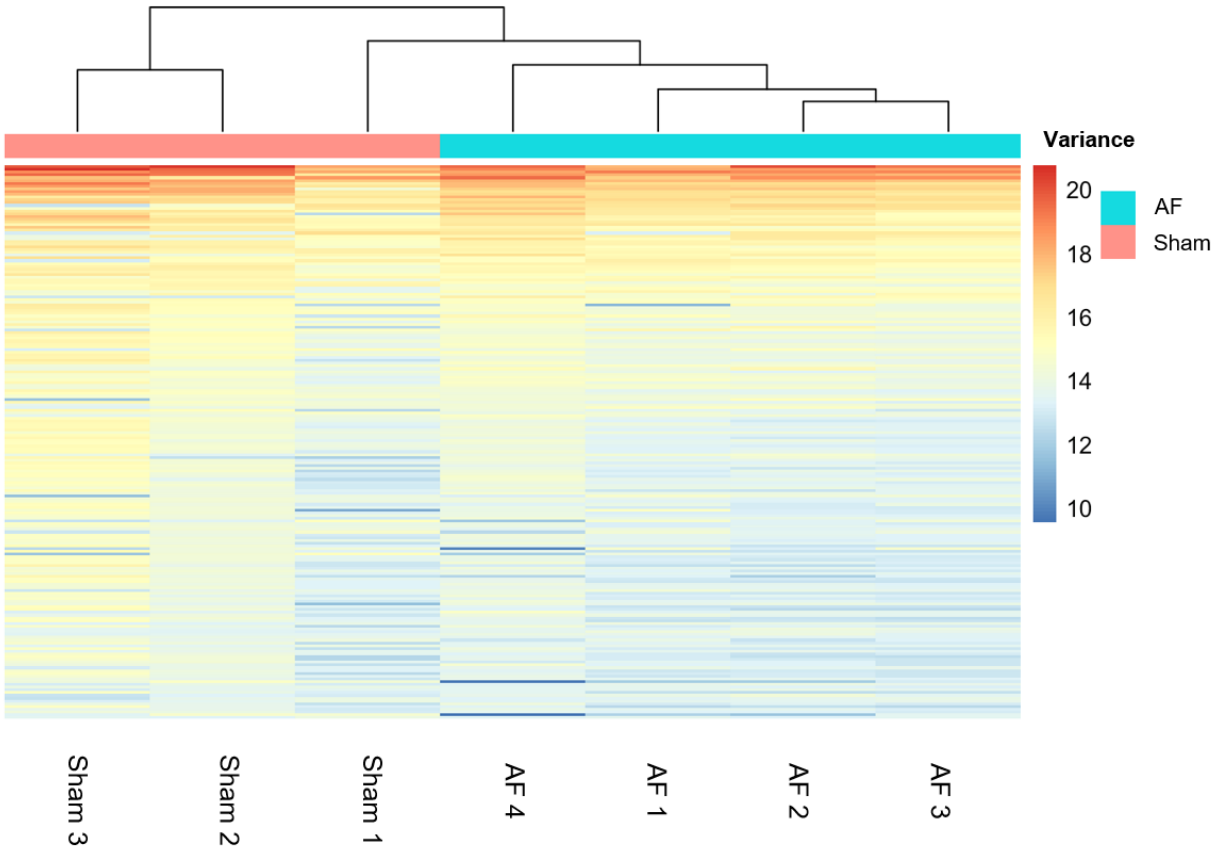

Figure 4:6: Heat map of the counts matrix. *Presented here is the heatmap of the top 200 most regulated genes to determine if the samples cluster together by the diseased or sham condition. The variance between the gene groups are presented over a colour bar, 10 or dark blue being down regulation and 20 or dark red being the up regulation. AF samples group colour code =bright teal and Sham samples group colour = Salmon pink.*

4.4.4 MA plot

Differentially expressed protein profiles between AF goat model and Sham models of LA were created using a, M and A values plot (MA plot). A Total of 230 genes were regulated in AF, with 119 genes significantly downregulated, and 111 upregulated showing the differential expression between the diseased and sham control conditions

at $p < 0.05$. The M stands for logged intensity ratio (M) and A stands for mean logged intensities (A) (Figure 4:7).

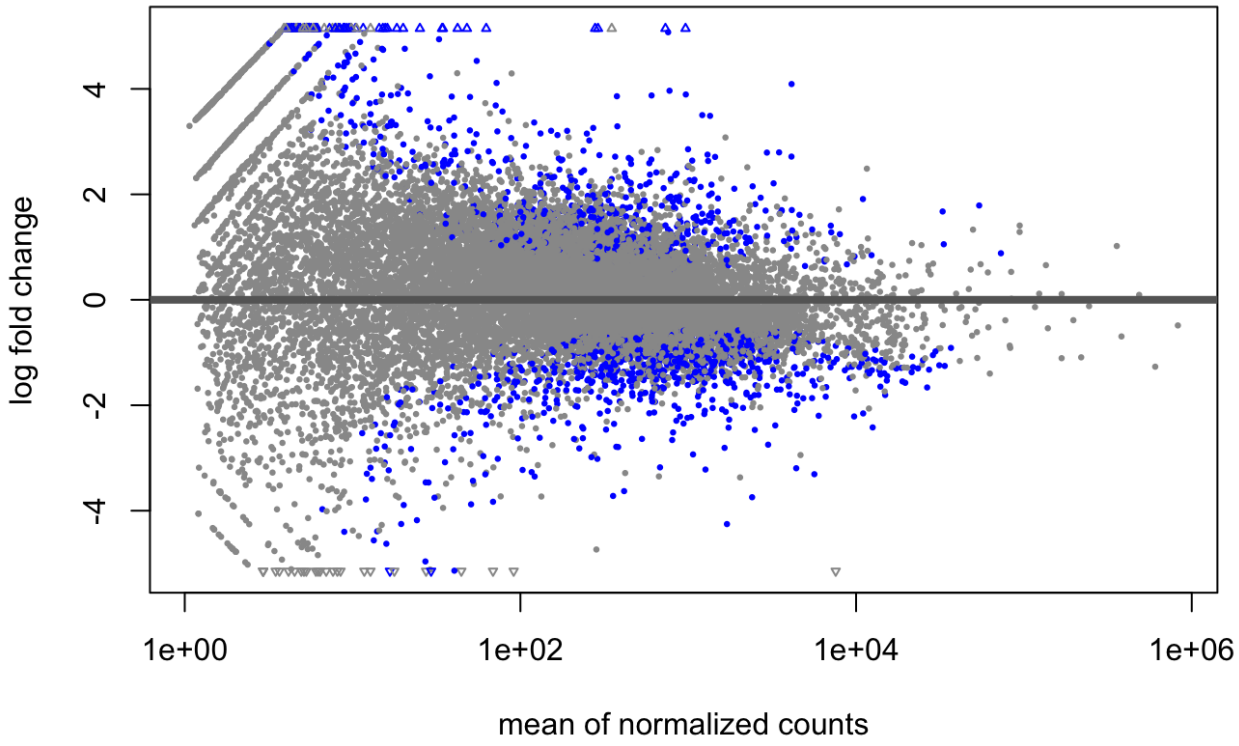

Figure 4:7: MA Plot presenting log2 fold changes attributable to a given variable over the mean of normalised counts. *The MA plot shows the gene expression changes between the AF and sham goat model groups. Genes with similar expression were clustered near M value =0 and further away + or – log fold change respectively presented genes either up regulated or down regulated. Genes with highest regulation levels are presented as open triangles outwards the 4 and -4 range. (Blue dots represent the highest regulated genes.*

4.5 Transcriptomics observations in goat AF tissue samples

4.5.1 Down regulation of the rRNA processing pathway in the nucleolus and cytosol

The AF goat model showed transcriptomic evidence that the dysregulations in the LA were due to increased cellular stress. This was indicated as the genes responsible for the rRNA processing and modification in protein synthesis (Grummt, 2013) were down-regulated (Figure 4:8).

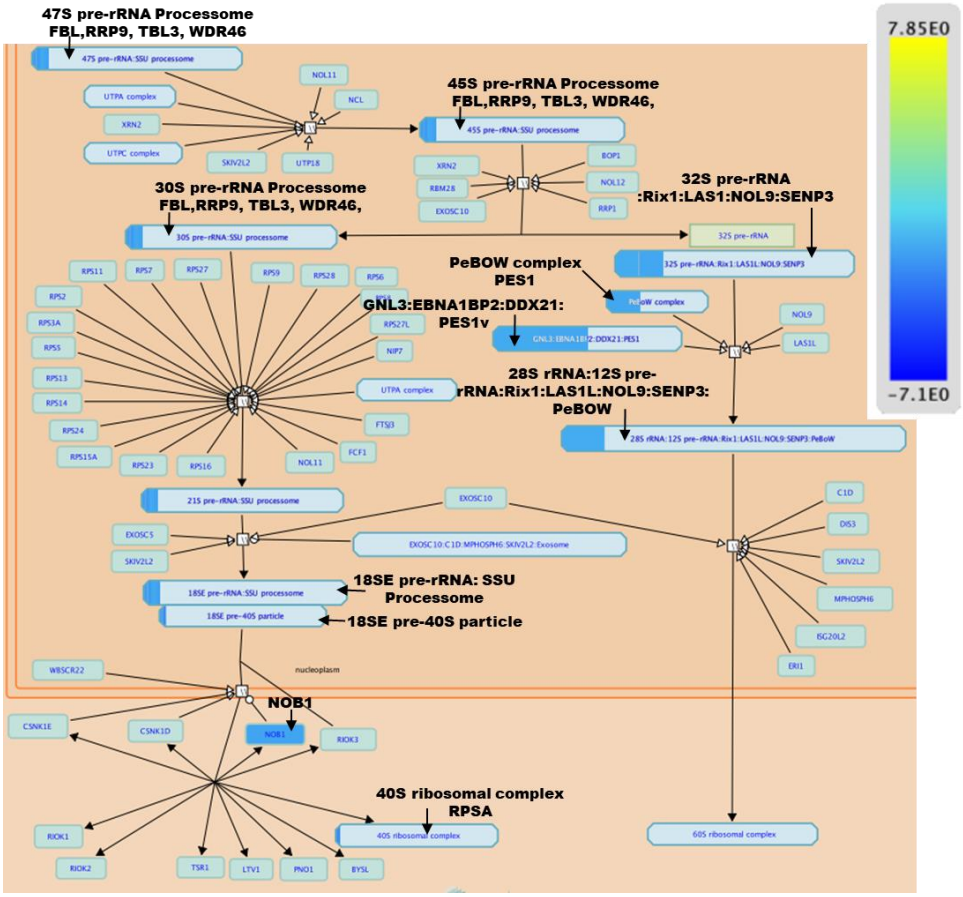

Figure 4:8: Down regulation of the rRNA processing pathway in the nucleolus and cytosol. *The observed protein complexes and their respective mRNA regulations are as follows: 47S- Pre-rRNA processome; this complex consists of proteins FBL (log2 -1.56), RRP9 (log2 -1.63), TBL3 (log2 -1.21), WDR46 (log2 -1.41).30S- Pre-rRNA processome; this complex consists of proteins FBL (log2 -1.56), RRP9 (log2 -1.63), TBL3 (log2 -1.21), WDR46 (log2 -1.41). 45S- Pre-rRNA processome; this complex consists of proteins FBL (log2 -1.56), RRP9 (log2 -1.63), TBL3 (log2 -1.21), WDR46 (log2 -1.41).32S pre-rRNA: Rix1: LAS1L:NOL9:SENP3; this complex consists of proteins PES1 (log2 -1.23), SENP3 (log2 -1.1). PeBOW complex; PES1 (log -1.23). GNL3:EBNA1BP2:DDX21:PES1; this complex consists of proteins EBNA1BP2 (log2-1.13), PES1 (log2 -1.23). 28S rRNA: 12S Pre-rRNA: Rix1: LAS1L, NOL9, SENP3: PeBOW; this complex consists of protein SENP3 (log2 -1.1). 40S ribosomal complex; this complex consists of protein RPSA (log2 -2.16). NOB1 (log2 -1.36). 18SE pre- 40S particle; this complex consists of proteins NOB1 (log -1.36), RPSA (log2 -2.16). 18SE pre- rRNA: SSU processome; this complex consists of proteins FBL (log2 -1.56), RRP9 (log2 -1.63), TBL3 (log2 -1.21), WDR46 (log2 -1.41). 21SE pre- rRNA: SSU processome; this complex consists of proteins FBL (log2 -1.56), RRP9 (log2 -1.63), TBL3 (log2 -1.21), WDR46 (log2 -1.41). (colour code=yellow to blue gradient, yellow represent highest up regulation while blue represent highest down regulation, highest upregulation log2 fold 7.85E0 and lowest log2 fold -7.1E0, The protein complexes with complete or part-coloured representation showed the total molecules present from the query data set to complete the complex. Arrow = Protein or protein complex name) Figure created using www.reactome.com pathway analysis. The given figure is a cropped version from the original elaborated figure for the discussion and the original version of this figure is provided in the Appendix figure A3:1.*

In the AF goat model, the genes encoding the rRNA processing in the nucleolus and cytosol were downregulated (Figure 4.8). These genes with the regulation levels are, given in the Table 4:1 below.

Gene Name	**Gene**	**Log2 Fold change**
Eukaryotic initiation factor 4A-I	EIF4A1	-1.10
40S ribosomal protein SA	RPSA	-2.16
Pescadillo homolog	PES1	-1.23
rRNA 2'-O-methyltransferase fibrillarin	FBL	-1.56
Transducin beta-like protein 3	TBL3	-1.21
Probable rRNA-processing protein EBP2	EBNA1BP2	-1.13
RNA-binding protein NOB1	NOB1	-1.36
WD repeat-containing protein 46	WDR46	-1.41
U3 small nucleolar RNA-interacting protein 2	RRP9	-1.63

Table 4:1: List of downregulated genes of rRNA processing in the nucleolus and cytosol pathway

Identifying the functional aspects of all the downregulated genes is vital to understanding the total transcriptomic regulation in rRNA processing. EIF4A1 is a subunit from the eIF4F complex involved in the mRNA recognition of the 5'end m7G cap (7-methylguansine triphosphate linked to the 5′ end of the mRNA via a 5′ → 5′ triphosphate linkage is a conserved modification of eukaryotic mRNA which is necessary for the mRNA to bind the ribosome to proceed the translation) (Zhong *et al.*, 2018) and (Iacobas *et al.*, 2008).

EBNA1BP2 is a 27s pre-rRNA processing protein, and RPSA is a ribosomal 40s subunit stabilising protein required for the 40S ribosomal subunit maturation. PES1 is a protein component of the Pes1, Bop1, and WDR12 complex (PeBOW), part of the ribosome biogenesis and cell cycle coordination process. It has been reported that depletion of PeBOW proteins led to dramatically suppressed, cell expansion, epidermal pavement, cell proliferation, and cell differentiation in *Arabidopsis thaliana plant.* FBL is a methylating enzyme that methylates both proteins and RNA (Iyer-Bierhoff *et al.*, 2018). Moreover, FBL is a pre-rRNA processing protein (Iyer-Bierhoff *et al.*, 2018). TBL3 is an RNA binding protein and is part of the WD40 group, which are regulatory proteins. WDR46 is a fundamental scaffold component of the nucleolar structure (Hirai *et al.*, 2013). RRP9 is a component of the small ribonucleoprotein particle SnoRNP (Granneman *et al.*, 2009), which plays a functional role in processing and modifying pre-rRNA. The RRP9 downregulation is predicted to have an effect on the translation (Figure 4:8).

4.5.2 AMPK activation of GLUT4 vesicle translocation to the plasma membrane

As discussed in Chapter 3, similarly, in the transcriptomics data, the Reactome pathway highlighted a possible upregulation in the GLUT4 vesicle translocation to the plasma membrane (Yamaguchi *et al.*, 2005). AMPK induced GLUT4 vesicle translocation to the plasma membrane was up-regulated (Figure 4:9). During the acute cell stress caused by energy depletion, it is vital to maintain cell homeostasis, and this is done by switching off the most energy-consuming pathways, such as protein synthesis (Iacobas *et al.*, 2008).

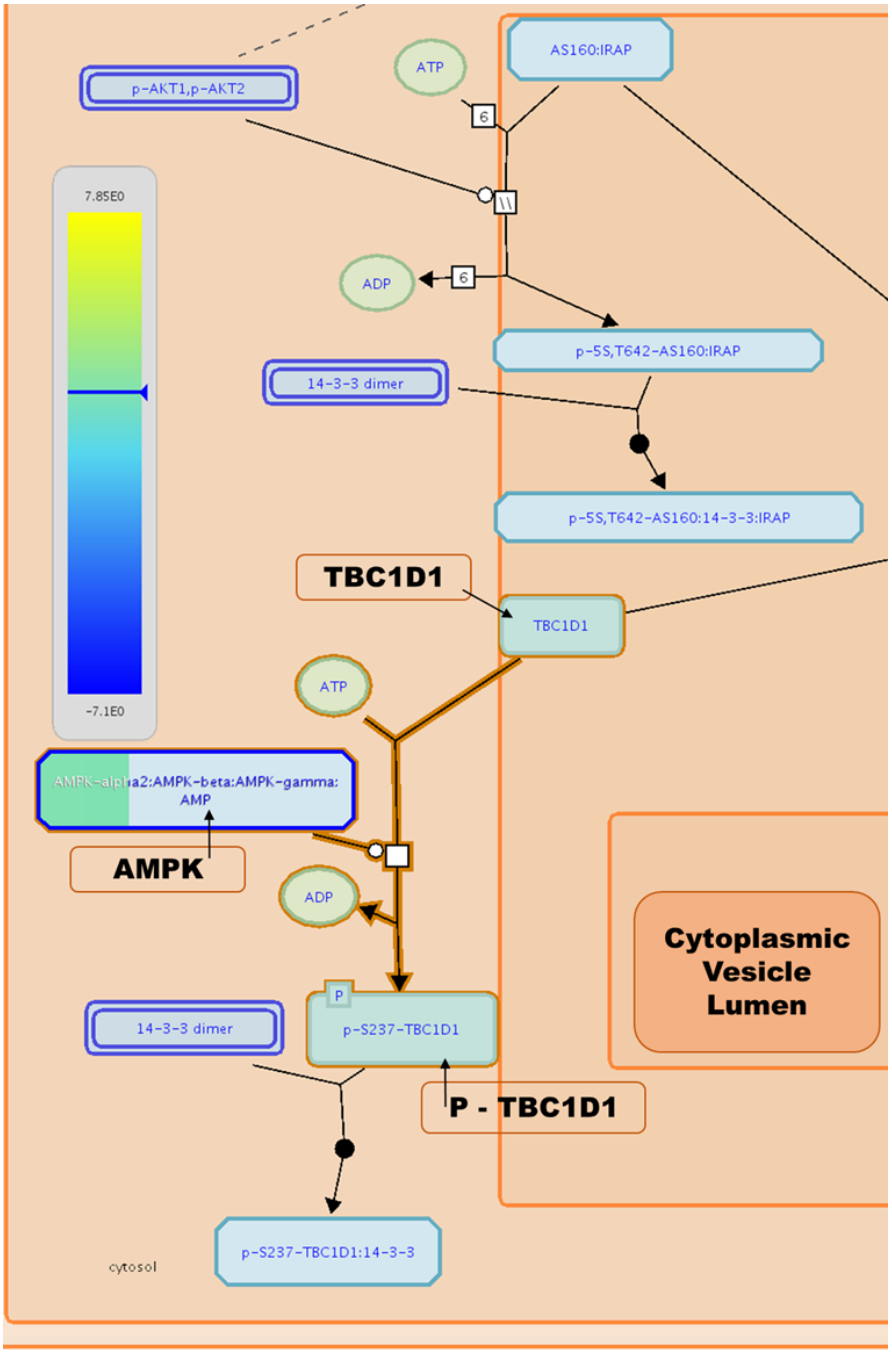

Figure 4:9: AMPK activation of GLUT4 vesicle translocation to the plasma membrane. *TBC1 domain family member 1 (TBC1D1) phosphorylation at AMPK to activate GLUT4 glucose uptake to the cell. (colour code=yellow to blue gradient, yellow represent highest up regulation while blue represent highest down regulation, highest upregulation log2 fold 7.85E0 and lowest log2 fold -7.1E0, The protein complexes with complete or part-coloured representation showed the total molecules present from the query data set to complete the complex. Arrow = Protein or protein complex name) Figure created using www.reactome.com pathway analysis. The given figure is a cropped version from the original elaborated figure for the discussion and the original version of this figure is provided in the Appendix figure A3:2.*

GLUT4 is from the family of glucose transporter proteins containing 12-transmembrane domains and expressed primarily in skeletal muscle and adipose tissue (Vargas *et al.*, 2021). As part of the endosomal-trans-Golgi network (TGN) system vesicle, GLUT4 translocates between the intracellular domain and cell membrane (Vargas *et al.*, 2021). Once internalised, GLUT4 vesicles fuse with early endosomes and are re-located back into intracellular vesicles (Bryant *et al.*, 2002). In the AF goat model of LA, the Reactome pathway indicated that GLUT4 pathway was associated with TBC1 domain family member 1 (TBC1D1). TBC1D1 is a Rab-GTPase – activating protein that is phosphorylated as a response to AMPK (Pehmøller *et al.*, 2009), insulin, and some growth factors (e.g.: insulin like growth factor IGF1) (Chen *et al.*, 2016) and stimulates glucose uptake (Vichaiwong *et al.*, 2010). Translocation of GLUT4 vesicles to the plasma membrane by AMPK pathway activation implicates cellular glucose demand to produce more ATP in the AF diseased condition (Zhao *et al.*, 2019).

4.5.3 AMPK Activation of macroautophagy

AMPK is activated under pathological conditions such as electrical stimulation, ischemia and energy demand (Qin, 2019). AMPK phosphorylates and activates multiple events through its kinase activity to increase the ATP availability and reduce

excess energy expenditure. Here in AF goat model AMPK activation has further acted upon the pathways, such as inhibition of anabolic processes, namely rRNA process and modification, and upregulated macroautophagy while inhibiting the ER stress related cell apoptosis. The above mentioned cascade of molecular regulations maintain the energy balance while supporting the homeostasis of cellular environment (Hardie *et al.*, 2016).

The Reactome pathway studies of the AF goat model interpreted, that the upregulated AMPK directly form heterodimers with ATG13, ULK1 and ATG101. Therefore, up regulated AMPK has a possibility to activate macroautophagy through a series of phosphorylation of the ATG13, ULK1 and ATG101 protein complexes (Li and Chen, 2019). ATG13 can be directly phosphorylated and activated by AMPK as well (Li and Chen, 2019). Therefore AMPK upregulation of macroautophagy can be hypothesized in AF goat model.

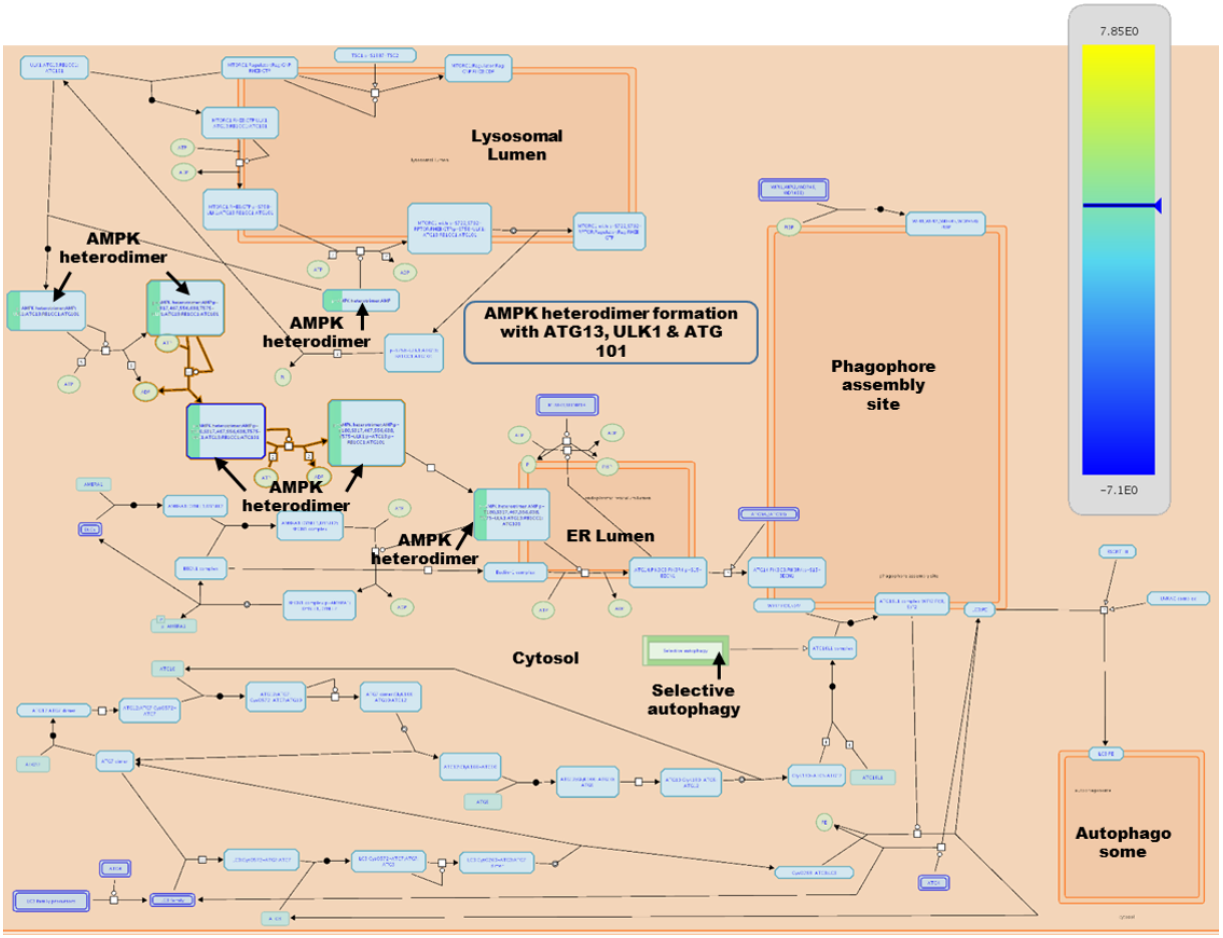

Figure 4:10: AMPK activation of Macrophagy. *AMPK or PRKAG3 log2 2.2 and PRKAA2 log2 2.3 fold up regulation was observed in the mRNA differential expression analysis. AMPK formed direct heterodimer with autophagy marker proteins such as ATG13, ATG101 and ULK1. Moreover, AMPK activation of selective autophagy was observed. (colour code=yellow to blue gradient, yellow represent highest up regulation while blue represent highest down regulation, highest upregulation log2 fold 7.85E0 and lowest log2 fold -7.1E0, The protein complexes with complete or part-coloured representation showed the total molecules present from the query data set to complete the complex. Arrow = Protein or protein complex name) Figure created using www.reactome.com pathway analysis. The given figure is a cropped version from the original elaborated figure for the discussion and the original version of this figure is provided in the Appendix figure A3:3.*

4.5.4 AMPK activation of Lipophagy

The autophagic degradation of lipid droplets or the lipid storage organelles of eukaryotic cells is called lipophagy (Kounakis *et al.*, 2019), a lysosomal degradation pathway. The general function of the lipid droplets is storing lipids that can later be utilized for energy production or the synthesis of membrane components. However, through lipolysis (a process that breaks down esters and triacylglycerols by lipase enzymes) (Zimmermann *et al.*, 2004) and lipophagy (Kounakis *et al.*, 2019), during nutrient deprivation (Kaushik and Cuervo, 2016) or energy demand the stored lipids can be accessed (Seo *et al.*, 2017). The lipid droplets are coated with a protective protein called perilipin (PLIN) (Kaushik and Cuervo, 2016) and (Ward *et al.*, 2016). When PLIN is degraded, the contents inside the droplet are associated with lysosomal degradative enzymes and break down into fatty acids (Schulze *et al.*, 2017) ; (Kaushik and Cuervo, 2016). As discussed in Chapter 3 extensively, we now know that AMPK is an energy regulator in the cell. Previous studies by Seo *et al*., 2017 and Kaushik, S., and Cuervo, A. M. et al., 2016 extensively showed the AMPK regulation of lipophagy occurs during energy deprivation. Therefore, AMPK mediated lipid droplet degradation is considered a mechanism that provides the cells with immediate energy requirements (Kaushik and Cuervo, 2016).

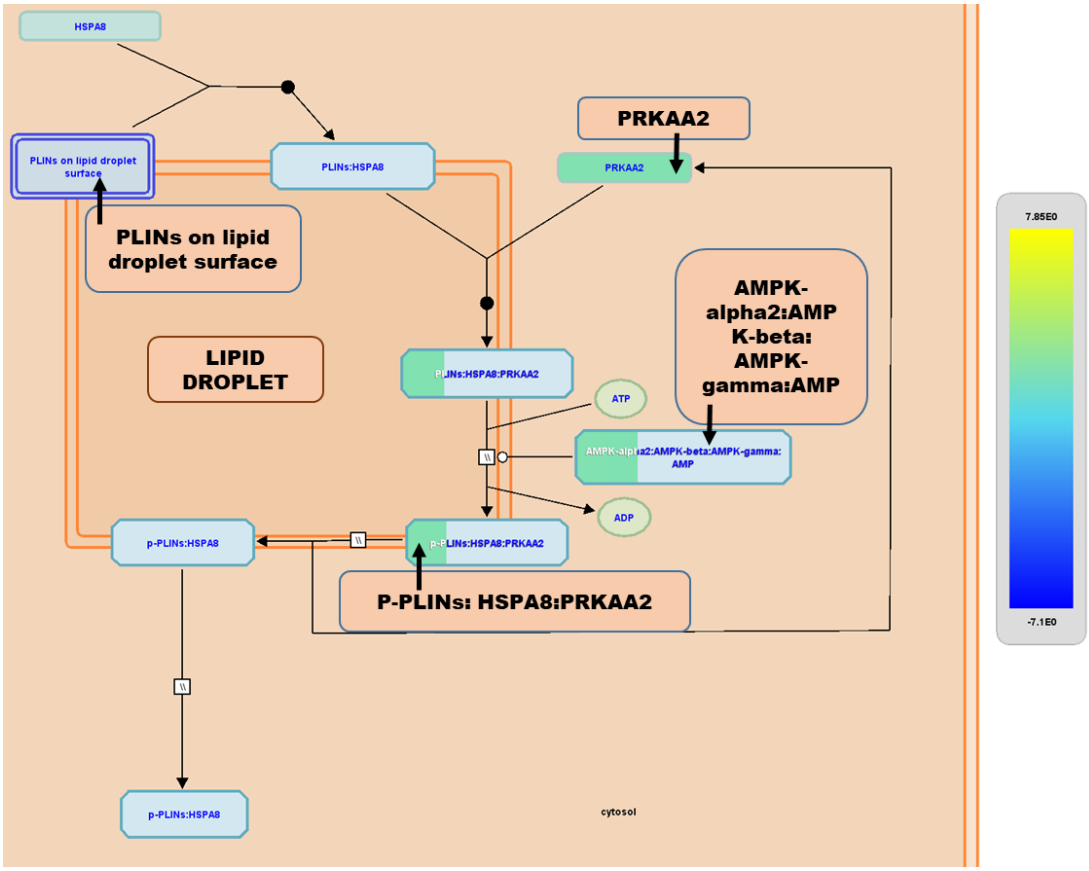

Figure 4:11: Lipophagy: *AMPK activated Lipophagy as interpreted in AF goat LA model. AMPK or PRKAG3 log2 2.2 and PRKAA2 log2 2.3 fold up regulated. The Perilipin (PLIN) protein was firstly interacted with the chaperone protein Heat shock protein 8 (HSP8) and then AMPK/PRKAA2 phosphorylated the PLIN protein to degrade through chaperone mediated autophagy. (colour code=yellow to blue gradient, yellow represent highest up regulation while blue represent highest down regulation, highest upregulation log2 fold 7.85E0 and lowest log2 fold -7.1E0, The protein complexes with complete or part-coloured representation showed the total molecules present from the query data set to complete the complex. Arrow = Protein or protein complex name). Figure created using www.reactome.com pathway analysis. The given figure is a cropped version from the original elaborated figure for the discussion and the original version of this figure is provided in the Appendix figure A3:4.*

In the AF goat model of LA the AMPK activation of Lipophagy was interpreted in the Reactome pathway studies. (Figure 4:11) and AMPK was log2 2.3 fold upregulated. The PLIN protein first interacted with the chaperone Heat shock protein 8 (HSPA8) and

the upregulated AMPK, then phosphorylated PLIN, to break down the PLIN protein from the lipid droplet membrane (Kaushik and Cuervo, 2016).

4.5.5 The mechanistic Target of Rapamycin (mTOR) antagonism by 4F2 cell-surface antigen heavy chain (SLC3A2)

The mechanistic Target of the Rapamycin (mTOR) signalling pathway is one of the most commonly dysregulated pathways found in pathological states of the cell, such as cardiovascular anomalies or cancer (Sciarretta *et al.*, 2018) and (Murugan, 2019). mTOR coordinates eukaryotic cell growth and regulates cellular metabolism by sensing nutrients such as amino acids and growth factors. The mTOR pathway has been extensively studied for tumor cell proliferation, metabolism and genomic instability (reviewed by Janku, Yap, and Meric-Bernstam, 2018) (Janku *et al.*, 2018) or nutrient and energy-deprived states of the cell (Nicklin *et al.*, 2009). mTORC1 regulates protein synthesis (Wang and Proud, 2006), de novo lipid synthesis such as fatty acid and cholesterol biosynthesis, and induces cell growth (Porstmann *et al.*, 2008).

The mTOR pathway plays a significant role in the regulation of nutrient-sensing (Fang *et al.*, 2001) and, depending on the cellular or pathological circumstance, coordinates the cell to proliferate or functionally differentiate (Howie *et al.*, 2014). Additionally, the amino acid glutamine is mainly associated with the mTORC1 signalling pathway. An extensive study conducted by Durán *et. al*.,2012 showed that mTORC1 is activated by combining glutamine and leucine. The glutamine, leucine combination enhances glutaminolysis and α-ketoglutarate production (Durán *et al.*, 2012). Therefore, suppression or inhibition of glutaminolysis prevents GTP association of Ras-related GTP-binding protein B (RagB) and mTORC1 activation through lysosomal translocation.

The active Rag heterodimer activates mTORC1 in the absence of glutaminolysis. Conversely, enhanced glutaminolysis stimulates lysosomal translocation and mTORC1 activation (Li *et al.*, 2013). Furthermore, autophagy and cell growth were found to be controlled by mTORC1 and were also regulated by glutaminolysis (Durán *et al.*, 2012). Consequently, mTORC1 senses and is activated by glutamine and leucine via glutaminolysis and α-ketoglutarate production upstream of Rag proteins (Durán *et al.*, 2012).

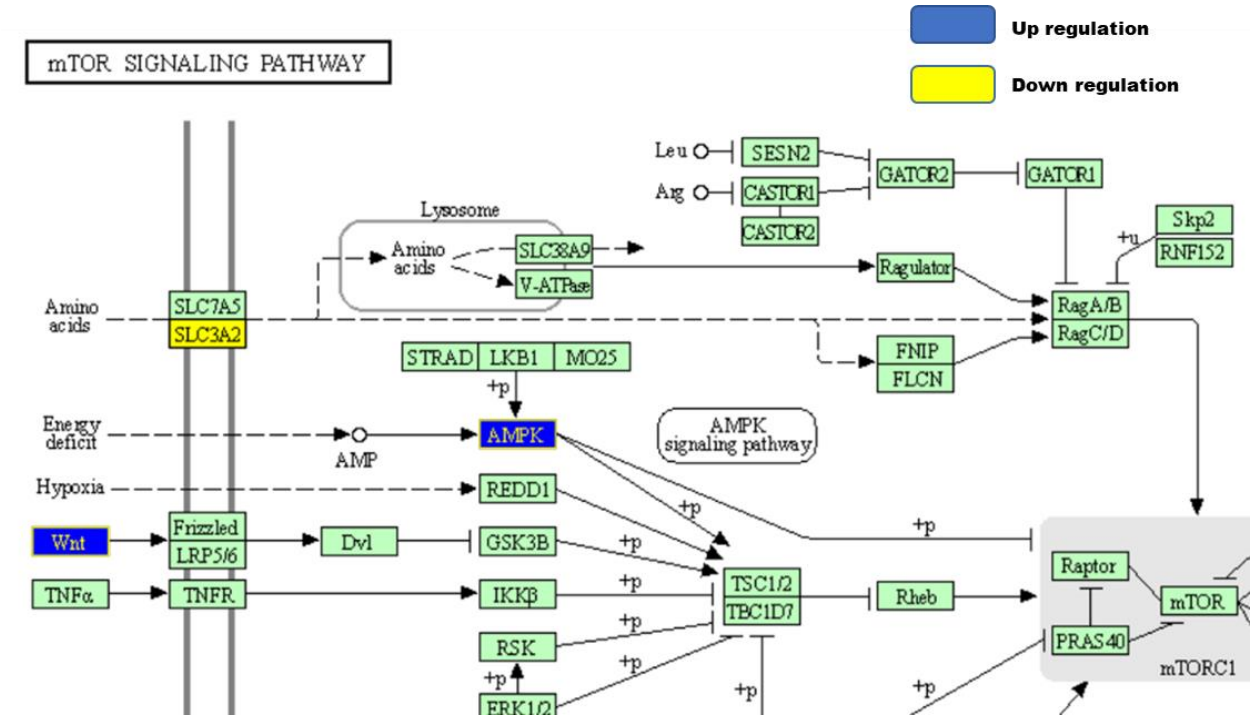

Figure 4:12: The mTOR signaling Pathway. *The mTOR signalling inhibition by the down regulation of SLC3A2 (log2 -1.6 fold), AMPK or PRKAG3 log2 2.2 and PRKAA2 log2 2.3 fold and WNT5A log2 2.3 fold up regulated. (Arrow = Gene name, Blue = up regulation (log2 fold change) and Yellow= down regulation (log2 fold change)). +P = phosphorylating events Pathway analysed using KeGG database. The given figure is a cropped version from the original elaborated figure for the discussion and the original version of this figure is provided in the Appendix figure A3:5.*

Furthermore, the Nicklin *et al*., 2009 studies on bidirectional transport of amino acids and regulation of both mTOR and autophagy, showed that L-glutamine up-taking of glucose and its efflux in the presence of essential amino acids is the rate-limiting step for mTOR activation. Here in the AF goat model of LA, a significant log2 -1.6 fold down-regulation of (SLC3A2) gene was observed. SLC3A2, a bidirectional transporter that regulates the efflux of the L-glutamine and intake L-leucine. According to the studies of Nicklin *et al*., 2009, L-glutamine is a rate-limiting step for mTORC1 activation, and SLC3A2 inhibition or down-regulation antagonises mTORC1 signaling by limiting

cellular uptake of L-glutamine (Nicklin *et al.*, 2009). Inhibition of mTOR signaling by withdrawing amino acids or adding rapamycin activates autophagy (Blommaart *et al.*, 1995). Here in the AF goat model transcriptomics studies, a SLC3A2 mediated mTORC pathway inhibition has occurred, showing that in the AF goat model LA, the mTOR pathway is antagonised, supporting the AMPK regulated cellular autophagy is induced.

4.6 Discussion

This chapter discusses the results from genomic expression analysis in LA tissue from the AF goat model compared to the sham goat model using the mRNA transcript counts. The highlights for the pathway interpretation for the mRNA expression were: up-regulation of the AMPK, and the AMPK induced autophagy pathway. The likely results of these changes are to balance energy consumption in the LA and accelerate the removal of ROS mediated cytotoxic material and maintain the cellular and molecular integrity.

Eukaryotes respond to cellular stresses that threaten homeostasis by downregulating rRNA (Grummt, 2013 and Bolster *et al.*, 2002), ribosome and global protein synthesis because these processes are considered the highest ATP consuming pathways (Grummt, 2013). Except for reducing ATP consumption, downregulation of protein

synthesis further supports cells by providing a better environment (Pakay *et al.*, 2002) and (Hand and Hardewig, 1996) to remove the accumulated stress-mediated cytotoxic waste through selective and macroautophagy (Maity *et al.*, 2016). As increased ROS reacts with newly synthesized proteins, misfolded protein aggregation increases (Mirzaei and Regnier, 2008). Hence, reduced protein synthesis can increase the cell survival state.

Upregulated AMPK both directly and indirectly reacts with molecular targets. Analysis of the genomic expression in the AF tissue predicts that up regulated AMPK has a tendency to form complexes with autophagic proteins such as ULK1 and ATGs to accelerate autophagic flux. Transcriptomic regulations observed in the AF goat model of LA did not indicate direct phenotypic changes to the lysosome, but indicated changes in lysosome directed macroautophagy. Dynein regulatory complex protein 9 (IQCG), a protein that is reported to be involved in the dynein-mediated autophagosome (AP) trafficking (Xu *et al.*, 2014), formation of autophago-lysosomes (APLs) and autophagic flux processes in coronary arterial myocytes, was identified as down-regulated by log2 -4.6 fold in the transcriptomics results. Similarly, cytoplasmic dynein 1 intermediate chain 2 (DYNC1I2), a protein that is Involved in membrane-transport, such as Golgi apparatus, late endosomes and lysosomes (Chanduri *et al.*, 2016), was down-regulated in the proteomic differential expression data. Caveolae-associated protein 2 (CAVIN2) was upregulated log2 2.6 in transcriptomics and similarly in proteomics Caveolin (CAV1) was upregulated by log2 0.5 fold.

The pathway analysis performed on the differential expression of mRNA studies suggests that cellular energy demand results in AMPK pathway activation in the AF model. As a result, mechanisms such as elevated macroautophagy, lipophagy and downregulated rRNA processing, GLUT4 translocation to the plasma membrane and induced autophagy through mTOR inhibition were highlighted through the Reactome and KeGG pathway analysis. These data further highlight pathological similarities that were identified in both the proteomics and transcriptomics data for the AF goat model. Therefore, the general pathology affecting the acidic organelle pathways, vesicle-mediated transport and autophago-lysosome motility share a similar proteomic and genomic profile in the AF goat model in LA tissue and prompt for further conformational studies such as RNAi or gene knock out in animal models.

Chapter 5

Quantitative Analysis of lysosomal proteins using biochemical assays

5.1 Introduction

Chapters 3 and 4 discussed proteomic and transcriptomic analyses in the LA goat AF model and how the proteins and genes were regulated. Here in this chapter, I present a quantitative analysis for some of the proteins regulated in the proteomic data and reported in the literature of AF. In this chapter I discuss molecular and biochemical techniques such as Western blotting and lysosome enzyme assays on various endo lysosomal proteins.

Western blotting or immunoblotting was first invented in 1979 by Harry Towbin (Towbin *et al.*, 1979). The term blotting refers to the concept of transferring biological samples such as protein from a gel base to a membrane, subsequently identifying by the specific antigen-antibody binding reaction. Even though Western blotting is technically a labour intensive and a high cost technique, the unique way of identifying a protein in a complex mixture of proteins, the ability to detect the protein regulations, and the ability to quantify using the protein band intensity (Towbin *et al.*, 1979) are some of the unique features that explain why to date researchers depend on this technique.

Christian De Duve performed the acidic enzyme assays in 1955, which led to the discovery of the lysosome (De Duve *et al.*, 1955). Ever since, lysosome enzyme assays are performed to identify the lysosomal lumen activity.

In this chapter, we look at Western blot results to probe regulation of Glycogenin-1 (GYG1). GYG1 serves as a primer protein in glycogen synthesis (Litwack, 2018). The proteomic data presented in chapter 3 demonstrated significant upregulation of SLCA4/ GLUT4 by log2 1.5-fold in the AF goat model of LA. Furthermore, the upregulation of lysosomal-α- glucosidase (GAA) was observed in the proteomic data obtained from the EL fraction of the AF goat model, which was by log2 0.4-fold. GAA is a lysosomal enzyme that degrades glycogen (Adeva-Andany *et al.*, 2016) in the lysosome (Zirin *et al.*, 2013), and an upregulation of GYG1 would provide evidence that either glycogen levels go up or an accumulation of glycogen takes place (Embi *et al.*, 2014 and Ausma

et al., 2003), which is considered a structural or a cellular remodeling of AF goat LA (Embi *et al.*, 2014) and (Ausma *et al.*, 2003).

Furthermore, I evaluated Rab11A upregulation that was observed in the proteomics data. Rab11A was found to be significantly up regulated in the TL fraction during proteomic analysis, exhibiting a log2 0.5-fold increase. Ras-related Rab11A, or Rab11A, is a small GTPase protein and is an essential regulatory protein in the vesicle-mediated transport system (Goswami *et al.*, 2021). Rab proteins switch between two conformations, a GDP-bound inactive form and an active GTP-bound form. Activated Rab binds with specific effectors such as Rab11 family-interacting protein 3 (RAB11FIP3) to promote vesicle trafficking (Hales *et al.*, 2001) , (Grosshans *et al.*, 2006 and Welz *et al.*, 2014) . These recruited effectors are involved in the formation of vesicles, fusion and tethering (Welz *et al.*, 2014). Rab11 is a localised trans-Golgi network protein involved in the cellular recycling pathway, supporting the traffic of membrane components to the plasma membrane (Urbé *et al.*, 1993).

In addition to the above, I used Western blotting to identify the protein regulation trends of cathepsin D (CTSD) in goat AF model LA and the AF patients' plasma to follow up on the preliminary proteomics data.

In addition to testing selected hits observed in the proteomics data set, I also carried out activity assays of the main lysosomal enzymes, β –galactosidase, β – hexosaminidase type A and β – hexosaminidase type B.

Lysosomes contain more than 50 acid hydrolases and are the primary location for the degrading of intracellular and extracellular macromolecules. The acidic hydrolases are active at the acidic pH of lysosomes (approximately 4.5) (Mindell, 2012), and are not active at the neutral cytosolic pH of 7.5 (Cooper, 2000). Therefore, even if the lysosomal membrane were to burst, the released acid hydrolases would be inactive due to the pH of the cytosol. Lysosomes actively transport H^+ into the lumen using lysosomal proton pumps to maintain their acidic environment (Mindell, 2012). Mutations in the genes that encode hydrolases give rise to more than 30 different forms of lysosomal storage diseases (Cooper, 2000 and Filocamo and Morrone, 2011) . Additionally, the hydrolase dysregulations lead to cardiac metabolic disorders, such as Fabry, Pompe and Danon disease (Filocamo and Morrone, 2011) ; (Nair *et al.*, 2019). Since the proteomics data of the AF goat model identified significant upregulation of GAA, which has been reported to be linked to Pompe disease with a cardiac phenotype (Nair *et al.*, 2019) ; (Kishnani *et al.*, 2006) and (van den Hout *et al.*, 2003), it is necessary to study lysosomal hydrolases to probe for possible changes in the enzymatic activity.

Similarly, the quantitative analyses of the preliminary proteomic data obtained from the technical replicates of n=1 biological samples of sham and AF group showed that the CTSD levels were altered in the goat AF sample. Therefore, a follow-up biochemical study was performed using Western blotting. Cathepsins are a part of the hydrolase family. The term 'cathepsin' is derived from the Greek terms 'kata' and 'hepsein', which means digest and boil down (Willstatter R and E, 1929). Cathepsins are categorised according to their catalytic site as either serine (cathepsins A and G), aspartic (cathepsins D and E) or cysteine proteases. CTSD is an aspartic lysosomal protease that is ubiquitously expressed throughout the human body and synthesised as pre-pro-CTSD in the endoplasmic reticulum (ER). Then, as a signal peptide chain, it is modified into cleaved forms. These forms are Pro CTSD at 50- 52 kDa and intermediate CTSD at 48 kDa, produced after removing 44 amino acids from the peptide chain (Wu *et al.*, 2017). Furthermore, proteolytic cleavage produces mature-CTSD heavy chain 34 kDa and mature-CTSD light chain 14 kDa (Laurent-Matha *et al.*, 2006). As reported in studies (Barrett *et al.*, 2004), pro-CTSD, found in the early stages of the endosomal sorting complexes required for transport (ESCRT) pathway (Barrett *et al.*, 2004), is enzymatically inactive (Butler *et al.*, 2019) and (Ikonomov *et al.*, 2003). Secretory components including ER, Golgi network, inter-Golgi vesicles, and endosomes contain the CTSD inactive form (Ikonomov *et al.*, 2003).

Active CTSD is abundant in the late endosomes and lysosomes (Barrett *et al.*, 2004).

Biologically inactive pro-CTSD can be secreted to the extracellular environment, for example, in human breast milk (Větvicka *et al.*, 1993), and enzymatically active CTSD can be secreted to the extracellular space during cellular damage or ischemic episodes (Větvicka *et al.*, 1993). Cellular CTSD levels increase under pathological conditions such as increased autophagy, where CTSD promotes autophagic flux for cell survival, and has been implicated in a protective role against the development of heart failure after myocardial infarction (Wu *et al.*, 2017). The CTSD enzyme has recently been recognised as a clinically useful histopathological biomarker in breast Cancer (Dubey and Luqman, 2017) ; (Abbott *et al.*, 2010).

In summary, this chapter presents a quantitative biochemical validation of selected proteins that were regulated or related to the regulated proteins in the proteomics results and a set of lysosomal enzyme assays to ascertain and identify dysregulations in the lysosomal enzyme activity in goat AF LA tissue.

5.2 Methods

5.2.1 Tissue homogenization

Frozen LA tissue biopsies from AF and Sham goat models (n=3 biological samples for each condition) were thoroughly cleaned in PBS and weighed. Each atrium was gently homogenised using a 7 mL Dounce homogeniser in Lysosome isolation buffer (LIB) [Containing 1:500 protease inhibitor cocktail (PIC) and phosphatase inhibitor (PHI) (Bio vision), (PhosSTOP Roche)]. Preparations were further homogenised in a 1 mL Dounce homogenizer and transferred to chilled 1.5 mL ultracentrifugation tubes (Beckmann coulter). Sample preparations were mixed by inverting tubes at a ratio of 1:1.5 Lysosome enrichment buffer [(LEB) (Biovision, containing 1:500 PIC)] to homogenate, and were stored on ice for 5 min before centrifugation. Samples were centrifuged at 13,000 g for 2 min at 4°C (TLX Beckmann Coulter Ultra Centrifuge) and the resulting supernatant, corresponding to the TL was collected (Ayagama *et al.*, 2021).

5.2.2 Human plasma sample selection

Human plasma samples (n=3 AF and n=3 age, sex, ethnicity matched controls) were purchased from Discovery life sciences (DLS). The patients and healthy donors were screened. All six patients were age matched, and didn't have any previous history of serious medical conditions such as cardiac ischemia, cancer etc. Patients were thoroughly screened for above parameters as CTSD regulation has been demonstrated in the case of certain medical conditions, such as cancer (Kang *et al.*, 2020) and ischemic heart disease (Wu *et al.*, 2017). Samples were stored in -80°C until use.

Age (Yrs)	Ethnicity	Sex	Condition
78	White	Male	Persistent AF
81	White	Male	Persistent AF
81	White	Female	Persistent AF
80	White	Male	Control
78	White	Male	Control
78	White	Male	Control

Table 4:1: The age, ethnicity and previous medical histories of the patients were checked. All the AF patients had persistent AF.

5.2.3 Protein quantitation assay for AF and sham goat tissue

Tissue lysates were mixed at a ratio of 1:1 with radio-immunoprecipitation (RIPA) buffer (Thermo Scientific). Protein concentrations of all tissue lysates were determined using the Bicinchoninic acid assay (BCA Protein Assay Kit, Thermo Scientific). Bovine serum albumin was used as a protein standard, and serial dilutions were prepared from the initial stock concentration of 2 mg/mL to prepare a standard curve. To ensure accuracy and reproducibility, protein assays were performed in triplicate. Absorbance values were measured at 562 nm. Protein concentrations were calculated by linear regression analysis (BMG Labtech).

5.2.4 Protein quantitation assay for human plasma samples

Human plasma samples from AF patients and healthy donors were mixed at a ratio of 1:1 with radio-immunoprecipitation (RIPA) buffer (Thermo Scientific). Then samples were 5-fold diluted with sterilized DDH_2O to avoid intensity saturation. Protein concentrations of all samples were determined using the Bicinchoninic acid assay

(BCA Protein Assay Kit, Thermo Scientific). The protein standards were prepared using serial dilutions as stated above in chapter 2 section 2.2.1.4. The absorbance values were detected at 562 nm and protein concentrations were calculated using linear regression.

5.2.5 SDS/PAGE gel preparation and Western blotting

Tissue lysates and human plasma samples were solubilised, and proteins denatured using SDS/PAGE loading buffer (bio rad) and 2-mercaptoethanol (Sigma-Aldrich). Proteins were separated by gel electrophoresis (NW04120BOX, NuPAGE 4%–12% Bis-Tris protein gels, 20X MES buffer). The gel was transferred to a nitrocellulose membrane (NC) (Bio-Rad) for protein transfer (X-cell-II blot module, Thermo Fischer Scientific). NC membrane was blocked by incubation in 5% skimmed milk. The primary antibodies anti CTSD (1:500, 219361-1 mL, Merck life science UK Ltd), RAB11 (1:1000, GTX54678, GeneTex), GYG 1(1: 500, GTX64944, GeneTex), GAPDH (1:3000, 60004-1-Ig, protein-tech) were incubated at 4 °C (cold room) overnight on a rocker. An HRP-conjugated goat anti-rabbit antibody (1:2,500, Dako P0448) was used as the secondary antibody. The secondary antibodies were detected via chemiluminescence using Westar Supernova (XLS3,0020, Cyanogen) and the protein bands were visualised in a ChemiDoc XRS + imager (Bio-rad with image Lab software).

5.2.6 Lysosome hydrolase activity assays

β – Galactosidase and β – Hexosaminidase

Lysosomal hydrolase activities were performed in the tissue lysates. To fluorometrically measure the lysosome enzyme levels, artificial sugar substrates containing the fluorophore 4-methylumbelliferone (4-MU) were used. For measuring β -hexosaminidase activity, 3 mM 4-MU N-acetyl-b-D-glucosaminide (Sigma Aldrich) in 200 mM sodium citrate buffer, pH 4.5 and 0.1% Triton X-100 was used as substrate. For β -galactosidase activity, 1 mM 4-MU b-D-galactopyranoside (Sigma Aldrich) in 200 mM sodium acetate buffer, pH 4.3, 100 mM NaCl, and 0.1% Triton X-100 was used as substrate. The reaction was stopped by adding chilled 0.5 M Na_2CO_3, and the released fluorescent 4-MU was measured in a Clariostar OPTIMA plate reader (BMG Labtech, Ortenberg, Germany) with an excitation at 360 nm and emission at 460 nm. A standard curve for free 4-MU was used to calculate the enzyme activity. Results were calculated as total units of enzyme activity (nmol/min/mg) and also normalised with respect to protein content.

5.2.7 Statistical analysis

Western blotting and lysosomal enzyme assay results were quantified and the graphs were created using GraphPad Prism v9.2.0. Data of the two groups and the statistical significance was observed using unpaired two-way t-test or one-way t-test as appropriate. Data are presented as mean±SD.

5.3 Results

5.3.1 Cathepsin D expression in goat model - Atrial fibrillation

Human CTSD is a lysosomal aspartic protease with an array of functional aspects in the cell and CTSD is synthesised as a single polypeptide that is proteolytically processed into mature CTSD that exists as a two-chain form: an amino terminal light chain (14 kDa) and a carboxyl-terminal heavy chain (34 kDa). These chains remain associated with each other by hydrophobic interactions (Zaidi *et al.*, 2008). For these experiments, analysis was carried out on the pro-CTSD chain and mature-heavy chain form(s).

I performed Western blotting experiments on n=3 biological samples of sham and AF goat models (Figure 5:1), and observed three distinct bands on the HEK293 (+) marker and in the goat sham and AF samples. Pro-CTSD at 52 kDa, also the mature-CTSD heavy chain at 34 kDa were prominently visible in the goat samples, however, the mature light chain of 14 kDa was only slightly visible in the goat samples and not used for analysis. The house keeping protein GAPDH was blotted against the same samples.

The Western blot protein band intensities of pro-CTSD, mature-heavy chain of CTSD and GAPDH were measured using imageJ software. The band intensities of pro-CTSD and mature-CTSD heavy chain were normalised to the band intensity of GAPDH and graphs were created using Graph Pad Prism software (Figure 5:2 and 5:3). The data are presented as mean±SD and the statistical tests were performed.

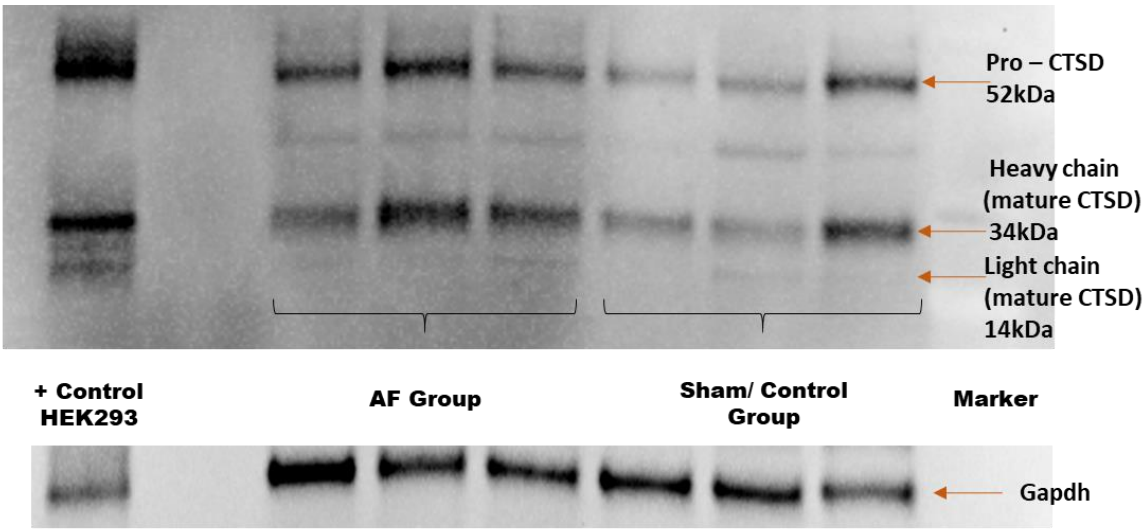

Figure 5:1 Western Blot bands showing CTSD expression in LA of AF goat model. *Western blots were performed on n=3 biological samples from each sham and AF groups. HEK 293 cell line was used as the (+) control lane. Pro CTSD was identified at 52 kDa and mature CTSD heavy chain at 34 kDa. The heavy chain associated light chain at 14 kDa was identified in the control HEK cell line but wasn't prominantly visible in the sham or AF goat samples. GAPDH is used as the housekeeping gene at molecular weight 37 kDa.*

The mean value for the pro-CTSD normalised band intensity was at 0.65±0.62 for control group and 0.90±0.38 for AF group. To analyse the intensity levels of AF group compared to the control group I conducted a two-way t-test and the pro-CTSD did not report any significant change (p= 0.58) in the AF group (Figure 5:2).

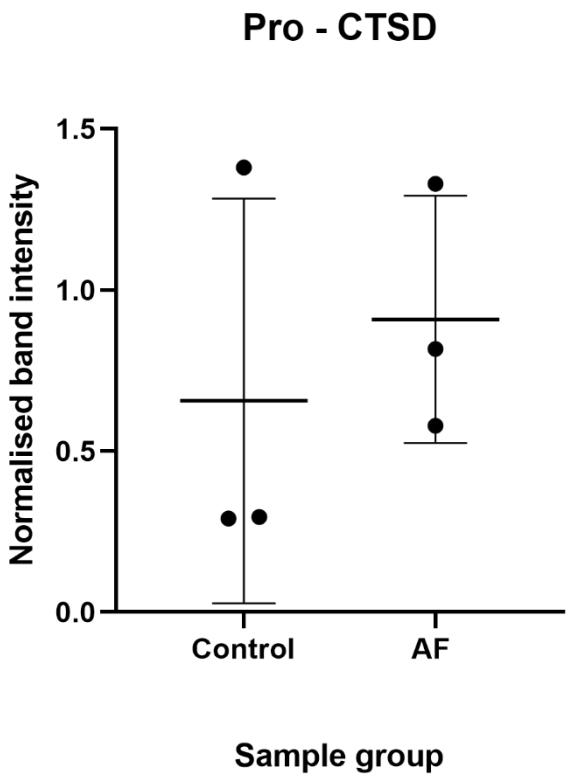

Figure 5:2: Pro - CTSD expression in AF goat model of LA*. Western blots were performed on n=3 biological samples from each sham and AF groups andband intensities of Pro-CTSD at 52 kDa data are presented as mean±SD. The normalised band intensity was at 0.65±0.62 for control group and 0.90±0.38 for AF group. Two-way t-test was performed and the protein band intensity of pro-CTSD did not show a significant regulation (p = 0.58).*

Similarly, for the mature-CTSD heavy chain normalised band intensities (Figure 5:3) data are presented as mean±SD, and the normalised band intensity was at 0.97±0.80 for control group and 1.24±0.70 for AF group. A two-way t-test was performed for the mature-CTSD Western blot normalised intensities to identify any regulation in AF compared to the control group, however, a statistically significant change was not identified (p = 0.68) in the AF group compared to the control group (Figure 5:3).

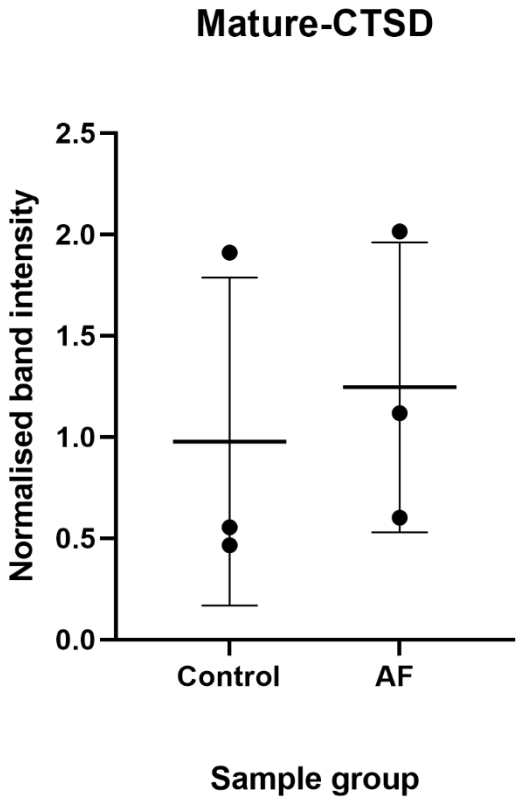

Figure 5:3: Mature-CTSD expression in LA of AF goat model. *Western blots were performed on n=3 biological samples from each sham and AF groups and band intensities of mature-CTSD (heavy chain) at 34 kDa, data are presented as mean±SD. Normalised band intensity was at 0.97±0.80 for control group and 1.24±0.70 for AF group. Two-way t-test was performed and the protein band intensity of mature - CTSD did not show a significant regulation (p = 0.68).*

5.3.2 Cathepsin D expression in human plasma - AF patients and healthy donors

In addition to the Western blotting analysis of goat AF model I performed a pilot study using Western blotting on AF patient plasma to determine whether increased plasma CTSD levels are observed in human AF (Figure 5:4 and 6:5). Three control and AF patients with no prior medical history of long term illnesses were selected, and the plasma of these patients were prepared for Western blotting a as explained in the methods section. The band intensity of the mature 34 kDa CTSD bands were measured. A house keeping protein wasn't used as this is not applicable for plasma (Tsai *et al.*, 2020) (Figure 5:4A), instead the SDS gel was stained with Coomassie blue stain after the protein transfer to NC membrane to verify the complete transfer of protein (Figure 5:4B). The mature-CTSD heavy chain band was completely transferred to the NC membrane and the band intensity was measured using image J software.

A

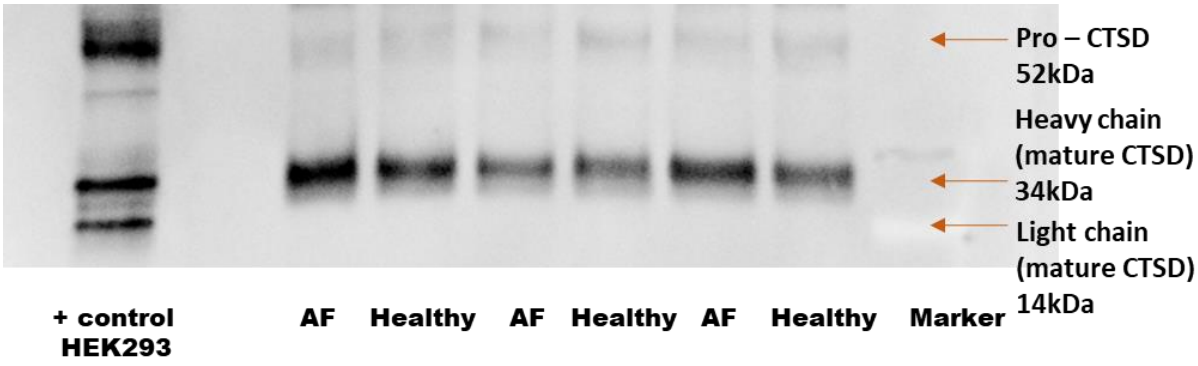

B

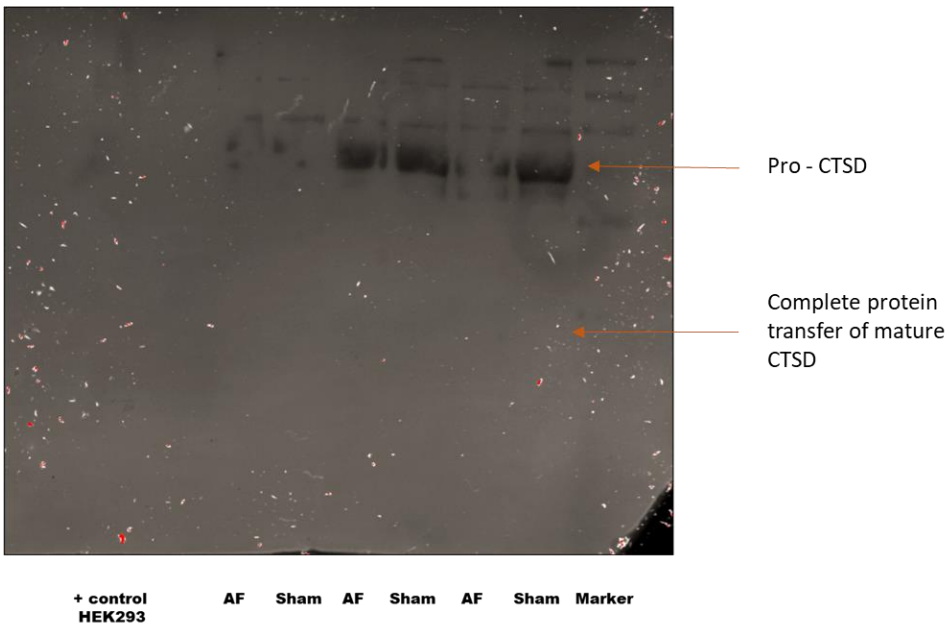

Figure 5:4: A. Western Blot bands showing CTSD expression in human plasma collected from the healthy and AF patients. *Western blots were performed on n=3 biological samples from each healthy and AF patients groups. HEK 293 cell line was used as the control lane. A. faint Pro CTSD was identified at 52 kDa and mature CTSD heavy chain at 34 kDa. The light chain at 14 kDa was identified in the control HEK cell line but wasn't visible in the healthy or AF patients groups. B. The gel image after the Western blot transfer showing a complete protein transfer of mature CTSD (A Housekeeping gene is not applicable to use on plasma samples (Tsai et al., 2020).*

The band intensity data are presented as mean±SD. Respectively, the band intensity was at 13817±3380 for control group and 17101±5603 for AF group (both n=3). A two-

way t-test was performed to identify any changes in the AF patients plasma mature-CTSD levels compared to the healthy patients. No significant (p = 0.43) regulation was observed in the mature-CTSD levels (Figure 5:5).

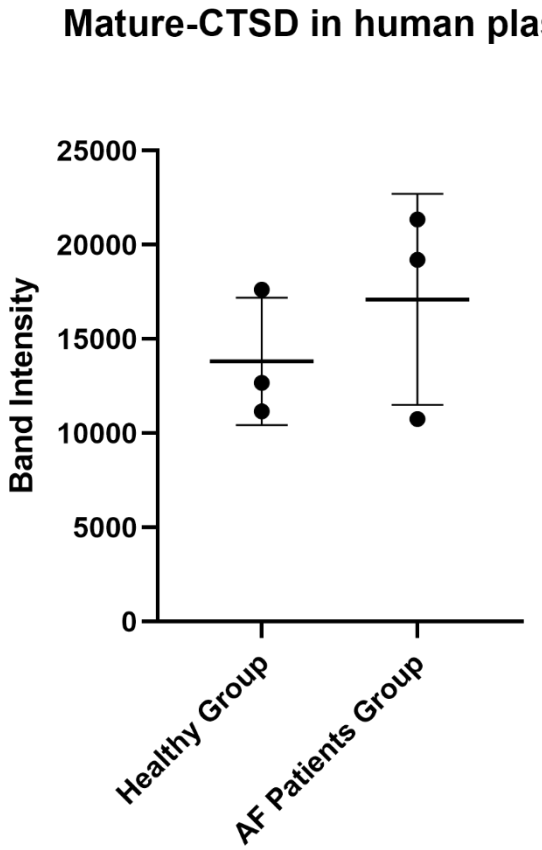

Figure 5:5: CTSD expression in human plasma of AF patients. *Western blots were performed on n=3 biological samples from each healthy and AF patients groups and band intensities of mature-CTSD (heavy chain) at 34 kDa, data are presented as mean±SD. The band intensity was at 13817±3380 for control group and 17101±5603 for AF group. Two-way t-test was performed and the protein band intensity of mature - CTSD did not show a significant regulation (p = 0.43).*

5.3.3 Western blotting evaluation for selected protein regulations observed in atrial fibrillation

5.3.3.1 Ras-related protein Rab-11A (Rab11A)

Rab11A protein showed a statistically significant up regulation in the AF goat model LA. Western blotting was performed to evaluate this finding (Figure 5:6 and 5:7). Western blotting was conducted on the n=3 biological samples retrieved from sham and AF goat models. GAPDH was used as the house keeping protein and the protein intensities of Rab11A and GAPDH were measured using imageJ software. The band intensities of Rab11A were normalised to the band intensities of the GAPDH, and these data are presented as mean±SD. The normalised band intensity was at 0.61±0.20 for control group and 0.90±0.20 for AF group (Figure 5:7). To identify whether the Rab11A is upregulated in AF, I conducted a one-way t-test. Although these data did not support a significant upregulation in Rab11A in these samples (n = 3), the p value of 0.07 suggests a trend towards Rab11A upregulation in the AF group (p = 0.07) when compared to sham controls.

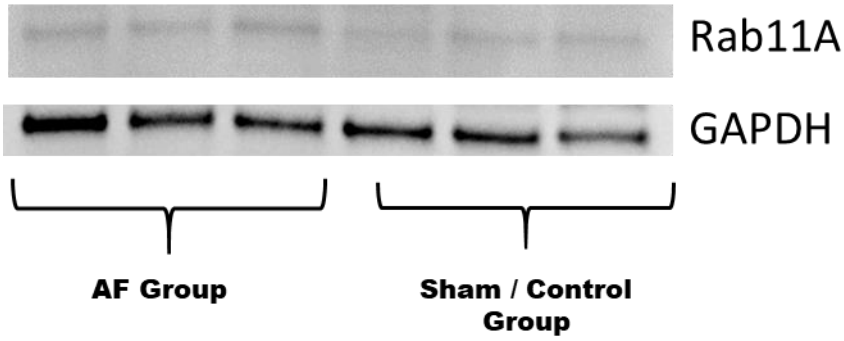

Figure 5:6: Western Blot bands showing Rab11A expression in LA of AF goat model. *Rab11A molecular weight is at 24- 25 kDa and GAPDH was used as the housekeeping gene .Molecular weight of GAPDH is at 37 kDa. Western blots were performed on n=3 biological samples from each sham and AF groups.*

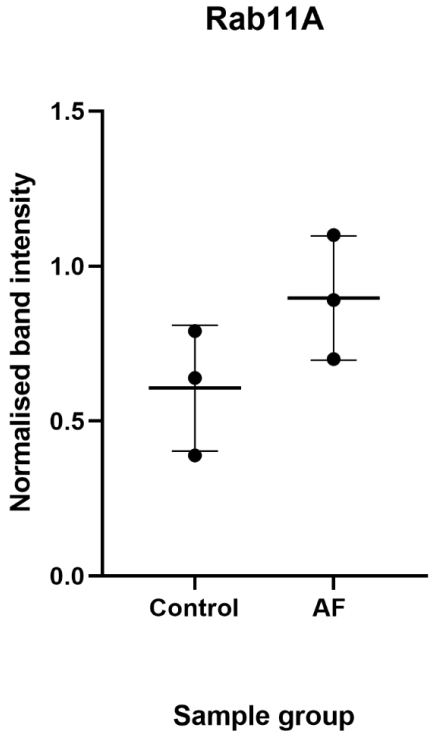

Figure 5:7: Rab11A expression in LA of AF goat model. *Western blots were performed on n=3 biological samples from each sham and AF groups and band intensities of Rab11A, data are presented as mean±SD. Normalised band intensity was at 0.61±0.20 for control group and 0.90±0.20 for AF group. -A one-way t test was performed on the normalised protein band intensity and observed a trend towards a significant upregulation in AF group (p = 0.07).*

5.3.3.2 Glycogenin – 1

Glycogenin-1 is an enzyme involved in glycogen metabolism, and therefore, plays a vital role in the conversion of glucose to glycogen. GYG1 is the isoform present in cardiac tissue, and downregulation of GYG1 is associated with glycogen storage disorder and related myopathies (Tarnopolsky, 2018).

GLUT4 as discussed in chapter 3 from its gene name SLC2A4 and GYG1 upregulation has been observed in human skeletal muscle during physical exercise (Kraniou *et al.*, 2000). The proteomics results in chapter 3 showed an upregulation of GLUT4 protein in the AF goat model. Energy storage in the heart and skeletal muscle occurs through the synthesis of glycogen (Jensen *et al.*, 2011), and muscle, including that of the heart, lacks glucose-6-phosphatase enzyme, which is necessary for glucose release into circulation (Zhang *et al.*, 2021). A viable goat antibody against GLUT4 was not found despite extensive testing, therefore another protein which serves as part of the glycogen synthesis/storage pathway was evaluated. Glycogenin serves as a core for glycogen (glycogen is a branching glucose polymer surrounding the core of GYG1) (Chaikuad *et al.*, 2011). Due to the multiple branching nature, stored glucose can be rapidly mobilised (Adeva-Andany *et al.*, 2016). Therefore, glycogen stores are used locally by muscles for energy needs (Jefferies *et al.*, 2017) and (Jensen *et al.*, 2011). In Chapter 3, I presented data from the Reactome pathway analysis suggesting the

upregulation of GLUT4 protein could have an effect on vesicle translocation to the plasma membrane, which would be expected to affect cellular glucose intake in AF (Koshy *et al.*, 2010).

In the Western blotting performed on GYG1, a significant 1.7-fold upregulation was observed in LA of the AF goat model (p=0.007), after conducting a two-way t- test (Figure 5:8, 5:9).Therefore, supporting the published data related to GLUT4 and GYG1 (Kraniou *et al.*, 2000). The mean values of the GYG1 normalised band intensity were 0.61±0.05 for control group and 0.90±0.02 for AF group (both n=3, Figure 5:9).

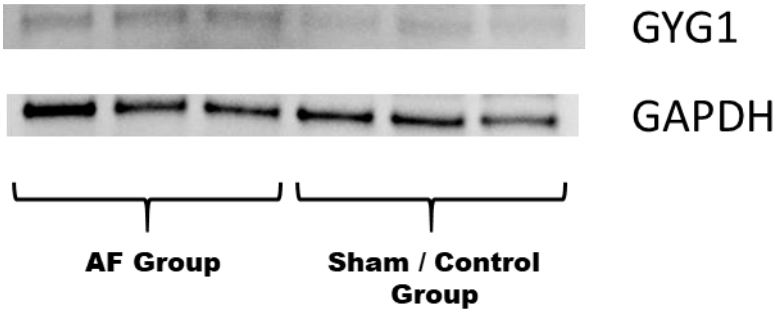

Figure 5:8: Western Blot bands showing GYG1 expression in LA of AF goat model. *GYG1 molecular weight is at 39k Da and the housekeeping gene GAPDH ; Molecular weight of GAPDH is at 37 kDa. Western blots were performed on n=3 biological samples from each group of sham and AF goat models.*

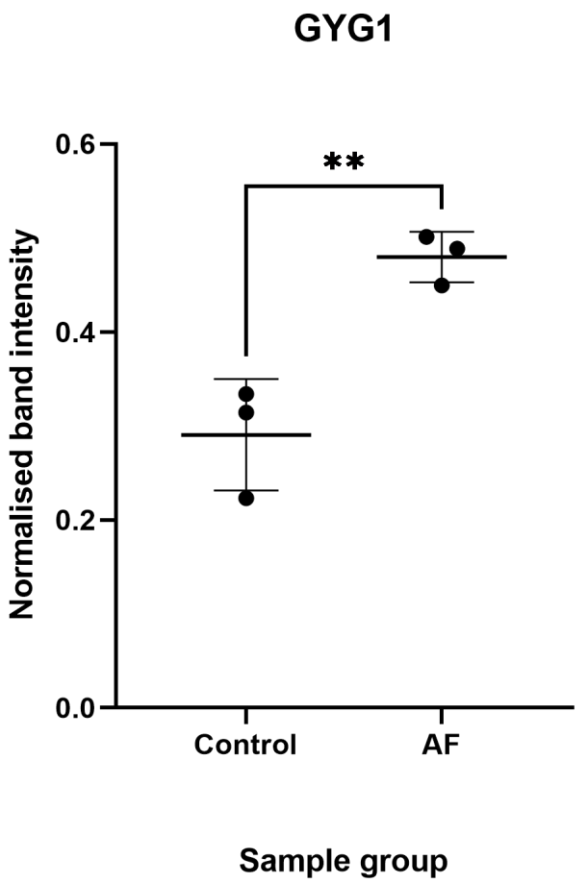

Figure 5:9: GYG1 expression in LA of AF goat model. *Western blots were performed on n=3 biological samples from each sham and AF groups and band intensities of GYG1 were normalised to GAPDH. The normalised data are presented as mean±SD. Normalised band intensity was at 0.61±0.05 for control group and 0.90±0.02 for AF group. A two-way t-test was performed and the nomalised protein band intensity of GYG1 showed a significant upregulation (p=0.007) in AF goat models compared to the control goats.*

5.3.4 Lysosome hydrolase activity assays

In order to investigate whether lysosomal enzyme activity is changed in goat AF, lysosomal enzyme activity assays were performed on three common lysosomal enzymes: β-hexosaminidase type A (Figure 5:10), β hexosaminidase type B (Figure 5:11) and β galactosidase (Figure 5:12). Lysosomal β–hexosaminidases type A and B remove terminal-β glycosidically bound N-acetyl-hexosamine residues from several glyco-conjugates (Hepbildikler *et al.*, 2002). β -galactosidase has two isoforms; isoform 1 cleaves β linked terminal galactosyl residues from gangliosides, glycoproteins and glycosaminoglycans (Morreau *et al.*, 1989), whilst isoform 2 is associated with the formation of extracellular elastic fibers or elastogenesis and the development of connective tissue (Hinek *et al.*, 2000).

5.3.4.1 β-Hexosaminidase A

The Sham and AF goat model n=3 biological replicates were carried out as described in the methods to detect β-Hexosaminidase A enzymatic activity. Enzymatic activity was analysed per nmol/min/mg and the data are presented as mean±SD, and the normalised band intensity was at 8.93±3.1 for control group and 6.75±0.11 for AF

group. A two-way t-test was performed to identify any statistical difference in the enzymatic activity of AF group compared to control group of goats. No significant difference (p=0.28) was detected between the groups (Figure 5:10).

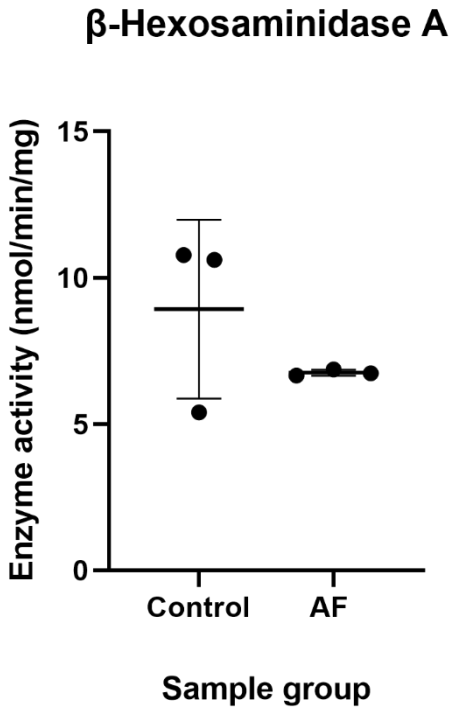

Figure 5:10: β hexosaminidase type A activity. *The sham group of goats LA (n=3 biological samples) showed respectively 5.4, 10.61 and 10.78 nmol/min/mg of β hexosaminidase type A activity, whist, AF group of goats LA showed respectively 6.66, 6.74 and 6.87 nmol/min/mg of β hexosaminidase type A activity. Data are presented as mean±SD. The normalised band intensity was at 8.93±3.1 for control group and 6.75±0.11 for AF group. A two-way t-test was performed but the β hexosaminidase type A activity of the AF group showed no significant regulation (p=0.28).*

5.3.4.2 β-Hexosaminidase B

To understand the β-Hexosaminidase B enzymatic activity levels in sham and AF tissue, n=3 biological replicates were prepared as described in the methods. The enzymatic activity was analysed per nmol/min/mg and the data are presented as mean±SD. The normalised band intensity was at 1.8±0.39 for control group and 1.6±0.11 for AF group. A two-way t-test was performed to identify any statistical difference in the enzymatic activity of AF group compared to control group of goats. No significant difference (p=0.56) was detected between the groups (Figure 5:11).

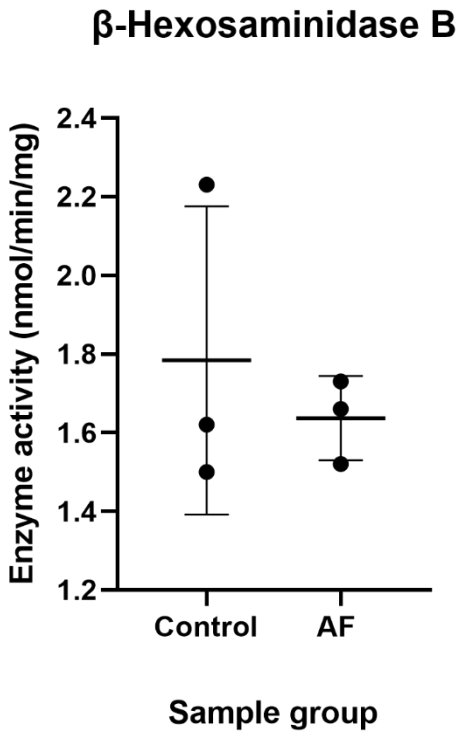

Figure 5:11: β hexosaminidase type B activity. *The sham group of goats LA (n=3 biological samples) showed respectively 1.5, 1.62 and 2.23 nmol/min/mg of β hexosaminidase type B activity, whist, AF group of goats LA showed respectively 1.52, 1.66 and 1.73 nmol/min/mg of β hexosaminidase type B activity. Data are presented as mean±SD. The normalised band intensity was at 1.8±0.39 for control group and 1.6±0.11 for AF group. . A two-way t-test was performed but the β hexosaminidase type B activity of the AF group showed no significant regulation (p=0.56)*

5.3.4.3 β-Galactosidase

The enzymatic activity of β-Galactosidase was analysed between Sham and AF goat model n=3 biological replicates. The samples were prepared as described in the methods, and the data processed to present as mean±SD. The normalised band intensity was at 3.57±1.8 for control group and 2.97±0.31 for AF group. A two-way t-

test was performed to identify significant difference in the enzymatic activity of AF group compared to control group of goats. No significant difference (p=0.60) was detected between the groups (Figure 5:12).

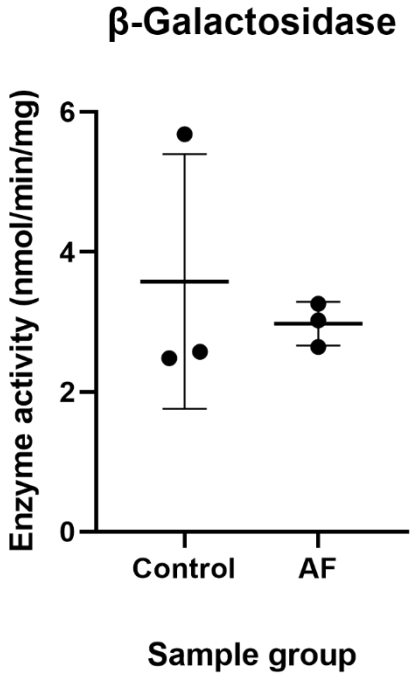

Figure 5:12: β galactosidase activity. *The sham group of goats LA (n=3 biological samples) showed respectively 2.48, 2.57 and 5.68 nmol/min/mg of β galactosidase activity, whist, AF group of goats LA showed respectively 2.64, 3.02 and 3.26 nmol/min/mg of β galactosidase activity. Data are presented as mean±SD. The normalised band intensity was at 3.57±1.8 for control group and 2.57±0.31 for AF group. A Two-way t-test was performed but the β galactosidase activity of the AF group showed no significant regulation (p=0.60).*

5.4 Discussion

Proteostasis, or protein homeostasis, is the sum of all protein regulated mechanisms in the cell (Powers and Balch, 2013). Protein degradation in the cell plays a vital role in cellular homeostasis. Primarily this task is completed through lysosomes and proteasomes. It has been reported that dysfunctions in lysosomes and proteasomes are linked to cardiac pathogenesis (Wang and Robbins, 2014).

This chapter used the same goat tissue used in proteomic studies to perform quantitative Western blot analysis to validate the proteomic data set. Additionally, quantitative analysis was performed on lysosomal enzyme activities to identify the enzymatic activity in the AF and sham-operated tissue. Due to our interest in endo lysosomes, it would seem logical to study the lysosomal enzymatic activity of the lysosomal lumen to understand the functionality of lysosomes in pathological events such as AF.

Notably, the SLC2A4 or GLUT4 protein, which uptakes glucose in the cells, showed a significant upregulation in the proteomic data. Furthermore, the EL fraction of the AF goat model LA presented a significant upregulation in the lysosomal GAA. We now know that GAA is the main glycogen degradation enzyme in the lysosome (Roig-Zamboni *et al.*, 2017). In this chapter, I presented data that demonstrates significant upregulation of GYG1 (Figure 5:9). GYG1 acts as the primer for the growing glycogen molecule at the center and self-attaches UDP-glucose molecules (Litwack, 2018) participating in the glycogen synthesis. As widely accepted in the published data (Embi *et al.*, 2014) and (Ausma *et al.*, 2003), this study provides further evidence for a possible increased glycogen level in the LA AF goat tissue.

GAA is the glycogen degrading enzyme (Roig-Zamboni *et al.*, 2017), and interestingly, the GAA enzyme upregulation was observed in the EL fraction proteomic results. The clinical study of Hout et al., 2001 indicated that in the skeletal and cardiac muscles, considerable high levels of recombinant human α-glucosidase may be needed to reduce the abnormal storage of glycogen (Van den Hout *et al.*, 2001) and (Zhu *et al.*, 2004) , and similarly the up regulated level of GAA observed in our data for AF goat LA highlights a potential link to the increased glycogen levels or glycogen synthesis in the AF goat model of LA (Embi and Scherlag, 2014). Furthermore, the observation of GAA significant upregulation was detected only in the EL fraction, further suggesting that the modified density gradient proteomics-based method to analyse endolysosomal

proteins in cardiac tissue is a suitable method for analysing endolysosomal protein composition (Ayagama *et al.*, 2021).

Rab11A contributes to the dynamics of the late endosome-lysosome system (Zulkefli *et al.*, 2019), and plays an extensive role as protein adaptors during the endocytic recycling of vesicles (Hales *et al.*, 2002). The proteomic upregulation of Rab11a was also evaluated by the Western blotting and showed a trend achieving significance towards the upregulation in the AF. Further investigations with increased n's are be warranted to determine if Rab11A is upregulated.

Lysosomal enzyme assays were conducted on some selected lysosomal enzymes to understand whether dysregulations had taken place in the biochemical activities of the lysosome in the AF goat model LA. However, neither β-hexosaminidase type A or B showed no significant change in the AF goat model of LA. Similarly, (Figure 5:10 and 5:11) β-galactosidase (Figure 5:12) showed no significant regulation in the AF goat model of LA. An interesting observation is the close clustering observed in all 3 enzymes in the AF group vs the sham controls.

CTSD regulation levels were studied in the AF and sham tissue as a follow-up study to the preliminary proteomics analysis performed at the early stages of the project. This

work was followed up in AF and healthy patients' plasma, with a scope to identify CTSD as a possible biomarker in AF. Published literature favours the possibility of CTSD as a biomarker as it has been reported to play a significant role in cardiac disorders and sudden cardiac death (Dai *et al.*, 2021) and (Kobayashi *et al.*, 2020) . Published reports show that the CTSD regulations in cardiovascular disorders are discordant (Kostin *et al.*, 2003) and (Ozkayar *et al.*, 2015). Decreased myocardial CTSD protein levels are detected in human dilated cardiomyopathy (DCM), (Kostin *et al.*, 2003) whilst disorders such as dysfunctional endothelial (Ozkayar *et al.*, 2015), atherogenesis (Lusis, 2000) and acute coronary syndrome exhibit an upregulation in CTSD levels (Ozkayar *et al.*, 2015; Yamac *et al.*, 2015). Therefore, I considered investigation of the CTSD regulation in the AF goat model. However, in the complete data set for proteomics (n=3), I did not detect a significant change in CTSD, and significant regulation of CTSD was not identified in either the goat AF model of LA (Figure 5:1 and 5:2) or human plasma (Figure 5:4). For a true biomarker study, large number of n's are required to draw statistical significance and the fact that I only analysed 3 samples might be a red herring in the story. Therefore, at this stage, it is not possible to conclude that CTSD would serve as a biomarker for AF based on these data.

5.5 Limitations to Study

The results discussed in this chapter are limited by the number of biological samples in goat and human. Acquiring more samples would have been beneficial to conduct further biochemical studies. However, the studies were affected by the COVID-19 pandemic, and the AF goat model facility was, and remains, closed, obstructing access to further samples from the same experimental groups. A more significant number of patient tissue biopsies and plasma samples must be examined, and more types of validation methods (e.g. RT-PCR) must be used to declare a protein as a confident biomarker in AF. This goes beyond the scope of my DPhil studies.

Additionally, the tissue was blotted against an array of antibodies, but not all antibodies were functional in detecting the proteins of interest in goat tissue. The antibodies were selected to match a minimum of 75% sequence alignment to that of the goat targeted proteins using the 'BLAST' sequence aligning tool. However, most of the antibodies failed to recognise the epitopes of the targeted proteins. Therefore, the paucity of the commercially available antibodies for the goat as a species was a limitation in this study.

Furthermore, in enzymatic activity assays, the variance among the Sham biological samples seen was high in comparison to the AF. In particular Sham goat 1 showed a variance among all the enzyme assays. It is not possible with the current n-number to determine with certainty whether these measurements represent an outlier or whether the Sham control activities are simply widely distributed. More samples would help in resolving this issue.

Chapter 6

Conclusions

Cardiovascular diseases are a leading cause of death worldwide and continue to increase in prevalence, partly due to of the growing ageing population. Atrial fibrillation (AF) is considered one of the most common arrhythmias and is associated with increased mortality and stroke incidences (Zoni-Berisso *et al.*, 2014) and (Samuthpongtorn *et al.*, 2021).

The observations of protein level changes from this thesis contribute new insight into the pathways and molecular mechanisms involved in the development and maintenance of AF, and allows the possibility to discover pilot information on pathway dysregulations linked to acidic organelles that can be studied further. Analysis of significantly regulated proteins in separated tissue lysate (TL), mitochondrial fraction (Mito) and endo-lysosome fractions (EL) (Ayagama *et al.*, 2021) increased the possibility of our ability to uncovering lysosome-specific proteins that were not identified in the TL, such as GAA and CLTB. Proteomics, transcriptomics and molecular biology techniques employed in this thesis are the main methods that allowed us to study molecular pathways in AF. Therefore, the work presented in this thesis paves the way for future targeted studies focused on drug discoveries and biomarker studies.

In Chapter 2, discusses a robust method to isolate endo-lysosomes to study the endolysosomal proteomic profile, specifically in frozen atrial biopsies. This offers many advantages. The first part of Chapter 2 describes a low-cost method to isolate endo-lysosomes from a minimum of 100mg of tissue biopsy, giving us an opportunity to study the endo-lysosome as an organelle and its proteome under physiological and pathological conditions. The endo-lysosome isolation protocol presented in this thesis did not require modifications or alterations to manipulate the nature of the endo-lysosomes, and is therefore an ideal method to isolate endo-lysosomes in any type of tissue biopsy.

Additionally, a modified differential density gradient method was used to produce a low-cost isolation protocol to make this research a much more affordable method versus existing complex methods such as the molecular tagging methods or techniques such as localisation of organelle proteins by isotope tagging (LOPIT) (Dunkley *et al*., 2004). The second part of Chapter 2 presents a robust method that allows us to confidently identify hits from an organelle proteomics data set and use biochemical assays to evaluate the contamination levels and determine the enrichment of the data. The final part of Chapter 2 describes various pathway analysis methods, namely Gene Ontology (GO), Cytoscape and Panther, that helps reveal the functional aspects of the most significantly abundant proteins in the endo-lysosomal fraction.

The modified density gradient proteomics-based method described in Chapter 2 was developed in the guinea pig atria model, a commonly used animal model in cardiac research. A long history of work from several groups (Fukuda, 1975) and (Dzimiri and Fricke, 1988) , including our own, has highlighted the value of using *C. porcellus* tissue to study Ca^{2+} handling in atrial cells (Capel et al., 2021; Capel and Terrar, 2015). Additionally, guinea pig cardiac electrophysiology, which includes the typical long plateau phase of the action potential, is closer to humans than mice or rats. In developing a method based on 100mg of tissue, this approach offers the advantage of scalability, involving utilising minimal quantities of heart biopsies, for instance, those obtainable during surgery (Ayagama *et al.*, 2021).

However, the detected yield of ion channel proteins was likely to underestimate the total ion channel proteins within samples, such as lysosomal ion channel proteins TPC (Wang et al., 2012) (Cang et al., 2013 and Grimm et al., 2014). Ion channel proteins are large and hydrophobic, and their highly folded transmembrane units cause it difficult for trypsin digestion, leaving them undetected during the proteomics screening (Vit and Petrak, 2017).

Chapter 3 presents a detailed account of applying the newly developed endolysosomal isolation method discussed in Chapter 2 on left atrial tissue (LA) from a goat AF model. The most significant proteins that were dysregulated in AF identified major pathways,

including AMPK signalling pathway, selective autophagy (Aggrephagy and proteasome pathway), NADPH oxidase pathway, gap junction assembly and degradation pathway, OXPHOS pathway, vesicle-mediated transport, protein processing and folding pathway, ESCRT, and lysosome vesicle biogenesis.

Interestingly, proteins and interpreted pathways identified in my study were previously identified or are increasingly recognised in cardiac research, either in clinical trials, animal models, or cell models (Sygitowicz *et al.*, 2021) and (Papathanasiou *et al.*, 2021), such as gap junctional remodelling (van der Velden *et al.*, 2000), NADPH oxidase (Kim *et al.*, 2005), metabolic stress caused by oxidative Stress, mitochondrial-bioenergetics and proteostasis (Papathanasiou *et al.*, 2021).

Excitation-contraction coupling utilises high amounts of ATP in the atria (Mason *et al*., 2020). Especially, myosin utilises the hydrolysis of the ATP molecule to ADP and Pi as kinetic energy. Furthermore, AF is considered a tachyarrhythmia with a high heart rate (Nesheiwat *et al*., 2022). Therefore, increased ATP consumption in AF would be expected to leave an energy demand in the atria (Rennison *et al*., 2021). ATP hydrolysis is the primary energy source in the cell, driving active and coupled membrane ion transport (Hasselbach, 1964) that controls intracellular ion concentrations to maintain the ion homeostasis (Grant, 2009). In the active transporting ion pumps, ions are transported from low concentrations to higher concentrations or

against the concentration gradient using the energy from ATP hydrolysis, catalysed by ATPase. Some of the examples for these ion pumps are sodium-potassium ATPase (Na+/K+ ATPase) which pump three Na+ out of the cell and transport two K+ into the cell, and build a chemical gradient between inner and outer membranes of the cell (Godbey, 2022). Calcium ATPase (Ca2+ ATPase/SERCA) which pump Ca+ from cytosol in to the SR lumen to relax the cardiomyocyte (Primeau *et al*., 2018), Proton ATPase utilise the hydrolysed ATP to pump H+ against the electro chemical gradient to acidify the acidic organelles such as lysosomes (Godbey, 2014). Therefore especially in cardiac energetics, an imbalance of ATP could disrupt the ion gradient between the outer and inner membranes leading to the failure of the cellular ion homeostasis (Grant, 2009).

Moreover, some ion channels exhibit ATP sensitivity, such as ATP-sensitive potassium channels (KATP). KATP channels open at the reduced ATP and increased Adenosine levels (Aziz *et al*., 2018) and are inhibited at higher intracellular ATP concentrations, leaving depolarisation of the membrane (Lima *et al*., 2022). Therefore during atrial energy depletion, the opening of KATP channels acts to shorten the action potential. This lessens force production, which is cardio-protective (Grant, 2009). During AF the KATP can increase its activity that would decrease the APD, and participate as a substrate for a re-entry (Balana *et al*., 2003). The increased re-entry mechanisms of AF with the shorter wavelengths is discussed in 1.2.2.2 in detail. Furthermore, proton transporters such as V-ATPase harness the ATP energy to acidify the lysosomes

(Godbey, 2014). An optimal luminal pH is required to activate the hydrolytic enzymes, which is vital for cellular homeostasis, and the disruption of V- ATPases affecting the lysosomal substrate degradation is reported in neurodegenerative disorders (Song *et al.*, 2020). Hence an ATP energy demand in the atria can indirectly cause a chemical imbalance in the acidic organelles such as lysosomes.

Proteins related to proteostasis were observed to be altered in the AF goat model LA. Most of the pathways identified were related to proteostasis, and were leading towards acidic organelles, namely protein processing, folding pathways, ESCRT, vesicle-mediated transport pathways, aggrephagy, proteasome pathway, lysosome biogenesis, gap junctional trafficking to lysosomes, gap junction internalisation and degradation. Additionally, up-regulation of the AMPK pathway and OXPHOS (Xie *et al.*, 2015) suggests that the upregulation of these two pathways could potentially increase the cellular ATP level in AF. Therefore, its plausible to conclude that, energy sensing AMPK upregulation may contribute to the increased ATP levels in AF, and as a side effect of increased ATP production through OXPHOS, free radicals or reactive oxygen species (ROS) (Xie *et al.*, 2015) were formed (Zhao *et al.*, 2019). ROS production can be hypothesised by the upregulated NOX2 levels in the AF tissue, and increased $O_2^{\cdot -}$ production in both the LA and left atrial appendage (LAA) has been reported in AF (Dudley *et al.*, 2005). Increased metabolic stress is commonly recognised in AF pathophysiology (Harada *et al.*, 2015). Here in our AF LA tissue, the increased OXPHOS (Zhao *et al.*, 2019), NADPH oxidase pathway (Magnani and

Mattevi, 2019) and the upregulated ROS defensive protein SOD2 (Suski *et al.*, 2018) points towards the increased ROS mediated oxidative stress in the AF goat model. Additionally, hsp70, hsp40, CDC37, HSP90B1, and HSPB1 were up-regulated in our AF tissue.

Oxidative stress increases in a cell due to the presence of highly reactive free radicals (Aruoma, 1998). At high concentrations, free radicals and radical-derived reactive species react and damage all major cellular constituents (Phaniendra *et al.*, 2015). ROS contain a minimum of one unpaired electron around the atomic nucleus. Examples of free radicals produced in the cell include oxygen radicals such as superoxide $O_2^{\bullet -}$, and hydroxyl (·OH) (Dröge, 2002). Naturally, the oxygen molecule itself has a radical nature to react with molecules, but the presence of two unpaired electrons makes it bi-radical. The high reactivity of the oxygen radicals tends to obtain another electron from molecules to achieve stability. When this phenomenon occurs in a cell, mainly lipids (Ylä-Herttuala, 1999), proteins (Stadtman and Levine, 2000), and nucleic acids (Marnett, 2000) react with ROS. After reacting with ROS, the protein molecule loses its integrity (Stadtman and Levine, 2000), and these oxidatively modified proteins are not degraded easily, leading to sequestration by chaperones.

Some degree of ROS formation is reported to be beneficial for cardio-protection (Matsushima *et al.*, 2013) (Simon *et al.*, 2021) (Cadenas, 2018) and (Kleikers *et al.*,

2012). For example, H_2O_2 oxidises the thiol group of the targeted protein during redox signalling, therefore functionally modifying the protein. However, reversal of the H_2O_2 to the threshold reverts the protein activity to the previous state, and importantly, in a study on protective effects of H_2O_2 on rat hearts, Yaguchi et al., (2003) showed that the cardio-protective nature of H_2O_2 depends on the low H_2O_2 concentration (2 µmol/L) in the heart (Yaguchi *et al.*, 2003), preserving the energy metabolism and improved contractile during short episodes of ischemia-reperfusion.

Cross-talk between the AMPK pathway and ROS has been reported in cancer cells, where inducing glycolysis through AMPK eventually increases NADPH levels in the cell as well as ATP synthesis (Zhao *et al.*, 2017) and (Upadhyay *et al.*, 2013).

Cellular survival mechanisms, such as chaperone proteins that mediate protein quality control (Gregersen and Bross, 2010), were up-regulated in the AF goat model. The observation of increased protein processing, chaperone-mediated protein folding pathway, selective autophagy (for instance, aggrephagy and vesicle-mediated membrane trafficking), might indicate that increased superoxide levels or free radicals have caused a shift in the balance between protein processing and degradation (Arrieta *et al.*, 2019). For instance, the ESCRT pathway showed a down-regulation in the ESCRT-II complex and its cargo proteins, such as ESCRT-II complex subunit VPS25 and Rab7a in AF. The downstream proteostasis pathways analysed in KeGG

and Reactome on these proteins suggest dysregulations in the above protein processing in the AF condition.

Rab7a and Rab2a are critical players in the transition of late endosomes to MVB in the ESCRT pathway (Vanlandingham and Ceresa, 2009), and autophago-lysosome formation (Press *et al.*, 1998 and Ding *et al.*, 2019). Additionally, VPS25 is one of the main regulatory components of the ESCRT complex-II that sort the endosomal cargo proteins to the MVB and recruits the ESCRT-III complex (Im *et al.*, 2009). In the AF goat model of LA, Rab7a, Rab2a and VPS25 were significantly downregulated.

DNM2, a vesicular trafficking processor protein associated with microtubules, actin, cytoskeleton, and membrane remodelling (Yu *et al.*, 2018b), was downregulated. DYNC1I2, a motor protein that links dynein protein to endocytic cargos, adapter proteins to regulate dynein function (Ansar *et al.*, 2019), was also found downregulated in AF goat model LA , suggesting a possible down-regulating pattern in tethering, fusion and motor proteins (Ansar *et al.*, 2019). These observations, therefore, support the dysregulation of transport of the vesicles along the cytoskeleton and microtubules in AF and subsequently downstream lysosomal function (McEwan *et al.*, 2015) and (Mukhopadhyay *et al.*, 1997).

Above all, the discussed intracellular cargo transport motor proteins and dynein or actin cytoskeleton proteins such as myosin that shuttle along the microtubule network are energy-dependent (Bruce A *et al.*, 2002 and Roberts *et al.*, 2013), and as mentioned before, in the proteomics results AMPK was upregulated. In the AF tissue I observed, mitochondrial ATP production OXPHOS complex proteins were upregulated, implying that ATP energy demand in AF goat model LA has occurred. The upregulated AMPK would be expected to reduce the energy-consuming processes to balance high energy demand. Additionally, transcriptomics studies presented in Chapter 4 revealed that high energy requiring protein translational steps such as rRNA biosynthesis (Grummt, 2013 and Hoppe *et al.*, 2009) were downregulated (Hoppe *et al.*, 2009). Since motor proteins consume ATP energy to function (Roberts *et al.*, 2013) and traffic vesicles along the microtubules (Bruce A *et al.*, 2002 and Roberts *et al.*, 2013), we can hypothesise that AMPK may have reduced the motor protein translation in the AF goat model.

Furthermore, proteomics highlighted an upregulation of CLTB protein in the AF condition. CLTB is known to play a role in lysosome membrane biogenesis with adaptor protein 1 and VAMP proteins (Saftig and Klumperman, 2009). CLTB and TUBA4A were upregulated and, as mentioned earlier, DNM2 and AP2A2 were downregulated in the gap junctional assembly pathway. Additionally, Reactome pathway analysis highlighted that the degradation of gap junctional plaques was presumably up-regulated in the lysosome. .

Chapter 4, focused on the transcriptomics studies performed in the goat sham and AF tissue, helping to understand the molecular pathway regulations at the gene level and evaluate the observed pathways in genomics. In the proteomics study, the upregulation in the macroautophagy related proteins, AMPK pathway proteins, cellular protein processing, and folding process chaperone proteins implied that the LA might have transitioned to a cell survival state in the AF disease tissue.

The proteomics regulations were supported by the gene regulations observed in the transcriptomics results of the AF goat model, such as AMPK induced macroautophagy and downregulation of rRNA biosynthesis. It has been reported that the upregulated AMPK could phosphorylate downstream autophagic complexes (Zhao and Klionsky, 2011). Furthermore, AMPK acts on autophagy through phosphorylation and could have activated autophagy-related protein complexes such as ATG13, ULK1 and ATG101 (Li and Chen, 2019), and the possibility of this phenomenon was interpreted in the Reactome pathway analysis in the AF goat model.

Additionally, in the AF goat model, the eukaryotic initiation factor 4A-I (EIF4A1) of the major initiation factor genes was downregulated. It has been observed in the Reactome pathway studies of the AF goat model that the protein translation might have been controlled by downregulating the translation initiation step (Grummt, 2013).

Chapter 5 presented Western blotting data demonstrating a significant upregulation of GYG1, which acts as the primer for the growing glycogen molecule at the centre and self-attaches UDP-glucose molecules (Litwack, 2018), participating in glycogen synthesis. In comparison, proteomic results show a significant upregulation of SLC2A4/ GLUT4, which uptakes glucose in the cells and GAA, which degrades glycogen. As widely accepted in the published data (Embi *et al.*, 2014) and (Ausma *et al.*, 2003), upregulation of GYG1, GLUT4 and GAA provides further evidence for a possible increased glycogen level in the AF goat model of LA, which is reported as structural remodelling (Embi *et al.*, 2014 and Yosefy *et al.*, 2021). Moreover, Rab11A, an essential regulatory protein in the vesicle-mediated transport system (Goswami *et al.*, 2021), and autophagosome formation (Longatti *et al.*, 2012), was identified as being upregulated in the proteomic results, and showed a trend towards an upregulation in the Western blotting.

Chapter 5 further examines the main lysosomal enzymes in the AF and sham control tissue. The enzymatic activity of β hexosaminidase type A, β galactosidase type B and β hexosaminidase type B were analysed. The lysosome storage disorders (LSD) such as Tay-Sachs disease caused by deficiency of hexosaminidase has the phenotype muscle weakness or muscle atrophy (Adam *et al.*, 1993), and galactosialidosis caused by the β galactosidase deficiency has phenotypes, cardiomegaly and cardiac failure

(Haverkamp *et al.*, 1996), which shows the importance of analyzing these enzyme levels in the AF tissue. However, none of the β hexosaminidase type A or B and β galactosidase type B showed any regulation in the enzymatic activity of the AF goat model.

6.1 Summary

This thesis discussed a method developed to study endolysosomal proteins and its successful application on AF goat model LA to learn possible lysosomal protein regulations and their interpreted pathways in AF pathology. The key findings of this project is summarised in table 1.

Summary of the key results
The method development stage of this project resulted in: • Development of a flexible, low-cost, method to study endo-lysosomal proteins Application of this method to a goat model of atrial fibrillation (AF) demonstrated: • Up regulation of AMPK is the primary pathway in AF goat model • GLUT4 glucose transporter, Glycogenin-1 and lysosomal α glucosidase enzyme upregulation showing possible structural remodelling of glycogen deposition • Upregulation of autophagy and proteasome degradation pathways. • ESCRT, MVB formation, autophago-lysosomal fusion proteins VPS25, Rab7A and Rab2A downregulation • Downregulation of vesicle tethering, fusion and motor proteins affecting the downstream lysosomal cargo. • Gap junctional plaques formation and degradation via lysosomes • mTORC1 inactivation

Table 1: A summary of the key results.

The proteomic, transcriptomic and biochemical assays performed on the AF goat model of LA tissue to understand the lysosomal regulations produced several possible conclusions. Direct lysosomal dysregulations were observed, such as the (i) possible structural remodelling of LA AF tissue through increased glycogen levels or glycogen synthesis, (ii) the compensated upregulation of GAA enzyme, and (iii) the downregulation of several lysosomal autophago-lysosomal fusion, tethering and motor proteins. Additionally, pathway analysis of the most regulated proteins and genes interpreted the AMPK pathway regulation and its downstream regulations leading towards the acidic organelles and endomembrane system, which can affect the lysosomes indirectly. These pathways include increased ROS production, vesicle-mediated trafficking, protein processing and folding, lysosome biogenesis, gap junctional degradation and Rag A/B activation of mTORC1.

6.2 Future directions

The modified density gradient proteomics-based method to analyze endolysosomal proteins in cardiac tissue developed in my studies presents a comprehensive protocol and data set of guinea pig atrial EL organelle proteomics using techniques also applicable to non-cardiac tissue.

The molecular pathways identified in this thesis can be applied to downstream pathway studies to identify novel sub pathways. Further biochemical assays and knockdown animal models exploring these pathways will be a useful approach to understanding the exact consequence of dysfunctional pathway interpretations in AF. The elevated cytokine levels in plasma are already studied as a biomarker indication in AF (Li *et al.*, 2017). Moreover, the ROS mediated damaged DNA component levels in the plasma are identified as a biomarker in AF (Ramos and Brundel, 2020). In this study conducted in AF goat tissue, oxidative stress induced metabolic stress was observed and additionally, the structural remodelling was observed with the direct involvement of lysosomes. The data learned in this study, such as detection of end products of glycogen degraded by GAA released to plasma (Murray, 2020) and plasma glucose levels can be directed for further biomarker tests for AF (Fu *et al.*, 2019).

References

Aarhus R, Dickey DM, Graeff RM, Gee KR, Walseth TF and Lee HC. (1996). Activation and inactivation of Ca2+ release by NAADP+. *J Biol Chem* **271,** 8513-8516.

Abbott DE, Margaryan NV, Jeruss JS, Khan S, Kaklamani V, Winchester DJ, Hansen N, Rademaker A, Khalkhali-Ellis Z and Hendrix MJ. (2010). Reevaluating cathepsin D as a biomarker for breast cancer: serum activity levels versus histopathology. *Cancer Biol Ther* **9,** 23-30.

Abunimer A, Smith K, Wu TJ, Lam P, Simonyan V and Mazumder R. (2014). Single-nucleotide variations in cardiac arrhythmias: prospects for genomics and proteomics based biomarker discovery and diagnostics. *Genes (Basel)* **5,** 254-269.

Actis Dato V, Benitez-Amaro A, de Gonzalo-Calvo D, Vazquez M, Bonacci G, Llorente-Cortés V and Chiabrando GA. (2020). LRP1-Mediated AggLDL Endocytosis Promotes Cholesteryl Ester Accumulation and Impairs Insulin Response in HL-1 Cells. *Cells* **9**.

Adam MP, Ardinger HH, Pagon RA, Wallace SE, Bean LJH, Mirzaa G and Amemiya A. (1993). GeneReviews.

Adam SS, McDuffie JR, Ortel TL and Williams JW. (2012). Comparative effectiveness of warfarin and new oral anticoagulants for the management of atrial fibrillation and venous thromboembolism: a systematic review. *Ann Intern Med* **157,** 796-807.

Adeva-Andany MM, González-Lucán M, Donapetry-García C, Fernández-Fernández C and Ameneiros-Rodríguez E. (2016). Glycogen metabolism in humans. *BBA Clin* **5,** 85-100.

AH Kashou, H Basit & A Malik. (2022). ST Segment. StatPearls Publishing.

Alaoui-Jamali MA and Xu YJ. (2006). Proteomic technology for biomarker profiling in cancer: an update. *J Zhejiang Univ Sci B* **7,** 411-420.

Alberts B, Johnson A and Lewis J. (2002). *Molecular Biology of the Cell*. Garland Science.

Allessie MA, Boyden PA, Camm AJ, Kléber AG, Lab MJ, Legato MJ, Rosen MR, Schwartz PJ, Spooner PM, Van Wagoner DR and Waldo AL. (2001). Pathophysiology and prevention of atrial fibrillation. *Circulation* **103,** 769-777.

Alvarez-Fernandez R, Penfold CA, Galvez-Valdivieso G, Exposito-Rodriguez M, Stallard EJ, Bowden L, Moore JD, Mead A, Davey PA, Matthews JSA, Beynon J, Buchanan-Wollaston V, Wild DL, Lawson T, Bechtold U, Denby KJ and Mullineaux PM. (2021). Time-series transcriptomics reveals a BBX32-directed control of acclimation to high light in mature Arabidopsis leaves. *Plant J* **107,** 1363-1386.

Anderson RH, Spicer DE, Hlavacek AM, Cook AC and Backer CL. (2013). *Wilcox's Surgical Anatomy of the Heart*. Cambridge University Press.

Ansar M, Ullah F, Paracha SA, Adams DJ, Lai A, Pais L, Iwaszkiewicz J, Millan F, Sarwar MT, Agha Z, Shah SF, Qaisar AA, Falconnet E, Zoete V, Ranza E, Makrythanasis P, Santoni FA, Ahmed J, Katsanis N, Walsh C, Davis EE and Antonarakis SE. (2019). Bi-allelic Variants in DYNC1I2 Cause Syndromic Microcephaly with Intellectual Disability, Cerebral Malformations, and Dysmorphic Facial Features. *Am J Hum Genet* **104,** 1073-1087.

Antoniades C, Demosthenous M, Reilly S, Margaritis M, Zhang MH, Antonopoulos A, Marinou K, Nahar K, Jayaram R, Tousoulis D, Bakogiannis C, Sayeed R, Triantafyllou C, Koumallos N, Psarros C, Miliou A, Stefanadis C, Channon KM and Casadei B. (2012). Myocardial redox state predicts in-hospital clinical outcome after cardiac surgery effects of short-term pre-operative statin treatment. *J Am Coll Cardiol* **59,** 60-70.

Arbel R, Sergienko R, Hammerman A, Dotan-Greenberg S, Batat E, Avnery O, Greenberg D and Ellis MH. (2019). Direct oral anticoagulation and mortality in moderate to high-risk atrial fibrillation. *Heart* **105,** 1487-1492.

Arighi CN, Hartnell LM, Aguilar RC, Haft CR and Bonifacino JS. (2004). Role of the mammalian retromer in sorting of the cation-independent mannose 6-phosphate receptor. *J Cell Biol* **165,** 123-133.

Ariyaratnam JP, Middeldorp M, Thomas G, Noubiap JJ, Lau D and Sanders P. (2020). Risk Factor Management Before and After Atrial Fibrillation Ablation. *Card Electrophysiol Clin* **12,** 141-154.

Arnold SM, Fessler LI, Fessler JH and Kaufman RJ. (2000). Two homologues encoding human UDP-glucose:glycoprotein glucosyltransferase differ in mRNA expression and enzymatic activity. *Biochemistry* **39,** 2149-2163.

Arrieta A, Blackwood EA, Stauffer WT and Glembotski CC. (2019). Integrating ER and Mitochondrial Proteostasis in the Healthy and Diseased Heart. *Front Cardiovasc Med* **6,** 193.

Aruoma OI. (1998). Free radicals, oxidative stress, and antioxidants in human health and disease. *J Am Oil Chem Soc* **75,** 199-212.

Aston D, Capel RA, Ford KL, Christian HC, Mirams GR, Rog-Zielinska EA, Kohl P, Galione A, Burton RA and Terrar DA. (2017). High resolution structural evidence suggests the Sarcoplasmic Reticulum forms microdomains with Acidic Stores (lysosomes) in the heart. *Sci Rep* **7,** 40620.

Athanasiou LS, Fotiadis DI & Michalis LK. (2017). Introduction Atherosclerotic Plaque Characterization Methods Based on Coronary Imaging,. In Atherosclerotic Plaque Characterization Methods Based on Coronary Imaging. Academic Press.

Au CE, Bell AW, Gilchrist A, Hiding J, Nilsson T and Bergeron JJ. (2007). Organellar proteomics to create the cell map. *Curr Opin Cell Biol* **19,** 376-385.

Ausma J, Coumans WA, Duimel H, Van der Vusse GJ, Allessie MA & Borgers M. (2000). Atrial high energy phosphate content and mitochondrial enzyme activity during chronic atrial fibrillation. Cardiovasc Res 47, 788-796.

Ausma J, van der Velden HM, Lenders MH, van Ankeren EP, Jongsma HJ, Ramaekers FC, Borgers M and Allessie MA. (2003). Reverse structural and gap-junctional remodeling after prolonged atrial fibrillation in the goat. *Circulation* **107,** 2051-2058.

Ayagama T, Bose SJ, Capel RA, Priestman DA, Berridge G, Fischer R, Galione A, Platt FM, Kramer H and Burton RAB. (2021). A modified density gradient proteomic-based method to analyze endolysosomal proteins in cardiac tissue. *iScience* **24,** 102949.

Aziz Q, Finlay M, Montaigne D, Ojake L, Li Y, Anderson N, Ludwig A & Tinker A. (2018). ATP-sensitive potassium channels in the sinoatrial node contribute to heart rate control and adaptation to hypoxia. J Biol Chem 293, 8912-8921.

Baars TL, Petri S, Peters C and Mayer A. (2007). Role of the V-ATPase in regulation of the vacuolar fission-fusion equilibrium. *Mol Biol Cell* **18,** 3873-3882.

Bagshaw RD, Mahuran DJ and Callahan JW. (2005). A proteomic analysis of lysosomal integral membrane proteins reveals the diverse composition of the organelle. *Mol Cell Proteomics* **4,** 133-143.

Bagshaw RD, Pasternak SH, Mahuran DJ and Callahan JW. (2003). Nicastrin is a resident lysosomal membrane protein. *Biochem Biophys Res Commun* **300,** 615-618.

Bak J, Billington RA, Timar G, Dutton AC and Genazzani AA. (2001). NAADP receptors are present and functional in the heart. *Curr Biol* **11,** 987-990.

Balana B, Dobrev D, Wettwer E, Christ T, Knaut M & Ravens U. (2003). Decreased ATP-sensitive K(+) current density during chronic human atrial fibrillation. J Mol Cell Cardiol 35, 1399-1405.

Barh D and Azevedo V. (2017). *Omics Technologies and Bio-Engineering Towards Improving Quality of Life*. Elsevier Inc.

Beck MA, Handy J and Levander OA. (2000). The role of oxidative stress in viral infections. *Ann N Y Acad Sci* **917,** 906-912.

Berg DD, Ruff CT and Morrow DA. (2021). Biomarkers for Risk Assessment in Atrial Fibrillation. *Clin Chem* **67,** 87-95.

Bergeron R, Russell RR, Young LH, Ren JM, Marcucci M, Lee A and Shulman GI. (1999). Effect of AMPK activation on muscle glucose metabolism in conscious rats. *Am J Physiol* **276,** E938-944.

Berthoud VM, Minogue PJ, Laing JG and Beyer EC. (2004). Pathways for degradation of connexins and gap junctions. *Cardiovasc Res* **62,** 256-267.

Betteridge DJ. (2000). What is oxidative stress? *Metabolism* **49,** 3-8.

Bilousova T, Melnik M, Miyoshi E, Gonzalez BL, Poon WW, Vinters HV, Miller CA, Corrada MM, Kawas C, Hatami A, Albay R, Glabe C and Gylys KH. (2019). Apolipoprotein E/Amyloid-β Complex Accumulates in Alzheimer Disease Cortical Synapses via Apolipoprotein E Receptors and Is Enhanced by APOE4. *Am J Pathol* **189,** 1621-1636.

Bissig C, Hurbain I, Raposo G & van Niel G. (2017). PIKfyve activity regulates reformation of terminal storage lysosomes from endolysosomes. Traffic 18, 747-757.

Bittihn P. (2015). *Complex Structure and Dynamics of the Heart*. Springer 2014.

Blommaart EF, Luiken JJ, Blommaart PJ, van Woerkom GM and Meijer AJ. (1995). Phosphorylation of ribosomal protein S6 is inhibitory for autophagy in isolated rat hepatocytes. *J Biol Chem* **270,** 2320-2326.

Boittin FX, Galione A and Evans AM. (2002). Nicotinic acid adenine dinucleotide phosphate mediates Ca2+ signals and contraction in arterial smooth muscle via a two-pool mechanism. *Circ Res* **91,** 1168-1175.

Bolster DR, Crozier SJ, Kimball SR and Jefferson LS. (2002). AMP-activated protein kinase suppresses protein synthesis in rat skeletal muscle through down-regulated mammalian target of rapamycin (mTOR) signaling. *J Biol Chem* **277,** 23977-23980.

Bose SJ, Ayagama T & Burton RAB. (2022). Chapter 3 - Lysosomal proteases and their role in signaling pathways Proteolytic Signaling in Health and Disease. In *Proteolytic Signaling in Health and Disease*, ed. Zelanis A, pp. 41-61. Academic Press.

Botto GL, Luzi M and A. Sagone. (2003). Atrial fibrillation: the remodelling phenomenon. European Heart Journal Supplements.

Boudeau J, Baas AF, Deak M, Morrice NA, Kieloch A, Schutkowski M, Prescott AR, Clevers HC and Alessi DR. (2003). MO25alpha/beta interact with STRADalpha/beta enhancing their ability to bind, activate and localize LKB1 in the cytoplasm. *EMBO J* **22,** 5102-5114.

Boulon S, Westman BJ, Hutten S, Boisvert FM and Lamond AI. (2010). The nucleolus under stress. *Mol Cell* **40,** 216-227.

Bravo-San Pedro JM, Kroemer G and Galluzzi L. (2017). Autophagy and Mitophagy in Cardiovascular Disease. *Circ Res* **120,** 1812-1824.

Bright NA, Davis LJ & Luzio JP. (2016). Endolysosomes Are the Principal Intracellular Sites of Acid Hydrolase Activity. Curr Biol 26, 2233-2245.

Brodsky FM. (2016). *Encyclopedia of Cell Biology, Clathrin and Clathrin-Dependent Endocytosis,*. Academic Press.

Brozinick JT, Berkemeier BA and Elmendorf JS. (2007). "Actin"g on GLUT4: membrane and cytoskeletal components of insulin action. *Curr Diabetes Rev* **3,** 111-122.

Bryant NJ, Govers R and James DE. (2002). Regulated transport of the glucose transporter GLUT4. *Nat Rev Mol Cell Biol* **3,** 267-277.

Burton R-AB and Terrar DA. (2021). Emerging Evidence for cAMP-calcium Cross Talk in Heart Atrial Nanodomains Where IP_3-Evoked Calcium Release Stimulates Adenylyl Cyclases. Contact.

Bustos V, Pulina MV, Bispo A, Lam A, Flajolet M, Gorelick FS and Greengard P. (2017). Phosphorylated Presenilin 1 decreases β-amyloid by facilitating autophagosome-lysosome fusion. *Proc Natl Acad Sci U S A* **114,** 7148-7153.

Butler VJ, Cortopassi WA, Argouarch AR, Ivry SL, Craik CS, Jacobson MP and Kao AW. (2019). Progranulin Stimulates the In Vitro Maturation of Pro-Cathepsin D at Acidic pH. *J Mol Biol* **431,** 1038-1047.

Byun S, Seok S, Kim YC, Zhang Y, Yau P, Iwamori N, Xu HE, Ma J, Kemper B and Kemper JK. (2020). Fasting-induced FGF21 signaling activates hepatic autophagy and lipid degradation via JMJD3 histone demethylase. *Nat Commun* **11,** 807.

Cadenas E and Davies KJ. (2000). Mitochondrial free radical generation, oxidative stress, and aging. *Free Radic Biol Med* **29,** 222-230.

Cadenas S. (2018). ROS and redox signaling in myocardial ischemia-reperfusion injury and cardioprotection. *Free Radic Biol Med* **117,** 76-89.

Calcraft PJ, Ruas M, Pan Z, Cheng X, Arredouani A, Hao X, Tang J, Rietdorf K, Teboul L, Chuang KT, Lin P, Xiao R, Wang C, Zhu Y, Lin Y, Wyatt CN, Parrington J, Ma J, Evans AM, Galione A and Zhu MX. (2009). NAADP mobilizes calcium from acidic organelles through two-pore channels. *Nature* **459,** 596-600.

Campden RI and Zhang Y. (2019). The role of lysosomal cysteine cathepsins in NLRP3 inflammasome activation. *Arch Biochem Biophys* **670,** 32-42.

Cancela JM, Churchill GC and Galione A. (1999). Coordination of agonist-induced Ca2+-signalling patterns by NAADP in pancreatic acinar cells. *Nature* **398,** 74-76.

Cang C, Zhou Y, Navarro B, Seo YJ, Aranda K, Shi L, Battaglia-Hsu S, Nissim I, Clapham DE and Ren D. (2013). mTOR regulates lysosomal ATP-sensitive two-pore Na(+) channels to adapt to metabolic state. *Cell* **152,** 778-790.

Capel RA, Bolton EL, Lin WK, Aston D, Wang Y, Liu W, Wang X, Burton RA, Bloor-Young D, Shade KT, Ruas M, Parrington J, Churchill GC, Lei M, Galione A and Terrar DA. (2015). Two-pore Channels (TPC2s) and Nicotinic Acid Adenine Dinucleotide Phosphate (NAADP) at Lysosomal-Sarcoplasmic Reticular Junctions Contribute to Acute and Chronic beta-Adrenoceptor Signaling in the Heart. *J Biol Chem* **290,** 30087-30098.

Carlson BM. (2019). Chapter 10 - The Circulatory System. In *The Human Body*, pp. 271-301. Academic Press.

Cataldo AM, Mathews PM, Boiteau AB, Hassinger LC, Peterhoff CM, Jiang Y, Mullaney K, Neve RL, Gruenberg J and Nixon RA. (2008). Down syndrome fibroblast model of Alzheimer-related endosome pathology: accelerated endocytosis promotes late endocytic defects. *Am J Pathol* **173,** 370-384.

Cecchini G. (2003). Function and structure of complex II of the respiratory chain. *Annu Rev Biochem* **72,** 77-109.

Chaikuad A, Froese DS, Berridge G, von Delft F, Oppermann U and Yue WW. (2011). Conformational plasticity of glycogenin and its maltosaccharide substrate during glycogen biogenesis. *Proc Natl Acad Sci U S A* **108,** 21028-21033.

Chakraborty P, Nattel S and Nanthakumar K. (2020). Linking cellular energy state to atrial fibrillation pathogenesis: Potential role of adenosine monophosphate-activated protein kinase. *Heart Rhythm* **17,** 1398-1404.

Chandramouli K and Qian PY. (2009). Proteomics: challenges, techniques and possibilities to overcome biological sample complexity. *Hum Genomics Proteomics* **2009**.

Chanduri M, Rai A, Malla AB, Wu M, Fiedler D, Mallik R and Bhandari R. (2016). Inositol hexakisphosphate kinase 1 (IP6K1) activity is required for cytoplasmic dynein-driven transport. *Biochem J* **473,** 3031-3047.

Chen J, Ou Y, Luo R, Wang J, Wang D, Guan J, Li Y, Xia P, Chen PR and Liu Y. (2021). SAR1B senses leucine levels to regulate mTORC1 signalling. *Nature* **596,** 281-284.

Chen L, Chen Q, Xie B, Quan C, Sheng Y, Zhu S, Rong P, Zhou S, Sakamoto K, MacKintosh C, Wang HY and Chen S. (2016). Disruption of the AMPK-TBC1D1 nexus increases lipogenic gene expression and causes obesity in mice via promoting IGF1 secretion. *Proc Natl Acad Sci U S A* **113,** 7219-7224.

Chen SA, Hsieh MH, Tai CT, Tsai CF, Prakash VS, Yu WC, Hsu TL, Ding YA and Chang MS. (1999). Initiation of atrial fibrillation by ectopic beats originating from the pulmonary veins: electrophysiological characteristics, pharmacological responses, and effects of radiofrequency ablation. *Circulation* **100,** 1879-1886.

Cheung KS and Leung WK. (2017). Gastrointestinal bleeding in patients on novel oral anticoagulants: Risk, prevention and management. *World J Gastroenterol* **23,** 1954-1963.

Christensen KA, Myers JT and Swanson JA. (2002). pH-dependent regulation of lysosomal calcium in macrophages. *J Cell Sci* **115,** 599-607.

Chung E and Leinwand LA. (2008). Rescuing cardiac malfunction: the roles of the chaperone-like small heat shock proteins. *Circ Res* **103,** 1351-1353.

Churchill GC and Galione A. (2001). NAADP induces Ca2+ oscillations via a two-pool mechanism by priming IP3- and cADPR-sensitive Ca2+ stores. *EMBO J* **20,** 2666-2671.

Churchill GC, Okada Y, Thomas JM, Genazzani AA, Patel S and Galione A. (2002). NAADP mobilizes Ca(2+) from reserve granules, lysosome-related organelles, in sea urchin eggs. *Cell* **111,** 703-708.

Chédin S, Laferté A, Hoang T, Lafontaine DL, Riva M and Carles C. (2007). Is ribosome synthesis controlled by pol I transcription? *Cell Cycle* **6,** 11-15.

Clague MJ, Urbé S, Aniento F and Gruenberg J. (1994). Vacuolar ATPase activity is required for endosomal carrier vesicle formation. *J Biol Chem* **269,** 21-24.

Clark DP. (2009). *Molecular Biology*. Elsevier Science & Technology.

Clauss S, Schüttler D, Bleyer C, Vlcek J, Shakarami M, Tomsits P, Schneider S, Maderspacher F, Chataut K, Trebo A, Wang C, Kleeberger J, Xia R, Baloch E, Hildebrand B, Massberg S, Wakili R and Kääb S. (2020). Characterization of a porcine model of atrial arrhythmogenicity in the context of ischaemic heart failure. *PLoS One* **15,** e0232374.

Collins TP, Bayliss R, Churchill GC, Galione A and Terrar DA. (2011). NAADP influences excitation-contraction coupling by releasing calcium from lysosomes in atrial myocytes. *Cell Calcium* **50,** 449-458.

Comolli R. (1971). Hydrolase activity and intracellular pH in liver, heart and diaphragm of aging rats. *Exp Gerontol* **6,** 219-225.

Comtois P, Kneller J and Nattel S. (2005). Of circles and spirals: bridging the gap between the leading circle and spiral wave concepts of cardiac reentry. *Europace* **7 Suppl 2,** 10-20.

Barrett AJ, Rawlings ND & Woessner JF. (2004). Handbook of Proteolytic Enzymes. Elsevier Academic.

Cooper GM. (2000). *The Cell A Molecular Approach* Sinauer Associates.

Cooper GM and Hausman RE. (2007). *The cell : a molecular approach*. ASM Press.

Cox J and Mann M. (2008). MaxQuant enables high peptide identification rates, individualized p.p.b.-range mass accuracies and proteome-wide protein quantification. *Nat Biotechnol* **26,** 1367-1372.

Crick F. (1970). Central dogma of molecular biology. *Nature* **227,** 561-563.

D'Souza Z, Blackburn JB, Kudlyk T, Pokrovskaya ID and Lupashin VV. (2019). Defects in COG-Mediated Golgi Trafficking Alter Endo-Lysosomal System in Human Cells. *Front Cell Dev Biol* **7,** 118.

Daboussi L, Costaguta G and Payne GS. (2012). Phosphoinositide-mediated clathrin adaptor progression at the trans-Golgi network. *Nat Cell Biol* **14,** 239-248.

Dai J, Zhang Q, Wan C, Liu J, Yu Y and Wang J. (2021). Significances of viable synergistic autophagy-associated cathepsin B and cathepsin D (CTSB/CTSD) as potential biomarkers for sudden cardiac death. *BMC Cardiovasc Disord* **21,** 233.

Dangelmaier C, Manne BK, Liverani E, Jin J, Bray P and Kunapuli SP. (2014). PDK1 selectively phosphorylates Thr(308) on Akt and contributes to human platelet functional responses. *Thromb Haemost* **111,** 508-517.

Daniloski Z, Jordan TX, Wessels HH, Hoagland DA, Kasela S, Legut M, Maniatis S, Mimitou EP, Lu L, Geller E, Danziger O, Rosenberg BR, Phatnani H, Smibert P, Lappalainen T, tenOever BR and Sanjana NE. (2021). Identification of Required Host Factors for SARS-CoV-2 Infection in Human Cells. *Cell* **184,** 92-105.e116.

David C, Halliwell J and Whitaker M. (1988). Some properties of the membrane currents underlying the fertilization potential in sea urchin eggs. *J Physiol* **402,** 139-154.

Davis S, Charles PD, He L, Mowlds P, Kessler BM and Fischer R. (2017). Expanding Proteome Coverage with CHarge Ordered Parallel Ion aNalysis (CHOPIN) Combined with Broad Specificity Proteolysis. *J Proteome Res* **16,** 1288-1299.

de Araujo MEG, Liebscher G, Hess MW and Huber LA. (2020). Lysosomal size matters. *Traffic* **21,** 60-75.

de Diego I, Schwartz F, Siegfried H, Dauterstedt P, Heeren J, Beisiegel U, Enrich C and Grewal T. (2002). Cholesterol modulates the membrane binding and intracellular distribution of annexin 6. *J Biol Chem* **277,** 32187-32194.

De Duve C, PRESSMAN BC, GIANETTO R, WATTIAUX R and APPELMANS F. (1955). Tissue fractionation studies. 6. Intracellular distribution patterns of enzymes in rat-liver tissue. *Biochem J* **60,** 604-617.

De Duve C and Wattiaux R. (1966). Functions of lysosomes. *Annu Rev Physiol* **28,** 435-492.

De Souza AI, Cardin S, Wait R, Chung YL, Vijayakumar M, Maguy A, Camm AJ and Nattel S. (2010). Proteomic and metabolomic analysis of atrial profibrillatory remodelling in congestive heart failure. *J Mol Cell Cardiol* **49,** 851-863.

Dhalla NS, Temsah RM and Netticadan T. (2000). Role of oxidative stress in cardiovascular diseases. *J Hypertens* **18,** 655-673.

Ding X, Jiang X, Tian R, Zhao P, Li L, Wang X, Chen S, Zhu Y, Mei M, Bao S, Liu W, Tang Z and Sun Q. (2019). RAB2 regulates the formation of autophagosome and autolysosome in mammalian cells. *Autophagy* **15,** 1774-1786.

Distefano MB, Kjos I, Bakke O and Progida C. (2015). Rab7b at the intersection of intracellular trafficking and cell migration. *Commun Integr Biol* **8,** e1023492.

Doeberitz MvK and Wentzensen N. (2008). *Comprehensive Cytopathology*. Elsevier Inc.

Doll S, Dreßen M, Geyer PE, Itzhak DN, Braun C, Doppler SA, Meier F, Deutsch MA, Lahm H, Lange R, Krane M and Mann M. (2017). Region and cell-type resolved quantitative proteomic map of the human heart. *Nat Commun* **8,** 1469.

Doykov ID, Heywood WE, Nikolaenko V, Śpiewak J, Hällqvist J, Clayton PT, Mills P, Warnock DG, Nowak A and Mills K. (2020). Rapid, proteomic urine assay for monitoring progressive organ disease in Fabry disease. *J Med Genet* **57,** 38-47.

Dröge W. (2002). Free radicals in the physiological control of cell function. *Physiol Rev* **82,** 47-95.

Dromparis P & Michelakis ED. (2013). Mitochondria in vascular health and disease. *Annu Rev Physiol* **75,** 95-126.

du Plessis L, Skunca N and Dessimoz C. (2011). The what, where, how and why of gene ontology--a primer for bioinformaticians. *Brief Bioinform* **12,** 723-735.

Dubey V and Luqman S. (2017). Cathepsin D as a Promising Target for the Discovery of Novel Anticancer Agents. *Curr Cancer Drug Targets* **17,** 404-422.

Dudley SC, Hoch NE, McCann LA, Honeycutt C, Diamandopoulos L, Fukai T, Harrison DG, Dikalov SI and Langberg J. (2005). Atrial fibrillation increases production of superoxide by the left atrium and left atrial appendage: role of the NADPH and xanthine oxidases. *Circulation* **112,** 1266-1273.

Dunkley TP, Watson R, Griffin JL, Dupree P and Lilley KS. (2004). Localization of organelle proteins by isotope tagging (LOPIT). *Mol Cell Proteomics* **3,** 1128-1134.

Durrer D, Schoo L, Schuilenburg RM and Wellens HJ. (1967). The role of premature beats in the initiation and the termination of supraventricular tachycardia in the Wolff-Parkinson-White syndrome. *Circulation* **36,** 644-662.

Durán RV, Oppliger W, Robitaille AM, Heiserich L, Skendaj R, Gottlieb E and Hall MN. (2012). Glutaminolysis activates Rag-mTORC1 signaling. *Mol Cell* **47,** 349-358.

Dytham C. (2011). *Choosing and Using Statistics : A Biologist's Guide*. John Wiley & Sons.

Dzimiri N and Fricke U. (1988). Lipophilicity and pharmacodynamics of cardiotonic steroids in guinea-pig isolated heart muscle preparations. *Br J Pharmacol* **93,** 281-288.

Echt DS, Liebson PR, Mitchell LB, Peters RW, Obias-Manno D, Barker AH, Arensberg D, Baker A, Friedman L and Greene HL. (1991). Mortality and morbidity in patients receiving encainide, flecainide, or placebo. The Cardiac Arrhythmia Suppression Trial. *N Engl J Med* **324,** 781-788.

Eckstein J, Maesen B, Linz D, Zeemering S, van Hunnik A, Verheule S, Allessie M and Schotten U. (2011). Time course and mechanisms of endo-epicardial electrical dissociation during atrial fibrillation in the goat. *Cardiovasc Res* **89,** 816-824.

Egan DF, Shackelford DB, Mihaylova MM, Gelino S, Kohnz RA, Mair W, Vasquez DS, Joshi A, Gwinn DM, Taylor R, Asara JM, Fitzpatrick J, Dillin A, Viollet B, Kundu M, Hansen M & Shaw RJ. (2011). Phosphorylation of ULK1 (hATG1) by AMP-activated protein kinase connects energy sensing to mitophagy. Science 331, 456-461.

Eijsbouts S, Ausma J, Blaauw Y, Schotten U, Duytschaever M and Allessie MA. (2006). Serial cardioversion by class IC Drugs during 4 months of persistent atrial fibrillation in the goat. *J Cardiovasc Electrophysiol* **17,** 648-654.

Embi AA and Scherlag BJ. (2014). An endocrine hypothesis for the genesis of atrial fibrillation: the hypothalamic-pituitary-adrenal axis response to stress and glycogen accumulation in atrial tissues. *N Am J Med Sci* **6,** 586-590.

Embi AA, Scherlag BJ and Ritchey JW. (2014). Glycogen and the propensity for atrial fibrillation: intrinsic anatomic differences in glycogen in the left and right atria in the goat heart. *N Am J Med Sci* **6,** 510-515.

Enslen H, Raingeaud J and Davis RJ. (1998). Selective activation of p38 mitogen-activated protein (MAP) kinase isoforms by the MAP kinase kinases MKK3 and MKK6. *J Biol Chem* **273,** 1741-1748.

Fabregat A, Sidiropoulos K, Viteri G, Forner O, Marin-Garcia P, Arnau V, D'Eustachio P, Stein L and Hermjakob H. (2017). Reactome pathway analysis: a high-performance in-memory approach. *BMC Bioinformatics* **18,** 142.

Fang Y, Vilella-Bach M, Bachmann R, Flanigan A and Chen J. (2001). Phosphatidic acid-mediated mitogenic activation of mTOR signaling. *Science* **294,** 1942-1945.

Farrell AP. (2011). DESIGN AND PHYSIOLOGY OF THE HEART | Physiology of Cardiac Pumping. In Encyclopedia of Fish Physiology, ed. Farrell AP, pp. 1030-1037. Academic Press.

Friedrichs, M., Graf, G., and Springer, B.: Skimming flow induced over a simulated polychaete tube lawn at low population densities, Mar. Ecol.-Prog. Ser., 192, 219–228, 2000

Fernández B, Fdez E, Gómez-Suaga P, Gil F, Molina-Villalba I, Ferrer I, Patel S, Churchill GC & Hilfiker S. (2016). Iron overload causes endolysosomal deficits modulated by NAADP-regulated 2-pore channels and RAB7A. Autophagy 12, 1487-1506.

Filocamo M and Morrone A. (2011). Lysosomal storage disorders: molecular basis and laboratory testing. *Hum Genomics* **5,** 156-169.

Frustaci A, Chimenti C, Bellocci F, Morgante E, Russo MA and Maseri A. (1997). Histological substrate of atrial biopsies in patients with lone atrial fibrillation. *Circulation* **96,** 1180-1184.

Fu L, Deng H, Lin WD, He SF, Liu FZ, Liu Y, Zhan XZ, Fang XH, Liao HT, Wei W, Liao ZL, Tang LH, Fu ZY, Zheng MR, Wu SL and Xue YM. (2019). Association between elevated blood glucose level and non-valvular atrial fibrillation: a report from the Guangzhou heart study. *BMC Cardiovasc Disord* **19,** 270.

Fukuda Y. (1975). Difference in calcium content of atrial and ventricular muscle. *Jpn J Physiol* **25,** 467-479.

Galione A, Morgan AJ, Arredouani A, Davis LC, Rietdorf K, Ruas M and Parrington J. (2010). NAADP as an intracellular messenger regulating lysosomal calcium-release channels. *Biochem Soc Trans* **38,** 1424-1431.

Galjart NJ, Morreau H, Willemsen R, Gillemans N, Bonten EJ and d'Azzo A. (1991). Human lysosomal protective protein has cathepsin A-like activity distinct from its protective function. *J Biol Chem* **266,** 14754-14762.

Ge SX, Jung D and Yao R. (2020). ShinyGO: a graphical gene-set enrichment tool for animals and plants. *Bioinformatics* **36,** 2628-2629.

Gemel J, Lin X, Collins R, Veenstra RD and Beyer EC. (2008). Cx30.2 can form heteromeric gap junction channels with other cardiac connexins. *Biochem Biophys Res Commun* **369,** 388-394.

Ghzally Y and Gerasimon G. (2020). *Catheter Ablation*. Statpearl publishing.

Ghezelbash S, Molina CE & Dobrev D. (2015). Altered atrial metabolism: an underappreciated contributor to the initiation and progression of atrial fibrillation. J Am Heart Assoc 4, e001808.

Gingras AC, Raught B and Sonenberg N. (1999). eIF4 initiation factors: effectors of mRNA recruitment to ribosomes and regulators of translation. *Annu Rev Biochem* **68,** 913-963.

Gladka MM, Molenaar B, de Ruiter H, van der Elst S, Tsui H, Versteeg D, Lacraz GPA, Huibers MMH, van Oudenaarden A and van Rooij E. (2018). Single-Cell Sequencing of the Healthy and Diseased Heart Reveals Cytoskeleton-Associated Protein 4 as a New Modulator of Fibroblasts Activation. *Circulation* **138,** 166-180.

Glick D, Barth S and Macleod KF. (2010). Autophagy: cellular and molecular mechanisms. *J Pathol* **221,** 3-12.

Godbey WT. (2014). Chapter 3 - Cellular Transport, An Introduction to Biotechnology. In An Introduction to Biotechnology. Woodhead Publishing.

Godbey WT. (2022). Chapter 2 - Voyage into the cell. In Biotechnology and its Application (Second) edn, pp. 11-46. Academic Press

Goldberger AL, Goldberger ZD & Shvilkin A. (2018). Goldberger's Clinical Electrocardiography (Ninth Edition) Chapter 23 - Interpreting ECGs: An Integrative Approach. Elsevier.

Golub TR, Slonim DK, Tamayo P, Huard C, Gaasenbeek M, Mesirov JP, Coller H, Loh ML, Downing JR, Caligiuri MA, Bloomfield CD and Lander ES. (1999). Molecular classification of cancer: class discovery and class prediction by gene expression monitoring. *Science* **286,** 531-537.

Goswami S, Balasubramanian I, D'Agostino L, Bandyopadhyay S, Patel R, Avasthi S, Yu S, Goldenring JR, Bonder EM and Gao N. (2021). RAB11A-mediated YAP localization to adherens and tight junctions is essential for colonic epithelial integrity. *J Biol Chem* **297,** 100848.

Graham JM. (2001). Isolation of lysosomes from tissues and cells by differential and density gradient centrifugation. *Curr Protoc Cell Biol* **Chapter 3,** Unit 3.6.

Grant AO. (2009). Cardiac ion channels. Circ Arrhythm Electrophysiol 2, 185-194.

Granneman S, Kudla G, Petfalski E and Tollervey D. (2009). Identification of protein binding sites on U3 snoRNA and pre-rRNA by UV cross-linking and high-throughput analysis of cDNAs. *Proc Natl Acad Sci U S A* **106,** 9613-9618.

Gray, M., and R.J. Botelho. 2017. Phagocytosis: Hungry, Hungry Cells. Methods Mol. Biol. 1519:1–16. https://doi.org/10.1007/978-1-4939-6581-6_1

Gregersen N and Bross P. (2010). Protein misfolding and cellular stress: an overview. *Methods Mol Biol* **648,** 3-23.

Grimm C, Holdt LM, Chen CC, Hassan S, Müller C, Jörs S, Cuny H, Kissing S, Schröder B, Butz E, Northoff B, Castonguay J, Luber CA, Moser M, Spahn S, Lüllmann-Rauch R, Fendel C, Klugbauer N, Griesbeck O, Haas A, Mann M, Bracher F, Teupser D, Saftig P, Biel M and Wahl-Schott C. (2014). High susceptibility to fatty liver disease in two-pore channel 2-deficient mice. *Nat Commun* **5,** 4699.

Grivennikova VG, Kapustin AN and Vinogradov AD. (2001). Catalytic activity of NADH-ubiquinone oxidoreductase (complex I) in intact mitochondria. evidence for the slow active/inactive transition. *J Biol Chem* **276,** 9038-9044.

Grosshans BL, Ortiz D and Novick P. (2006). Rabs and their effectors: achieving specificity in membrane traffic. *Proc Natl Acad Sci U S A* **103,** 11821-11827.

Grummt I. (2013). The nucleolus—guardian of cellular homeostasis and genome integrity. *Chromosoma* **122,** 487-497.

Grummt I and Voit R. (2010). Linking rDNA transcription to the cellular energy supply. *Cell Cycle* **9,** 225-226.

Gudmundsson H, Hund TJ, Wright PJ, Kline CF, Snyder JS, Qian L, Koval OM, Cunha SR, George M, Rainey MA, Kashef FE, Dun W, Boyden PA, Anderson ME, Band H and Mohler PJ. (2010). EH domain proteins regulate cardiac membrane protein targeting. *Circ Res* **107,** 84-95.

Guerra F and Bucci C. (2016). Multiple Roles of the Small GTPase Rab7. *Cells* **5**.

Guo R, Rowe PS, Liu S, Simpson LG, Xiao ZS and Quarles LD. (2002). Inhibition of MEPE cleavage by Phex. *Biochem Biophys Res Commun* **297,** 38-45.

Gutierrez MG, Munafó DB, Berón W and Colombo MI. (2004). Rab7 is required for the normal progression of the autophagic pathway in mammalian cells. *J Cell Sci* **117,** 2687-2697.

Gwinn DM, Shackelford DB, Egan DF, Mihaylova MM, Mery A, Vasquez DS, Turk BE and Shaw RJ. (2008). AMPK phosphorylation of raptor mediates a metabolic checkpoint. *Mol Cell* **30,** 214-226.

Gómez-Garre P, Jesús S, Carrillo F, Cáceres-Redondo MT, Bernal-Bernal I, Carballo M, Gao L and Mir P. (2012). PSMC1 Gene in Parkinson's Disease. *Eur Neurol* **68,** 193-198.

Göktuna S. (2018). IKBKE inhibits TSC1 to activate the mTOR/S6K pathway for oncogenic transformation. *Turk J Biol* **42,** 268-278.

Hahn S. (2004). Structure and mechanism of the RNA polymerase II transcription machinery. *Nat Struct Mol Biol* **11,** 394-403.

Hales CM, Griner R, Hobdy-Henderson KC, Dorn MC, Hardy D, Kumar R, Navarre J, Chan EK, Lapierre LA and Goldenring JR. (2001). Identification and characterization of a family of Rab11-interacting proteins. *J Biol Chem* **276,** 39067-39075.

Hales CM, Vaerman JP and Goldenring JR. (2002). Rab11 family interacting protein 2 associates with Myosin Vb and regulates plasma membrane recycling. *J Biol Chem* **277,** 50415-50421.

Hand SC and Hardewig I. (1996). Downregulation of cellular metabolism during environmental stress: mechanisms and implications. *Annu Rev Physiol* **58,** 539-563.

Harada M, Tadevosyan A, Qi X, Xiao J, Liu T, Voigt N, Karck M, Kamler M, Kodama I, Murohara T, Dobrev D and Nattel S. (2015). Atrial Fibrillation Activates AMP-Dependent Protein Kinase and its Regulation of Cellular Calcium Handling: Potential Role in Metabolic Adaptation and Prevention of Progression. *J Am Coll Cardiol* **66,** 47-58.

Hardbower DM, de Sablet T, Chaturvedi R and Wilson KT. (2013). Chronic inflammation and oxidative stress: the smoking gun for Helicobacter pylori-induced gastric cancer? *Gut Microbes* **4,** 475-481.

Hardie DG. (2011). AMP-activated protein kinase: an energy sensor that regulates all aspects of cell function. *Genes Dev* **25,** 1895-1908.

Hardie DG, Ross FA and Hawley SA. (2012). AMPK: a nutrient and energy sensor that maintains energy homeostasis. *Nat Rev Mol Cell Biol* **13,** 251-262.

Hardie DG, Schaffer BE and Brunet A. (2016). AMPK: An Energy-Sensing Pathway with Multiple Inputs and Outputs. *Trends Cell Biol* **26,** 190-201.

Harrison RE, Bucci C, Vieira OV, Schroer TA and Grinstein S. (2003). Phagosomes fuse with late endosomes and/or lysosomes by extension of membrane protrusions along microtubules: role of Rab7 and RILP. *Mol Cell Biol* **23,** 6494-6506.

Hart RG, Pearce LA and Aguilar MI. (2007). Meta-analysis: antithrombotic therapy to prevent stroke in patients who have nonvalvular atrial fibrillation. *Ann Intern Med* **146,** 857-867.

Hasselbach W. (1964). ATP-driven active transport of calcium in the membranes of the sarcoplasmic reticulum. Proc R Soc Lond B Biol Sci 160, 501-504.

Haverkamp F, Jacobs D, Cantz M, Hansmann M, Fahnenstich H and Zerres K. (1996). Nonimmune hydrops fetalis with galactosialidosis: consequences for family planning. *Fetal Diagn Ther* **11,** 114-119.

Hay N and Sonenberg N. (2004). Upstream and downstream of mTOR. *Genes Dev* **18,** 1926-1945.

Haïssaguerre M, Jaïs P, Shah DC, Takahashi A, Hocini M, Quiniou G, Garrigue S, Le Mouroux A, Le Métayer P and Clémenty J. (1998). Spontaneous initiation of atrial fibrillation by ectopic beats originating in the pulmonary veins. *N Engl J Med* **339,** 659-666.

He H and Kogut MH. (2003). CpG-ODN-induced nitric oxide production is mediated through clathrin-dependent endocytosis, endosomal maturation, and activation of PKC, MEK1/2 and p38 MAPK, and NF-kappaB pathways in avian macrophage cells (HD11). *Cell Signal* **15,** 911-917.

He K, Sun H, Zhang J, Zheng R, Gu J, Luo M and Shao Y. (2019). Rab7-mediated autophagy regulates phenotypic transformation and behavior of smooth muscle cells via the Ras/Raf/MEK/ERK signaling pathway in human aortic dissection. *Mol Med Rep* **19,** 3105-3113.

Healy SJ, Verfaillie T, Jäger R, Agostinis P and Samali A. (2012). *Biology of the Endoplasmic Reticulum*. Springer, Dordrecht.

Heide Pvd. (2014). *Secondary Ion Mass Spectrometry: An Introduction to Principles and Practices*. Wiley.

Heijman J, Voigt N, Wehrens XH and Dobrev D. (2014). Calcium dysregulation in atrial fibrillation: the role of CaMKII. *Front Pharmacol* **5,** 30.

Hendley DD and Strehler BL. (1965). Enzymic activities of lipofuscin age pigments: comparative histochemical and biochemical studies. *Biochim Biophys Acta* **99,** 406-417.

Hepbildikler ST, Sandhoff R, Kolzer M, Proia RL and Sandhoff K. (2002). Physiological substrates for human lysosomal beta -hexosaminidase S. *J Biol Chem* **277,** 2562-2572.

Heras-Bautista CO, Mikhael N, Lam J, Shinde V, Katsen-Globa A, Dieluweit S, Molcanyi M, Uvarov V, Jütten P, Sahito RGA, Mederos-Henry F, Piechot A, Brockmeier K, Hescheler J, Sachinidis A and Pfannkuche K. (2019). Cardiomyocytes facing fibrotic conditions re-express extracellular matrix transcripts. *Acta Biomater* **89,** 180-192.

Hermans MM, Kroos MA, van Beeumen J, Oostra BA and Reuser AJ. (1991). Human lysosomal alpha-glucosidase. Characterization of the catalytic site. *J Biol Chem* **266,** 13507-13512.

Hibbs RG, Ferrans VJ, Walsh JJ and Burch GE. (1965). Electron microscopic observations on lysosomes and related cytoplasmic components of normal and pathological cardiac muscle. *Anat Rec* **153,** 173-185.

Hilenski LL, Clempus RE, Quinn MT, Lambeth JD and Griendling KK. (2004). Distinct subcellular localizations of Nox1 and Nox4 in vascular smooth muscle cells. *Arterioscler Thromb Vasc Biol* **24,** 677-683.

Hill MF and Singal PK. (1996). Antioxidant and oxidative stress changes during heart failure subsequent to myocardial infarction in rats. *Am J Pathol* **148,** 291-300.

Hinek A, Zhang S, Smith AC and Callahan JW. (2000). Impaired elastic-fiber assembly by fibroblasts from patients with either Morquio B disease or infantile GM1-gangliosidosis is linked to deficiency in the 67-kD spliced variant of beta-galactosidase. *Am J Hum Genet* **67,** 23-36.

Hinrichsen L, Harborth J, Andrees L, Weber K and Ungewickell EJ. (2003). Effect of clathrin heavy chain- and alpha-adaptin-specific small inhibitory RNAs on endocytic accessory proteins and receptor trafficking in HeLa cells. *J Biol Chem* **278,** 45160-45170.

Hirai Y, Louvet E, Oda T, Kumeta M, Watanabe Y, Horigome T and Takeyasu K. (2013). Nucleolar scaffold protein, WDR46, determines the granular compartmental localization of nucleolin and DDX21. *Genes Cells* **18,** 780-797.

Hoefsloot LH, Hoogeveen-Westerveld M, Kroos MA, van Beeumen J, Reuser AJ and Oostra BA. (1988). Primary structure and processing of lysosomal alpha-

glucosidase; homology with the intestinal sucrase-isomaltase complex. *EMBO J* **7,** 1697-1704.

Hoffert JD, Pisitkun T, Wang G, Shen RF and Knepper MA. (2006). Quantitative phosphoproteomics of vasopressin-sensitive renal cells: regulation of aquaporin-2 phosphorylation at two sites. *Proc Natl Acad Sci U S A* **103,** 7159-7164.

Hoffman NJ and Elmendorf JS. (2011). Signaling, cytoskeletal and membrane mechanisms regulating GLUT4 exocytosis. *Trends Endocrinol Metab* **22,** 110-116.

Hoppe S, Bierhoff H, Cado I, Weber A, Tiebe M, Grummt I and Voit R. (2009). AMP-activated protein kinase adapts rRNA synthesis to cellular energy supply. *Proc Natl Acad Sci U S A* **106,** 17781-17786.

Howie D, Waldmann H and Cobbold S. (2014). Nutrient Sensing via mTOR in T Cells Maintains a Tolerogenic Microenvironment. *Front Immunol* **5,** 409.

Huang J and Manning BD. (2009). A complex interplay between Akt, TSC2 and the two mTOR complexes. *Biochem Soc Trans* **37,** 217-222.

Hubert V, Peschel A, Langer B, Gröger M, Rees A and Kain R. (2016). LAMP-2 is required for incorporating syntaxin-17 into autophagosomes and for their fusion with lysosomes. *Biol Open* **5,** 1516-1529.

Hurley, J.H. and Schulman, B.A. (2014) Atomistic Autophagy: The Structures of Cellular Self-Digestion. Cell, 157, 300-311.

Husser D, Cannom DS, Bhandari AK, Stridh M, Sörnmo L, Olsson SB & Bollmann A. (2007). Electrocardiographic characteristics of fibrillatory waves in new-onset atrial fibrillation. Europace 9, 638-642

Hylek EM, Go AS, Chang Y, Jensvold NG, Henault LE, Selby JV and Singer DE. (2003). Effect of intensity of oral anticoagulation on stroke severity and mortality in atrial fibrillation. *N Engl J Med* **349,** 1019-1026.

Iacobas DA, Fan C, Iacobas S and Haddad GG. (2008). Integrated transcriptomic response to cardiac chronic hypoxia: translation regulators and response to stress in cell survival. *Funct Integr Genomics* **8,** 265-275.

Ikonomov OC, Sbrissa D, Foti M, Carpentier JL and Shisheva A. (2003). PIKfyve controls fluid phase endocytosis but not recycling/degradation of endocytosed receptors or sorting of procathepsin D by regulating multivesicular body morphogenesis. *Mol Biol Cell* **14,** 4581-4591.

Im YJ, Wollert T, Boura E and Hurley JH. (2009). Structure and function of the ESCRT-II-III interface in multivesicular body biogenesis. *Dev Cell* **17,** 234-243.

Inoki K, Zhu T and Guan KL. (2003). TSC2 mediates cellular energy response to control cell growth and survival. *Cell* **115,** 577-590.

Inpanathan S and Botelho RJ. (2019). The Lysosome Signaling Platform: Adapting With the Times. *Front Cell Dev Biol* **7,** 113.

Itoh T and Takenawa T. (2002). Phosphoinositide-binding domains: Functional units for temporal and spatial regulation of intracellular signalling. *Cell Signal* **14,** 733-743.

Iwasaki YK, Nishida K, Kato T and Nattel S. (2011). Atrial fibrillation pathophysiology: implications for management. *Circulation* **124,** 2264-2274.

Iyer-Bierhoff A, Krogh N, Tessarz P, Ruppert T, Nielsen H and Grummt I. (2018). SIRT7-Dependent Deacetylation of Fibrillarin Controls Histone H2A Methylation and rRNA Synthesis during the Cell Cycle. *Cell Rep* **25,** 2946-2954.e2945.

Janku F, Yap TA & Meric-Bernstam F. (2018). Targeting the PI3K pathway in cancer: are we making headway? *Nat Rev Clin Oncol* **15,** 273-291.

Jalife J and Kaur K. (2015). Atrial remodeling, fibrosis, and atrial fibrillation. *Trends Cardiovasc Med* **25,** 475-484.

Jang EJ, Kim SC, Lee JH, Lee JR, Kim IK, Baek SY and Kim YW. (2018). Fucoxanthin, the constituent of Laminaria japonica, triggers AMPK-mediated cytoprotection and autophagy in hepatocytes under oxidative stress. *BMC Complement Altern Med* **18,** 97.

January CT, Wann LS, Alpert JS, Calkins H, Cigarroa JE, Cleveland JC, Conti JB, Ellinor PT, Ezekowitz MD, Field ME, Murray KT, Sacco RL, Stevenson WG, Tchou PJ, Tracy CM, Yancy CW and Guidelines ACoCAHATFoP. (2014). 2014 AHA/ACC/HRS guideline for the management of patients with atrial fibrillation: a report of the American College of Cardiology/American Heart Association Task Force on Practice Guidelines and the Heart Rhythm Society. *J Am Coll Cardiol* **64,** e1-76.

Jefferies JL, Blaxall BC, Robbins J and Towbin JA. (2017). *Cardioskeletal Myopathies in Children and Young Adults*. Elsevier Inc.

Jeganathan J, Saraf R, Mahmood F, Pal A, Bhasin MK, Huang T, Mittel A, Knio Z, Simons R, Khabbaz K, Senthilnathan V, Liu D, Sellke F and Matyal R. (2017). Mitochondrial Dysfunction in Atrial Tissue of Patients Developing Postoperative Atrial Fibrillation. *Ann Thorac Surg* **104,** 1547-1555.

Jensen J, Rustad PI, Kolnes AJ and Lai YC. (2011). The role of skeletal muscle glycogen breakdown for regulation of insulin sensitivity by exercise. *Front Physiol* **2,** 112.

Jeon SM. (2016). Regulation and function of AMPK in physiology and diseases. *Exp Mol Med* **48,** e245.

Jewell JL, Russell RC and Guan KL. (2013). Amino acid signalling upstream of mTOR. *Nat Rev Mol Cell Biol* **14,** 133-139.

Jiang F, Zhang Y and Dusting GJ. (2011). NADPH oxidase-mediated redox signaling: roles in cellular stress response, stress tolerance, and tissue repair. *Pharmacol Rev* **63,** 218-242.

Jiang L, Wang M, Lin S, Jian R, Li X, Chan J, Dong G, Fang H, Robinson AE, Snyder MP and Consortium G. (2020). A Quantitative Proteome Map of the Human Body. *Cell* **183,** 269-283.e219.

Johnson JN, Tester DJ, Perry J, Salisbury BA, Reed CR and Ackerman MJ. (2008). Prevalence of early-onset atrial fibrillation in congenital long QT syndrome. *Heart Rhythm* **5,** 704-709.

Johnson JN & Ackerman MJ. (2009). QTc: how long is too long? Br J Sports Med 43, 657-662.

K D and A R. (2014). Reactive oxygen species (ROS) and response of antioxidants as ROS-scavengers during environmental stress in plants. Frontiers Environmental Science.

Kalifa J, Maixent JM, Chalvidan T, Dalmasso C, Colin D, Cozma D, Laurent P, Deharo JC, Djiane P, Cozzone P & Bernard M. (2008). Energetic metabolism during acute stretch-related atrial fibrillation. Mol Cell Biochem 317, 69-75.

Kang J, Yu Y, Jeong S, Lee H, Heo HJ, Park JJ, Na HS, Ko DS and Kim YH. (2020). Prognostic role of high cathepsin D expression in breast cancer: a systematic review and meta-analysis. *Ther Adv Med Oncol* **12,** 1758835920927838.

Kanzaki M and Pessin JE. (2003). Insulin signaling: GLUT4 vesicles exit via the exocyst. *Curr Biol* **13,** R574-576.

Katoh Y, Ritter B, Gaffry T, Blondeau F, Höning S and McPherson PS. (2009). The clavesin family, neuron-specific lipid- and clathrin-binding Sec14 proteins regulating lysosomal morphology. *J Biol Chem* **284,** 27646-27654.

Katz and M A. (2010). *Physiology of the Heart*. Wolters Kluwer Health.

Kaushik S & Cuervo AM. (2012). Chaperone-mediated autophagy: a unique way to enter the lysosome world. *Trends Cell Biol* **22,** 407-417.

Kaushik S and Cuervo AM. (2016). AMPK-dependent phosphorylation of lipid droplet protein PLIN2 triggers its degradation by CMA. *Autophagy* **12,** 432-438.

Kessler A, Tomas E, Immler D, Meyer HE, Zorzano A and Eckel J. (2000). Rab11 is associated with GLUT4-containing vesicles and redistributes in response to insulin. *Diabetologia* **43,** 1518-1527.

Kim E, Goraksha-Hicks P, Li L, Neufeld TP and Guan KL. (2008). Regulation of TORC1 by Rag GTPases in nutrient response. *Nat Cell Biol* **10,** 935-945.

Kim MS, Pinto SM, Getnet D, Nirujogi RS, Manda SS, Chaerkady R, Madugundu AK, Kelkar DS, Isserlin R, Jain S, Thomas JK, Muthusamy B, Leal-Rojas P, Kumar P, Sahasrabuddhe NA, Balakrishnan L, Advani J, George B, Renuse S, Selvan LD, Patil AH, Nanjappa V, Radhakrishnan A, Prasad S, Subbannayya T, Raju R, Kumar M, Sreenivasamurthy SK, Marimuthu A, Sathe GJ, Chavan S, Datta KK, Subbannayya Y, Sahu A, Yelamanchi SD, Jayaram S, Rajagopalan P, Sharma J, Murthy KR, Syed N, Goel R, Khan AA, Ahmad S, Dey G, Mudgal K, Chatterjee A, Huang TC, Zhong J, Wu X, Shaw PG, Freed D, Zahari MS, Mukherjee KK, Shankar S, Mahadevan A, Lam H, Mitchell CJ, Shankar SK, Satishchandra P, Schroeder JT, Sirdeshmukh R, Maitra A, Leach SD, Drake CG, Halushka MK, Prasad TS, Hruban RH, Kerr CL, Bader GD, Iacobuzio-Donahue CA, Gowda H and Pandey A. (2014). A draft map of the human proteome. *Nature* **509,** 575-581.

Kim YC and Guan KL. (2015). mTOR: a pharmacologic target for autophagy regulation. *J Clin Invest* **125,** 25-32.

Kim YC, Park HW, Sciarretta S, Mo JS, Jewell JL, Russell RC, Wu X, Sadoshima J and Guan KL. (2014). Rag GTPases are cardioprotective by regulating lysosomal function. *Nat Commun* **5,** 4241.

Kim YM, Guzik TJ, Zhang YH, Zhang MH, Kattach H, Ratnatunga C, Pillai R, Channon KM and Casadei B. (2005). A myocardial Nox2 containing NAD(P)H oxidase contributes to oxidative stress in human atrial fibrillation. *Circ Res* **97,** 629-636.

King JB, Azadani PN, Suksaranjit P, Bress AP, Witt DM, Han FT, Chelu MG, Silver MA, Biskupiak J, Wilson BD, Morris AK, Kholmovski EG and Marrouche N. (2017). Left Atrial Fibrosis and Risk of Cerebrovascular and Cardiovascular Events in Patients With Atrial Fibrillation. *J Am Coll Cardiol* **70,** 1311-1321.

Kinnear NP, Wyatt CN, Clark JH, Calcraft PJ, Fleischer S, Jeyakumar LH, Nixon GF and Evans AM. (2008). Lysosomes co-localize with ryanodine receptor subtype 3 to form a trigger zone for calcium signalling by NAADP in rat pulmonary arterial smooth muscle. *Cell Calcium* **44,** 190-201.

Kirchhof P, Benussi S, Kotecha D, Ahlsson A, Atar D, Casadei B, Castella M, Diener HC, Heidbuchel H, Hendriks J, Hindricks G, Manolis AS, Oldgren J, Popescu BA, Schotten U, Van Putte B, Vardas P, Agewall S, Camm J, Baron Esquivias G, Budts W, Carerj S, Casselman F, Coca A, De Caterina R, Deftereos S, Dobrev D, Ferro JM, Filippatos G, Fitzsimons D, Gorenek B, Guenoun M, Hohnloser SH, Kolh P, Lip GY, Manolis A, McMurray J, Ponikowski P, Rosenhek R, Ruschitzka F, Savelieva I, Sharma S, Suwalski P, Tamargo JL, Taylor CJ, Van Gelder IC, Voors AA, Windecker S, Zamorano JL and Zeppenfeld K. (2016). 2016 ESC Guidelines for the management of atrial fibrillation developed in collaboration with EACTS. *Eur J Cardiothorac Surg* **50,** e1-e88.

Kishnani PS, Steiner RD, Bali D, Berger K, Byrne BJ, Case LE, Case L, Crowley JF, Downs S, Howell RR, Kravitz RM, Mackey J, Marsden D, Martins AM, Millington DS, Nicolino M, O'Grady G, Patterson MC, Rapoport DM, Slonim A, Spencer CT, Tifft CJ, Watson MS and Disease AWGoMoP. (2006). Pompe disease diagnosis and management guideline. *Genet Med* **8,** 267-288.

Kleikers PW, Wingler K, Hermans JJ, Diebold I, Altenhöfer S, Radermacher KA, Janssen B, Görlach A and Schmidt HH. (2012). NADPH oxidases as a source of oxidative stress and molecular target in ischemia/reperfusion injury. *J Mol Med (Berl)* **90,** 1391-1406.

Klip A. (2009). The many ways to regulate glucose transporter 4. *Appl Physiol Nutr Metab* **34,** 481-487.

Klip A, Schertzer JD, Bilan PJ, Thong F and Antonescu C. (2009). Regulation of glucose transporter 4 traffic by energy deprivation from mitochondrial compromise. *Acta Physiol (Oxf)* **196,** 27-35.

Ko D, Benson MD, Ngo D, Yang Q, Larson MG, Wang TJ, Trinquart L, McManus DD, Lubitz SA, Ellinor PT, Vasan RS, Gerszten RE, Benjamin EJ and Lin H. (2019). Proteomics Profiling and Risk of New-Onset Atrial Fibrillation: Framingham Heart Study. *J Am Heart Assoc* **8,** e010976.

Kobayashi S, Zhao F, Kobayashi T, Hagiwara M, Kaminaris A, Li C, Cai F, Huang Y and Liang Q. (2020). Hyperglycemia-induced cardiomyocyte death is mediated by lysosomal membrane injury and aberrant expression of cathepsin D. *Biochem Biophys Res Commun* **523,** 239-245.

Koerdt SN and Gerke V. (2017). Annexin A2 is involved in Ca. *Biochim Biophys Acta Mol Cell Res* **1864,** 1046-1053.

Kohl P and Camelliti P. (2007). Cardiac myocyte-nonmyocyte electrotonic coupling: implications for ventricular arrhythmogenesis. *Heart Rhythm* **4,** 233-235.

Korshunov SS, Skulachev VP and Starkov AA. (1997). High protonic potential actuates a mechanism of production of reactive oxygen species in mitochondria. *FEBS Lett* **416,** 15-18.

Koshy S, Alizadeh P, Timchenko LT and Beeton C. (2010). Quantitative measurement of GLUT4 translocation to the plasma membrane by flow cytometry. *J Vis Exp*.

Kostin S, Pool L, Elsässer A, Hein S, Drexler HC, Arnon E, Hayakawa Y, Zimmermann R, Bauer E, Klövekorn WP and Schaper J. (2003). Myocytes die by multiple mechanisms in failing human hearts. *Circ Res* **92,** 715-724.

Kotadia I, Whitaker J, Roney C, Niederer S, O'Neill M, Bishop M and Wright M. (2020). Anisotropic Cardiac Conduction. *Arrhythm Electrophysiol Rev* **9,** 202-210.

Kottkamp H, Bender R and Berg J. (2015). Catheter ablation of atrial fibrillation: how to modify the substrate? *J Am Coll Cardiol* **65,** 196-206.

Kottmeier CA and Wheat MW. (1967). Myocardial lysosomes in experimental atrial septal defects. *Circ Res* **21,** 17-24.

Kounakis K, Chaniotakis M, Markaki M and Tavernarakis N. (2019). Emerging Roles of Lipophagy in Health and Disease. *Front Cell Dev Biol* **7,** 185.

Kraft C, Peter M and Hofmann K. (2010). Selective autophagy: ubiquitin-mediated recognition and beyond. *Nat Cell Biol* **12,** 836-841.

Krajcovic M, Krishna S, Akkari L, Joyce JA & Overholtzer M. (2013). mTOR regulates phagosome and entotic vacuole fission. Mol Biol Cell 24, 3736-3745.

Kraniou Y, Cameron-Smith D, Misso M, Collier G and Hargreaves M. (2000). Effects of exercise on GLUT-4 and glycogenin gene expression in human skeletal muscle. *J Appl Physiol (1985)* **88,** 794-796.

Krebs JE, Goldstein ES and Kilpatrick ST. (2017). *Lewin's GENES XII*. Jones and Bartlett Learning.

Krishna S, Palm W, Lee Y, Yang W, Bandyopadhyay U, Xu H, Florey O, Thompson CB & Overholtzer M. (2016). PIKfyve Regulates Vacuole Maturation and Nutrient Recovery following Engulfment. Dev Cell 38, 536-547.

Laing JG and Beyer EC. (1995). The gap junction protein connexin43 is degraded via the ubiquitin proteasome pathway. *J Biol Chem* **270,** 26399-26403.

Laing JG, Tadros PN, Westphale EM and Beyer EC. (1997). Degradation of connexin43 gap junctions involves both the proteasome and the lysosome. *Exp Cell Res* **236,** 482-492.

Laird DW. (2006). Life cycle of connexins in health and disease. *Biochem J* **394,** 527-543.

Laird DW. (2010). The gap junction proteome and its relationship to disease. *Trends Cell Biol* **20,** 92-101.

Lamberti G, de Araújo ME and Huber LA. (2015). Isolation of Macrophage Early and Late Endosomes by Latex Bead Internalization and Density Gradient Centrifugation. *Cold Spring Harb Protoc* **2015,** pdb.prot083451.

Langston RG and Cookson MR. (2020). Pathways of protein synthesis and degradation in PD pathogenesis. *Prog Brain Res* **252,** 217-270.

Larance M and Lamond AI. (2015). Multidimensional proteomics for cell biology. *Nat Rev Mol Cell Biol* **16,** 269-280.

Laurent-Matha V, Derocq D, Prébois C, Katunuma N and Liaudet-Coopman E. (2006). Processing of human cathepsin D is independent of its catalytic function and auto-activation: involvement of cathepsins L and B. *J Biochem* **139,** 363-371.

Lavandero S, Troncoso R, Rothermel BA, Martinet W, Sadoshima J, Hill JA (2013) Cardiovascular autophagy: concepts, controversies, and perspectives. Autophagy 9, 1455–1466

Lee HC. (2013). Electrical remodeling in human atrial fibrillation. *Chin Med J (Engl)* **126,** 2380-2383.

Lee HC and Aarhus R. (1995). A derivative of NADP mobilizes calcium stores insensitive to inositol trisphosphate and cyclic ADP-ribose. *J Biol Chem* **270,** 2152-2157.

Lee HC and Aarhus R. (2000). Functional visualization of the separate but interacting calcium stores sensitive to NAADP and cyclic ADP-ribose. *J Cell Sci* **113 Pt 24,** 4413-4420.

Lefkir Y, de Chassey B, Dubois A, Bogdanovic A, Brady RJ, Destaing O, Bruckert F, O'Halloran TJ, Cosson P and Letourneur F. (2003). The AP-1 clathrin-adaptor is required for lysosomal enzymes sorting and biogenesis of the contractile vacuole complex in Dictyostelium cells. *Mol Biol Cell* **14,** 1835-1851.

Lenders M & Brand E. (2021). Fabry Disease: The Current Treatment Landscape. Drugs 81, 635-645.

Letronne F, Laumet G, Ayral AM, Chapuis J, Demiautte F, Laga M, Vandenberghe ME, Malmanche N, Leroux F, Eysert F, Sottejeau Y, Chami L, Flaig A, Bauer C, Dourlen P, Lesaffre M, Delay C, Huot L, Dumont J, Werkmeister E, Lafont F, Mendes T, Hansmannel F, Dermaut B, Deprez B, Hérard AS, Dhenain M, Souedet N, Pasquier F, Tulasne D, Berr C, Hauw JJ, Lemoine Y, Amouyel P, Mann D, Déprez R, Checler F, Hot D, Delzescaux T, Gevaert K and Lambert JC. (2016). ADAM30 Downregulates APP-Linked Defects Through Cathepsin D Activation in Alzheimer's Disease. *EBioMedicine* **9,** 278-292.

Levin R, Grinstein S, Canton J (2016) The life cycle of phagosomes: formation,maturation, and resolution.Immunol Rev 273:156–179.

Lewin B, Krebs J, Kilpatrick ST and Goldstein ES. (2011). *Lewin's GENES X*. Jones and Bartlett Learning.

Li CM, Park JH, He X, Levy B, Chen F, Arai K, Adler DA, Disteche CM, Koch J, Sandhoff K and Schuchman EH. (1999). The human acid ceramidase gene (ASAH): structure, chromosomal location, mutation analysis, and expression. *Genomics* **62,** 223-231.

Li JY, He Y, Ke HH, Jin Y, Jiang ZY and Zhong GQ. (2017). Plasma oxidative stress and inflammatory biomarkers are associated with the sizes of the left atrium and pulmonary vein in atrial fibrillation patients. *Clin Cardiol* **40,** 89-94.

Li M, Khambu B, Zhang H, Kang JH, Chen X, Chen D, Vollmer L, Liu PQ, Vogt A and Yin XM. (2013). Suppression of lysosome function induces autophagy via a feedback down-regulation of MTOR complex 1 (MTORC1) activity. *J Biol Chem* **288,** 35769-35780.

Li Y and Chen Y. (2019). AMPK and Autophagy. *Adv Exp Med Biol* **1206,** 85-108.

Li Z, Agrawal V, Ramratnam M, Sharma RK, D'Auria S, Sincoular A, Jakubiak M, Music ML, Kutschke WJ, Huang XN, Gifford L & Ahmad F. (2019). Cardiac sodium-dependent glucose cotransporter 1 is a novel mediator of ischaemia/reperfusion injury. Cardiovasc Res 115, 1646-1658.

Liang K-H. (2013). *Bioinformatics for Biomedical Science and Clinical Applications*. Woodhead publishing.

Liang X, Zhang Q, Wang X, Yuan M, Zhang Y, Xu Z, Li G and Liu T. (2018). Reactive oxygen species mediated oxidative stress links diabetes and atrial fibrillation. *Mol Med Rep* **17,** 4933-4940.

Lima TdC, Santos DdO & Lotufo CMdC (2022). Chapter 13 - ATP-sensitive potassium channels in pain and analgesia The Neurobiology, Physiology, and Psychology of Pain. In The Neurobiology, Physiology, and Psychology of Pain. Academic Press.

Linhart A and Elliott PM. (2007). The heart in Anderson-Fabry disease and other lysosomal storage disorders. *Heart* **93,** 528-535.

Litwack G. (2018). Chapter 7 - Glycogen and Glycogenolysis. In Human Biochemistry, pp. 161-181. Academic Press.

Liu J, Aoki M, Illa I, Wu C, Fardeau M, Angelini C, Serrano C, Urtizberea JA, Hentati F, Hamida MB, Bohlega S, Culper EJ, Amato AA, Bossie K, Oeltjen J, Bejaoui K, McKenna-Yasek D, Hosler BA, Schurr E, Arahata K, de Jong PJ and Brown

RH. (1998). Dysferlin, a novel skeletal muscle gene, is mutated in Miyoshi myopathy and limb girdle muscular dystrophy. *Nat Genet* **20,** 31-36.

Liu S-s. (1998). *Oxidative Stress in Cancer, AIDS, and Neurodegenerative Diseases*. CRC Press.

Lomako J, Lomako WM and Whelan WJ. (2004). Glycogenin: the primer for mammalian and yeast glycogen synthesis. *Biochim Biophys Acta* **1673,** 45-55.

Long J, Wang Y, Liu XC, Yu M, Wang YL, Huang X and Zhao M. (2017). [Effect of oxidative stress on myocardial apoptosis, endoplasmic reticulum stress and apoptosis factor in suckling mouse atria myocardium]. *Zhongguo Ying Yong Sheng Li Xue Za Zhi* **33,** 185-188.

Long YC and Zierath JR. (2006). AMP-activated protein kinase signaling in metabolic regulation. *J Clin Invest* **116,** 1776-1783.

Longatti A, Lamb CA, Razi M, Yoshimura S, Barr FA and Tooze SA. (2012). TBC1D14 regulates autophagosome formation via Rab11- and ULK1-positive recycling endosomes. *J Cell Biol* **197,** 659-675.

Lovrić J. (2011). *Introducing proteomics from concepts to sample preparation , mass spectrometry and data analysis*. A John Wiley and Sons.

Lumb RA and Bulleid NJ. (2002). Is protein disulfide isomerase a redox-dependent molecular chaperone? *EMBO J* **21,** 6763-6770.

Lundholm K and Scherstén T. (1975). Leucine incorporation into proteins and cathepsin -D activity in human skeletal muscles. The influence of the age of the subject. *Exp Gerontol* **10,** 155-159.

Lusis AJ. (2000). Atherosclerosis. *Nature* **407,** 233-241.

Lübke T, Lobel P and Sleat DE. (2009). Proteomics of the lysosome. *Biochim Biophys Acta* **1793,** 625-635.

Ma L, Chen Z, Erdjument-Bromage H, Tempst P and Pandolfi PP. (2005). Phosphorylation and functional inactivation of TSC2 by Erk implications for tuberous sclerosis and cancer pathogenesis. *Cell* **121,** 179-193.

Macgregor AT, Rakovic S, Galione A and Terrar DA. (2007). Dual effects of cyclic ADP-ribose on sarcoplasmic reticulum Ca2+ release and storage in cardiac myocytes isolated from guinea-pig and rat ventricle. *Cell Calcium* **41,** 537-546.

Maesen B, Zeemering S, Afonso C, Eckstein J, Burton RA, van Hunnik A, Stuckey DJ, Tyler D, Maessen J, Grau V, Verheule S, Kohl P and Schotten U. (2013). Rearrangement of atrial bundle architecture and consequent changes in anisotropy of conduction constitute the 3-dimensional substrate for atrial fibrillation. *Circ Arrhythm Electrophysiol* **6,** 967-975.

Magnani F and Mattevi A. (2019). Structure and mechanisms of ROS generation by NADPH oxidases. *Curr Opin Struct Biol* **59,** 91-97.

Mahadevan V. (2014). Anatomy of the heart. Surgery (Oxford) 33, 47-51.

Maity S, Rajkumar A, Matai L, Bhat A, Ghosh A, Agam G, Kaur S, Bhatt NR, Mukhopadhyay A, Sengupta S and Chakraborty K. (2016). Oxidative Homeostasis Regulates the Response to Reductive Endoplasmic Reticulum Stress through Translation Control. *Cell Rep* **16,** 851-865.

Mantini G, Vallés AM, Le Large TYS, Capula M, Funel N, Pham TV, Piersma SR, Kazemier G, Bijlsma MF, Giovannetti E and Jimenez CR. (2020). Co-expression analysis of pancreatic cancer proteome reveals biology and prognostic biomarkers. *Cell Oncol (Dordr)* **43,** 1147-1159.

Marnett LJ. (2000). Oxyradicals and DNA damage. *Carcinogenesis* **21,** 361-370.

Martin-Serrano J, Yarovoy A, Perez-Caballero D, Bieniasz PD and Yaravoy A. (2003). Divergent retroviral late-budding domains recruit vacuolar protein sorting factors by using alternative adaptor proteins. *Proc Natl Acad Sci U S A* **100,** 12414-12419.

Maslov LN, Khaliulin IG, Pei J and Zhang I. (2011). [Role of heat shock proteins in the mechanism of cardioprotective effect of transient hyperthermia and delayed preconditioning]. *Patol Fiziol Eksp Ter***,** 64-73.

Mason FE, Pronto JRD, Alhussini K, Maack C & Voigt N. (2020). Cellular and mitochondrial mechanisms of atrial fibrillation. Basic Res Cardiol 115, 72.

Masters TA, Tumbarello DA, Chibalina MV and Buss F. (2017). MYO6 Regulates Spatial Organization of Signaling Endosomes Driving AKT Activation and Actin Dynamics. *Cell Rep* **19,** 2088-2101.

Mathieu C, Li de la Sierra-Gallay I, Duval R, Xu X, Cocaign A, Léger T, Woffendin G, Camadro JM, Etchebest C, Haouz A, Dupret JM and Rodrigues-Lima F. (2016). Insights into Brain Glycogen Metabolism: The Structure Of Human Brain Glycogen Phosphorylase. *J Biol Chem* **291,** 18072-18083.

Matsushima S, Kuroda J, Ago T, Zhai P, Ikeda Y, Oka S, Fong GH, Tian R and Sadoshima J. (2013). Broad suppression of NADPH oxidase activity exacerbates ischemia/reperfusion injury through inadvertent downregulation of hypoxia-inducible factor-1α and upregulation of peroxisome proliferator-activated receptor-α. *Circ Res* **112,** 1135-1149.

Mattiazzi A and Kranias EG. (2011). CaMKII regulation of phospholamban and SR Ca2+ load. *Heart Rhythm* **8,** 784-787.

Maulik SK and Kumar S. (2012). Oxidative stress and cardiac hypertrophy: a review. *Toxicol Mech Methods* **22,** 359-366.

Mauri P, Petretto A, Cuccabita D, Basilico F, Silvestre DD, Levreri I and Melioli G. (2008). *Current Pharmaceutical Analysis*, vol. 4. Bentham Science Publisher.

McEwan DG, Popovic D, Gubas A, Terawaki S, Suzuki H, Stadel D, Coxon FP, Miranda de Stegmann D, Bhogaraju S, Maddi K, Kirchof A, Gatti E, Helfrich MH, Wakatsuki S, Behrends C, Pierre P and Dikic I. (2015). PLEKHM1 regulates autophagosome-lysosome fusion through HOPS complex and LC3/GABARAP proteins. *Mol Cell* **57,** 39-54.

Menon S, Dibble CC, Talbott G, Hoxhaj G, Valvezan AJ, Takahashi H, Cantley LC and Manning BD. (2014). Spatial control of the TSC complex integrates insulin and nutrient regulation of mTORC1 at the lysosome. *Cell* **156,** 771-785.

Mezghrani A, Courageot J, Mani JC, Pugniere M, Bastiani P and Miquelis R. (2000). Protein-disulfide isomerase (PDI) in FRTL5 cells. pH-dependent thyroglobulin/PDI interactions determine a novel PDI function in the post-endoplasmic reticulum of thyrocytes. *J Biol Chem* **275,** 1920-1929.

Mi H, Ebert D, Muruganujan A, Mills C, Albou LP, Mushayamaha T and Thomas PD. (2021). PANTHER version 16: a revised family classification, tree-based classification tool, enhancer regions and extensive API. *Nucleic Acids Res* **49,** D394-D403.

Mighiu AS, Recalde A, Ziberna K, Carnicer R, Tomek J, Bub G, Brewer AC, Verheule S, Shah AM, Simon JN and Casadei B. (2021). Inducibility, but not stability, of atrial fibrillation is increased by NOX2 overexpression in mice. *Cardiovasc Res* **117,** 2354-2364.

Mihaylova MM and Shaw RJ. (2011). The AMPK signalling pathway coordinates cell growth, autophagy and metabolism. *Nat Cell Biol* **13,** 1016-1023.

Miller SL. (1953). A production of amino acids under possible primitive earth conditions. *Science* **117,** 528-529.

Mindell JA. (2012). Lysosomal acidification mechanisms. *Annu Rev Physiol* **74,** 69-86.

Minokoshi Y, Toda C and Okamoto S. (2012). Regulatory role of leptin in glucose and lipid metabolism in skeletal muscle. *Indian J Endocrinol Metab* **16,** S562-568.

Mirzaei H and Regnier F. (2008). Protein:protein aggregation induced by protein oxidation. *J Chromatogr B Analyt Technol Biomed Life Sci* **873,** 8-14.

Mizushima N, Levine B, Cuervo AM & Klionsky DJ. (2008). Autophagy fights disease through cellular self-digestion. Nature 451, 1069-1075.

Moheimani F, Kim CH, Rahmanto AS, van Reyk DM and Davies MJ. (2012). Inhibition of lysosomal function in macrophages incubated with elevated glucose concentrations: a potential contributory factor in diabetes-associated atherosclerosis. *Atherosclerosis* **223,** 144-151.

Mor A and Philips MR. (2006). Compartmentalized Ras/MAPK signaling. *Annu Rev Immunol* **24,** 771-800.

Morreau H, Galjart NJ, Gillemans N, Willemsen R, van der Horst GT and d'Azzo A. (1989). Alternative splicing of beta-galactosidase mRNA generates the classic lysosomal enzyme and a beta-galactosidase-related protein. *J Biol Chem* **264,** 20655-20663.

Morris JH, Apeltsin L, Newman AM, Baumbach J, Wittkop T, Su G, Bader GD and Ferrin TE. (2011). clusterMaker: a multi-algorithm clustering plugin for Cytoscape. *BMC Bioinformatics* **12,** 436.

Mukhopadhyay A, Funato K and Stahl PD. (1997). Rab7 regulates transport from early to late endocytic compartments in Xenopus oocytes. *J Biol Chem* **272,** 13055-13059.

Murayama A, Ohmori K, Fujimura A, Minami H, Yasuzawa-Tanaka K, Kuroda T, Oie S, Daitoku H, Okuwaki M, Nagata K, Fukamizu A, Kimura K, Shimizu T and Yanagisawa J. (2008). Epigenetic control of rDNA loci in response to intracellular energy status. *Cell* **133,** 627-639.

Murphy MP. (2009). How mitochondria produce reactive oxygen species. *Biochem J* **417,** 1-13.

Murray AK. (2020). The Release of a Soluble Glycosylated Protein from Glycogen by Recombinant Lysosomal α-Glucosidase (rhGAA) In Vitro and Its Presence in Serum In Vivo. *Biomolecules* **10**.

Murugan AK. (2019). mTOR: Role in cancer, metastasis and drug resistance. *Semin Cancer Biol* **59,** 92-111.

Nair V, Belanger EC and Veinot JP. (2019). Lysosomal storage disorders affecting the heart: a review. *Cardiovasc Pathol* **39,** 12-24.

Nakai A, Yamaguchi O, Takeda T, Higuchi Y, Hikoso S, Taniike M, Omiya S, Mizote I, Matsumura Y, Asahi M, Nishida K, Hori M, Mizushima N and Otsu K. (2007). The role of autophagy in cardiomyocytes in the basal state and in response to hemodynamic stress. *Nat Med* **13,** 619-624.

Nakatsu F, Hase K and Ohno H. (2014). The Role of the Clathrin Adaptor AP-1: Polarized Sorting and Beyond. *Membranes (Basel)* **4,** 747-763.

Nakatsu F and Ohno H. (2003). Adaptor protein complexes as the key regulators of protein sorting in the post-Golgi network. *Cell Struct Funct* **28,** 419-429.

Nattel S. (2017). Molecular and Cellular Mechanisms of Atrial Fibrosis in Atrial Fibrillation. *JACC Clin Electrophysiol* **3,** 425-435.

Nattel S and Dobrev D. (2016). Electrophysiological and molecular mechanisms of paroxysmal atrial fibrillation. *Nat Rev Cardiol* **13,** 575-590.

Nebel M, Schwoerer AP, Warszta D, Siebrands CC, Limbrock AC, Swarbrick JM, Fliegert R, Weber K, Bruhn S, Hohenegger M, Geisler A, Herich L, Schlegel S, Carrier L, Eschenhagen T, Potter BV, Ehmke H and Guse AH. (2013). Nicotinic acid adenine dinucleotide phosphate (NAADP)-mediated calcium signaling and arrhythmias in the heart evoked by β-adrenergic stimulation. *J Biol Chem* **288,** 16017-16030.

Nelson DL and Cox M. (2008). *Lehninger Principles of Biochemistry*. W.H.Freeman and Co Ltd.

Nesheiwat Z, Goyal A & Jagtap M. (2022). Atrial Fibrillation In: StatPearls. Treasure Island (FL): StatPearls Publishing.

Nguyen DH and D'haeseleer P. (2006). Deciphering principles of transcription regulation in eukaryotic genomes. *Mol Syst Biol* **2,** 2006.0012.

Nguyen ON, Grimm C, Schneider LS, Chao YK, Atzberger C, Bartel K, Watermann A, Ulrich M, Mayr D, Wahl-Schott C, Biel M and Vollmar AM. (2017). Two-Pore Channel Function Is Crucial for the Migration of Invasive Cancer Cells. *Cancer Res* **77,** 1427-1438.

Nicklin P, Bergman P, Zhang B, Triantafellow E, Wang H, Nyfeler B, Yang H, Hild M, Kung C, Wilson C, Myer VE, MacKeigan JP, Porter JA, Wang YK, Cantley LC, Finan PM and Murphy LO. (2009). Bidirectional transport of amino acids regulates mTOR and autophagy. *Cell* **136,** 521-534.

NIH. (2012). LiverTox: Clinical and Research Information on Drug-Induced Liver Injury.

Nolte H, MacVicar TD, Tellkamp F and Krüger M. (2018). Instant Clue: A Software Suite for Interactive Data Visualization and Analysis. *Sci Rep* **8,** 12648.

Ouyang H, Ali YO, Ravichandran M, Dong A, Qiu W, MacKenzie F, Dhe-Paganon S, Arrowsmith CH and Zhai RG. (2012). Protein aggregates are recruited to aggresome by histone deacetylase 6 via unanchored ubiquitin C termini. *J Biol Chem* **287,** 2317-2327.

Ozcan C, Battaglia E, Young R and Suzuki G. (2015). LKB1 knockout mouse develops spontaneous atrial fibrillation and provides mechanistic insights into human disease process. *J Am Heart Assoc* **4,** e001733.

Ozcan C, Li Z, Kim G, Jeevanandam V and Uriel N. (2019). Molecular Mechanism of the Association Between Atrial Fibrillation and Heart Failure Includes Energy Metabolic Dysregulation Due to Mitochondrial Dysfunction. *J Card Fail* **25,** 911-920.

Ozkayar N, Piskinpasa S, Akyel F, Turgut D, Bulut M, Turhan T and Dede F. (2015). Relation between serum cathepsin D levels and endothelial dysfunction in patients with chronic kidney disease. *Nefrologia* **35,** 72-79.

Pakay JL, Withers PC, Hobbs AA and Guppy M. (2002). In vivo downregulation of protein synthesis in the snail Helix apersa during estivation. *Am J Physiol Regul Integr Comp Physiol* **283,** R197-204.

Papathanasiou KA, Giotaki SG, Vrachatis DA, Siasos G, Lambadiari V, Iliodromitis KE, Kossyvakis C, Kaoukis A, Raisakis K, Deftereos G, Papaioannou TG, Giannopoulos G, Avramides D and Deftereos SG. (2021). Molecular Insights in Atrial Fibrillation Pathogenesis and Therapeutics: A Narrative Review. *Diagnostics (Basel)* **11**.

Papp Z, Czuriga D, Balogh L, Balogh Á and Borbély A. (2012). How cardiomyocytes make the heart old. *Curr Pharm Biotechnol* **13,** 2515-2521.

Patil M, Saheera S, Dubey PK, Kahn-Krell A, Kumar Govindappa P, Singh S, Tousif S, Zhang Q, Lal H, Zhang J, Qin G and Krishnamurthy P. (2021). Novel Mechanisms of Exosome-Mediated Phagocytosis of Dead Cells in Injured Heart. *Circ Res* **129,** 1006-1020.

Paul and Iaizzo A. (2015). *Handbook of Cardiac Anatomy, Physiology, and Devices*. Springer, Cham.

Pehmøller C, Treebak JT, Birk JB, Chen S, Mackintosh C, Hardie DG, Richter EA and Wojtaszewski JF. (2009). Genetic disruption of AMPK signaling abolishes both contraction- and insulin-stimulated TBC1D1 phosphorylation and 14-3-3 binding in mouse skeletal muscle. *Am J Physiol Endocrinol Metab* **297,** E665-675.

Perez-Lugones A, McMahon JT, Ratliff NB, Saliba WI, Schweikert RA, Marrouche NF, Saad EB, Navia JL, McCarthy PM, Tchou P, Gillinov AM and Natale A. (2003). Evidence of specialized conduction cells in human pulmonary veins of patients with atrial fibrillation. *J Cardiovasc Electrophysiol* **14,** 803-809.

Persson PB and Mueller M. (2015). Transcription. *Acta Physiol (Oxf)* **215,** 159-160.

Peters TJ and De Duve C. (1974). Lysosomes of the arterial wall. II. Subcellular fractionation of aortic cells from rabbits with experimantal atheroma. *Exp Mol Pathol* **20,** 228-256.

Phaniendra A, Jestadi DB and Periyasamy L. (2015). Free radicals: properties, sources, targets, and their implication in various diseases. *Indian J Clin Biochem* **30,** 11-26.

Piehl M, Lehmann C, Gumpert A, Denizot JP, Segretain D and Falk MM. (2007). Internalization of large double-membrane intercellular vesicles by a clathrin-dependent endocytic process. *Mol Biol Cell* **18,** 337-347.

Pinto AR, Ilinykh A, Ivey MJ, Kuwabara JT, D'Antoni ML, Debuque R, Chandran A, Wang L, Arora K, Rosenthal NA and Tallquist MD. (2016). Revisiting Cardiac Cellular Composition. *Circ Res* **118,** 400-409.

Pizzale S, Gollob MH, Gow R and Birnie DH. (2008). Sudden death in a young man with catecholaminergic polymorphic ventricular tachycardia and paroxysmal atrial fibrillation. *J Cardiovasc Electrophysiol* **19,** 1319-1321.

Pons M, Grewal T, Rius E, Schnitgerhans T, Jäckle S and Enrich C. (2001). Evidence for the Involvement of annexin 6 in the trafficking between the endocytic compartment and lysosomes. *Exp Cell Res* **269,** 13-22.

Pool L, Wijdeveld LFJM, de Groot NMS and Brundel BJJM. (2021). The Role of Mitochondrial Dysfunction in Atrial Fibrillation: Translation to Druggable Target and Biomarker Discovery. *Int J Mol Sci* **22**.

Porstmann T, Santos CR, Griffiths B, Cully M, Wu M, Leevers S, Griffiths JR, Chung YL and Schulze A. (2008). SREBP activity is regulated by mTORC1 and contributes to Akt-dependent cell growth. *Cell Metab* **8,** 224-236.

Potter LR, Abbey-Hosch S and Dickey DM. (2006). Natriuretic peptides, their receptors, and cyclic guanosine monophosphate-dependent signaling functions. *Endocr Rev* **27,** 47-72.

Powers ET and Balch WE. (2013). Diversity in the origins of proteostasis networks--a driver for protein function in evolution. *Nat Rev Mol Cell Biol* **14,** 237-248.

Press B, Feng Y, Hoflack B and Wandinger-Ness A. (1998). Mutant Rab7 causes the accumulation of cathepsin D and cation-independent mannose 6-phosphate receptor in an early endocytic compartment. *J Cell Biol* **140,** 1075-1089.

Primeau JO, Armanious GP, Fisher MLE & Young HS. (2018). The SarcoEndoplasmic Reticulum Calcium ATPase. In Membrane Protein Complexes: Structure and Function, ed. Harris JR & Boekema EJ, pp. 229-258. Springer Singapore, Singapore.

Pullen N, Dennis PB, Andjelkovic M, Dufner A, Kozma SC, Hemmings BA and Thomas G. (1998). Phosphorylation and activation of p70s6k by PDK1. *Science* **279,** 707-710.

Pullikuth AK and Catling AD. (2007). Scaffold mediated regulation of MAPK signaling and cytoskeletal dynamics: a perspective. *Cell Signal* **19,** 1621-1632.

Qi X, Pohl NM, Loesch M, Hou S, Li R, Qin JZ, Cuenda A and Chen G. (2007). p38alpha antagonizes p38gamma activity through c-Jun-dependent ubiquitin-proteasome pathways in regulating Ras transformation and stress response. *J Biol Chem* **282,** 31398-31408.

Qin Z-H. (2019). *Autophagy: Biology and Diseases*. Springer.

Rabanal-Ruiz Y, Otten EG and Korolchuk VI. (2017). mTORC1 as the main gateway to autophagy. *Essays Biochem* **61,** 565-584.

Ramos KS and Brundel BJJM. (2020). DNA Damage, an Innocent Bystander in Atrial Fibrillation and Other Cardiovascular Diseases? *Front Cardiovasc Med* **7,** 67.

Redeker V. (2010). Mass spectrometry analysis of C-terminal posttranslational modifications of tubulins. *Methods Cell Biol* **95,** 77-103.

Rennison JH, Li L, Lin CR, Lovano BS, Castel L, Wass SY, Cantlay CC, McHale M, Gillinov AM, Mehra R, Willard BB, Smith JD, Chung MK, Barnard J & Van Wagoner DR. (2021). Atrial fibrillation rhythm is associated with marked changes in metabolic and myofibrillar protein expression in left atrial appendage. Pflugers Arch 473, 461-475.

Richter JD and Sonenberg N. (2005). Regulation of cap-dependent translation by eIF4E inhibitory proteins. *Nature* **433,** 477-480.

Rinné S, Kiper AK, Schmidt C, Ortiz-Bonnin B, Zwiener S, Seebohm G and Decher N. (2017). Stress-Kinase Regulation of TASK-1 and TASK-3. *Cell Physiol Biochem* **44,** 1024-1037.

Riquelme G, Llanos P, Tischner E, Neil J and Campos B. (2004). Annexin 6 modulates the maxi-chloride channel of the apical membrane of syncytiotrophoblast isolated from human placenta. *J Biol Chem* **279,** 50601-50608.

Roberts AJ, Kon T, Knight PJ, Sutoh K and Burgess SA. (2013). Functions and mechanics of dynein motor proteins. *Nat Rev Mol Cell Biol* **14,** 713-726.

Roberts RA, Laskin DL, Smith CV, Robertson FM, Allen EM, Doorn JA and Slikker W. (2009). Nitrative and oxidative stress in toxicology and disease. *Toxicol Sci* **112,** 4-16.

Rogalla T, Ehrnsperger M, Preville X, Kotlyarov A, Lutsch G, Ducasse C, Paul C, Wieske M, Arrigo AP, Buchner J and Gaestel M. (1999). Regulation of Hsp27 oligomerization, chaperone function, and protective activity against oxidative stress/tumor necrosis factor alpha by phosphorylation. *J Biol Chem* **274,** 18947-18956.

Roig-Zamboni V, Cobucci-Ponzano B, Iacono R, Ferrara MC, Germany S, Bourne Y, Parenti G, Moracci M and Sulzenbacher G. (2017). Structure of human lysosomal acid α-glucosidase-a guide for the treatment of Pompe disease. *Nat Commun* **8,** 1111.

Roselli C, Chaffin MD, Weng LC, Aeschbacher S, Ahlberg G, Albert CM, Almgren P, Alonso A, Anderson CD, Aragam KG, Arking DE, Barnard J, Bartz TM, Benjamin EJ, Bihlmeyer NA, Bis JC, Bloom HL, Boerwinkle E, Bottinger EB, Brody JA, Calkins H, Campbell A, Cappola TP, Carlquist J, Chasman DI, Chen LY, Chen YI, Choi EK, Choi SH, Christophersen IE, Chung MK, Cole JW, Conen D, Cook J, Crijns HJ, Cutler MJ, Damrauer SM, Daniels BR, Darbar D, Delgado G, Denny JC, Dichgans M, Dörr M, Dudink EA, Dudley SC, Esa N, Esko T, Eskola M, Fatkin D, Felix SB, Ford I, Franco OH, Geelhoed B, Grewal RP, Gudnason V, Guo X, Gupta N, Gustafsson S, Gutmann R, Hamsten A, Harris TB, Hayward C, Heckbert SR, Hernesniemi J, Hocking LJ, Hofman A, Horimoto ARVR, Huang J, Huang PL, Huffman J, Ingelsson E, Ipek EG, Ito K, Jimenez-Conde J, Johnson R, Jukema JW, Kääb S, Kähönen M, Kamatani Y, Kane JP, Kastrati A, Kathiresan S, Katschnig-Winter P, Kavousi M, Kessler T, Kietselaer BL, Kirchhof P, Kleber ME, Knight S, Krieger JE, Kubo M, Launer LJ, Laurikka J, Lehtimäki T, Leineweber K, Lemaitre RN, Li M, Lim HE, Lin HJ, Lin H, Lind L, Lindgren CM, Lokki ML, London B, Loos RJF, Low SK, Lu Y, Lyytikäinen LP, Macfarlane PW, Magnusson PK, Mahajan A, Malik R, Mansur AJ, Marcus GM, Margolin L, Margulies KB, März W, McManus DD, Melander O, Mohanty S, Montgomery JA, Morley MP, Morris AP, Müller-Nurasyid M, Natale A, Nazarian S, Neumann B, Newton-Cheh C, Niemeijer MN, Nikus K, Nilsson P, Noordam R, Oellers H, Olesen MS, Orho-Melander M, Padmanabhan S, Pak HN, Paré G, Pedersen NL, Pera J, Pereira A, Porteous D, Psaty BM, Pulit SL, Pullinger CR, Rader DJ, Refsgaard L, Ribasés M, Ridker PM, Rienstra M, Risch L, Roden DM, Rosand J, Rosenberg MA, Rost N, Rotter JI, Saba S, Sandhu RK, Schnabel RB, Schramm K, Schunkert H, Schurman C, Scott SA, Seppälä I, Shaffer C, Shah S, Shalaby AA, Shim J, Shoemaker MB, Siland JE, Sinisalo J, Sinner MF, Slowik A, Smith AV, Smith BH, Smith JG, Smith JD, Smith NL, Soliman EZ, Sotoodehnia N, Stricker BH, Sun A, Sun H, Svendsen JH, Tanaka T, Tanriverdi K, Taylor KD, Teder-Laving M, Teumer A, Thériault S, Trompet S, Tucker NR, Tveit A, Uitterlinden AG, Van Der Harst P, Van Gelder IC, Van Wagoner DR, Verweij N, Vlachopoulou E, Völker U, Wang B, Weeke PE, Weijs B, Weiss R, Weiss S, Wells QS, Wiggins KL, Wong JA, Woo D, Worrall BB, Yang PS, Yao J, Yoneda ZT, Zeller T, Zeng L, Lubitz SA, Lunetta KL and Ellinor PT. (2018). Multi-ethnic genome-wide association study for atrial fibrillation. *Nat Genet* **50,** 1225-1233.

Rubi L, Gawali VS, Kubista H, Todt H, Hilber K and Koenig X. (2015). Proper Voltage-Dependent Ion Channel Function in Dysferlin-Deficient Cardiomyocytes. *Cell Physiol Biochem* **36,** 1049-1058.

Rudenok MM, Alieva AK, Nikolaev MA, Kolacheva AA, Ugryumov MV, Pchelina SN, Slominsky PA and Shadrina MI. (2019). [Possible Involvement of Genes Related to Lysosomal Storage Disorders in the Pathogenesis of Parkinson's Disease]. *Mol Biol (Mosk)* **53,** 28-36.

Ruigómez A, Johansson S, Wallander MA and García Rodríguez LA. (2002). Risk of mortality in a cohort of patients newly diagnosed with chronic atrial fibrillation. *BMC Cardiovasc Disord* **2,** 5.

Russo A and Russo G. (2017). Ribosomal Proteins Control or Bypass p53 during Nucleolar Stress. *Int J Mol Sci* **18**.

Sabath N, Levy-Adam F, Younis A, Rozales K, Meller A, Hadar S, Soueid-Baumgarten S and Shalgi R. (2020). Cellular proteostasis decline in human senescence. *Proc Natl Acad Sci U S A* **117,** 31902-31913.

Saftig P and Klumperman J. (2009). Lysosome biogenesis and lysosomal membrane proteins: trafficking meets function. *Nat Rev Mol Cell Biol* **10,** 623-635.

Samuthpongtorn C, Jereerat T and Suwanwela NC. (2021). Stroke risk factors, subtypes and outcome in elderly Thai patients. *BMC Neurol* **21,** 322.

Sancak Y, Peterson TR, Shaul YD, Lindquist RA, Thoreen CC, Bar-Peled L and Sabatini DM. (2008). The Rag GTPases bind raptor and mediate amino acid signaling to mTORC1. *Science* **320,** 1496-1501.

Sarbassov DD, Ali SM and Sabatini DM. (2005). Growing roles for the mTOR pathway. *Curr Opin Cell Biol* **17,** 596-603.

Schröder B, Wrocklage C, Pan C, Jäger R, Kösters B, Schäfer H, Elsässer HP, Mann M and Hasilik A. (2007). Integral and associated lysosomal membrane proteins. *Traffic* **8,** 1676-1686.

Schröder BA, Wrocklage C, Hasilik A and Saftig P. (2010). The proteome of lysosomes. *Proteomics* **10,** 4053-4076.

Schröder K, Weissmann N and Brandes RP. (2017). Organizers and activators: Cytosolic Nox proteins impacting on vascular function. *Free Radic Biol Med* **109,** 22-32.

Schulze RJ, Drižytė K, Casey CA and McNiven MA. (2017). Hepatic Lipophagy: New Insights into Autophagic Catabolism of Lipid Droplets in the Liver. *Hepatol Commun* **1,** 359-369.

Schüttler D, Bapat A, Kääb S, Lee K, Tomsits P, Clauss S and Hucker WJ. (2020). Animal Models of Atrial Fibrillation. *Circ Res* **127,** 91-110.

Sciarretta S, Forte M, Frati G and Sadoshima J. (2018). New Insights Into the Role of mTOR Signaling in the Cardiovascular System. *Circ Res* **122,** 489-505.

Seddon M, Looi YH and Shah AM. (2007). Oxidative stress and redox signalling in cardiac hypertrophy and heart failure. *Heart* **93,** 903-907.

Segretain D and Falk MM. (2004). Regulation of connexin biosynthesis, assembly, gap junction formation, and removal. *Biochim Biophys Acta* **1662,** 3-21.

Seo AY, Lau PW, Feliciano D, Sengupta P, Gros MAL, Cinquin B, Larabell CA and Lippincott-Schwartz J. (2017). AMPK and vacuole-associated Atg14p orchestrate μ-lipophagy for energy production and long-term survival under glucose starvation. *Elife* **6**.

Sestili P and Fimognari C. (2015). Cytotoxic and Antitumor Activity of Sulforaphane: The Role of Reactive Oxygen Species. *Biomed Res Int* **2015,** 402386.

Sevier CS and Kaiser CA. (2002). Formation and transfer of disulphide bonds in living cells. *Nat Rev Mol Cell Biol* **3,** 836-847.

Sha QQ, Dai XX, Dang Y, Tang F, Liu J, Zhang YL and Fan HY. (2017). A MAPK cascade couples maternal mRNA translation and degradation to meiotic cell cycle progression in mouse oocytes. *Development* **144,** 452-463.

Shannon P, Markiel A, Ozier O, Baliga NS, Wang JT, Ramage D, Amin N, Schwikowski B and Ideker T. (2003). Cytoscape: a software environment for integrated models of biomolecular interaction networks. *Genome Res* **13,** 2498-2504.

Shen K, Tu T, Yuan Z, Yi J, Zhou Y, Liao X, Liu Q and Zhou X. (2017). DNA methylation dysregulations in valvular atrial fibrillation. *Clin Cardiol* **40,** 686-691.

Shi KH, Tao H, Yang JJ, Wu JX, Xu SS and Zhan HY. (2013). Role of microRNAs in atrial fibrillation: new insights and perspectives. *Cell Signal* **25,** 2079-2084.

Shi Y, Xia YY, Wang L, Liu R, Khoo KS and Feng ZW. (2012). Neural cell adhesion molecule modulates mesenchymal stromal cell migration via activation of MAPK/ERK signaling. *Exp Cell Res* **318,** 2257-2267.

Shingu Y, Takada S, Yokota T, Shirakawa R, Yamada A, Ooka T, Katoh H, Kubota S & Matsui Y. (2020). Correlation between increased atrial expression of genes related to fatty acid metabolism and autophagy in patients with chronic atrial fibrillation. PLoS One 15, e0224713.

Siitari H, H K and T K. (2004). Proteomics: Challenges and Possibilities in Finland. Tekes.

Simard JC, Girard D and Tessier PA. (2010). Induction of neutrophil degranulation by S100A9 via a MAPK-dependent mechanism. *J Leukoc Biol* **87,** 905-914.

Simon JN, Vrellaku B, Monterisi S, Chu SM, Rawlings N, Lomas O, Marchal GA, Waithe D, Syeda F, Gajendragadkar PR, Jayaram R, Sayeed R, Channon KM, Fabritz L, Swietach P, Zaccolo M, Eaton P and Casadei B. (2021). Oxidation of Protein Kinase A Regulatory Subunit PKARIα Protects Against Myocardial

Ischemia-Reperfusion Injury by Inhibiting Lysosomal-Triggered Calcium Release. *Circulation* **143,** 449-465.

Singh U and Jialal I. (2006). Oxidative stress and atherosclerosis. *Pathophysiology* **13,** 129-142.

Sirokmány G, Szidonya L, Káldi K, Gáborik Z, Ligeti E and Geiszt M. (2006). Sec14 homology domain targets p50RhoGAP to endosomes and provides a link between Rab and Rho GTPases. *J Biol Chem* **281,** 6096-6105.

Skrinjar P, Schwarz M, Lexmüller S, Mechtler TP, Zeyda M, Greber-Platzer S, Trometer J, Kasper DC and Mikula H. (2018). Rapid and Modular Assembly of Click Substrates To Assay Enzyme Activity in the Newborn Screening of Lysosomal Storage Disorders. *ACS Cent Sci* **4,** 1688-1696.

Sleat DE, Della Valle MC, Zheng H, Moore DF and Lobel P. (2008). The mannose 6-phosphate glycoprotein proteome. *J Proteome Res* **7,** 3010-3021.

Song S, Zhang R, Mo B, Chen L, Liu L, Yu Y, Cao W, Fang G, Wan Y, Gu Y, Wang Y, Li Y and Wang Q. (2019). EZH2 as a novel therapeutic target for atrial fibrosis and atrial fibrillation. *J Mol Cell Cardiol* **135,** 119-133.

Song Q, Meng B, Xu H & Mao Z. (2020). The emerging roles of vacuolar-type ATPase-dependent Lysosomal acidification in neurodegenerative diseases. Transl Neurodegener 9, 17.

Spies D and Ciaudo C. (2015). Dynamics in Transcriptomics: Advancements in RNA-seq Time Course and Downstream Analysis. *Comput Struct Biotechnol J* **13,** 469-477.

Spronk HMH, Padro T, Siland JE, Prochaska JH, Winters J, van der Wal AC, Posthuma JJ, Lowe G, d'Alessandro E, Wenzel P, Coenen DM, Reitsma PH, Ruf W, van Gorp RH, Koenen RR, Vajen T, Alshaikh NA, Wolberg AS, Macrae FL, Asquith N, Heemskerk J, Heinzmann A, Moorlag M, Mackman N, van der Meijden P, Meijers JCM, Heestermans M, Renné T, Dólleman S, Chayouâ W, Ariëns RAS, Baaten CC, Nagy M, Kuliopulos A, Posma JJ, Harrison P, Vries

MJ, Crijns HJGM, Dudink EAMP, Buller HR, Henskens YMC, Själander A, Zwaveling S, Erküner O, Eikelboom JW, Gulpen A, Peeters FECM, Douxfils J, Olie RH, Baglin T, Leader A, Schotten U, Scaf B, van Beusekom HMM, Mosnier LO, van der Vorm L, Declerck P, Visser M, Dippel DWJ, Strijbis VJ, Pertiwi K, Ten Cate-Hoek AJ and Ten Cate H. (2018). Atherothrombosis and Thromboembolism: Position Paper from the Second Maastricht Consensus Conference on Thrombosis. *Thromb Haemost* **118,** 229-250.

Stadtman ER and Levine RL. (2000). Protein oxidation. *Ann N Y Acad Sci* **899,** 191-208.

Stillitano F, Lonardo G, Zicha S, Varro A, Cerbai E, Mugelli A and Nattel S. (2008). Molecular basis of funny current (If) in normal and failing human heart. *J Mol Cell Cardiol* **45,** 289-299.

Strous GJ and van Kerkhof P. (2002). The ubiquitin-proteasome pathway and the regulation of growth hormone receptor availability. *Mol Cell Endocrinol* **197,** 143-151.

Sulke N, Sayers F, Lip GY and fibrillation GDGftNcgftmoa. (2007). Rhythm control and cardioversion. *Heart* **93,** 29-34.

Surawicz B & Knilans TK. (2008). Chapter 1 - Normal Electrocardiogram: Origin and Description Chou's Electrocardiography in Clinical Practice. W.B. Saunders.

Surya SL, Long MJC, Urul DA, Zhao Y, Mercer EJ, Elsaid IM, Evans T and Aye Y. (2018). Cardiovascular Small Heat Shock Protein HSPB7 Is a Kinetically Privileged Reactive Electrophilic Species (RES) Sensor. *ACS Chem Biol* **13,** 1824-1831.

Suski J, Lebiedzinska M, Bonora M, Pinton P, Duszynski J and Wieckowski MR. (2018). Relation Between Mitochondrial Membrane Potential and ROS Formation. *Methods Mol Biol* **1782,** 357-381.

Sygitowicz G, Maciejak-Jastrzębska A and Sitkiewicz D. (2021). A Review of the Molecular Mechanisms Underlying Cardiac Fibrosis and Atrial Fibrillation. *J Clin Med* **10**.

Sánchez-Lanzas R and Castaño JG. (2018). Inhibitors of lysosomal function or serum starvation in control or LAMP2 deficient cells do not modify the cellular levels of Parkinson disease-associated DJ-1/PARK 7 protein. *PLoS One* **13,** e0201152.

Sühling M, Wolke C, Scharf C and Lendeckel U. (2018). Proteomics and transcriptomics in atrial fibrillation. *Herzschrittmacherther Elektrophysiol* **29,** 70-75.

Taji B, Chan ADC & Shirmohammadi S. (2018). False Alarm Reduction in Atrial Fibrillation Detection Using Deep Belief Networks. IEEE Transactions on Instrumentation and Measurement 67, 1124-1131

Takemasu S, Nigorikawa K, Yamada M, Tsurumi G, Kofuji S, Takasuga S and Hazeki K. (2019). Phosphorylation of TMEM55B by Erk/MAPK regulates lysosomal positioning. *J Biochem* **166,** 175-185.

Takenouchi T, Sekiyama K, Tsukimoto M, Iwamaru Y, Fujita M, Sugama S, Kitani H and Hashimoto M. (2015). *Autophagy: Cancer, Other Pathologies, Inflammation, Immunity, Infection, and Aging*. Academic Press.

Tan EHN and Tang BL. (2019). Rab7a and Mitophagosome Formation. *Cells* **8**.

Tanaka N, Kyuuma M and Sugamura K. (2008). Endosomal sorting complex required for transport proteins in cancer pathogenesis, vesicular transport, and non-endosomal functions. *Cancer Sci* **99,** 1293-1303.

Tang X, Luo YX, Chen HZ and Liu DP. (2014). Mitochondria, endothelial cell function, and vascular diseases. *Front Physiol* **5,** 175.

Tang Y, Nyengaard JR, Andersen JB, Baandrup U and Gundersen HJ. (2009). The application of stereological methods for estimating structural parameters in the human heart. *Anat Rec (Hoboken)* **292,** 1630-1647.

Tarnopolsky MA. (2018). Myopathies Related to Glycogen Metabolism Disorders. *Neurotherapeutics* **15,** 915-927.

Terman A, Dalen H, Eaton JW, Neuzil J and Brunk UT. (2003). Mitochondrial recycling and aging of cardiac myocytes: the role of autophagocytosis. *Exp Gerontol* **38,** 863-876.

Terman A, Kurz T, Gustafsson B and Brunk UT. (2008). The involvement of lysosomes in myocardial aging and disease. *Curr Cardiol Rev* **4,** 107-115.

Terrar DA, Wilson CM, Graham SG, Bryant SM and Heath BM. (2007). Comparison of guinea-pig ventricular myocytes and dog Purkinje fibres for in vitro assessment of drug-induced delayed repolarization. *J Pharmacol Toxicol Methods* **56,** 171-185.

Tharkeshwar AK, Trekker J, Vermeire W, Pauwels J, Sannerud R, Priestman DA, Te Vruchte D, Vints K, Baatsen P, Decuypere JP, Lu H, Martin S, Vangheluwe P, Swinnen JV, Lagae L, Impens F, Platt FM, Gevaert K and Annaert W. (2017). A novel approach to analyze lysosomal dysfunctions through subcellular proteomics and lipidomics: the case of NPC1 deficiency. *Sci Rep* **7,** 41408.

Thomas AM, Cabrera CP, Finlay M, Lall K, Nobles M, Schilling RJ, Wood K, Mein CA, Barnes MR, Munroe PB and Tinker A. (2019). Differentially expressed genes for atrial fibrillation identified by RNA sequencing from paired human left and right atrial appendages. *Physiol Genomics* **51,** 323-332.

Thong PS, Selley M and Watt F. (1996). Elemental changes in atherosclerotic lesions using nuclear microscopy. *Cell Mol Biol (Noisy-le-grand)* **42,** 103-110.

Thottath J, Vellarikkal SK, Jayarajan R, Verma A, Manamel M, Singh A, Rajendran VR, Sivasubbu S and Scaria V. (2019). A novel cathepsin D mutation in 2 siblings with late infantile neuronal ceroid lipofuscinosis. *Neurol Genet* **5,** e302.

Towbin H, Staehelin T and Gordon J. (1979). Electrophoretic transfer of proteins from polyacrylamide gels to nitrocellulose sheets: procedure and some applications. *Proc Natl Acad Sci U S A* **76,** 4350-4354.

Traurig HH. (1976). Lysosomal acid hydrolase activities in the lungs of fetal, neonatal, adult, and senile mice. *Gerontology* **22,** 419-427.

Tsai CW, Tsai CF, Lin KH, Chen WJ, Lin MS, Hsieh CC and Lin CC. (2020). An investigation of the correlation between the S-glutathionylated GAPDH levels in blood and Alzheimer's disease progression. *PLoS One* **15,** e0233289.

Tyanova S, Temu T, Sinitcyn P, Carlson A, Hein MY, Geiger T, Mann M and Cox J. (2016). The Perseus computational platform for comprehensive analysis of (prote)omics data. *Nat Methods* **13,** 731-740.

Upadhyay M, Samal J, Kandpal M, Singh OV and Vivekanandan P. (2013). The Warburg effect: insights from the past decade. *Pharmacol Ther* **137,** 318-330.

Urbé S, Huber LA, Zerial M, Tooze SA and Parton RG. (1993). Rab11, a small GTPase associated with both constitutive and regulated secretory pathways in PC12 cells. *FEBS Lett* **334,** 175-182.

van den Hout HM, Hop W, van Diggelen OP, Smeitink JA, Smit GP, Poll-The BT, Bakker HD, Loonen MC, de Klerk JB, Reuser AJ and van der Ploeg AT. (2003). The natural course of infantile Pompe's disease: 20 original cases compared with 133 cases from the literature. *Pediatrics* **112,** 332-340.

Van den Hout JM, Reuser AJ, de Klerk JB, Arts WF, Smeitink JA and Van der Ploeg AT. (2001). Enzyme therapy for pompe disease with recombinant human alpha-glucosidase from rabbit milk. *J Inherit Metab Dis* **24,** 266-274.

van der Velden HM, Ausma J, Rook MB, Hellemons AJ, van Veen TA, Allessie MA and Jongsma HJ. (2000). Gap junctional remodeling in relation to stabilization of atrial fibrillation in the goat. *Cardiovasc Res* **46,** 476-486.

Van Gelder IC, Rienstra M, Crijns HJ and Olshansky B. (2016). Rate control in atrial fibrillation. *Lancet* **388,** 818-828.

van Hunnik A, Zeemering S, Podziemski P, Simons J, Gatta G, Hannink L, Maesen B, Kuiper M, Verheule S and Schotten U. (2018). Stationary Atrial Fibrillation Properties in the Goat Do Not Entail Stable or Recurrent Conduction Patterns. *Front Physiol* **9,** 947.

Vanlandingham PA and Ceresa BP. (2009). Rab7 regulates late endocytic trafficking downstream of multivesicular body biogenesis and cargo sequestration. *J Biol Chem* **284,** 12110-12124.

Vargas E, Podder V, Alicia M and Sepulveda C. (2021). *Physiology, Glucose Transporter Type 4*. StatPearls publishing.

Vemu A, Atherton J, Spector JO, Moores CA and Roll-Mecak A. (2017). Tubulin isoform composition tunes microtubule dynamics. *Mol Biol Cell* **28,** 3564-3572.

Verheule S, Tuyls E, Gharaviri A, Hulsmans S, van Hunnik A, Kuiper M, Serroyen J, Zeemering S, Kuijpers NH and Schotten U. (2013). Loss of continuity in the thin epicardial layer because of endomysial fibrosis increases the complexity of atrial fibrillatory conduction. *Circ Arrhythm Electrophysiol* **6,** 202-211.

Verheule S, Tuyls E, van Hunnik A, Kuiper M, Schotten U and Allessie M. (2010). Fibrillatory conduction in the atrial free walls of goats in persistent and permanent atrial fibrillation. *Circ Arrhythm Electrophysiol* **3,** 590-599.

Vetter, F. J., and McCulloch, A. D. (1998). Three-dimensional analysis of regional cardiac function: a model of rabbit ventricular anatomy. Prog. Biophys. Mol. Biol. 69: 157-183.

Vichaiwong K, Purohit S, An D, Toyoda T, Jessen N, Hirshman MF and Goodyear LJ. (2010). Contraction regulates site-specific phosphorylation of TBC1D1 in skeletal muscle. *Biochem J* **431,** 311-320.

Victorino J, Alvarez-Franco A and Manzanares M. (2021). Functional genomics and epigenomics of atrial fibrillation. *J Mol Cell Cardiol* **157,** 45-55.

Vit O and Petrak J. (2017). Integral membrane proteins in proteomics. How to break open the black box? *J Proteomics* **153,** 8-20.

Větvicka V, Vágner J, Baudys M, Tang J, Foundling SI and Fusek M. (1993). Human breast milk contains procathepsin D--detection by specific antibodies. *Biochem Mol Biol Int* **30,** 921-928.

Wakimoto H, Maguire CT, Kovoor P, Hammer PE, Gehrmann J, Triedman JK and Berul CI. (2001). Induction of atrial tachycardia and fibrillation in the mouse heart. *Cardiovasc Res* **50,** 463-473.

Walker MW and Lloyd-Evans E. (2015). A rapid method for the preparation of ultrapure, functional lysosomes using functionalized superparamagnetic iron oxide nanoparticles. *Methods Cell Biol* **126,** 21-43.

Wang C, Michener CM, Belinson JL, Vaziri S, Ganapathi R and Sengupta S. (2010). Role of the 18:1 lysophosphatidic acid-ovarian cancer immunoreactive antigen domain containing 1 (OCIAD1)-integrin axis in generating late-stage ovarian cancer. *Mol Cancer Ther* **9,** 1709-1718.

Wang X and Proud CG. (2006). The mTOR pathway in the control of protein synthesis. *Physiology (Bethesda)* **21,** 362-369.

Wang X and Robbins J. (2014). Proteasomal and lysosomal protein degradation and heart disease. *J Mol Cell Cardiol* **71,** 16-24.

Wang X, Zhang X, Dong XP, Samie M, Li X, Cheng X, Goschka A, Shen D, Zhou Y, Harlow J, Zhu MX, Clapham DE, Ren D and Xu H. (2012). TPC proteins are phosphoinositide- activated sodium-selective ion channels in endosomes and lysosomes. *Cell* **151,** 372-383.

Wang Y, Li C, Shi L, Chen X, Cui C, Huang J, Chen B, Hall DD, Pan Z, Lu M, Hong J, Song LS and Zhao S. (2020). Integrin β1D Deficiency-Mediated RyR2 Dysfunction Contributes to Catecholamine-Sensitive Ventricular Tachycardia in ARVC. *Circulation*.

Wang Y, Liang B, Lau WB, Du Y, Guo R, Yan Z, Gan L, Yan W, Zhao J, Gao E, Koch W and Ma XL. (2017). Restoring diabetes-induced autophagic flux arrest in ischemic/reperfused heart by ADIPOR (adiponectin receptor) activation involves both AMPK-dependent and AMPK-independent signaling. *Autophagy* **13,** 1855-1869.

Wang YK, Ma Z, Quinn DF and Fu EW. (2002). Inverse 15N-metabolic labeling/mass spectrometry for comparative proteomics and rapid identification of protein markers/targets. *Rapid Commun Mass Spectrom* **16,** 1389-1397.

Ward C, Martinez-Lopez N, Otten EG, Carroll B, Maetzel D, Singh R, Sarkar S and Korolchuk VI. (2016). Autophagy, lipophagy and lysosomal lipid storage disorders. *Biochim Biophys Acta* **1861,** 269-284.

Ward RJ, Zucca FA, Duyn JH, Crichton RR and Zecca L. (2014). The role of iron in brain ageing and neurodegenerative disorders. *Lancet Neurol* **13,** 1045-1060.

Wasmer K, Eckardt L and Breithardt G. (2017). Predisposing factors for atrial fibrillation in the elderly. *J Geriatr Cardiol* **14,** 179-184.

Watson RT and Pessin JE. (2007). GLUT4 translocation: the last 200 nanometers. *Cell Signal* **19,** 2209-2217.

Wei B, Wei H and Jin JP. (2015). Dysferlin deficiency blunts β-adrenergic-dependent lusitropic function of mouse heart. *J Physiol* **593,** 5127-5144.

Welz T, Wellbourne-Wood J and Kerkhoff E. (2014). Orchestration of cell surface proteins by Rab11. *Trends Cell Biol* **24,** 407-415.

Wheat MW. (1964). Lysosomes in human myocardium.

Wheat MW. (1965). Ultrastructure autoradiography and lysosome studies in myocardium. *J Mt Sinai Hosp N Y* **32,** 107-121.

Whitaker. (2010). Robert H. Whitaker, Anatomy of the heart,. *Medicine*

Volume 38, 333-335.

Whitaker M. (2006). Calcium at fertilization and in early development. *Physiol Rev* **86,** 25-88.

Wijesurendra RS and Casadei B. (2019). Mechanisms of atrial fibrillation. *Heart* **105,** 1860-1867.

Wijffels MC, Dorland R and Allessie MA. (1999). Pharmacologic cardioversion of chronic atrial fibrillation in the goat by class IA, IC, and III drugs: a comparison between hydroquinidine, cibenzoline, flecainide, and d-sotalol. *J Cardiovasc Electrophysiol* **10,** 178-193.

Wijffels MC, Kirchhof CJ, Dorland R and Allessie MA. (1995). Atrial fibrillation begets atrial fibrillation. A study in awake chronically instrumented goats. *Circulation* **92,** 1954-1968.

Wildenthal K and Decker RS. (1980). The role of lysosomes in the heart. *Adv Myocardiol* **2,** 349-358.

Wildenthal K, Decker RS, Poole AR and Dingle JT. (1977). Age-related alterations in cardiac lysosomes. *J Mol Cell Cardiol* **9,** 859-866.

Willstatter R and E B. (1929). The protoease of stomach lining. First essay on the enzymes of leukoctyes. Hoppe-Seylers Zeitschrift Fur Physiologische Chemie.

Wilson PD. (1972). Enzyme patterns in young and old mouse livers and lungs. *Gerontologia* **18,** 36-54.

Wolff DA and Pertoft H. (1972). The purification of lysosomes from HeLa cells by centrifugation in colloidal silica density gradients. *Biochim Biophys Acta* **286,** 197-204.

Wolinsky H, Capron L, Goldfischer S, Capron F, Coltoff-Schiller B and Kasak LE. (1978). Hydrolase activities in the rat aorta. II. Effects of hypertension alone and in combination with diabetes mellitus. *Circ Res* **42,** 831-839.

Woods A, Dickerson K, Heath R, Hong SP, Momcilovic M, Johnstone SR, Carlson M and Carling D. (2005). Ca2+/calmodulin-dependent protein kinase kinase-beta acts upstream of AMP-activated protein kinase in mammalian cells. *Cell Metab* **2,** 21-33.

Wright E, Scism-Bacon JL and Glass LC. (2006). Oxidative stress in type 2 diabetes: the role of fasting and postprandial glycaemia. *Int J Clin Pract* **60,** 308-314.

Wu K, Huang C, Shi X, Chen F, Xu YH, Pan YX, Luo Z and Liu X. (2016a). Role and mechanism of the AMPK pathway in waterborne Zn exposure influencing the hepatic energy metabolism of Synechogobius hasta. *Sci Rep* **6,** 38716.

Wu M, Gu J, Guo R, Huang Y and Yang M. (2016b). Structure of Mammalian Respiratory Supercomplex I. *Cell* **167,** 1598-1609.e1510.

Wu P, Yuan X, Li F, Zhang J, Zhu W, Wei M, Li J and Wang X. (2017). Myocardial Upregulation of Cathepsin D by Ischemic Heart Disease Promotes Autophagic Flux and Protects Against Cardiac Remodeling and Heart Failure. *Circ Heart Fail* **10**.

Wullschleger S, Loewith R and Hall MN. (2006). TOR signaling in growth and metabolism. *Cell* **124,** 471-484.

Wyse DG, Waldo AL, DiMarco JP, Domanski MJ, Rosenberg Y, Schron EB, Kellen JC, Greene HL, Mickel MC, Dalquist JE, Corley SD and Investigators AFF-uIoRMA. (2002). A comparison of rate control and rhythm control in patients with atrial fibrillation. *N Engl J Med* **347,** 1825-1833.

Xi Y and Cheng J. (2015). Dysfunction of the autonomic nervous system in atrial fibrillation. *J Thorac Dis* **7,** 193-198.

Xia G, Zhu T, Li X, Jin Y, Zhou J and Xiao J. (2018). ROS-mediated autophagy through the AMPK signaling pathway protects INS-1 cells from human islet amyloid polypeptide-induced cytotoxicity. *Mol Med Rep* **18,** 2744-2752.

Xia Z, Chen Y, Fan Q and Xue M. (2014). Oxidative stress-mediated reperfusion injury: mechanism and therapies. *Oxid Med Cell Longev* **2014,** 373081.

Xiao YF. (2011). Cardiac arrhythmia and heart failure: From bench to bedside. *J Geriatr Cardiol* **8,** 131-132.

Xie W, Santulli G, Reiken SR, Yuan Q, Osborne BW, Chen BX and Marks AR. (2015). Mitochondrial oxidative stress promotes atrial fibrillation. *Sci Rep* **5,** 11427.

Xu M, Li XX, Chen Y, Pitzer AL, Zhang Y and Li PL. (2014). Enhancement of dynein-mediated autophagosome trafficking and autophagy maturation by ROS in mouse coronary arterial myocytes. *J Cell Mol Med* **18,** 2165-2175.

Xu P and Derynck R. (2010). Direct activation of TACE-mediated ectodomain shedding by p38 MAP kinase regulates EGF receptor-dependent cell proliferation. *Mol Cell* **37,** 551-566.

Yacine A-S & Dacheng X. (2017). Principal Component Analysis of High Frequency Data. *Chicago Booth Research Paper*.

Yaguchi Y, Satoh H, Wakahara N, Katoh H, Uehara A, Terada H, Fujise Y and Hayashi H. (2003). Protective effects of hydrogen peroxide against ischemia/reperfusion injury in perfused rat hearts. *Circ J* **67,** 253-258.

Yamac AH, Sevgili E, Kucukbuzcu S, Nasifov M, Ismailoglu Z, Kilic E, Ercan C, Jafarov P, Uyarel H and Bacaksiz A. (2015). Role of cathepsin D activation in major adverse cardiovascular events and new-onset heart failure after STEMI. *Herz* **40,** 912-920.

Yamaguchi S, Katahira H, Ozawa S, Nakamichi Y, Tanaka T, Shimoyama T, Takahashi K, Yoshimoto K, Imaizumi MO, Nagamatsu S and Ishida H. (2005). Activators of AMP-activated protein kinase enhance GLUT4 translocation and its glucose transport activity in 3T3-L1 adipocytes. *Am J Physiol Endocrinol Metab* **289,** E643-649.

Yang Q and Guan KL. (2007). Expanding mTOR signaling. *Cell Res* **17,** 666-681.

Yeh YH, Wakili R, Qi XY, Chartier D, Boknik P, Kääb S, Ravens U, Coutu P, Dobrev D and Nattel S. (2008). Calcium-handling abnormalities underlying atrial arrhythmogenesis and contractile dysfunction in dogs with congestive heart failure. *Circ Arrhythm Electrophysiol* **1,** 93-102.

Yeung ML, Teng JLL, Jia L, Zhang C, Huang C, Cai JP, Zhou R, Chan KH, Zhao H, Zhu L, Siu KL, Fung SY, Yung S, Chan TM, To KK, Chan JF, Cai Z, Lau SKP, Chen Z, Jin DY, Woo PCY and Yuen KY. (2021). Soluble ACE2-mediated cell entry of SARS-CoV-2 via interaction with proteins related to the renin-angiotensin system. *Cell* **184,** 2212-2228.e2212.

Ylä-Herttuala S. (1999). Oxidized LDL and atherogenesis. *Ann N Y Acad Sci* **874,** 134-137.

Yosefy O, Sharon B, Yagil C, Shlapoberski M, Livoff A, Novitski I, Beeri R, Yagil Y and Yosefy C. (2021). Diabetes induces remodeling of the left atrial appendage independently of atrial fibrillation in a rodent model of type-2 diabetes. *Cardiovasc Diabetol* **20,** 149.

Yoshida M, Muneyuki E and Hisabori T. (2001). ATP synthase--a marvellous rotary engine of the cell. *Nat Rev Mol Cell Biol* **2,** 669-677.

You YH, Okada S, Ly S, Jandeleit-Dahm K, Barit D, Namikoshi T and Sharma K. (2013). Role of Nox2 in diabetic kidney disease. *Am J Physiol Renal Physiol* **304,** F840-848.

Youhotsky-Gore I and Pathmanathan K. (1968). Some comparative observations on the lysosomal status of muscle from young and old mice. *Exp Gerontol* **3,** 281-286.

Youn JY, Zhang J, Zhang Y, Chen H, Liu D, Ping P, Weiss JN and Cai H. (2013). Oxidative stress in atrial fibrillation: an emerging role of NADPH oxidase. *J Mol Cell Cardiol* **62,** 72-79.

Yu FPS, Amintas S, Levade T and Medin JA. (2018a). Acid ceramidase deficiency: Farber disease and SMA-PME. *Orphanet J Rare Dis* **13,** 121.

Yu L, Chen Y and Tooze SA. (2018b). Autophagy pathway: Cellular and molecular mechanisms. *Autophagy* **14,** 207-215.

Yu S & Melia TJ. (2017). The coordination of membrane fission and fusion at the end of autophagosome maturation. Curr Opin Cell Biol 47, 92-98.

Yuan Y, Meng L, Zhou Y and Lu N. (2017). Genetic polymorphism of angiotensin-converting enzyme and hypertrophic cardiomyopathy risk: A systematic review and meta-analysis. *Medicine (Baltimore)* **96,** e8639.

Zaidi N, Maurer A, Nieke S and Kalbacher H. (2008). Cathepsin D: a cellular roadmap. *Biochem Biophys Res Commun* **376,** 5-9.

Zeqiraj E, Filippi BM, Deak M, Alessi DR and van Aalten DM. (2009). Structure of the LKB1-STRAD-MO25 complex reveals an allosteric mechanism of kinase activation. *Science* **326,** 1707-1711.

Zhang H, Ma J, Tang K and Huang B. (2021). Beyond energy storage: roles of glycogen metabolism in health and disease. *FEBS J* **288,** 3772-3783.

Zhang J, Naslavsky N and Caplan S. (2012). EHDs meet the retromer: Complex regulation of retrograde transport. *Cell Logist* **2,** 161-165.

Zhang M, Chen L, Wang S and Wang T. (2009). Rab7: roles in membrane trafficking and disease. *Biosci Rep* **29,** 193-209.

Zhang M, Liu L, Lin X, Wang Y, Li Y, Guo Q, Li S, Sun Y, Tao X, Zhang D, Lv X, Zheng L and Ge L. (2020). A Translocation Pathway for Vesicle-Mediated Unconventional Protein Secretion. *Cell* **181,** 637-652.e615.

Zhao M and Klionsky DJ. (2011). AMPK-dependent phosphorylation of ULK1 induces autophagy. *Cell Metab* **13,** 119-120.

Zhao P, Tian D, Song G, Ming Q, Liu J, Shen J, Liu QH and Yang X. (2019). Neferine Promotes GLUT4 Expression and Fusion With the Plasma Membrane to Induce Glucose Uptake in L6 Cells. *Front Pharmacol* **10,** 999.

Zhao RZ, Jiang S, Zhang L and Yu ZB. (2019). Mitochondrial electron transport chain, ROS generation and uncoupling (Review). *Int J Mol Med* **44,** 3-15.

Zhao Y, Gu TX, Zhang GW, Liu HG and Wang C. (2013). Losartan affects the substrate for atrial fibrillation maintenance in a rabbit model. *Cardiovasc Pathol* **22,** 383-388.

Zhao Y, Hu X, Liu Y, Dong S, Wen Z, He W, Zhang S, Huang Q and Shi M. (2017). ROS signaling under metabolic stress: cross-talk between AMPK and AKT pathway. *Mol Cancer* **16,** 79.

Zhong X, Persaud L, Muharam H, Francis A, Das D, Aktas BH and Sauane M. (2018). Eukaryotic Translation Initiation Factor 4A Down-Regulation Mediates Interleukin-24-Induced Apoptosis through Inhibition of Translation. *Cancers (Basel)* **10**.

Zhou S, Chang CM, Wu TJ, Miyauchi Y, Okuyama Y, Park AM, Hamabe A, Omichi C, Hayashi H, Brodsky LA, Mandel WJ, Ting CT, Fishbein MC, Karagueuzian HS and Chen PS. (2002). Nonreentrant focal activations in pulmonary veins in canine model of sustained atrial fibrillation. *Am J Physiol Heart Circ Physiol* **283,** H1244-1252.

Zhou XY, van der Spoel A, Rottier R, Hale G, Willemsen R, Berry GT, Strisciuglio P, Morrone A, Zammarchi E, Andria G and d'Azzo A. (1996). Molecular and biochemical analysis of protective protein/cathepsin A mutations: correlation with clinical severity in galactosialidosis. *Hum Mol Genet* **5,** 1977-1987.

Zhu MX, Ma J, Parrington J, Calcraft PJ, Galione A and Evans AM. (2010). Calcium signaling via two-pore channels: local or global, that is the question. *Am J Physiol Cell Physiol* **298,** C430-441.

Zhu Y, Li X, Kyazike J, Zhou Q, Thurberg BL, Raben N, Mattaliano RJ and Cheng SH. (2004). Conjugation of mannose 6-phosphate-containing oligosaccharides to acid alpha-glucosidase improves the clearance of glycogen in pompe mice. *J Biol Chem* **279,** 50336-50341.

Zimmermann R, Strauss JG, Haemmerle G, Schoiswohl G, Birner-Gruenberger R, Riederer M, Lass A, Neuberger G, Eisenhaber F, Hermetter A and Zechner R. (2004). Fat mobilization in adipose tissue is promoted by adipose triglyceride lipase. *Science* **306,** 1383-1386.

Zirin J, Nieuwenhuis J and Perrimon N. (2013). Role of autophagy in glycogen breakdown and its relevance to chloroquine myopathy. *PLoS Biol* **11,** e1001708.

Zoni-Berisso M, Lercari F, Carazza T and Domenicucci S. (2014). Epidemiology of atrial fibrillation: European perspective. *Clin Epidemiol* **6,** 213-220.

Zulkefli KL, Houghton FJ, Gosavi P and Gleeson PA. (2019). A role for Rab11 in the homeostasis of the endosome-lysosomal pathway. *Exp Cell Res* **380,** 55-68.

Żwirowski S, Kłosowska A, Obuchowski I, Nillegoda NB, Piróg A, Ziętkiewicz S, Bukau B, Mogk A and Liberek K. (2017). Hsp70 displaces small heat shock proteins from aggregates to initiate protein refolding. *EMBO J* **36,** 783-796.

Webpage references

Jonas. (2021). Violin Plots for plotting multiple distributions. Access Year: 2021 Access Date: 07.24.2021 URL: www.mathworks.com

Heart disease atrial fibrillation. Access Year: 2021 Access Date: 21.08.2021 URL: www.cdc.gov

European Bioinformatics Institute (EMBL-EBI). Access Year: 2021 Access Date: 12.07.2021 URL: www.ebi.ac.uk

Medications for Arrhythmia. Access Year: 2021 Access Date: 24.07.2021 URL: www.heart.org

Health Topic Atrial Fibrillation. Access Year: 2021 Access Date: 04.08.2021 URL: www.nhlbi.nih.gov

Atrial fibrillation: diagnosis and management NICE guideline [NG196] Access Year: 2021 Access Date: 24.07.2021 URL: www.nice.org.uk

Reactome Pathway Database. Access Year: 2021 Access Date: 02.02.2021 URL: www.reactome.org

Appendix

Appendix 1

1.1 Key proteins identified in EL fraction of guinea pig atria

Protein	Gene Name/ UniprotKB	Protein function	Disease	Reference
Intracellular acidification				
V-type proton ATPase subunits	*ATP6V1E1/ A0A286X946, A0A286XJE1/ ATP6V1F, A0A286XMG7/ ATP6V1G1, A0A286XU99/ ATP6V1G2, A0A286Y5L6/ ATP6V1H, H0UWY1/ ATP6V1B2, H0VFT3/*	Lysosomal acidification, lysosome/autophagy system		Kang HT et al 2017

	ATP6V1C1 , H0VJ49/ ATP6V0A1,			
V-type proton ATPase catalytic subunit A	*ATP6V1A/ H0VLR3*	Autophagy		Chung CY et al 2019
V-type proton ATPase subunit B, brain isoform	*ATP6V1B2/ H0UWY1*	Intracelllular acidification	autophagic flux	Wang F et al 2019
Endocytosis				
Ras-related proteins Rab-1A, 1B, 6A, 11B, 11A, 7a	*RAB1A/ A0A286X8 E8, RAB1B/ H0VS12 , Rab6a/ A0A286XD T1, RAB11B/ A0A286X9 A2, RAB11A/ A0A286X7 V8, RAB7A/ A0A286Y5 02,*	Endocytosis		Martinez O et al 1998
Rab3 GTPase-activating protein catalytic subunit	*RAB3GAP 1/ H0VCU4*	Endocytosis		Martinez O et al 1998
Rab GTPase-binding effector protein 1	*RABEP1/ H0V1E5,*	Endocytosis		Martinez O et al 1998[120]

AP-2 complex subunit mu	*AP2M1/ H0VLH9*	Endocytosis	Developmental and Epileptic Encephalopathy	Helbig I et al 2019
AP-2 complex subunit beta	*AP2B1/ A0A286XBQ1*	Endocytosis		Sjödin S et al 2019
Caveolin -1	*CAV1/ Q07E12*	Endocytosis	Pulmonary arterial hypertension	Scheidel N. et al 2018
				Austin ED. Et al 2012
Heat shock protein HSP 90-alpha	*HSP90AA1 / H0UXJ8*	Clathrin dependent endo-lysosomal pathway		Macri C at al 2015
Heat shock cognate 71 kDa protein	*HSPA8/ H0V2J1*	Chaperone-mediated autophagy		Orenstein SJ. Et al 2010
				Rudenok, M. M. et al 2019
Clathrin light chain A	*CLTA/ A0A286XQF8*	Clathrin-mediated endocytosis		Anderson RH et al 2018
Clathrin heavy chain 1	*CLTC/ A0A286X7P2*	Clathrin-mediated endocytosis		Chang CC et al 2014
Transferrin receptor protein 1	*TFRC/ H0VQ12*	Endosomal sorting proteins		Chen C et al 2013
Optineurin	*OPTN/ H0VAE0*	Endocytic trafficking from early to late endosomes	Adult-onset primary open-angle glaucoma	Vaibhava V. et al 2012
				Rezaie T 2002
Beta-arrestin-1	*ARRB1/ A0A286XT09*	Clathrin endocytic pathway		Bhattacharyya S et al 2011
Cdc42-interacting protein 4	*TRIP10/ H0VRG7*	Endocytic vesicles		Erasmus JC et al 2016

		formation/Lysosomal		
Transport regulators and trafficking pathway mediators				
Endosome-associated protein p162/ Early endosome antigen 1	*EEA1/ H0VR73*	Transport regulators and retrograde trafficking mediators		Itoh, T. and Takenawa, T et al 2002
EH domain-containing proteins 2 and 4	*EHD2/ H0W104, EHD4/ H0VT72*	Transport regulators and retrograde trafficking mediators		Zhang, J. et al 2012
AP-2 complex subunit alpha-1	*AP2A1/ A0A286XJ44*	key regulator in the endosomal/lysosomal protein sorting pathway		Nakatsu, F. and Ohno, H. et al 2003
Ankyrin-3	*ANK3/ A0A286X9J0*	Lysosomes/late endosomal pathway		Hoock TC et al 1997
Prolow-density lipoprotein receptor-related protein 1/ LDL receptor related protein 1	*LRP1/ A0A286XIH8*	1.Cholesterol metabolism 2. endocytosis pathway		Actis Dato, V. et al. 2020
Apo lipoprotein E	*APOE/ H0V9M0*	1.Cholesterol metabolism 2. endocytosis pathway		Bilousova, T. et al 2019
T-complex protein 1 subunit beta/ Chaperonin containing	*CCT2/ A0A286XZI0*	Molecular chaperon in Apoptosis		Wang Q et al 2019

TCP1 subunit 2				
Vacuolar protein sorting-associated proteins Vps4A, Vps26, Vps28, Vps29, Vps35	*Vps4A/H0VQZ5, Vps26/A0A286XUV0, Vps28/H0V681, Vps29/A0A286XC75, VPS35/A0A286XSU9*	Endosomal cargo protein	Parkinsons disease	Kostelansky et al 2006, Hamdan et al 2014, Nguyen et al 2019, Ye et al 2020
Peroxi-redoxin-6	*PRDX6/A0A286Y2Y5*	Thiol-specific peroxidase		Kook S. et al 2016
Glycogenin-1	*GYG1/H0UWB0*	Glycogen metabolism	Glycogen storage disease XV/ Skeletal myopathy or cardiomyopathy.	Hedberg-Oldfors C et al. 2019
Ca^{2+} sensors and transporters				
Dysferlin	*DYSF/A0A286XJT8*	calcium ion sensor/ Ca(2+)-dependent, vesicle-mediated membrane repair	Limb-girdle muscular dystrophy type 2B	Liu, J. et al 1998
Ankyrin-2	*ANK2/A0A286XYD0*	Membrane stabilization of ion transporters	Cardiac arrhythmias in inherited long-QT syndrome	Mohler PJ et al 2003
Sodium/ potassium-transporting ATPase subunit alpha-1	*Atp1a1/A0A286XK64*	Endocrine and other factor-regulated Ca^{2+} reabsorption pathway		Bilousova, T. et al 2019

Annexin-A1	*ANXA1/ H0VRE3*	Calcium-binding/associated proteins		Dera AA et al 2019
Annexin-2	*ANXA2/ H0V7P8*	calcium binding		De Seranno et al 2006
Annexin-6	*ANXA6/ A0A286XBC0*	calcium binding to late endosomes		de Diego, I. et al 2002
Dysfunctional lysosomal proteins and related diseases				
Lysosomal Pro-X carboxy-peptidase	*PRCP/ A0A286XWA1*	Lysosomal peptidase	Cardiovascular diseases	Gittleman HR et al 2016
Clusterin	*Clu/ H0VVP2*	Lysosome-proteasome functional aspects	1.mucopolysaccharidosis-related to arterial disease 2. myocardial infarction	Khalid O. et al. 2016
Glycogen phosphorylase, brain form/ Alpha-1,4 glucan phosphorylase	*PYGB/ H0WCW9*	Regulate glycogen mobilization	Fabry disease	Doykov, I. D. et al 2020
Lysosomal alpha-mannosidase	*MAN2B1/ A0A0C3SFZ0*	Cleave alpha-mannosidic linkages	Alpha mannosidosis	Zielonka, M et al 2019
Cathepsin B	*CTSB/ H0VDW9*	Endo-lysosomal thiol protease	Lipolysis dysfunction	Mizunoe Y et al 2020
Cathepsin C	*CTSC/ H0VRZ6*	Hydrolase/ intracellular protein degradation	Hypertension	Gu et al 2017
Cathepsin D	*CTSD/ H0VCH6*	Acid protease/ intracellular protein degradation	ceroid lipofuscinosis/ Batten disease	Cárcel-Trullols J et al 2017
Cathepsin Z	*CTSZ/ H0W265*	Hydrolase		Li J. et al 2020

Lysosomal alpha-glucosidase	*GAA/ H0V6Y7*	Lysosomal enzyme	Pompe disease	Salabarria, S. M. et al. 2020
Glucocerebrosidase	*GBA/H0V090*	Gaucher Disease	Gaucher Disease	Hallett et al., 2018
Versican core protein	*VCAN/ A0A286X7M1*	Glycosaminoglycan metabolism	vitreoretinopathy	Tang P.H. et al 2019
Mimecan/ Osteoglycin	*OGN/ A0A286Y5R4*	Proteoglycans	Degenerative mitral valve disease /Cardiac remodelling	Tan HT et al 2015
Decorin	*DCN/ B5APS7*	Proteoglycans	1.cardiac fibrosis or fibrotic stiffness	Määttä, A., Järveläinen et al 1994
			2. Aspartylglucosaminuria	
Lumican	*LUM/ A0A286XVU9*	Cellular structural constituent	cardiac fibrosis	Mohammadzadeh N et al 2020
Ceruloplasmin	*CP/ H0VMS1*	Endocytic transporter and ion binding	Aceruloplasminemia/ Niemann-Pick disease type C	Levi S et al 2014
				Hung.Y.H et al 2014

Table A1:1 Key proteins identified from C. porcellus EL fraction are listed according to the functions and related diseases. *Related to figure 2:6*

1.2 Enzyme assay activities from Tissue Lysate, Mitochondrial fraction and Endo-lysosome and remainder fractions

β -galactosidase						
	Vol (ml)	mg/ml	Total mg	nmol/hr/ml	nmol/hr	nmol/hr/mg
TL	2.1	0.607	1.258	230	479	380
Mitos	2.1	0.354	0.728	100	207	285
EL	1.35	0.123	0.163	46.7	63	380
Remainder	1.2	0.057	0.0684	3.65	4.4	41
beta-hexosaminidase						
	Vol (ml)	mg/ml	Total mg	µmol/hr/ml	µmol/hr	µmol/hr/mg
TL	2.1	0.607	1.258	2.64	5.49	4.35
Mitos	2.1	0.354	0.728	1.21	2.5	3.42
EL	1.35	0.123	0.163	0.42	0.57	3.41
Remainder	1.2	0.057	0.068	0.02	0.02	0.04

Table A1:2 Table of enzyme activities, *related to Figure 2:4A*

1.3 GO analysis enrichment for cell component

Enrichment FDR	Genes in list	Total genes	Functional Category	Genes
1.04E-40	161	2326	Extracellular organelle	LAP3 PRKAR2B PON1 SPAG9 MDH1 ERP44 VIM CD44 MAT2B CP THRAP3 PHPT1 PKM RHOA PFN2 RPL31 FBLN1 EPB41L2 RPS5 EIF3I CHMP5 HUWE1 NID2 BLVRB MYL6 NANS HSP90AB1 HNRNPM ST13 ATP6V1D PSME2 GSS NDRG3 CTSZ AHCY USP14 F9 NUTF2 CPQ TSTA3 GSR NUCB1 RPS19 CDC37 NAMPT SSBP1 HSPB1 XPNPEP1 RPL28 CTSC HSPA8 VWF GPLD1 CUTA DNPH1 HSPA9 SUB1 NIT2 PRKAR2A NCL ACTR1B PPP1R7 RAB3GAP1 NID1 STMN1 GOT1 ACAT2 HSPH1 CAT PRDX4 TRIP10 SNRPD2 PSMA1 ATP6V1E1 EIF2S1 YWHAQ PSAT1 PRPH GLUL ABI1 GRHPR ACTR2 ACTR1A AOX1 RAP1GDS1 ANXA3 ESD FBLN5 NPEPPS SCRN2 PSMB6 SH3BGRL3 PSMA5 TPM3 RPS27A ALDH1L1 AHSG GC TKFC ITIH2 ACE PDXK G6PD PGLYRP2 ITIH3 CMPK1 ACOT11 FBLN2 CLEC3B TKT APEH RPS14 PGAM2 YWHAZ VCP CRYL1 PACSIN3 CKB HSP90B1 YWHAB PDIA3 HDHD2 TPM4 OTUB1 HINT1 YWHAG NUDT9 GAA EFEMP2 CORO1B GLRX CSPG4 TOM1L2 RUVBL1 SFN A2M IMPDH2 MPI PFAS F2 COL18A1 ACTG1 KRT6B ANKFY1 RPL14 RPE ADH5

				HRNR TXNRD1 COPS8 APRT NAGA KRT6A CLIC1 DDAH2 PPP1CB RPS28 MIF UBE2V1 DPP3 IDE
1.04E-40	160	2300	Extracellular exosome	LAP3 PRKAR2B PON1 SPAG9 MDH1 ERP44 VIM CD44 MAT2B CP THRAP3 PHPT1 PKM RHOA PFN2 RPL31 FBLN1 EPB41L2 RPS5 EIF3I CHMP5 HUWE1 NID2 BLVRB MYL6 NANS HSP90AB1 HNRNPM ST13 ATP6V1D PSME2 GSS NDRG3 CTSZ AHCY USP14 F9 NUTF2 CPQ TSTA3 GSR NUCB1 RPS19 CDC37 NAMPT SSBP1 HSPB1 XPNPEP1 RPL28 CTSC HSPA8 VWF GPLD1 CUTA DNPH1 HSPA9 SUB1 NIT2 PRKAR2A NCL ACTR1B PPP1R7 RAB3GAP1 NID1 STMN1 GOT1 ACAT2 HSPH1 CAT PRDX4 TRIP10 SNRPD2 PSMA1 ATP6V1E1 EIF2S1 YWHAQ PSAT1 PRPH GLUL ABI1 GRHPR ACTR2 ACTR1A AOX1 RAP1GDS1 ANXA3 ESD FBLN5 NPEPPS SCRN2 PSMB6 SH3BGRL3 PSMA5 TPM3 RPS27A ALDH1L1 AHSG GC TKFC ITIH2 ACE PDXK G6PD PGLYRP2 ITIH3 CMPK1 ACOT11 CLEC3B TKT APEH RPS14 PGAM2 YWHAZ VCP CRYL1 PACSIN3 CKB HSP90B1 YWHAB PDIA3 HDHD2

				TPM4 OTUB1 HINT1 YWHAG NUDT9 GAA EFEMP2 CORO1B GLRX CSPG4 TOM1L2 RUVBL1 SFN A2M IMPDH2 MPI PFAS F2 COL18A1 ACTG1 KRT6B ANKFY1 RPL14 RPE ADH5 HRNR TXNRD1 COPS8 APRT NAGA KRT6A CLIC1 DDAH2 PPP1CB RPS28 MIF UBE2V1 DPP3 IDE
1.04E-40	161	2324	Extracellular vesicle	LAP3 PRKAR2B PON1 SPAG9 MDH1 ERP44 VIM CD44 MAT2B CP THRAP3 PHPT1 PKM RHOA PFN2 RPL31 FBLN1 EPB41L2 RPS5 EIF3I CHMP5 HUWE1 NID2 BLVRB MYL6 NANS HSP90AB1 HNRNPM ST13 ATP6V1D PSME2 GSS NDRG3 CTSZ AHCY USP14 F9 NUTF2 CPQ TSTA3 GSR NUCB1 RPS19 CDC37 NAMPT SSBP1 HSPB1 XPNPEP1 RPL28 CTSC HSPA8 VWF GPLD1 CUTA DNPH1 HSPA9 SUB1 NIT2 PRKAR2A NCL ACTR1B PPP1R7 RAB3GAP1 NID1 STMN1 GOT1 ACAT2 HSPH1 CAT PRDX4 TRIP10 SNRPD2 PSMA1 ATP6V1E1 EIF2S1 YWHAQ PSAT1 PRPH GLUL ABI1 GRHPR ACTR2 ACTR1A AOX1 RAP1GDS1 ANXA3 ESD FBLN5 NPEPPS SCRN2 PSMB6 SH3BGRL3 PSMA5 TPM3 RPS27A ALDH1L1 AHSG GC TKFC ITIH2 ACE PDXK G6PD PGLYRP2 ITIH3 CMPK1 ACOT11 FBLN2 CLEC3B TKT APEH RPS14 PGAM2 YWHAZ VCP CRYL1 PACSIN3 CKB HSP90B1 YWHAB PDIA3 HDHD2 TPM4 OTUB1 HINT1 YWHAG NUDT9 GAA EFEMP2 CORO1B GLRX CSPG4 TOM1L2 RUVBL1 SFN A2M IMPDH2 MPI PFAS F2 COL18A1 ACTG1 KRT6B ANKFY1 RPL14 RPE ADH5 HRNR TXNRD1 COPS8 APRT NAGA

				KRT6A CLIC1 DDAH2 PPP1CB RPS28 MIF UBE2V1 DPP3 IDE
2.18E-27	176	3479	Extracellular space	LAP3 NDUFAF7 PRKAR2B PON1 SPAG9 DCN MDH1 ERP44 VIM CD44 MAT2B CP THRAP3 PHPT1 PKM RHOA PFN2 RPL31 FBLN1 EPB41L2 RPS5 EIF3I CHMP5 HUWE1 NID2 LTBP4 BLVRB MYL6 NANS HSP90AB1 HNRNPM ST13 ATP6V1D PSME2 GSS NDRG3 CTSZ AHCY USP14 F9 NUTF2 CPQ TSTA3 GSR NUCB1 RPS19 CDC37 NAMPT SSBP1 HSPB1 XPNPEP1 RPL28 CTSC HSPA8 VWF MRPL18 GPLD1 CUTA DNPH1 HSPA9 SUB1 NIT2 PRKAR2A NCL ACTR1B PPP1R7 RAB3GAP1 NID1 STMN1 GOT1 ACAT2 HSPH1 CAT PRDX4 TRIP10 SNRPD2 PSMA1 ATP6V1E1 EIF2S1 YWHAQ PSAT1 CSN2 PRPH GLUL ABI1 GRHPR ACTR2 ACTR1A AOX1 RAP1GDS1 ANXA3 ESD FBLN5 NPEPPS SCRN2 PSMB6 SH3BGRL3 PSMA5 HDGF TPM3 RPS27A ALDH1L1 AHSG GC TKFC ITIH2 ACE PDXK G6PD PGLYRP2 ITIH3 CMPK1 ACOT11 CLEC3B TKT APEH RPS14 PGAM2 YWHAZ VCP CRYL1 PACSIN3 CKB HSP90B1 YWHAB PDIA3 HDHD2 TPM4 OTUB1 HINT1 YWHAG NUDT9 GAA EFEMP2 CORO1B GLRX CSPG4 TOM1L2 RUVBL1 SFN A2M IMPDH2 MPI PFAS F2 COL18A1 ACTG1 KRT6B ANKFY1 RPL14 RPE ADH5 HRNR TXNRD1 COPS8 APRT NAGA KRT6A CLIC1 DDAH2 PPP1CB RPS28 MIF UBE2V1 DPP3 SPON1 PCSK1N SPARC IGFBP5 PROC IDE FAU PDIA4 CKM C1QBP AIMP1
8.82E-26	179	3693	Extracellular region part	LAP3 NDUFAF7 PRKAR2B PON1 SPAG9 DCN MDH1 ERP44 VIM CD44 MAT2B CP

				THRAP3 PHPT1 PKM RHOA PFN2 RPL31 FBLN1 EPB41L2 RPS5 EIF3I CHMP5 HUWE1 NID2 LTBP4 BLVRB MYL6 NANS HSP90AB1 HNRNPM ST13 ATP6V1D PSME2 GSS NDRG3 CTSZ AHCY USP14 F9 NUTF2 CPQ TSTA3 GSR NUCB1 RPS19 CDC37 NAMPT SSBP1 HSPB1 XPNPEP1 RPL28 CTSC HSPA8 VWF MRPL18 GPLD1 CUTA DNPH1 HSPA9 SPARC SUB1 NIT2 PRKAR2A NCL ACTR1B PPP1R7 RAB3GAP1 NID1 STMN1 GOT1 ACAT2 HSPH1 CAT PRDX4 TRIP10 SNRPD2 PSMA1 ATP6V1E1 EIF2S1 YWHAQ PSAT1 CSN2 PRPH GLUL ABI1 GRHPR ACTR2 ACTR1A AOX1 RAP1GDS1 ANXA3 ESD FBLN5 NPEPPS SCRN2 PSMB6 SH3BGRL3 PSMA5 HDGF TPM3 RPS27A ALDH1L1 AHSG GC TKFC ITIH2 ACE PDXK G6PD PGLYRP2 ITIH3 CMPK1 ACOT11 FBLN2 CLEC3B TKT APEH RPS14 PGAM2 YWHAZ VCP CRYL1 PACSIN3 CKB HSP90B1 YWHAB PDIA3 HDHD2 TPM4 OTUB1 HINT1 YWHAG NUDT9 GAA EFEMP2 CORO1B GLRX CSPG4 TOM1L2 RUVBL1 SFN A2M IMPDH2 MPI PFAS F2 COL18A1 ACTG1 KRT6B ANKFY1 RPL14 RPE ADH5 HRNR TXNRD1 COPS8 APRT NAGA KRT6A CLIC1 DDAH2 PPP1CB RPS28 MIF UBE2V1 DPP3 SPON1 PCSK1N IGFBP5 PROC PPP1R13L IDE GSTM1 FAU PDIA4 CKM C1QBP AIMP1
1.56E-23	81	985	Ribonucleoprotein complex	RPL31 RPS5 RPS19 RPL28 RPS6 RPS27A FAU RPL29 RPS14 RPL13 RPS7 RPS17 RPS23 RPL14 RPS28 MRPS35 U2AF2 SF3B2 CIRBP HNRNPM SNU13 NOP56 FMR1 LSM5 EIF4H RWDD1 MRPS30 MRPL3 NCL MRPS14

				MRPS2 SNRPD2 MRPS26 RBM38 EIF2S1 MRPS9 G3BP2 MRPS5 DIS3L2 G3BP1 SRP19 MRPL10 U2AF1 LSM3 MRPL52 LSM2 EIF1 MRPL11 MRPL48 MRPL41 RPS27L MRPL46 AKAP8L VIM CBX5 HSPA8 MRPL18 ILF3 MRPL35 SRSF1 MRPL39 VCP SRRM2 SF1 MRPL14 GIGYF2 RBM8A MRPL45 ROCK1 EIF3I KHSRP EIF3D SSB HAX1 API5 RUVBL1 EIF3K GADD45GIP1 APEX1 RRBP1 PSMA1
1.33E-22	188	4252	Vesicle	LAP3 PRKAR2B PON1 SPAG9 MDH1 ERP44 VIM CD44 MAT2B CP THRAP3 PHPT1 PKM RHOA PFN2 RPL31 FBLN1 EPB41L2 RPS5 EIF3I CHMP5 HUWE1 NID2 BLVRB MYL6 NANS HSP90AB1 HNRNPM ST13 ATP6V1D PSME2 GSS NDRG3 CTSZ AHCY USP14 F9 NUTF2 CPQ TSTA3 GSR NUCB1 RPS19 CDC37 NAMPT SSBP1 HSPB1 XPNPEP1 RPL28 CTSC HSPA8 VWF GPLD1 CUTA DNPH1 HSPA9 SUB1 NIT2 PRKAR2A NCL ACTR1B PPP1R7 RAB3GAP1 NID1 STMN1 GOT1 ACAT2 HSPH1 CAT PRDX4 TRIP10 SNRPD2 PSMA1 ATP6V1E1 EIF2S1 YWHAQ PSAT1 PRPH GLUL ABI1 GRHPR ACTR2 ACTR1A AOX1 RAP1GDS1 ANXA3 ESD FBLN5 NPEPPS SCRN2 PSMB6 SH3BGRL3 PSMA5 TPM3 RPS27A ALDH1L1 AHSG GC TKFC ITIH2 ACE PDXK G6PD PGLYRP2 ITIH3 CMPK1 ACOT11 FBLN2 CLEC3B TKT APEH RPS14 PGAM2 YWHAZ VCP CRYL1 PACSIN3 CKB HSP90B1 YWHAB PDIA3 HDHD2 TPM4 OTUB1 HINT1 YWHAG NUDT9 GAA EFEMP2 CORO1B GLRX CSPG4 TOM1L2 RUVBL1 SFN A2M IMPDH2 MPI PFAS F2 COL18A1 ACTG1

				KRT6B ANKFY1 RPL14 RPE ADH5 HRNR TXNRD1 COPS8 APRT NAGA KRT6A CLIC1 DDAH2 PPP1CB RPS28 MIF UBE2V1 DPP3 AP3D1 VAC14 CLTA COPG1 EIPR1 SPARC TUBG1 AKT1 GIGYF2 EPS15 SH3GLB1 PCSK1N SGTA OSBPL9 OPTN CD93 UBQLN1 CALCOCO2 HAX1 PDIA4 NAP1L1 PLN ATP6V1G2 IDE CAMK2B ROCK1 CD207 PSMD6
1.98E-22	56	497	Mitochondrial matrix	MRPS35 BCKDHB SSBP1 GRPEL1 MRPS30 MRPL3 MRPS14 MRPS2 SARDH MRPS26 MRPS9 MRPS5 MRPL10 MRPL52 MRPL11 MRPL48 MRPL41 GLRX5 DNAJC19 MRPL46 DNAJA3 MRPL18 HSPA9 ACADM MCCC2 MRPL35 MRPL39 CCAR2 MRPL14 NFS1 MRPL45 HAGH IARS2 REXO2 C1QBP PCCB ACADL FDX1 MMUT ALDH4A1 SDHAF2 PCCA NDUFAF7 MCAT DECR1 GSR COQ3 PPA2 GCSH ACP6 ACSF2 ACAA2 NUDT9 TRMT61B GADD45GIP1 TXNRD2
2.80E-20	104	1724	Mitochondrion	PKM HSP90AB1 TIMM8A PLN NDUFAF7 MRPS35 ME1 IARS2 REXO2 BCKDHB MCAT DNAJA3 GSR DMPK SSBP1 C1QBP GRPEL1 MRPL18 MRPS30 HSPA9 MRPL3 ACADL ACADM IDE MRPS14 ACAT2 ECHDC2 MRPS2

				SARDH MRPS26 MCCC2 MRPL35 MRPS9 KYAT3 MRPS5 MRPL39 MRPL10 ACAA2 SDHAF2 NFU1 TRMT61B THOP1 MRPL52 MRPL11 MRPL48 MRPL14 MRPL41 GLRX5 NIPSNAP1 TXNRD2 TXNRD1 DNAJC19 MRPL46 MRPL45 CIAPIN1 SELENOO APEX1 DECR1 AARS2 ILF3 COQ3 DCAF8 GLUL FDX1 RAP1GDS1 HAX1 CCAR2 ACP6 TPPP METAP1D CAVIN1 GADD45GIP1 GPN1 NFS1 GATC HAGH SH3GLB1 PCCB CAT CLYBL YWHAQ ECHDC3 USP15 VARS2 PPA2 GCSH AKT1 MMUT OGT ALDH4A1 GATD3A YWHAZ YWHAB ACSF2 YWHAG NUDT9 PPM1E PCCA SFN FHIT ADH5 DDAH2 NDRG4 RPS27A
1.61E-19	40	282	Ribosome	RPL31 RPS5 RPS19 RPL28 RPS6 RPS27A FAU RPL29 RPS14 RPL13 RPS7 RPS17 RPS23 RPL14 RPS28 MRPS35 MRPS30 MRPL3 MRPS14 MRPS2 MRPS26 MRPS9 MRPS5 MRPL10 MRPL52 MRPL11 MRPL48 MRPL41 RPS27L MRPL46 MRPL18 MRPL35 MRPL39 MRPL14 MRPL45 GADD45GIP1 SF1 APEX1 FMR1 RRBP1

Table A1:3 Enrichment ShinyGo pathway analysis, *related to figure 2.7*

1.4 Comparison of proteomic data between human and guinea pig atria

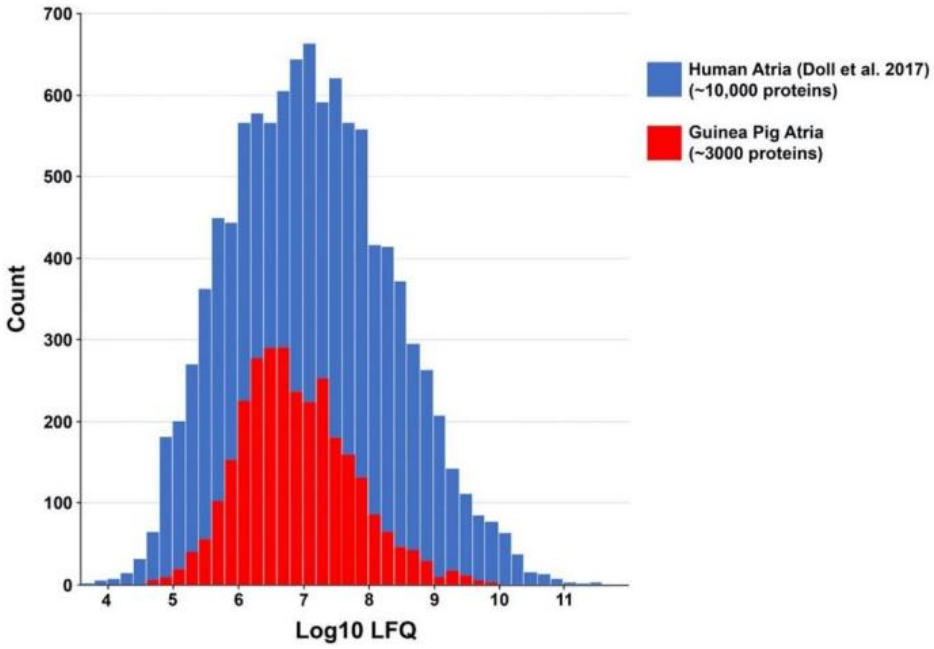

Figure A1:1 (related to Figure 2:4) Comparison of proteomic data between human and guinea pig atria. *Histograms total proteins identified in the TL from C. porcellus proteomics study (red) compared to published proteins from human total atrial tissue samples (blue) in the study by Doll et al. (Doll et al.,2017) (Figure reproduced with permission from Ayagama et al. 2021).*

Appendix 2

2.1 Complete figures of proteomic pathway analysis

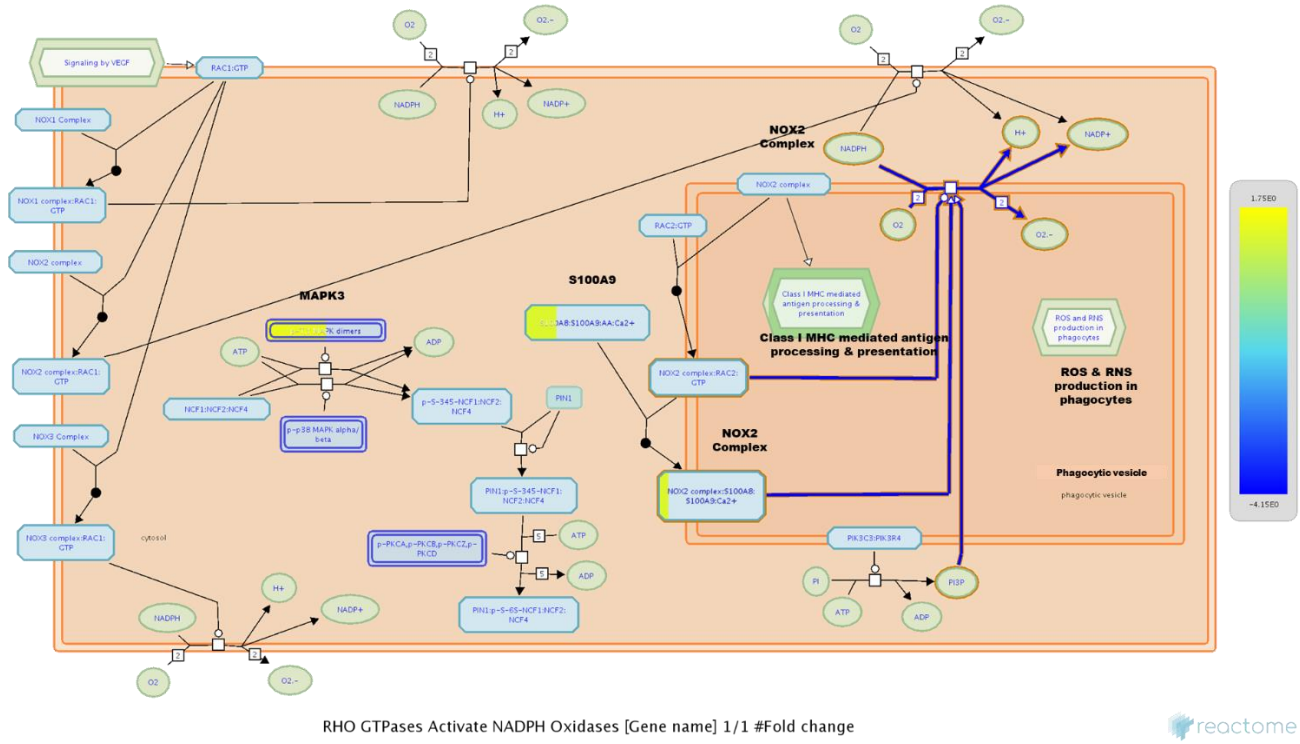

Figure A2:1 (Related to Figure 3:24): RHO GTPase activation of NADPH Oxidase. *The downstream reactions of the RHO GTPase activation of NOX2 signaling in AF included; the induced production of phagocyte oxygen radicals by NOX2 complex bound to Ras-related C3 botulinum toxin substrate 2 (RAC2) and Guanosine-5'-triphosphate (GTP), MAPK1 or MAPK3 phosphorylation of Neutrophil cytosol factor 1 (NCF1) at Serine/threonine-protein kinase Chk1 (Ser345) and S100A8:S100A9:AA:Ca(2+) binding to NOX2 complex. Protein S100-A9 (S100A9 with) log2 1.17, Mitogen-activated protein kinase 3 (MAPK3) with log2 1.4, Mitogen-activated protein kinase 12 (MAPK12) with log2 0.5 and Mitogen-activated protein kinase 14 (MAPK14) with log2 0.4 fold were upregulated (colour code=yellow to blue gradient yellow represent highest up regulation while blue represent highest down regulation, highest upregulation log2 fold 1.75E0 and lowest log2 fold -4.15E0. The protein complexes with complete or part-coloured representation showed the total molecules present from the query data set to complete the complex. Arrow = Protein, protein complex name or protein function) Figure created using www.reactome.com pathway analysis.*

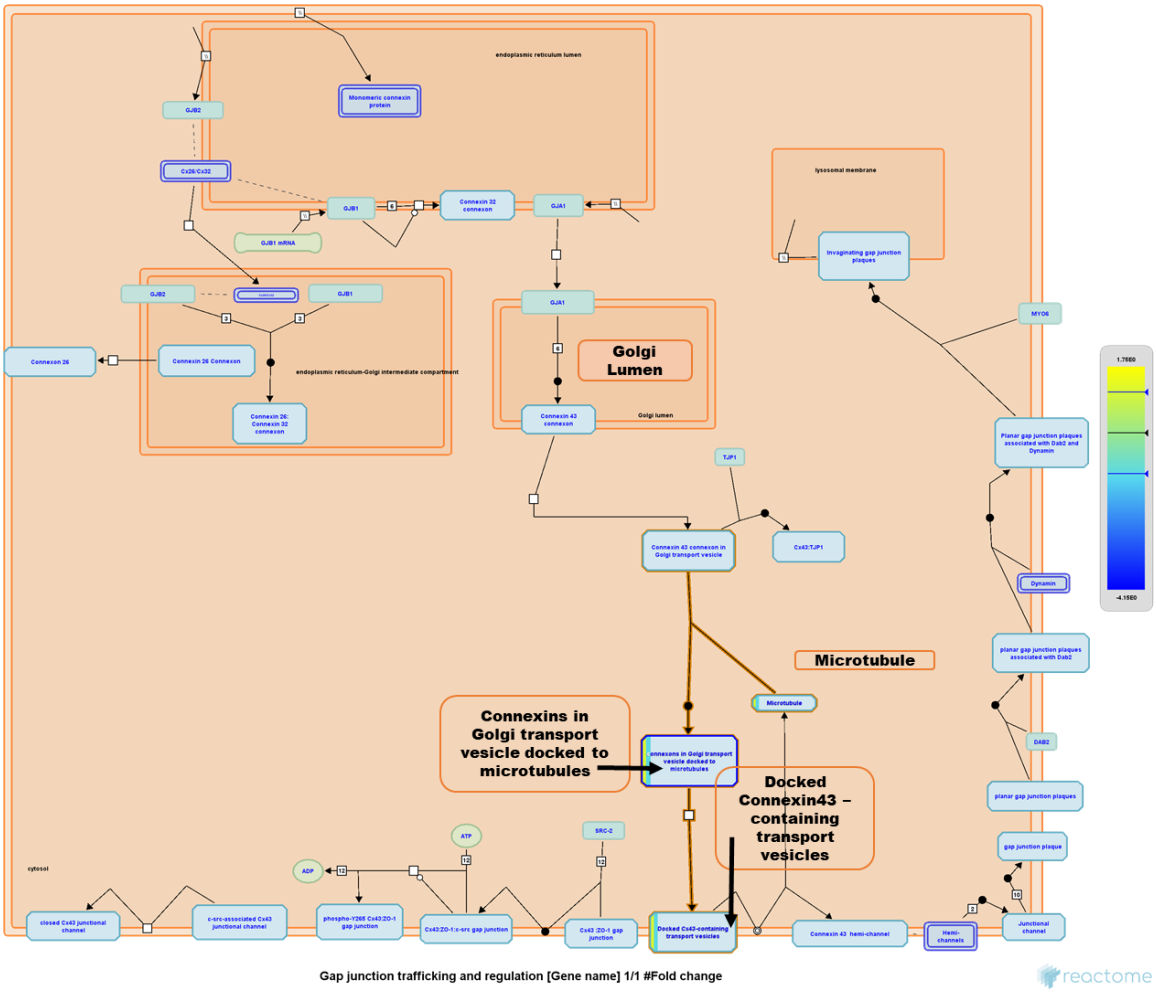

Figure A2:2 (Related to Figure 3:26): Gap junction assembly. *The pathway diagram showing the transport of connexons to the plasma membrane while using the discordantly regulated microtubule dependent trafficking from Golgi to plasma membrane. The assembly of gap junctions involves (1) synthesis of Connexin polypeptides at the membrane sites of ER, (2) Homomeric and heteromeric oligomerization into connexon or hemi-channels, (3) Hemi-channel transport through the Golgi stacks, (4) Trans Golgi membrane storage of the hemi channels, (5) trafficking of connexons along the microtubules, (6) insertion of Connexons into the plasma membrane, (7) lateral diffusion of hemi channels in the plasma membrane, (8) aggregation of gap junction channels into plaques, and (9) stabilization of peripheral microtubule plus-ends by binding to Connexin43- gap junctions (Segretain and Falk, 2004). Upregulated proteins were CLTB with log2 1.5 fold, TUBA4A with log2 1.088 fold, and down regulated proteins were AP2A2 with log2 -0.3 fold, and DNM2 with a log2 -0.6 fold. Arrow marks pointing to the events with protein regulations. (colour code=yellow to blue gradient yellow represent highest up regulation while blue represent most down regulated, highest upregulation log2 fold 1.75E0 and lowest log2 fold -4.15E0. The protein complexes with complete or part-coloured representation showed the total molecules present from the query data set to complete the complex. Arrow = Protein, protein complex name or protein function). Figure created using www.Reactome.com pathway analysis.*

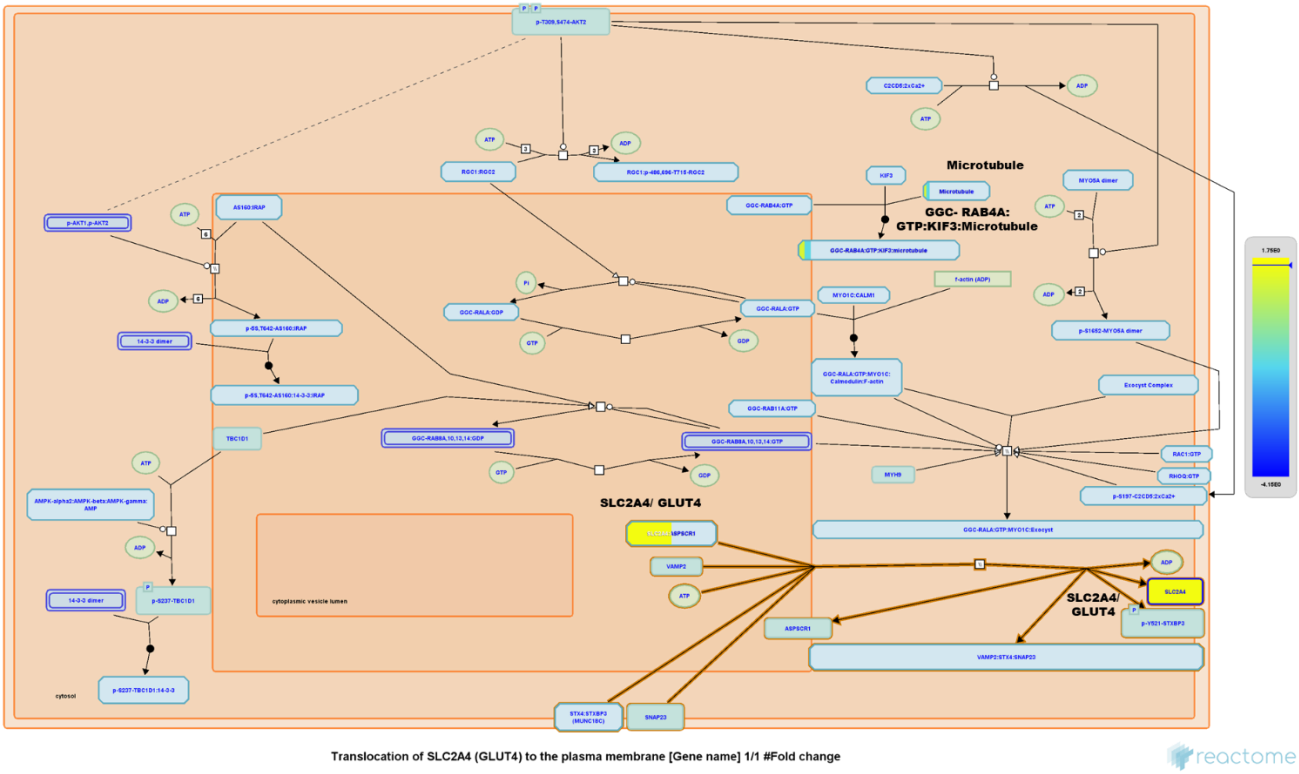

Figure A2:3 (Related to Figure 3:39): GLUT4 translocation to plasma membrane: *The pathway analysis of Reactome exhibited a possible interaction between the plasma membrane and GLUT4 vesicle trafficking. Under this pathway all the detected proteins were upregulated, such as, SLC2A4 or GLUT4 by log2 1.55, CAV1 by log2 0.6-fold, and NSF by log2 1.55. (colour code=yellow to blue gradient yellow represent highest up regulation while blue represent highest down regulation, highest upregulation log2 fold 1.75E0 and lowest log2 fold -4.15E0. The protein complexes with complete or part-coloured representation showed the total molecules present from the query data set to complete the complex. Arrow = Protein, protein complex name or protein function) Figure created using www.reactome.com pathway analysis.*

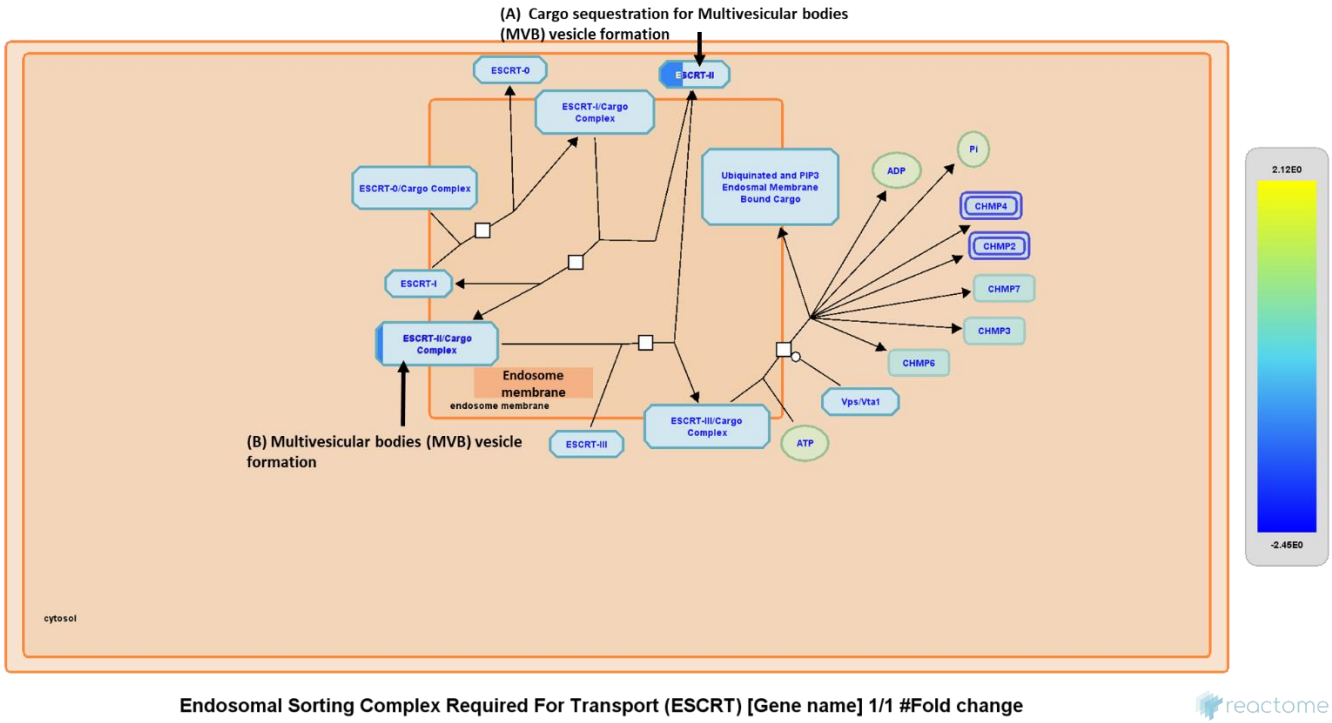

Figure A2:4 (Related to Figure 3:41): ESCRT pathway. *The left atrial cells of the AF goat model showed a possible down regulation of the multivesicular body formation in the ESCRT pathway. I observed a down regulation in the proteins such as ESCRT-II complex subunit VPS25 (VPS25) and Ras-related protein Rab-7a (Rab7a) respectively by log2 -1.03 fold and log2 -0.5 fold. (Colour code = yellow to blue gradient yellow represent highest up regulation while blue represent highest down regulation. Highest upregulation log2 1.75E0 fold and lowest log2 -4.15E0 fold. The protein complexes with complete or part-coloured representation showed the total molecules present from the query data set to complete the complex. Arrow = Protein, protein complex name or protein function) Figure created using www.reactome.com pathway analysis.*

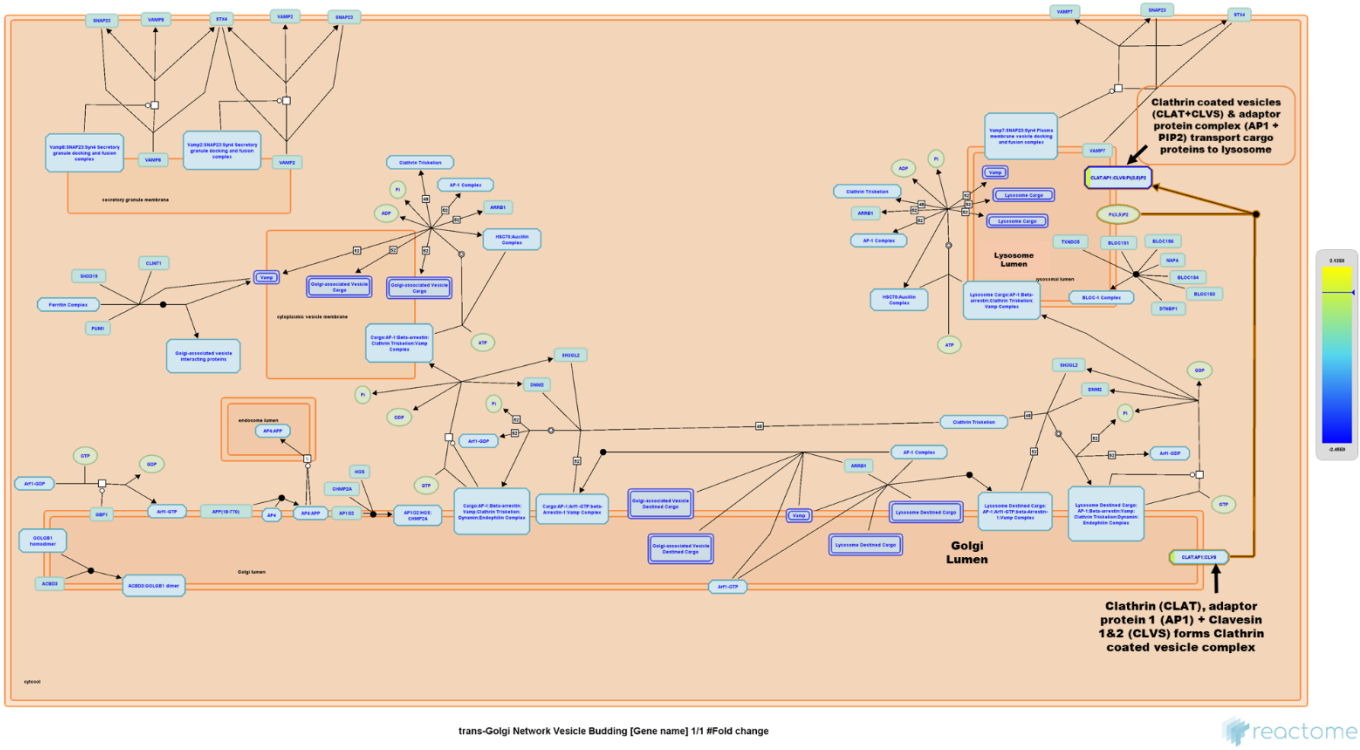

Figure A2:5 (Related to Figure 3:43): Lysosome biogenesis path. *Lysosome destined cargo is carried to the lysosome through clathrin mediated transport. Clathrin triskelions complex associate with lysosome destined cargo, AP1, beta-Arrestin and Vamp proteins, and dynamin form a collar around the vesicle budding for fission. This process is driven by GTPase. In the LA of the got AF model I observed an over expression of Clathrin coated vesicle traffic to the lysosome membrane. Formation of vesicles with Clathrin, AP1 protein complex and Clavesin proteins and its pathway to the lysosome was highlighted in the Reactome studies. (Colour code=yellow to blue gradient; yellow represent highest up regulation while blue represent highest down regulation. Highest upregulation log2 2.12E0 fold and lowest log2 -2.45E0 fold. The protein complexes with complete or part-coloured representation showed the total molecules present from the query data set to complete the complex. Arrow = Protein, protein complex name or protein function). Figure created using www.reactome.com pathway analysis.*

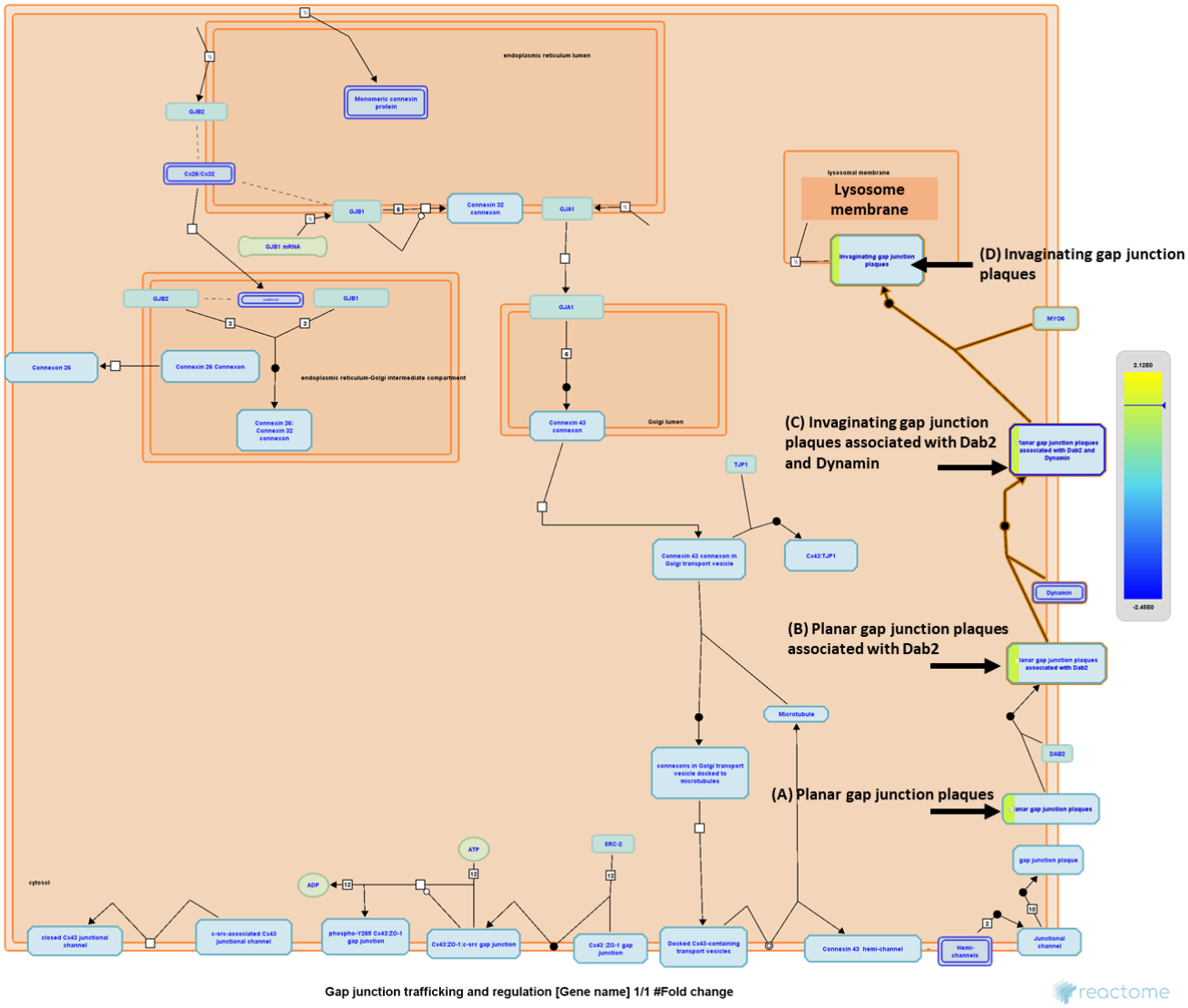

Figure A2:6 (Related to Figure 3:44): Pathway representation of gap junction trafficking to lysosomes, internalization and degradation. *In the AF goat model I observed; (A) increased planar gap junction plaques formation (B) Disabled homolog 2 (Dab2) protein of the plasma membrane associates with the hemi channels or planar gap junctions (C) Invagination of gap junctions form double membraned annular gap junctional plaque vesicles and transported to lysosome membrane by dynamin (D) internalization of gap junctional annular plaque vesicles at the lysosomal membrane for the degradation. (Colour code=yellow to blue gradient; yellow represent highest up regulation while blue represent highest down regulation. Highest upregulation log2 2.12E0 fold and lowest log2 -2.45E0 fold. The protein complexes with complete or part-coloured representation showed the total molecules present from the query data set to complete the complex. Arrow = Protein, protein complex name or protein function). Figure created using www.reactome.com pathway analysis.*

2.2 The Most significantly regulated proteins – Tissue Lysate (TL) fraction

Protein Name (TL fraction)	Accession	Protein ID	Protein/Gene	Log2 Fold change
Eukaryotic translation initiation factor 3 subunit M	A0A452EB00	A0A452EB00_CAPHI	EIF3M	1.753548
Myomesin-2	A0A452E9Y7	A0A452E9Y7_CAPHI	MYOM2	1.730804
Protein preY, mitochondrial	A0A452E134	A0A452E134_CAPHI	PYURF	1.550902
Glucose transporter type 4, insulin-responsive	A0A452FEB3	A0A452FEB3_CAPHI	SLC2A4	1.547994
Vesicle-fusing ATPase	A0A452EEQ2	A0A452EEQ2_CAPHI	NSF	1.545545
3-hydroxyisobutyryl-CoA hydrolase, mitochondrial	A0A452FTN3	A0A452FTN3_CAPHI	HIBCH	1.434621
Plastin-3	A0A452F5Y9	A0A452F5Y9_CAPHI	PLS3	1.434353
ATP-binding cassette sub-family E member 1	A0A452F8U9	A0A452F8U9_CAPHI	ABCE1	1.426301
MARVEL domain-containing protein	A0A452DTB9	A0A452DTB9_CAPHI	SYPL1	1.418171
Amine oxidase	A0A452FZL6	A0A452FZL6_CAPHI	MAOB	1.414722
MICOS complex subunit MIC10	A0A452FSW2	A0A452FSW2_CAPHI	MICOS10	1.403165
Mitogen-activated protein kinase	A0A452EU65	A0A452EU65_CAPHI	MAPK3	1.371264
Complex I-MNLL	A0A452ERZ9	A0A452ERZ9_CAPHI	NDUFB1	1.365012
Chromobox protein homolog 3	A0A452E268	A0A452E268_CAPHI	CBX3	1.359527
Calcium-transporting ATPase	A0A452F5R6	A0A452F5R6_CAPHI	ATP2A3	1.327052
Huntingtin-interacting protein K	A0A452DV61	A0A452DV61_CAPHI	HYPK	1.324654
DCN1-like protein	A0A452ED15	A0A452ED15_CAPHI	DCUN1D1	1.317841
Tuftelin-interacting protein 11	A0A452EYY0	A0A452EYY0_CAPHI	TFIP11	1.316593
Alpha-actinin-4	A0A452E7A9	A0A452E7A9_CAPHI	ACTN4	1.296948
Thioredoxin	A0A452EGP3	A0A452EGP3_CAPHI	TXN	1.292154
ATP synthase subunit a	D2KMK0	D2KMK0_CAPHI	ATP6	1.235089
2-phospho-D-glycerate hydro-lyase	A0A452FB24	A0A452FB24_CAPHI	ENO3	1.225511
Histone H3	A0A452DRQ7	A0A452DRQ7_CAPHI	H3C1	1.21935
NADH dehydrogenase (Ubiquinone) 1 alpha subcomplex 4	A5JSS3	A5JSS3_CAPHI	NDUFA4	1.218856
SAP domain-containing protein	A0A452DL17	A0A452DL17_CAPHI	CCAR1	1.209533
SERPIN domain-containing protein	A0A452EWZ3	A0A452EWZ3_CAPHI	LOC102174166	1.194336
BolA-like protein 2	A0A452FYK7	A0A452FYK7_CAPHI	BOLA2B	1.179847
Calgranulin-B	A0A452EXE8	A0A452EXE8_CAPHI	S100A9	1.167027

Methionine adenosyltransferase 2 subunit beta	A0A452GAJ0	A0A452GAJ0_CAPHI	MAT2B	1.103554
Pentatricopeptide repeat domain-containing protein 3, mitochondrial	A0A452EAC5	A0A452EAC5_CAPHI	PTCD3	1.087719
Tubulin alpha chain	A0A452DNE3	A0A452DNE3_CAPHI	TUBA4A	1.087668
Spectrin beta chain	A0A452EPS0	A0A452EPS0_CAPHI	SPTBN4	1.079849
NADH dehydrogenase [ubiquinone] iron-sulfur protein 6, mitochondrial	A0A452FDC1	A0A452FDC1_CAPHI	NDUFS6	1.079732
Peptidylprolyl isomerase	A0A452DYZ1	A0A452DYZ1_CAPHI	LOC108634682	1.071696
Hemoglobin subunit alpha-1	P0CH25	HBA1_CAPHI	HBA1	1.062692
Protein arginine methyltransferase NDUFAF7	A0A452FZM5	A0A452FZM5_CAPHI	NDUFAF7	1.060264
PKS_ER domain-containing protein	A0A452EZS5	A0A452EZS5_CAPHI	CRYZ	1.058466
IF rod domain-containing protein	A0A452G757	A0A452G757_CAPHI	NES	1.050134
ANK_REP_REGION domain-containing protein	A0A452F5N4	A0A452F5N4_CAPHI	MTPN	1.046287
Matrix-remodeling-associated protein 7	A0A452DZF9	A0A452DZF9_CAPHI	MXRA7	1.042658
NADH dehydrogenase [ubiquinone] 1 beta sub-complex subunit 8, mitochondrial	A0A452EKC1	A0A452EKC1_CAPHI	NDUFB8	1.020162
Serine/threonine-protein phosphatase 2A regulatory subunit B'' subunit alpha	A0A452E1L0	A0A452E1L0_CAPHI	PPP2R3A	1.017538
Superoxide dismutase	A0A452E294	A0A452E294_CAPHI	SOD2	1.013015
CMP/dCMP-type deaminase domain-containing protein	A0A452G6Y9	A0A452G6Y9_CAPHI	APOBEC2	1.011512
Complex I-49kD	A0A452FXF1	A0A452FXF1_CAPHI	NDUFS2	1.007449
Peptidase M20 domain-containing protein 2	A0A452ERD0	A0A452ERD0_CAPHI	PM20D2	1.007222
Calsequestrin	A0A452EKU0	A0A452EKU0_CAPHI	CASQ2	0.996356
Phosphoglycerate mutase	A0A452DR91	A0A452DR91_CAPHI	PGAM2	0.985742
Heterogeneous nuclear ribonucleoprotein H3	A0A452G7L1	A0A452G7L1_CAPHI	HNRNPH3	0.970102
Calumenin	A0A452G3A0	A0A452G3A0_CAPHI	CALU	0.969315
Prefoldin subunit 1	A0A452E6Y1	A0A452E6Y1_CAPHI	PFDN1	0.969292
Cytochrome P450 2D14	A0A452EE06	A0A452EE06_CAPHI	LOC102169002	0.969083
Reticulocalbin-2	A0A452EW53	A0A452EW53_CAPHI	RCN2	0.966087
Myosin regulatory light chain 2	A0A452FC01	A0A452FC01_CAPHI	MYL2	0.964058
Protein-tyrosine-phosphatase	A0A452FRP1	A0A452FRP1_CAPHI	EPM2A	0.95713
Sodium/potassium-transporting ATPase subunit beta	A0A452DMV1	A0A452DMV1_CAPHI	ATP1B4	0.957118
Complex I-B18	A0A452EGT0	A0A452EGT0_CAPHI	NDUFB7	0.950796
FHA domain-containing protein	A0A452E102	A0A452E102_CAPHI	SLMAP	0.949906
Tubulin-specific chaperone A	A0A452FI28	A0A452FI28_CAPHI	TBCA	0.947628
Annexin	A0A452E8X0	A0A452E8X0_CAPHI	ANXA3	0.94074
Tropomyosin beta chain	A0A452EN00	A0A452EN00_CAPHI	TPM2	0.936792
PDZ domain-containing protein	A0A452EQ10	A0A452EQ10_CAPHI	AHNAK	0.928654

Peroxiredoxin-6	A0A452EUX2	A0A452EUX2_CAPHI	PRDX6	0.928186
Acetyl-coenzyme A synthetase	A0A452FKE9	A0A452FKE9_CAPHI	ACSS1	0.926547
II alpha globin	C6ZP52	C6ZP52_CAPHI	HBAII	0.926373
Cystatin domain-containing protein	A0A452F4D3	A0A452F4D3_CAPHI	LOC102186806	0.923698
NADH dehydrogenase [ubiquinone] iron-sulfur protein 4, mitochondrial	A0A452G117	A0A452G117_CAPHI	NDUFS4	0.920454
Phosphorylase kinase	A0A452FGA5	A0A452FGA5_CAPHI	PHKG1	0.919327
Cytochrome b-c1 complex subunit 9	A0A452G6M6	A0A452G6M6_CAPHI	LOC102187154	0.917656
Protein-arginine deiminase	A0A452F1S1	A0A452F1S1_CAPHI	PADI2	0.916605
Complex I-B12	A0A452FQM9	A0A452FQM9_CAPHI	NDUFB3	0.905559
Spectrin alpha chain, erythrocytic 1	A0A452E834	A0A452E834_CAPHI	SPTA1	0.899963
Long-chain specific acyl-CoA dehydrogenase, mitochondrial	A0A452ECL8	A0A452ECL8_CAPHI	ACADL	0.899062
Calnexin	A0A452DM15	A0A452DM15_CAPHI	CANX	0.898036
Glycerol-3-phosphate dehydrogenase [NAD(+)]	A0A452E8U3	A0A452E8U3_CAPHI	GPD1L	0.88475
Endoplasmic reticulum resident protein 29	A0A452ECE5	A0A452ECE5_CAPHI	ERP29	0.87909
GTP-binding protein SAR1b	A0A452FNY5	A0A452FNY5_CAPHI	SAR1B	0.865904
Enoyl-CoA hydratase, mitochondrial	A0A452DLQ3	A0A452DLQ3_CAPHI	ECHS1	0.846677
Prefoldin subunit 6	A0A452FHF8	A0A452FHF8_CAPHI	PFDN6	0.84645
Sulfotransferase	A0A452F929	A0A452F929_CAPHI	LOC102183750	0.842231
AAA domain-containing protein	A0A452EY56	A0A452EY56_CAPHI	PSMC1	0.836968
ADP-ribosylation factor-like protein 8B	A0A452EAA3	A0A452EAA3_CAPHI	ARL8B	0.809175
Catechol O-methyltransferase domain-containing protein 1	A0A452DRF4	A0A452DRF4_CAPHI	COMTD1	0.801046
C-1-tetrahydrofolate synthase, cytoplasmic	A0A452DNI3	A0A452DNI3_CAPHI	MTHFD1	0.801027
Plectin	A0A452FMX3	A0A452FMX3_CAPHI	PLEC	0.798788
Calcyclin-binding protein	A0A452FJL5	A0A452FJL5_CAPHI	CACYBP	0.791136
S_100 domain-containing protein	A0A452DSQ1	A0A452DSQ1_CAPHI	S100A13	0.787987
SERPIN domain-containing protein	A0A452ETQ5	A0A452ETQ5_CAPHI	SERPINB9	0.780706
Phosphoglucomutase-1	A0A452F6I3	A0A452F6I3_CAPHI	PGM1	0.780198
Filamin-A	A0A452E7C9	A0A452E7C9_CAPHI	FLNA	0.778448
Serine/threonine-protein phosphatase 2A 65 kDa regulatory subunit A beta isoform	A0A452FC43	A0A452FC43_CAPHI	PPP2R1B	0.770544
Malate dehydrogenase	A0A452EQW7	A0A452EQW7_CAPHI	MDH1	0.770526
5'-AMP-activated protein kinase subunit gamma-1	A0A452FEA0	A0A452FEA0_CAPHI	PRKAG1	0.770019
RNA helicase	A0A452EBN6	A0A452EBN6_CAPHI	EIF4A2	0.768036
Creatine kinase	A0A452F2L8	A0A452F2L8_CAPHI	CKB	0.75861
26S proteasome non-ATPase regulatory subunit 9	A0A452FD51	A0A452FD51_CAPHI	PSMD9	0.750197
Pyridoxal 5'-phosphate synthase	A0A452DR09	A0A452DR09_CAPHI	PNPO	0.748333
Myopalladin	A0A452EPN2	A0A452EPN2_CAPHI	MYPN	0.745106

ATP synthase subunit epsilon, mitochondrial	A0A452FTG4	A0A452FTG4_CAPHI	ATP5F1E	0.742881
Sodium/potassium-transporting ATPase subunit alpha	A0A452FAW7	A0A452FAW7_CAPHI	ATP4A	0.740566
Beta-taxilin	A0A452G9A6	A0A452G9A6_CAPHI	TXLNB	0.731552
Heat shock 27 kDa protein	A0A452ESU7	A0A452ESU7_CAPHI	HSPB1	0.728128
DnaJ homolog subfamily A member 2	A0A452FTT1	A0A452FTT1_CAPHI	DNAJA2	0.720631
Apolipoprotein E	A0A452FL25	A0A452FL25_CAPHI	APOE	0.717812
UDP-glucose:glycoprotein glucosyltransferase 1	A0A452F043	A0A452F043_CAPHI	UGGT1	0.71579
Cytochrome c oxidase subunit 7A1, mitochondrial	A0A452EN08	A0A452EN08_CAPHI	COX7A1	0.709961
4-alpha-glucanotransferase	A0A452FWP3	A0A452FWP3_CAPHI	AGL	0.694387
Histidine-rich glycoprotein	A0A452G2Y4	A0A452G2Y4_CAPHI	HRG	0.692853
Sulfotransferase	A0A452EH52	A0A452EH52_CAPHI	SULT1C4	0.687469
Junctophilin	A0A452G3E6	A0A452G3E6_CAPHI	JPH2	0.686543
Calpain inhibitor	A0A452GB29	A0A452GB29_CAPHI	CAST	0.684368
Phosphorylase b kinase regulatory subunit	A0A452FL74	A0A452FL74_CAPHI	PHKA1	0.675629
SGNH_hydro domain-containing protein	A0A452EVP3	A0A452EVP3_CAPHI	IAH1	0.674795
Ras-related GTP-binding protein	A0A452DQZ4	A0A452DQZ4_CAPHI	RRAGA	0.66284
Histone H2A	A0A452DR58	A0A452DR58_CAPHI	H2AC6	0.655662
PDZ and LIM domain protein 5	A0A452DXY8	A0A452DXY8_CAPHI	PDLIM5	0.649108
Calcium/calmodulin-dependent protein kinase	A0A452E1R3	A0A452E1R3_CAPHI	CAMK2D	0.645605
Serum paraoxonase/arylesterase 2	A0A452FRI2	A0A452FRI2_CAPHI	PON2	0.64348
MPN domain-containing protein	A0A452F0S3	A0A452F0S3_CAPHI	PRPF8	0.639889
Nucleosome assembly protein 1-like 1	A0A452DUC4	A0A452DUC4_CAPHI	LOC102176008	0.63902
Epoxide hydrolase	A0A452F2I2	A0A452F2I2_CAPHI	EPHX1	0.636609
Phosphomannomutase	A0A452FM48	A0A452FM48_CAPHI	PMM2	0.633934
Tropomyosin alpha-3 chain	A0A452F0W7	A0A452F0W7_CAPHI	TPM3	0.633623
Serine and arginine rich splicing factor 3	A0A452E0R7	A0A452E0R7_CAPHI	SRSF3	0.63287
Nucleobindin-2	A0A452G1R9	A0A452G1R9_CAPHI	NUCB2	0.629403
Calmegin	A0A452EPL0	A0A452EPL0_CAPHI	CLGN	0.629065
Cathelicidin-2	A0A452F973	A0A452F973_CAPHI	CATHL2	0.625811
Actin, alpha skeletal muscle	A0A452EFE3	A0A452EFE3_CAPHI	ACTA1	0.619035
Peptidyl-prolyl cis-trans isomerase D	A0A452E5T3	A0A452E5T3_CAPHI	PPID	0.617126
Flavodoxin_2 domain-containing protein	A0A452G4A1	A0A452G4A1_CAPHI	NQO1	0.60844
14 kDa phosphohistidine phosphatase	A0A452DLG8	A0A452DLG8_CAPHI	PHPT1	0.607832
Cytosolic 5'-nucleotidase 1A	A0A452G9I1	A0A452G9I1_CAPHI	NT5C1A	0.603282
Protein NDRG4	A0A452FKQ2	A0A452FKQ2_CAPHI	NDRG4	0.59439
TPR_REGION domain-containing protein	A0A452F1P8	A0A452F1P8_CAPHI	ST13	0.582433
Protein phosphatase methylesterase 1	A0A452EHZ0	A0A452EHZ0_CAPHI	PPME1	0.575427

Protein disulfide-isomerase	A0A452G7V5	A0A452G7V5_CAPHI	P4HB	0.57506
Elongation factor 1-alpha	A0A452EWA5	A0A452EWA5_CAPHI	EEF1A2	0.57406
Caveolin	A0A452F8Y4	A0A452F8Y4_CAPHI	CAV1	0.570164
Thioredoxin domain-containing protein	A0A452GB70	A0A452GB70_CAPHI	ERP44	0.568227
Pyridoxal kinase	A0A452DXH7	A0A452DXH7_CAPHI	PDXK	0.567871
Hsp90 chaperone protein kinase-targeting subunit	A0A452DMC5	A0A452DMC5_CAPHI	CDC37	0.565205
Protein-serine/threonine kinase	A0A452EB53	A0A452EB53_CAPHI	PDK1	0.564358
2'-deoxynucleoside 5'-phosphate N-hydrolase 1	A0A452EMT6	A0A452EMT6_CAPHI	DNPH1	0.564068
Fibrinogen C-terminal domain-containing protein	A0A452FZU7	A0A452FZU7_CAPHI	MFAP4	0.56355
Succinate dehydrogenase cytochrome b560 subunit, mitochondrial	A0A452DYA9	A0A452DYA9_CAPHI	SDHC	0.558444
Importin N-terminal domain-containing protein	A0A452FTN8	A0A452FTN8_CAPHI	TNPO1	0.55633
14-3-3 protein theta	A0A452ECX7	A0A452ECX7_CAPHI	YWHAQ	0.553241
Tryptophanyl-tRNA synthetase	A0A452EGV3	A0A452EGV3_CAPHI	WARS2	0.545106
Neuropilin	A0A452DVS7	A0A452DVS7_CAPHI	NRP1	0.542856
Alpha(B)-crystallin	A0A452EJN6	A0A452EJN6_CAPHI	CRYAB	0.542451
Calcium-binding protein 39	A0A452FY20	A0A452FY20_CAPHI	CAB39	0.535436
Ras-related protein Rab-11A	A0A452EBK8	A0A452EBK8_CAPHI	RAB11A	0.532548
UBC core domain-containing protein	A0A452DLH9	A0A452DLH9_CAPHI	UBE2L3	0.52506
HIT domain-containing protein	A0A452E2L2	A0A452E2L2_CAPHI	HINT2	0.517671
Lipoma-preferred partner	A0A452FIK7	A0A452FIK7_CAPHI	LPP	0.514742
Cardiomyopathy-associated protein 5	A0A452G8K6	A0A452G8K6_CAPHI	CMYA5	0.514668
Nudix hydrolase domain-containing protein	A0A452FDJ0	A0A452FDJ0_CAPHI	NUDT9	0.514399
Kinesin-like protein	A0A452F874	A0A452F874_CAPHI	KIF5B	0.513384
COP9 signalosome complex subunit 2	A0A452FJG6	A0A452FJG6_CAPHI	COPS2	0.512563
Mitogen-activated protein kinase	A0A452EVI4	A0A452EVI4_CAPHI	MAPK12	0.512523
Rhodanese domain-containing protein	A0A452G3X4	A0A452G3X4_CAPHI	TSTD1	0.512291
Medium-chain acyl-CoA ligase ACSF2, mitochondrial	A0A452G8P5	A0A452G8P5_CAPHI	ACSF2	0.486525
Inorganic diphosphatase	A0A452DW40	A0A452DW40_CAPHI	PPA2	0.485303
Microsomal prostaglandin E synthase 2	A0A452G9H8	A0A452G9H8_CAPHI	PTGES2	0.472668
Inorganic diphosphatase	A0A452DWB5	A0A452DWB5_CAPHI	PPA2	0.470099
L-lactate dehydrogenase	A0A452E480	A0A452E480_CAPHI	LDHB	0.467515
Methylmalonyl-CoA isomerase	A0A452FS81	A0A452FS81_CAPHI	MMUT	0.449462
5-formyltetrahydrofolate cyclo-ligase	A0A452EUI1	A0A452EUI1_CAPHI	LOC102172393	0.44129
14_3_3 domain-containing protein	A0A452EU44	A0A452EU44_CAPHI	YWHAH	0.440295
NAD(P)-bd_dom domain-containing protein	A0A452FK08	A0A452FK08_CAPHI	BLVRB	0.433077
Calcium-activated neutral proteinase small subunit	A0A452EWE8	A0A452EWE8_CAPHI	CAPNS1	0.432237

Ras-related protein Rab-11B	A0A452FNL4	A0A452FNL4_CAPHI	RAB11B	0.4313
ADP-ribosylation factor 4	A0A452DS03	A0A452DS03_CAPHI	LOC108633910	0.429005
FERM domain-containing protein	A0A452F2C6	A0A452F2C6_CAPHI	EZR	0.424073
Fumarate hydratase, mitochondrial	A0A452DPJ7	A0A452DPJ7_CAPHI	FH	0.421047
Insulin-degrading enzyme	A0A452EWG8	A0A452EWG8_CAPHI	IDE	0.420459
Mitogen-activated protein kinase	A0A452DM03	A0A452DM03_CAPHI	MAPK14	0.419722
Pyr_redox_2 domain-containing protein	A0A452E9Y1	A0A452E9Y1_CAPHI	SQOR	0.419116
Elongation factor 1-gamma	A0A452FNW0	A0A452FNW0_CAPHI	EEF1G	0.416686
Peptidase_M3 domain-containing protein	A0A452EIW8	A0A452EIW8_CAPHI	THOP1	0.411928
Pyruvate kinase	A0A452ET82	A0A452ET82_CAPHI	PKM	0.408366
Pyruvate kinase	A0A452EU77	A0A452EU77_CAPHI	PKM	0.40792
Ig-like domain-containing protein	A0A452DYV8	A0A452DYV8_CAPHI	AZGP1	0.406659
1,4-alpha-glucan branching enzyme	A0A452G133	A0A452G133_CAPHI	GBE1	0.402056
Electron transfer flavoprotein-ubiquinone oxidoreductase	A0A452FRH5	A0A452FRH5_CAPHI	ETFDH	0.397831
Glyoxalase domain-containing protein 4	A0A452DZ71	A0A452DZ71_CAPHI	GLOD4	0.396202
Ubiquitin carboxyl-terminal hydrolase	A0A452EC09	A0A452EC09_CAPHI	USP5	0.392993
Ras GTPase-activating-like protein IQGAP1	A0A452E2E2	A0A452E2E2_CAPHI	IQGAP1	0.387255
Creatine kinase	A0A452FZ73	A0A452FZ73_CAPHI	CKM	0.385153
Alpha-1,4 glucan phosphorylase	A0A452G5W4	A0A452G5W4_CAPHI	PYGB	0.363848
ADP-ribosylation factor 1	A0A452E633	A0A452E633_CAPHI	ARF1	0.360695
PCI domain-containing protein	A0A452DW82	A0A452DW82_CAPHI	PSMD11	0.357048
HATPase_c domain-containing protein	A0A452E1G9	A0A452E1G9_CAPHI	HSP90B1	0.347101
ATP-dependent RNA helicase DDX1	A0A452E6Q6	A0A452E6Q6_CAPHI	DDX1	0.333734
Cytochrome b5 heme-binding domain-containing protein	A0A452G0B4	A0A452G0B4_CAPHI	NENF	0.321792
15S Mg(2+)-ATPase p97 subunit	A0A452F4B6	A0A452F4B6_CAPHI	VCP	0.320552
Annexin	A0A452EVG2	A0A452EVG2_CAPHI	ANXA6	0.310045
Guanine nucleotide-binding protein G(i) subunit alpha-2	A0A452E1P4	A0A452E1P4_CAPHI	GNAI2	-0.25125
Glutamate dehydrogenase (NAD(P)(+))	A0A452DLE1	A0A452DLE1_CAPHI	GLUD1	-0.25844
AP-2 complex subunit alpha	A0A452G2Q0	A0A452G2Q0_CAPHI	AP2A2	-0.26594
Proteasome subunit alpha type	A0A452FB11	A0A452FB11_CAPHI	PSMA1	-0.26733
Protein kinase domain-containing protein	A0A452G4G0	A0A452G4G0_CAPHI	NRBP1	-0.28148
Actin-related protein 2/3 complex subunit	A0A452EHP3	A0A452EHP3_CAPHI	ARPC1A	-0.31001
Proteasome subunit alpha type	B9VR86	B9VR86_CAPHI	PSMA6	-0.3118
Haloacid dehalogenase-like hydrolase domain-containing 5	A0A452EJE6	A0A452EJE6_CAPHI	HDHD5	-0.32867
Heterogeneous nuclear ribonucleoprotein R	A0A452FWA5	A0A452FWA5_CAPHI	HNRNPR	-0.33539
Tetraspanin	A0A452E0U0	A0A452E0U0_CAPHI	CD81	-0.34245
Proteasome subunit beta	A0A452E813	A0A452E813_CAPHI	PSMB5	-0.34445

Methylcrotonoyl-CoA carboxylase beta chain, mitochondrial	A0A452FSB8	A0A452FSB8_CAPHI	MCCC2	-0.36232
Proteasome subunit alpha type	A0A452EWR7	A0A452EWR7_CAPHI	PSMA3	-0.36718
Ectonucleotide pyrophosphatase/phosphodiesterase family member 1	A0A452FZ57	A0A452FZ57_CAPHI	ENPP1	-0.38767
Spectrin alpha chain, non-erythrocytic 1	A0A452EHE9	A0A452EHE9_CAPHI	SPTAN1	-0.38793
Spectrin alpha chain, non-erythrocytic 1	A0A452EHD5	A0A452EHD5_CAPHI	SPTAN1	-0.38906
Delta(3,5)-Delta(2,4)-dienoyl-CoA isomerase, mitochondrial	A0A452G3I1	A0A452G3I1_CAPHI	ECH1	-0.39057
Macrophage-capping protein	A0A452FGC9	A0A452FGC9_CAPHI	CAPG	-0.39416
Alpha-centractin	A0A452ELK2	A0A452ELK2_CAPHI	ACTR1A	-0.39721
28S ribosomal protein S22, mitochondrial	A0A452GAM6	A0A452GAM6_CAPHI	MRPS22	-0.40668
Cytosol aminopeptidase	A0A452DVV1	A0A452DVV1_CAPHI	LAP3	-0.41265
Decorin	A0A452F311	A0A452F311_CAPHI	DCN	-0.41785
acidPPc domain-containing protein	A0A452FPG6	A0A452FPG6_CAPHI	PLPP3	-0.43454
ADP-ribose glycohydrolase ARH3	A0A452E8X2	A0A452E8X2_CAPHI	ADPRS	-0.43592
Aminomethyltransferase	A0A452F0W6	A0A452F0W6_CAPHI	AMT	-0.44151
E3 ubiquitin-protein ligase CHIP	A0A452E6Z8	A0A452E6Z8_CAPHI	STUB1	-0.45723
VOC domain-containing protein	A0A452FD94	A0A452FD94_CAPHI	MCEE	-0.4631
Helix-destabilizing protein	A0A452G1G3	A0A452G1G3_CAPHI	HNRNPA1	-0.46438
Fructose-bisphosphate aldolase	A0A452DZ70	A0A452DZ70_CAPHI	ALDOC	-0.46899
Ras-related protein Rab-7a	A0A452DMR1	A0A452DMR1_CAPHI	RAB7A	-0.4712
Heterogeneous nuclear ribonucleoprotein D0	A0A452FMV1	A0A452FMV1_CAPHI	HNRNPD	-0.47652
t-SNARE coiled-coil homology domain-containing protein	A0A452EI11	A0A452EI11_CAPHI	STX4	-0.48277
Cytokeratin-1	A0A452GA47	A0A452GA47_CAPHI	KRT1	-0.48878
Heme-binding protein 1	A0A452DLZ9	A0A452DLZ9_CAPHI	HEBP1	-0.48933
Serine/arginine-rich splicing factor 2	A0A452EXY9	A0A452EXY9_CAPHI	SRSF2	-0.50036
IF rod domain-containing protein	A0A452EML6	A0A452EML6_CAPHI	KRT75	-0.50163
60S ribosomal protein L30	A0A452EXP6	A0A452EXP6_CAPHI	RPL30	-0.50589
Peptidyl-prolyl cis-trans isomerase E	A0A452ECN5	A0A452ECN5_CAPHI	PPIE	-0.51248
Junction plakoglobin	A0A452G6Z9	A0A452G6Z9_CAPHI	JUP	-0.51789
Complement factor H	A0A452FFD7	A0A452FFD7_CAPHI	CFH	-0.51985
40S ribosomal protein S15a	A0A452DNF8	A0A452DNF8_CAPHI	LOC102173911	-0.52674
(3R)-3-hydroxyacyl-CoA dehydrogenase	A0A452F211	A0A452F211_CAPHI	HSD17B8	-0.53067
Spectrin beta chain	A0A452E729	A0A452E729_CAPHI	SPTB	-0.53429
Hydroxyacyl-coenzyme A dehydrogenase, mitochondrial	A0A452EHJ6	A0A452EHJ6_CAPHI	HADH	-0.53503
40S ribosomal protein S16	A0A452FWU9	A0A452FWU9_CAPHI	RPS16	-0.53696
High mobility group protein B1	A0A452F540	A0A452F540_CAPHI	HMGB1	-0.54139
Eukaryotic translation initiation factor 3 subunit K	A0A452FS00	A0A452FS00_CAPHI	EIF3K	-0.54728

Apolipoprotein H	A0A452FZ04	A0A452FZ04_CAPHI	APOH	-0.54802
Septin-2	A0A452G8J5	A0A452G8J5_CAPHI	SEPTIN2	-0.55217
Dynamin GTPase	A0A452G5F8	A0A452G5F8_CAPHI	DNM2	-0.55427
Actin-related protein 2/3 complex subunit 3	A0A452FVB0	A0A452FVB0_CAPHI	ARPC3	-0.55802
Lactotransferrin	Q29477	TRFL_CAPHI	LTF	-0.55999
Protein-synthesizing GTPase	A0A452DQ55	A0A452DQ55_CAPHI	EIF2S3	-0.56503
CSD_1 domain-containing protein	A0A452EQN7	A0A452EQN7_CAPHI	CARHSP1	-0.57221
RNA-binding protein 39	A0A452G0J5	A0A452G0J5_CAPHI	RBM39	-0.57473
Malic enzyme	A0A452EKF4	A0A452EKF4_CAPHI	ME3	-0.57901
Mammalian ependymin-related protein 1	A0A452F7G3	A0A452F7G3_CAPHI	EPDR1	-0.57926
Guanine nucleotide-binding protein subunit alpha-11	A0A452EAS1	A0A452EAS1_CAPHI	GNA11	-0.57941
Post-proline cleaving enzyme	A0A452F9B9	A0A452F9B9_CAPHI	PREP	-0.58721
Utrophin	A0A452DQU9	A0A452DQU9_CAPHI	UTRN	-0.59497
RRM domain-containing protein	A0A452FP83	A0A452FP83_CAPHI	HNRNPC	-0.60159
Macrophage migration inhibitory factor	A0A452FQK5	A0A452FQK5_CAPHI	MIF	-0.61685
Laminin subunit alpha-4	A0A452FAG1	A0A452FAG1_CAPHI	LAMA4	-0.61738
Protein-serine/threonine kinase	A0A452E6M1	A0A452E6M1_CAPHI	PDK3	-0.61752
Fructose-bisphosphate aldolase	A0A452EH63	A0A452EH63_CAPHI	ALDOA	-0.62541
Hydrolase_4 domain-containing protein	A0A452E6R4	A0A452E6R4_CAPHI	MGLL	-0.63103
Keratin, type I cytoskeletal 25	A0A452EQ71	A0A452EQ71_CAPHI	KRT25	-0.63593
Protein S100	A0A452G7N6	A0A452G7N6_CAPHI	S100A16	-0.63732
40S ribosomal protein S9	A0A452FX42	A0A452FX42_CAPHI	RPS9	-0.63967
Poly(rC)-binding protein 1	A0A452DVL8	A0A452DVL8_CAPHI	PCBP1	-0.64376
PHB domain-containing protein	A0A452E9N0	A0A452E9N0_CAPHI	STOM	-0.64989
60S ribosomal protein L36	A0A452EMZ1	A0A452EMZ1_CAPHI	RPL36	-0.66075
GST class-pi	A0A452ERH0	A0A452ERH0_CAPHI	LOC102184041	-0.67183
Acid ceramidase	A0A452E0H9	A0A452E0H9_CAPHI	ASAH1	-0.67802
60S ribosomal protein L23	A0A452DR46	A0A452DR46_CAPHI	LOC102169182	-0.68061
WD_REPEATS_REGION domain-containing protein	A0A452G2P0	A0A452G2P0_CAPHI	DYNC1I2	-0.69076
IF rod domain-containing protein	A0A452FER9	A0A452FER9_CAPHI	KRT7	-0.69561
Cytochrome c oxidase subunit 2	D2KMJ8	D2KMJ8_CAPHI	MT-CO2	-0.71383
Biglycan	A0A452DTM3	A0A452DTM3_CAPHI	BGN	-0.71995
Ecto-5'-nucleotidase	A0A452E4U4	A0A452E4U4_CAPHI	NT5E	-0.74684
IF rod domain-containing protein	A0A452F3I2	A0A452F3I2_CAPHI	KRT12	-0.7623
KAT8 regulatory NSL complex subunit 3	A0A452EG01	A0A452EG01_CAPHI	KANSL3	-0.76793
RNA-binding protein FUS	A0A452DQG8	A0A452DQG8_CAPHI	FUS	-0.76915
Tetraspanin	A0A452DYP4	A0A452DYP4_CAPHI	CD9	-0.77398
40S ribosomal protein S8	A0A452FDR2	A0A452FDR2_CAPHI	RPS8	-0.78631
Palmdelphin	A0A452G5M5	A0A452G5M5_CAPHI	PALMD	-0.7961
EF-hand domain-containing protein	A0A452G6U6	A0A452G6U6_CAPHI	TESC	-0.82531

Adipsin	A0A452F6V7	A0A452F6V7_CAPHI	CFD	-0.82905
Early endosome antigen 1	A0A452FIX8	A0A452FIX8_CAPHI	EEA1	-0.84786
A_deaminase domain-containing protein	A0A452DR44	A0A452DR44_CAPHI	ADAL	-0.8484
Alpha-S1-casein	P18626	CASA1_CAPHI	CSN1S1	-0.85646
C-terminal-binding protein 1	A0A452G220	A0A452G220_CAPHI	CTBP1	-0.86849
Prolow-density lipoprotein receptor-related protein 1	A0A452FYK1	A0A452FYK1_CAPHI	LRP1	-0.87083
Alpha-S2-casein	P33049	CASA2_CAPHI	CSN1S2	-0.87083
39S ribosomal protein L46, mitochondrial	A0A452ET13	A0A452ET13_CAPHI	MRPL46	-0.89112
Sodium/potassium-transporting ATPase subunit alpha	A0A452G969	A0A452G969_CAPHI	ATP1A2	-0.90575
CCT-alpha	A0A452EVX4	A0A452EVX4_CAPHI	TCP1	-0.90927
Protein kinase domain-containing protein	A0A452DYE7	A0A452DYE7_CAPHI	TNK1	-0.94237
S-methyl-5'-thioadenosine phosphorylase	A0A452EN12	A0A452EN12_CAPHI	MTAP	-0.94402
H15 domain-containing protein	A0A452E5I0	A0A452E5I0_CAPHI	H1-3	-0.94809
WD repeat-containing protein 81	A0A452G9D8	A0A452G9D8_CAPHI	WDR81	-1.00024
Interleukin-6	Q28319	IL6_CAPHI	IL6	-1.04147
Complement factor I	A0A452DTU9	A0A452DTU9_CAPHI	CFI	-1.04186
RNA helicase	A0A452G600	A0A452G600_CAPHI	DDX6	-1.04338
IF rod domain-containing protein	A0A452G0P6	A0A452G0P6_CAPHI	KRT10	-1.04531
Tubulin beta chain	A0A452G3J7	A0A452G3J7_CAPHI	TUBB2A	-1.07237
IF rod domain-containing protein	A0A452ECG5	A0A452ECG5_CAPHI	LOC102176997	-1.07315
CTD domain-containing protein	A0A452E7D3	A0A452E7D3_CAPHI	SRRM2	-1.07353
Acidic leucine-rich nuclear phosphoprotein 32 family member E	A0A452DNV7	A0A452DNV7_CAPHI	ANP32E	-1.08378
Golgin subfamily B member 1	A0A452GBN0	A0A452GBN0_CAPHI	GOLGB1	-1.11186
IF rod domain-containing protein	A0A452FN18	A0A452FN18_CAPHI	KRT3	-1.12512
Tropomyosin alpha-4 chain	A0A452E0A4	A0A452E0A4_CAPHI	TPM4	-1.14356
Myosin-7B	A0A452F3X0	A0A452F3X0_CAPHI	MYH7B	-1.14602
Interleukin-12 subunit alpha	O02814	IL12A_CAPHI	IL12A	-1.15324
OCIA domain-containing protein	A0A452FY19	A0A452FY19_CAPHI	OCIAD1	-1.18684
IF rod domain-containing protein	A0A452G2U2	A0A452G2U2_CAPHI	LOC108635997	-1.19764
Complement component C7	A0A452EW11	A0A452EW11_CAPHI	C7	-1.20913
Serum amyloid A protein	A0A452FTY4	A0A452FTY4_CAPHI	LOC102168979	-1.21767
IF rod domain-containing protein	A0A452EME0	A0A452EME0_CAPHI	KRT14	-1.2698
Cytochrome b	Q8WF85	Q8WF85_CAPHI	cytb	-1.45505
Arginase	A0A452FLB4	A0A452FLB4_CAPHI	ARG1	-1.45682
Coronin	A0A452FJC1	A0A452FJC1_CAPHI	CORO1A	-1.4663
Glyceraldehyde-3-phosphate dehydrogenase	A0A452E0Z2	A0A452E0Z2_CAPHI	GAPDHS	-1.6073
U3 small nucleolar RNA-associated protein 25 homolog	A0A452FJP9	A0A452FJP9_CAPHI	UTP25	-1.66228

Dihydropyrimidine dehydrogenase [NADP(+)]	A0A452EUG4	A0A452EUG4_CAPHI	DPYD	-1.69687
Lamin-B2	A0A452EGA4	A0A452EGA4_CAPHI	LMNB2	-1.71162
Hemoglobin subunit beta-C	A0A452FX49	A0A452FX49_CAPHI	HBBC	-1.75556
TCTP domain-containing protein	A0A452E2E4	A0A452E2E4_CAPHI	LOC102168398	-1.87502
SWIM-type domain-containing protein	A0A452DJR4	A0A452DJR4_CAPHI	ZSWIM8	-1.93934
Structural maintenance of chromosomes protein	A0A452DY79	A0A452DY79_CAPHI	SMC1A	-2.01977
Mitochondrial import inner membrane translocase subunit TIM16	A0A452DRC3	A0A452DRC3_CAPHI	PAM16	-4.15329

Table A3:1 The Most significantly regulated proteins – Tissue Lysate (TL) fraction

2.3 The Most significantly regulated proteins Mitochondrial (Mito) fraction

Protein Name (Mito fraction)	Accession	Protein ID	Protein/Gene	Log2Fold change
SAP domain-containing protein	A0A452DL17	A0A452DL17_CAPHI	CCAR1	2.679643383
Myomesin-2	A0A452E9Y7	A0A452E9Y7_CAPHI	MYOM2	1.864306981
Transmembrane protein 182	A0A452FJJ0	A0A452FJJ0_CAPHI	TMEM182	1.737569451
Cerebral dopamine neurotrophic factor	A0A452F8A8	A0A452F8A8_CAPHI	CDNF	1.736772949
BolA-like protein 2	A0A452FYK7	A0A452FYK7_CAPHI	BOLA2B	1.702977777
2-phospho-D-glycerate hydro-lyase	A0A452FB24	A0A452FB24_CAPHI	ENO3	1.689024791
Rib_recp_KP_reg domain-containing protein	A0A452FQG0	A0A452FQG0_CAPHI	RRBP1	1.652441065
SH3 domain-containing kinase-binding protein 1	A0A452EMI7	A0A452EMI7_CAPHI	LOC108634607	1.616510739
Chondroitin sulfate proteoglycan 4	A0A452FNK5	A0A452FNK5_CAPHI	CSPG4	1.586058338
Autism susceptibility gene 2 protein	A0A452EW73	A0A452EW73_CAPHI	AUTS2	1.556596494
Cathelicidin-2	A0A452F973	A0A452F973_CAPHI	CATHL2	1.527757913
Calcium-transporting ATPase	A0A452F5R6	A0A452F5R6_CAPHI	ATP2A3	1.520948403
PDZ and LIM domain protein 5	A0A452DXY8	A0A452DXY8_CAPHI	PDLIM5	1.513670524
PRA1 family protein	A0A452FJJ3	A0A452FJJ3_CAPHI	ARL6IP5	1.442342828
IF rod domain-containing protein	A0A452G757	A0A452G757_CAPHI	NES	1.385065352
NADH dehydrogenase (Ubiquinone) 1 alpha subcomplex 4	A5JSS3	A5JSS3_CAPHI	NDUFA4	1.381476854
SHSP domain-containing protein	A0A452G662	A0A452G662_CAPHI	HSPB7	1.362984546
60S ribosomal protein L14	A0A452F9G8	A0A452F9G8_CAPHI	RPL14	1.341212511
Cytochrome c oxidase subunit 7A1, mitochondrial	A0A452EN08	A0A452EN08_CAPHI	COX7A1	1.328395451

Clathrin light chain	A0A452F3N4	A0A452F3N4_CAPHI	CLTB	1.300505525
Phosphomannomutase	A0A452FM48	A0A452FM48_CAPHI	PMM2	1.258902599
Glucose transporter type 4, insulin-responsive	A0A452FEB3	A0A452FEB3_CAPHI	SLC2A4	1.254747565
Serine/threonine-protein phosphatase 2A 65 kDa regulatory subunit A beta isoform	A0A452FC43	A0A452FC43_CAPHI	PPP2R1B	1.227426584
Heat shock 27 kDa protein	A0A452ESU7	A0A452ESU7_CAPHI	HSPB1	1.20855701
Alpha-actinin-4	A0A452E7A9	A0A452E7A9_CAPHI	ACTN4	1.190868288
Peroxiredoxin-6	A0A452EUX2	A0A452EUX2_CAPHI	PRDX6	1.190308454
Tropomyosin beta chain	A0A452EN00	A0A452EN00_CAPHI	TPM2	1.179895292
Sodium/potassium-transporting ATPase subunit beta	A0A452DMV1	A0A452DMV1_CAPHI	ATP1B4	1.128908515
Genetic suppressor element 1	A0A452G1G7	A0A452G1G7_CAPHI	GSE1	1.12015748
Cystatin domain-containing protein	A0A452F4D3	A0A452F4D3_CAPHI	LOC102186806	1.119886837
Calumenin	A0A452G3A0	A0A452G3A0_CAPHI	CALU	1.118333469
Complex I-MNLL	A0A452ERZ9	A0A452ERZ9_CAPHI	NDUFB1	1.082844466
Spectrin alpha chain, erythrocytic 1	A0A452E834	A0A452E834_CAPHI	SPTA1	1.078825346
Lipoma-preferred partner	A0A452FIK7	A0A452FIK7_CAPHI	LPP	1.071918091
Gal_mutarotas_2 domain-containing protein	A0A452FP74	A0A452FP74_CAPHI	GANAB	1.023952086
Complex I-B12	A0A452FQM9	A0A452FQM9_CAPHI	NDUFB3	1.018589171
NAD-dependent protein deacetylase	A0A452EPW1	A0A452EPW1_CAPHI	SIRT3	1.006681614
Tubulin alpha chain	A0A452DNE3	A0A452DNE3_CAPHI	TUBA4A	0.990908046
Actin, cytoplasmic 1-like	A0A452EU47	A0A452EU47_CAPHI	LOC102180084	0.937859297
ATP synthase peripheral stalk subunit	A0A452E2H1	A0A452E2H1_CAPHI	ATP5PO	0.892853598
Nucleobindin-2	A0A452G1R9	A0A452G1R9_CAPHI	NUCB2	0.89032195
Mitogen-activated protein kinase	A0A452EU65	A0A452EU65_CAPHI	MAPK3	0.883618345
Amine oxidase	A0A452FZL6	A0A452FZL6_CAPHI	MAOB	0.880046725
Tropomyosin alpha-3 chain	A0A452F0W7	A0A452F0W7_CAPHI	TPM3	0.844483445
Filamin-A	A0A452E7C9	A0A452E7C9_CAPHI	FLNA	0.831979021
Filamin-B	A0A452ETD8	A0A452ETD8_CAPHI	FLNB	0.830764545
Epoxide hydrolase	A0A452F2I2	A0A452F2I2_CAPHI	EPHX1	0.822289386
Reticulocalbin-2	A0A452EW53	A0A452EW53_CAPHI	RCN2	0.820237198
Beta-taxilin	A0A452G9A6	A0A452G9A6_CAPHI	TXLNB	0.806409746
Hsp90 chaperone protein kinase-targeting subunit	A0A452DMC5	A0A452DMC5_CAPHI	CDC37	0.792134276
RNA helicase	A0A452DQY2	A0A452DQY2_CAPHI	DDX39B	0.789986856
Ras-related GTP-binding protein	A0A452DQZ4	A0A452DQZ4_CAPHI	RRAGA	0.778333694
NADH dehydrogenase [ubiquinone] iron-sulfur protein 4, mitochondrial	A0A452G117	A0A452G117_CAPHI	NDUFS4	0.762397677
Protein phosphatase methylesterase 1	A0A452EHZ0	A0A452EHZ0_CAPHI	PPME1	0.725795858
Transket_pyr domain-containing protein	A0A452FP45	A0A452FP45_CAPHI	OGDHL	0.712171872

Calnexin	A0A452DM15	A0A452DM15_CAPHI	CANX	0.710042725
14 kDa phosphohistidine phosphatase	A0A452DLG8	A0A452DLG8_CAPHI	PHPT1	0.707391791
Acetyl-coenzyme A synthetase	A0A452FKE9	A0A452FKE9_CAPHI	ACSS1	0.696863155
Myosin-4	A0A452E568	A0A452E568_CAPHI	MYH4	0.691417993
ATP synthase subunit epsilon, mitochondrial	A0A452FTG4	A0A452FTG4_CAPHI	ATP5F1E	0.684425908
Eukaryotic translation initiation factor 4 gamma 1	A0A452E1M0	A0A452E1M0_CAPHI	EIF4G1	0.674328705
B-cell receptor-associated protein	A0A452ED36	A0A452ED36_CAPHI	BCAP31	0.668274879
TPR_REGION domain-containing protein	A0A452F1P8	A0A452F1P8_CAPHI	ST13	0.657224317
Peptidylprolyl isomerase	A0A452F711	A0A452F711_CAPHI	FKBP3	0.643492396
Protein preY, mitochondrial	A0A452E134	A0A452E134_CAPHI	PYURF	0.627047648
Neuropilin	A0A452DVS7	A0A452DVS7_CAPHI	NRP1	0.621326605
Ras-related protein Rab-11A	A0A452EBK8	A0A452EBK8_CAPHI	RAB11A	0.587331372
COP9 signalosome complex subunit 4	A0A452EN27	A0A452EN27_CAPHI	COPS4	0.573800287
KOW domain-containing protein	A0A452G1I8	A0A452G1I8_CAPHI	RPL26	0.526351285
6-phosphogluconolactonase	A0A452FZF1	A0A452FZF1_CAPHI	PGLS	0.499311574
Fructose-bisphosphate aldolase	A0A452DZ70	A0A452DZ70_CAPHI	ALDOC	-0.46849859
Cytosol aminopeptidase	A0A452DVV1	A0A452DVV1_CAPHI	LAP3	-0.481266379
Sulfatase domain-containing protein	A0A452EHN0	A0A452EHN0_CAPHI	ARSA	-0.556893745
Hypoxia up-regulated protein 1	A0A452F0T8	A0A452F0T8_CAPHI	HYOU1	-0.579841052
Peroxin-19	A0A452EGH5	A0A452EGH5_CAPHI	PEX19	-0.595367932
Poly(rC)-binding protein 1	A0A452DVL8	A0A452DVL8_CAPHI	PCBP1	-0.639672975
Proteasome subunit alpha type	A0A452EWR7	A0A452EWR7_CAPHI	PSMA3	-0.659320295
S-methyl-5'-thioadenosine phosphorylase	A0A452EN12	A0A452EN12_CAPHI	MTAP	-0.727276062
Ras-related protein Rab-2A	I1W1N0	I1W1N0_CAPHI	RAB2A	-0.738402245
Arginase	A0A452FLB4	A0A452FLB4_CAPHI	ARG1	-0.741209502
Coronin	A0A452FJC1	A0A452FJC1_CAPHI	CORO1A	-0.770637751
Apolipoprotein H	A0A452FZ04	A0A452FZ04_CAPHI	APOH	-0.78832525
Actin-related protein 2/3 complex subunit 3	A0A452FVB0	A0A452FVB0_CAPHI	ARPC3	-0.824847415
Hydroxyacyl-coenzyme A dehydrogenase, mitochondrial	A0A452EHJ6	A0A452EHJ6_CAPHI	HADH	-0.825262278
OCIA domain-containing protein	A0A452FY19	A0A452FY19_CAPHI	OCIAD1	-0.82801342
26S proteasome non-ATPase regulatory subunit 5	A0A452FI84	A0A452FI84_CAPHI	PSMD5	-0.849809865
Acid ceramidase	A0A452E0H9	A0A452E0H9_CAPHI	ASAH1	-0.887602528
Proteasome assembly chaperone 2	A0A452DTJ6	A0A452DTJ6_CAPHI	PSMG2	-0.893549422
Eukaryotic translation initiation factor 3 subunit L	A0A452EL27	A0A452EL27_CAPHI	EIF3L	-0.925396701
DZF domain-containing protein	A0A452EA62	A0A452EA62_CAPHI	ILF2	-0.93170774
IF rod domain-containing protein	A0A452FN18	A0A452FN18_CAPHI	KRT3	-0.937678327

Collagen type XI alpha 2 chain	A0A452EBR1	A0A452EBR1_CAPHI	COL11A2	-0.956333848
Ribose-5-phosphate isomerase	A0A452EW09	A0A452EW09_CAPHI	RPIA	-0.957096597
Serine/arginine-rich splicing factor 2	A0A452EXY9	A0A452EXY9_CAPHI	SRSF2	-0.958351582
Protein kinase C	A0A452FXS0	A0A452FXS0_CAPHI	PRKCA	-1.117050548
Myosin-7B	A0A452F3X0	A0A452F3X0_CAPHI	MYH7B	-1.150230295
WD_REPEATS_REGION domain-containing protein	A0A452DNL3	A0A452DNL3_CAPHI	GNB2	-1.234709526
Interleukin-6	Q28319	IL6_CAPHI	IL6	-1.242234449
Macrophage migration inhibitory factor	A0A452FQK5	A0A452FQK5_CAPHI	MIF	-1.314031025
U6 snRNA-associated Sm-like protein LSm2	A0A452ETL0	A0A452ETL0_CAPHI	LSM2	-1.317363163
Sestrin-3	A0A452G353	A0A452G353_CAPHI	SESN3	-1.394218663
Hemoglobin subunit beta-C	A0A452FX49	A0A452FX49_CAPHI	HBBC	-1.511518228
Syntenin-1	A0A452F195	A0A452F195_CAPHI	SDCBP	-1.566873374
TCTP domain-containing protein	A0A452E2E4	A0A452E2E4_CAPHI	LOC102168398	-1.598622466
Protein kinase domain-containing protein	A0A452DYE7	A0A452DYE7_CAPHI	TNK1	-1.73113354
SWIM-type domain-containing protein	A0A452DJR4	A0A452DJR4_CAPHI	ZSWIM8	-1.886654228
Lamin-B2	A0A452EGA4	A0A452EGA4_CAPHI	LMNB2	-1.977324466

Table A3:2 The Most significantly regulated proteins – Mitochondrial (Mito) fraction

2.4 The Most significantly regulated proteins – Endolysosomal (EL) fraction

Protein name (EL fraction)	**Accession**	**Protein ID**	**Protein/Gene**	**Log2 Fold change**
Prefoldin subunit 4	A0A452F9W2	A0A452F9W2_CAPHI	PFDN4	2.119092
Single-pass membrane and coiled-coil domain-containing protein 4	A0A452DN27	A0A452DN27_CAPHI	SMCO4	2.012148
Structural maintenance of chromosomes protein	A0A452DY79	A0A452DY79_CAPHI	SMC1A	2.012094
SAP domain-containing protein	A0A452DL17	A0A452DL17_CAPHI	CCAR1	1.991
E3 ubiquitin-protein ligase HECTD3	A0A452G2Z7	A0A452G2Z7_CAPHI	HECTD3	1.832324
WD_REPEATS_REGION domain-containing protein	A0A452DPX9	A0A452DPX9_CAPHI	WDR78	1.789756
Reticulon	A0A452EJX2	A0A452EJX2_CAPHI	RTN3	1.782796

SHSP domain-containing protein	A0A452G662	A0A452G662_CAPHI	HSPB7	1.772209
RING finger protein 17	A0A452G8P6	A0A452G8P6_CAPHI	RNF17	1.752444
Calponin-homology (CH) domain-containing protein	A0A452DM61	A0A452DM61_CAPHI	NAV2	1.716669
E3 ubiquitin-protein ligase PPP1R11	A0A452F797	A0A452F797_CAPHI	PPP1R11	1.705649
cAMP-dependent protein kinase inhibitor	A0A452FPZ5	A0A452FPZ5_CAPHI	PKIG	1.681201
1,4-alpha-glucan branching enzyme	A0A452G133	A0A452G133_CAPHI	GBE1	1.66558
Cytochrome c oxidase subunit	A0A452F8B4	A0A452F8B4_CAPHI	COX6A2	1.561108
SHSP domain-containing protein	A0A452G4I2	A0A452G4I2_CAPHI	HSPB2	1.554888
2-phospho-D-glycerate hydro-lyase	A0A452F5D8	A0A452F5D8_CAPHI	ENO2	1.510925
ATP synthase-coupling factor 6, mitochondrial	A0A452FLK7	A0A452FLK7_CAPHI	ATP5PF	1.472771
Actin, alpha cardiac muscle 1	A0A452DQP7	A0A452DQP7_CAPHI	ACTC1	1.46661
DNA-directed RNA polymerase III subunit RPC4	A0A452EBL3	A0A452EBL3_CAPHI	POLR3D	1.462928
Clathrin light chain	A0A452F3N4	A0A452F3N4_CAPHI	CLTB	1.453916
Splicing factor, proline- and glutamine-rich	A0A452FRY3	A0A452FRY3_CAPHI	SFPQ	1.431758
Mitochondrial import inner membrane translocase subunit TIM16	A0A452DRC3	A0A452DRC3_CAPHI	PAM16	1.389762
Complex I-MNLL	A0A452ERZ9	A0A452ERZ9_CAPHI	NDUFB1	1.365012
D-beta-hydroxybutyrate dehydrogenase, mitochondrial	A0A452G711	A0A452G711_CAPHI	BDH1	1.322843
Protein cordon-bleu	A0A452FQ01	A0A452FQ01_CAPHI	COBL	1.253796
Prefoldin subunit 1	A0A452E6Y1	A0A452E6Y1_CAPHI	PFDN1	1.215183
PRA1 family protein	A0A452FJJ3	A0A452FJJ3_CAPHI	ARL6IP5	1.195813
Microtubule-actin cross-linking factor 1, isoforms 1/2/3/5	A0A452DY71	A0A452DY71_CAPHI	MACF1	1.18684
Lipoma-preferred partner	A0A452FIK7	A0A452FIK7_CAPHI	LPP	1.181124
Cathelicidin-2	A0A452F973	A0A452F973_CAPHI	CATHL2	1.156658
Myosin phosphatase Rho-interacting protein	A0A452EW34	A0A452EW34_CAPHI	MPRIP	1.138741
PDZ domain-containing protein	A0A452EQJ4	A0A452EQJ4_CAPHI	AHNAK	1.136853
Coxsackievirus and adenovirus receptor	A0A452FP52	A0A452FP52_CAPHI	CXADR	1.105928
Protein phosphatase 1 regulatory subunit	A0A452F158	A0A452F158_CAPHI	PPP1R12C	1.10205
NADH dehydrogenase [ubiquinone] iron-sulfur protein 6, mitochondrial	A0A452FDC1	A0A452FDC1_CAPHI	NDUFS6	1.079732
Prelamin-A/C	A0A452FQ33	A0A452FQ33_CAPHI	LMNA	1.071665
Diacylglycerol kinase	A0A452G3Z1	A0A452G3Z1_CAPHI	DGKD	1.055565
Microtubule-associated protein	A0A452EIY1	A0A452EIY1_CAPHI	MAP4	1.045073
Prefoldin subunit 6	A0A452FHF8	A0A452FHF8_CAPHI	PFDN6	1.043646
Autism susceptibility gene 2 protein	A0A452EW73	A0A452EW73_CAPHI	AUTS2	1.038308
NADH dehydrogenase [ubiquinone] 1 beta subcomplex subunit 8, mitochondrial	A0A452EKC1	A0A452EKC1_CAPHI	NDUFB8	1.020162
Ubiquitinyl hydrolase 1	A0A452FL98	A0A452FL98_CAPHI	USP9X	1.004248
Hsp90 chaperone protein kinase-targeting subunit	A0A452DMC5	A0A452DMC5_CAPHI	CDC37	1.002968

BolA-like protein 2	A0A452FYK7	A0A452FYK7_CAPHI	BOLA2B	1.002693
TRASH domain-containing protein	A0A452E9A8	A0A452E9A8_CAPHI	RPL24	0.997535
Ubiquitin-fold modifier-conjugating enzyme 1	A0A452FDZ6	A0A452FDZ6_CAPHI	UFC1	0.997205
Protein-cysteine N-palmitoyltransferase HHAT-like protein	A0A452FSE0	A0A452FSE0_CAPHI	HHATL	0.996004
Dynein light chain roadblock	A0A452F2G4	A0A452F2G4_CAPHI	DYNLRB1	0.977814
IF rod domain-containing protein	A0A452G757	A0A452G757_CAPHI	NES	0.964974
ATP synthase subunit d, mitochondrial	A0A452G5E3	A0A452G5E3_CAPHI	ATP5PD	0.957897
Complex I-B18	A0A452EGT0	A0A452EGT0_CAPHI	NDUFB7	0.950796
Gal_mutarotas_2 domain-containing protein	A0A452FP74	A0A452FP74_CAPHI	GANAB	0.937815
Leucyl-tRNA synthetase	A0A452ENN3	A0A452ENN3_CAPHI	LARS1	0.931774
Vesicle-associated membrane protein-associated protein A	A0A452DKF1	A0A452DKF1_CAPHI	VAPA	0.92626
Cystatin domain-containing protein	A0A452F4D3	A0A452F4D3_CAPHI	LOC102186806	0.922918
NAD-dependent protein deacetylase	A0A452EPW1	A0A452EPW1_CAPHI	SIRT3	0.907779
Cytochrome b5 heme-binding domain-containing protein	A0A452G0B4	A0A452G0B4_CAPHI	NENF	0.90682
N-lysine methyltransferase SMYD2	A0A452F760	A0A452F760_CAPHI	SMYD2	0.899039
Matrix-remodeling-associated protein 7	A0A452DZF9	A0A452DZF9_CAPHI	MXRA7	0.874135
Short/branched chain specific acyl-CoA dehydrogenase	A0A452FYY0	A0A452FYY0_CAPHI	ACADSB	0.866711
NADH dehydrogenase (Ubiquinone) 1 alpha subcomplex 4	A5JSS3	A5JSS3_CAPHI	NDUFA4	0.863957
GRASP55_65 domain-containing protein	A0A452EKQ0	A0A452EKQ0_CAPHI	GORASP2	0.858305
Glutaredoxin domain-containing protein	A0A452FF94	A0A452FF94_CAPHI	GLRX	0.850176
Complex I-B22	A0A452FEX6	A0A452FEX6_CAPHI	NDUFB9	0.84649
Fibronectin	A0A452FJK2	A0A452FJK2_CAPHI	FN1	0.840795
Plasminogen (Fragment)	Q7M323	PLMN_CAPHI	PLG	0.814164
Complex I-B12	A0A452FQM9	A0A452FQM9_CAPHI	NDUFB3	0.808344
Helix-destabilizing protein	A0A452G1G3	A0A452G1G3_CAPHI	HNRNPA1	0.806895
60S acidic ribosomal protein P2	A0A452F1F7	A0A452F1F7_CAPHI	RPLP2	0.773711
Peroxiredoxin-6	A0A452EUX2	A0A452EUX2_CAPHI	PRDX6	0.758201
Myomesin-2	A0A452E9Y7	A0A452E9Y7_CAPHI	MYOM2	0.737294
Transgelin	A0A452GB99	A0A452GB99_CAPHI	TAGLN2	0.709685
Epoxide hydrolase	A0A452F2I2	A0A452F2I2_CAPHI	EPHX1	0.679334
Sodium/potassium-transporting ATPase subunit alpha	A0A452FAW7	A0A452FAW7_CAPHI	ATP4A	0.67095
Heat shock 27 kDa protein	A0A452ESU7	A0A452ESU7_CAPHI	HSPB1	0.63215
Cerebral dopamine neurotrophic factor	A0A452F8A8	A0A452F8A8_CAPHI	CDNF	0.601148
NADH dehydrogenase [ubiquinone] 1 alpha subcomplex subunit 6	A0A452EI29	A0A452EI29_CAPHI	NDUFA6	0.599446
Tubulin-specific chaperone A	A0A452FI28	A0A452FI28_CAPHI	TBCA	0.58214
EH domain-containing protein 1	A0A452FFI1	A0A452FFI1_CAPHI	EHD1	0.567712
CCT-beta	A0A452G4D6	A0A452G4D6_CAPHI	CCT2	0.546448

PCI domain-containing protein	A0A452EF68	A0A452EF68_CAPHI	COPS7A	0.475299
Metaxin-2	A0A452DXZ3	A0A452DXZ3_CAPHI	MTX2	0.461069
Lysosomal alpha-glucosidase	A0A452EV92	A0A452EV92_CAPHI	GAA	0.438701
Filamin-B	A0A452ETD8	A0A452ETD8_CAPHI	FLNB	0.413626
Ribonuclease inhibitor	A0A452ERC8	A0A452ERC8_CAPHI	RNH1	-0.40701
ADP/ATP translocase 3	A0A452EB34	A0A452EB34_CAPHI	SLC25A6	-0.43075
Malic enzyme	A0A452FQE3	A0A452FQE3_CAPHI	ME1	-0.43373
Ras-related protein Rab-7a	A0A452DMR1	A0A452DMR1_CAPHI	RAB7A	-0.50202
Myosin-7B	A0A452F3X0	A0A452F3X0_CAPHI	MYH7B	-0.57003
Mediator of ErbB2-driven cell motility 1	A0A452DSU6	A0A452DSU6_CAPHI	MEMO1	-0.61283
Lactamase_B domain-containing protein	A0A452EI23	A0A452EI23_CAPHI	ETHE1	-0.61666
Nuclear receptor corepressor 2	A0A452E1G5	A0A452E1G5_CAPHI	NCOR2	-0.6196
Poly(rC)-binding protein 1	A0A452DVL8	A0A452DVL8_CAPHI	PCBP1	-0.7003
Dystonin	A0A452G6A1	A0A452G6A1_CAPHI	DST	-0.70095
Importin N-terminal domain-containing protein	A0A452F3M1	A0A452F3M1_CAPHI	IPO5	-0.70269
Fructose-bisphosphate aldolase	A0A452EH63	A0A452EH63_CAPHI	ALDOA	-0.7152
NEDD8-activating enzyme E1 regulatory subunit	A0A452DZ25	A0A452DZ25_CAPHI	NAE1	-0.76313
Exosome complex protein LRP1	A0A452FYK1	A0A452FYK1_CAPHI	LRP1	-0.76378
Pyridoxal phosphate homeostasis protein	A0A452FU89	A0A452FU89_CAPHI	PLPBP	-0.7791
PABS domain-containing protein	A0A452DU00	A0A452DU00_CAPHI	SMS	-0.78733
PKS_ER domain-containing protein	A0A452E7Y7	A0A452E7Y7_CAPHI	RTN4IP1	-0.78797
Interleukin-6	Q28319	IL6_CAPHI	IL6	-0.85769
IF rod domain-containing protein	A0A452FN18	A0A452FN18_CAPHI	KRT3	-0.86257
Glyoxylate reductase/hydroxypyruvate reductase	A0A452FAD3	A0A452FAD3_CAPHI	GRHPR	-0.87396
CSD_1 domain-containing protein	A0A452EQN7	A0A452EQN7_CAPHI	CARHSP1	-0.91712
Pyridoxal phosphate phosphatase	A0A452EKB8	A0A452EKB8_CAPHI	PDXP	-0.92183
Proteasome subunit beta	A0A452FAZ1	A0A452FAZ1_CAPHI	PSMB4	-0.94255
Tubulin beta chain	A0A452G1A9	A0A452G1A9_CAPHI	TUBB6	-0.94606
Serine/arginine-rich splicing factor 2	A0A452EXY9	A0A452EXY9_CAPHI	SRSF2	-0.95347
Glycerol-3-phosphate dehydrogenase [NAD(+)]	A0A452FD14	A0A452FD14_CAPHI	GPD1	-0.97373
Farnesyl pyrophosphate synthase	A0A452FCU2	A0A452FCU2_CAPHI	FDPS	-0.97921
Chromobox protein homolog 1	A0A452E698	A0A452E698_CAPHI	CBX1	-0.98289
4a-hydroxytetrahydrobiopterin dehydratase	A0A452FV62	A0A452FV62_CAPHI	PCBD2	-0.98343
Eukaryotic translation initiation factor 3 subunit E	A0A452DRD5	A0A452DRD5_CAPHI	EIF3E	-0.98571
Phospholipase B-like	A0A452FVJ7	A0A452FVJ7_CAPHI	PLBD1	-0.98619
Perilipin	A0A452FUU5	A0A452FUU5_CAPHI	PLIN3	-0.9974
RRM domain-containing protein	A0A452FP83	A0A452FP83_CAPHI	HNRNPC	-1.00172
ESCRT-II complex subunit VPS25	A0A452ES90	A0A452ES90_CAPHI	VPS25	-1.0375
OCIA domain-containing protein	A0A452FY19	A0A452FY19_CAPHI	OCIAD1	-1.04266

Hydroxyacyl-coenzyme A dehydrogenase, mitochondrial	A0A452EHJ6	A0A452EHJ6_CAPHI	HADH	-1.04854
EGF domain-specific O-linked N-acetylglucosamine transferase	A0A452EJR1	A0A452EJR1_CAPHI	EOGT	-1.06245
Protein-synthesizing GTPase	A0A452DQ55	A0A452DQ55_CAPHI	EIF2S3	-1.06575
Non-specific serine/threonine protein kinase	A0A452EIV8	A0A452EIV8_CAPHI	MAPKAPK3	-1.07881
Small nuclear ribonucleoprotein Sm D3	A0A452DKT5	A0A452DKT5_CAPHI	SNRPD3	-1.20843
Early endosome antigen 1	A0A452FIX8	A0A452FIX8_CAPHI	EEA1	-1.21445
CCT-alpha	A0A452EVX4	A0A452EVX4_CAPHI	TCP1	-1.22985
Palmdelphin	A0A452G5M5	A0A452G5M5_CAPHI	PALMD	-1.2299
Caveolae-associated protein 1	A0A452FLJ3	A0A452FLJ3_CAPHI	CAVIN1	-1.25635
Coronin	A0A452FNA0	A0A452FNA0_CAPHI	CORO1C	-1.27662
S-adenosylmethionine synthase	A0A452G7L4	A0A452G7L4_CAPHI	MAT2A	-1.31437
Actin-related protein 2/3 complex subunit 3	A0A452FVB0	A0A452FVB0_CAPHI	ARPC3	-1.31705
Hemoglobin subunit beta-C	A0A452FX49	A0A452FX49_CAPHI	HBBC	-1.38286
Cytochrome b	Q8WF85	Q8WF85_CAPHI	Cytb	-1.45505
SWIM-type domain-containing protein	A0A452DJR4	A0A452DJR4_CAPHI	ZSWIM8	-1.47698
VWFA domain-containing protein	A0A452DS40	A0A452DS40_CAPHI	ITGAX	-1.47766
Beta-MPP	A0A452F341	A0A452F341_CAPHI	PMPCB	-1.86277
Argininosuccinate synthase	A0A452F1Z3	A0A452F1Z3_CAPHI	ASS1	-2.45124

Table A3:3 The Most significantly regulated proteins – Endolysosomal (EL) fraction

Appendix 3

3.1 The complete pathways of transcriptomic pathway analysis

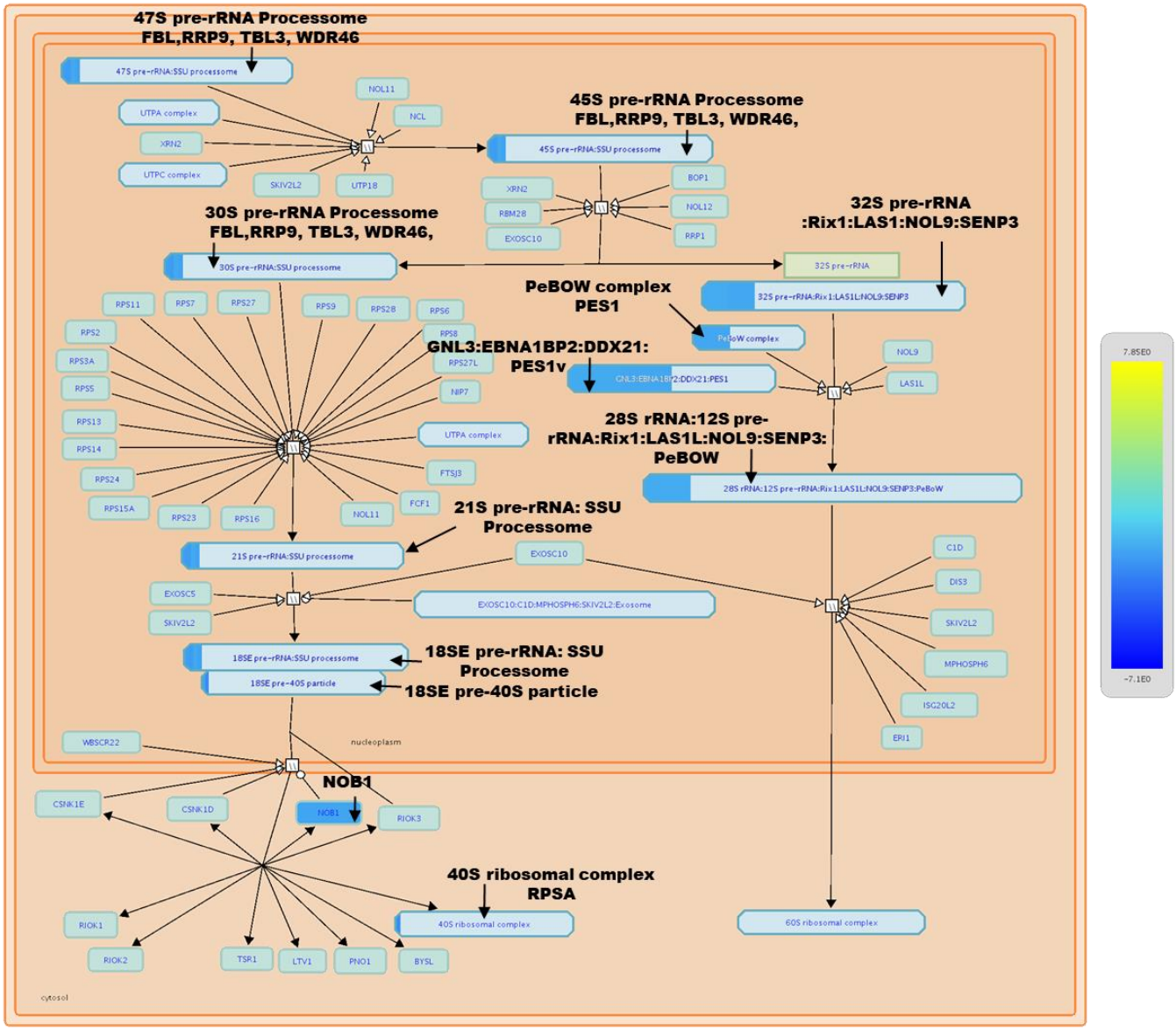

Major pathway of rRNA processing in the nucleolus and cytosol [gene name] 1/1 #log2FoldChange

Figure A3:1: (Related to Figure 4:8): Down regulation of the rRNA processing pathway in the nucleolus and cytosol. *The observed protein complexes and their respective mRNA regulations are as follows: 47S- Pre-rRNA processome; this complex consists of proteins FBL (log2 -1.56), RRP9 (log2 -1.63), TBL3 (log2 -1.21), WDR46 (log2 -1.41).30S- Pre-rRNA processome; this complex consists of proteins FBL (log2 -1.56), RRP9 (log2 -1.63), TBL3 (log2 -1.21), WDR46 (log2 -1.41). 45S- Pre-rRNA processome; this complex consists of proteins FBL (log2 -1.56), RRP9 (log2 -1.63), TBL3 (log2 -1.21), WDR46 (log2 -1.41).32S pre-rRNA: Rix1: LAS1L:NOL9:SENP3; this complex consists of proteins PES1 (log2 -1.23), SENP3 (log2 -1.1). PeBOW complex; PES1 (log -1.23). GNL3:EBNA1BP2:DDX21:PES1; this complex consists of proteins EBNA1BP2 (log2-1.13), PES1 (log2 -1.23). 28S rRNA: 12S Pre-rRNA: Rix1: LAS1L, NOL9, SENP3: PeBOW; this complex consists of protein SENP3 (log2 -1.1). 40S ribosomal complex; this complex consists of protein RPSA (log2 -2.16). NOB1 (log2 -1.36). 18SE pre-40S particle; this complex consists of proteins NOB1 (log -1.36), RPSA (log2 -2.16). 18SE pre- rRNA: SSU processome; this complex consists of proteins FBL (log2 -1.56), RRP9 (log2 -1.63), TBL3 (log2 -1.21), WDR46 (log2 -1.41). 21SE pre- rRNA: SSU processome; this complex consists of proteins FBL (log2 -1.56), RRP9 (log2 -1.63), TBL3 (log2 -1.21), WDR46 (log2 -1.41). (colour code=yellow to blue gradient, yellow represent highest up regulation while blue represent highest down regulation, highest upregulation log2 fold 7.85E0 and lowest log2 fold -7.1E0, The protein complexes with complete or part-coloured representation showed the total molecules present from the query data set to complete the complex. Arrow = Protein or protein complex name) Figure created using www.reactome.com pathway analysis.*

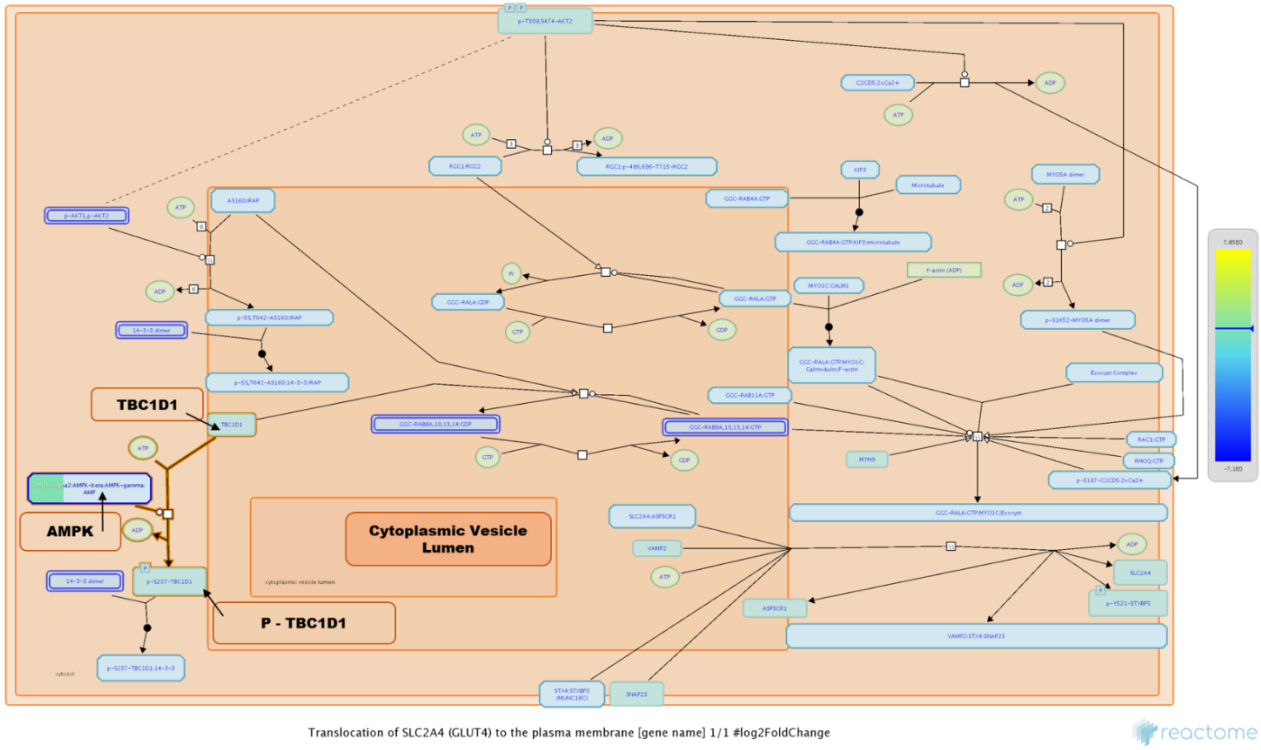

Figure A3:2: (Related to Figure 4:9): AMPK activation of GLUT4 vesicle translocation to the plasma membrane. *TBC1 domain family member 1 (TBC1D1) phosphorylation at AMPK to activate GLUT4 glucose uptake to the cell. (colour code=yellow to blue gradient, yellow represent highest up regulation while blue represent highest down regulation, highest upregulation log2 fold 7.85E0 and lowest log2 fold -7.1E0, The protein complexes with complete or part-coloured representation showed the total molecules present from the query data set to complete the complex. Arrow = Protein or protein complex name) Figure created using www.reactome.com pathway analysis.*

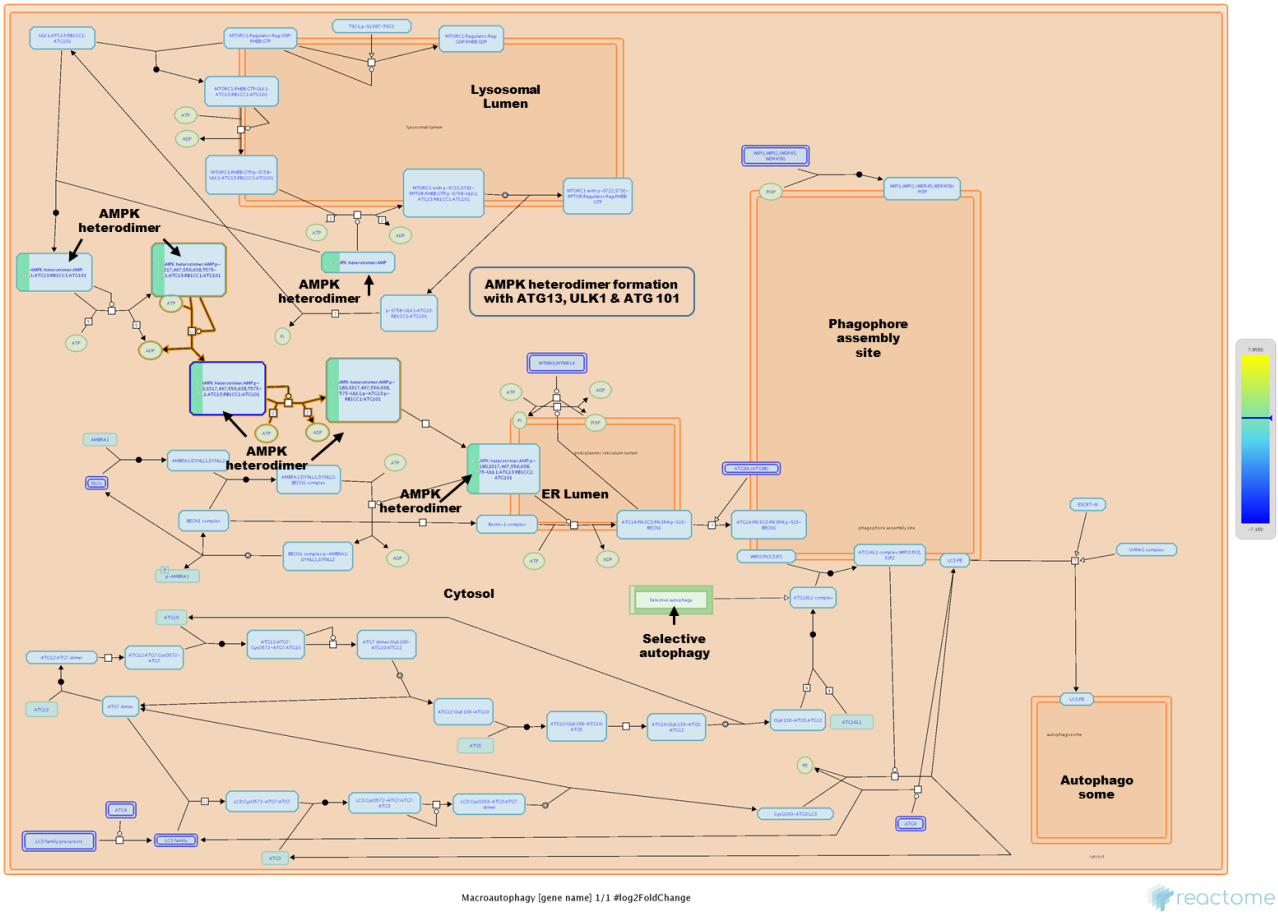

Figure A3:3: (Related to Figure 4:10): AMPK activation of Macrophagy. *AMPK or PRKAG3 log2 2.2 and PRKAA2 log2 2.3 fold up regulation was observed in the mRNA differential expression analysis. AMPK formed direct heterodimer with autophagy marker proteins such as ATG13, ATG101 and ULK1. Moreover, AMPK activation of selective autophagy was observed. (colour code=yellow to blue gradient, yellow represent highest up regulation while blue represent highest down regulation, highest upregulation log2 fold 7.85E0 and lowest log2 fold -7.1E0, The protein complexes with complete or part-coloured representation showed the total molecules present from the query data set to complete the complex. Arrow = Protein or protein complex name) Figure created using www.reactome.com pathway analysis.*

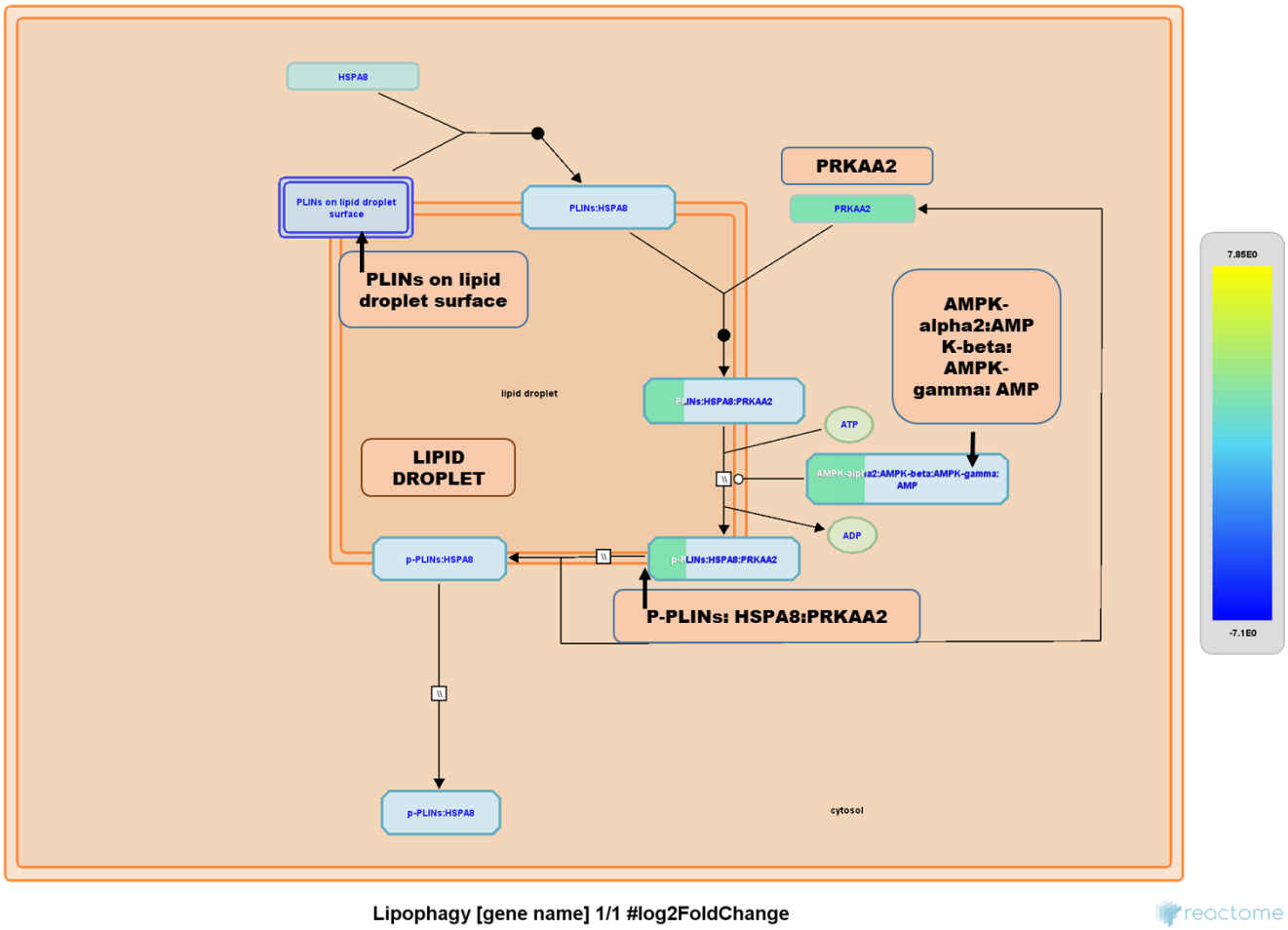

Figure A3:4: (Related to Figure 4:11): AMPK activated Lipophagy as interpreted in AF goat LA model. *AMPK or PRKAG3 log2 2.2 and PRKAA2 log2 2.3 fold up regulated. The Perilipin (PLIN) protein was firstly interacted with the chaperone protein Heat shock protein 8 (HSP8) and then AMPK/PRKAA2 phosphorylated the PLIN protein to degrade through chaperone mediated autophagy. (colour code=yellow to blue gradient, yellow represent highest up regulation while blue represent highest down regulation, highest upregulation log2 fold 7.85E0 and lowest log2 fold -7.1E0, The protein complexes with complete or part-coloured representation showed the total molecules present from the query data set to complete the complex. Arrow = Protein or protein complex name). Figure created using www.reactome.com pathway analysis.*

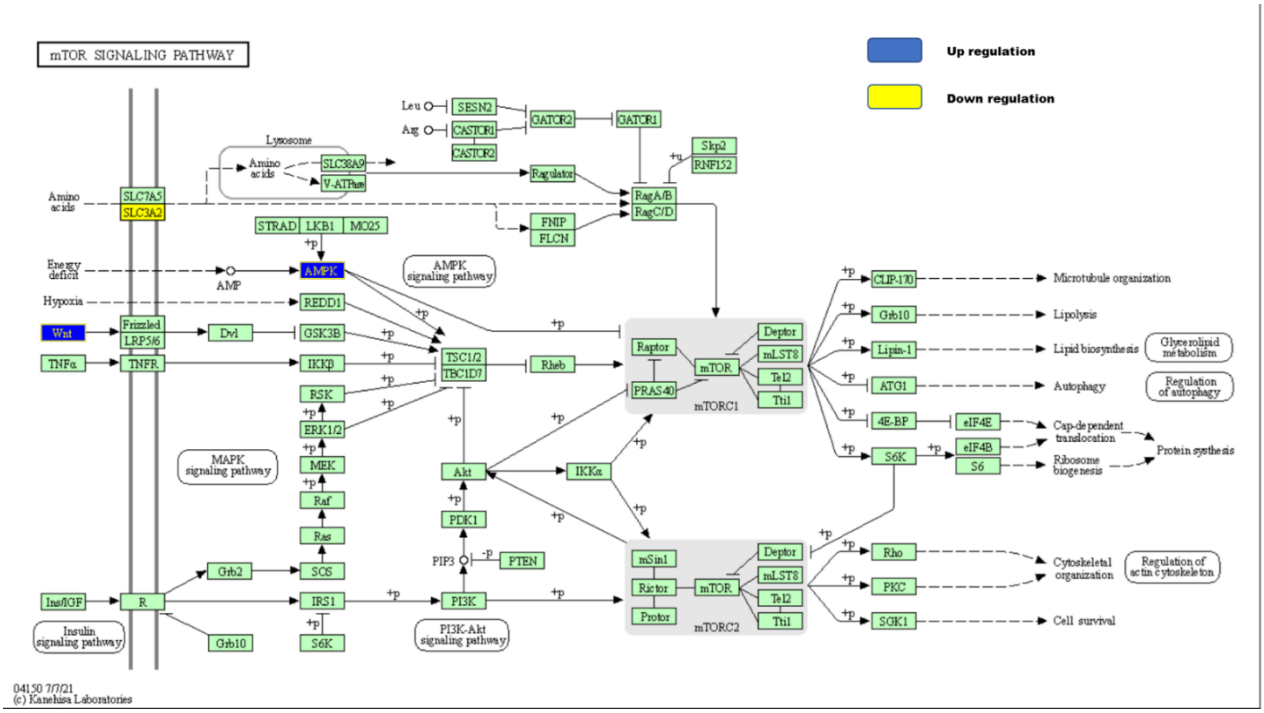

Figure A3:5 (Related to Figure 4:12): The mTOR signaling Pathway. *The mTOR signalling inhibition by the down regulation of SLC3A2 (log2 -1.6 fold), AMPK or PRKAG3 log2 2.2 and PRKAA2 log2 2.3 fold and WNT5A log2 2.3 fold up regulated. (Arrow = Gene name, Blue = up regulation (log2 fold change) and Yellow= down regulation (log2 fold change)). +P = phosphorylating events Pathway analysed using KeGG database.*

Appendix 4

Full publications related to this Thesis

Ayagama T, Bose SJ, Capel RA, Priestman DA, Berridge G, Fischer R, Galione A, Platt FM, Kramer H and Burton RAB. (2021). A modified density gradient proteomic-based method to analyze endolysosomal proteins in cardiac tissue. *iScience* **24,** 102949.

Bose SJ, Ayagama T & Burton RAB. (2022). Chapter 3 - Lysosomal proteases and their role in signaling pathways In *Proteolytic Signaling in Health and Disease*, ed. Zelanis A, pp. 41-61. Academic Press.